Novel Bio-Hybrid Nanoscale Carriers Engineered for High Therapeutic Payload and Controllable Extended Release Using Nucleic Acid Aptamers

by

Padma Priya Mohana Sundaram

A Dissertation Submitted to the Graduate Faculty of
Auburn University
In Partial Fulfillment of the
Requirements for the Degree of
Doctor of Philosophy

Auburn, Alabama
May 4, 2014

Keywords: Drug, Delivery Carrier, Gold Nanoparticles, DNA, Aptamers, Neomycin, Daunomycin

Copyright 2014 by Padma Priya Mohana Sundaram

Approved by

Mark E. Byrne, Chair, Daniel F & Josephine Breeden Associate Professor of Chemical Engineering
Jacek Wower, Co-Chair, Professor of Animal Sciences
Christopher B. Robert, Uthlaut Professor of Chemical Engineering
Elizabeth A. Lipke, Assistant Professor of Chemical Engineering
Valery A. Petrenko, Professor of Pathology

Abstract

Controlled delivery of therapeutics to target tissues constitutes a great challenge of modern medicine, especially in the field of cancer treatment where malignant cells have to be killed without damaging the surrounding healthy cells. A drug delivery carrier capable of releasing drug in a controlled manner for an extended period of time would greatly impact the field of medicine. Such a carrier has to be small in size, non-toxic, and it should not cause any immune response. Recently, gold nanoparticles (AuNps) and nucleic acids were found to be potential tools for drug delivery. AuNps have been studied as drug delivery platforms because of their non-toxic gold core, ease of preparation of mono-dispersed particles, ease of functionalization of small molecules, and efficient cellular uptake. Nucleic acid aptamers are emerging as important drug targets and versatile therapeutic agents due to their ability to fold into complex three-dimensional structures and bind therapeutically important small molecules. A number of studies demonstrated that nucleic acids constitute attractive materials for nanotechnology, as these macromolecules can be easily programmed to carry out specific functions. Our strategy is to exploit the nucleic acid's response to different physical and chemical triggers such as temperature and binding affinity to produce controlled and extended drug release.

In this work, we have developed gold nanoparticles and DNA-based drug delivery nano-carriers which utilizes the versatile properties of nucleic acids for controlled and

extended release of drugs. The drug delivery carrier consists of 15 nm gold nanoparticles (AuNps) functionalized with drug binding DNA aptamers via a single stranded (ss) anchor DNA. The presence of ssDNA makes the nano-carrier flexible to be reprogrammed for aptamers that either bind different drugs or display different affinities for the same drug. Under the optimum binding conditions (0.4 M NaCl and 4 μM DNA), a maximum of 101±8 anchor DNA strands were conjugated per particle. Changes in number density influenced the mean diameter of DNA-conjugated AuNps which was determined using dynamic light scattering. The mean diameter of DNA-conjugated AuNps was also affected by conformational changes of DNA strands. Our studies revealed that short DNA strands exist in a stretched conformation while longer DNA strands adopt coiled conformation when functionalized on AuNps.

For the first time, we demonstrated that neomycin could bind to DNA aptamer with very high affinity (K_d= 98.101 nM). The nano-carrier for neomycin was constructed by binding DNA-aptamer:drug complexes to the anchor DNA functionalized AuNps. Controlled and extended release of drug from the synthesized carrier was obtained by temperature and affinity modulations. The nano-carrier when modified for the anticancer drug daunomycin, demonstrated very high loading of 1157 ± 18 drug molecule per particle. The hydrodynamic size of the nano-carrier was found to be 41 ± 2 nm. This size of the nano-carrier makes it suitable for passive targeting of drug to cancer cells. The in-vitro release of daunomycin at 37^{o}C demonstrated controlled release of drug from the nano-carrier for an extended period of time. After 6 days of release only about 75% of the bound daunomycin was released from the nano-carrier which implies that the release can be

extended much further. Furthermore, the physiological relevance of the nano-carrier was demonstrated by testing the cell viability of MCF7 breast cancers cells after incubating them with the drug loaded nano-carrier. The nano-carriers displayed excellent cellular uptake, were found to be non-toxic, and invoked cell death which was observed to be proportional to the concentration of the daunomycin loaded nano-carrier. At any tested concentration, cell death by the daunomycin loaded nano-carrier was higher or equal to the cell death induced by the same concentration of free daunomycin. This nano-carrier with a very high payload and efficient drug delivery is a potentially powerful, yet flexible, tool for fighting cancer. Being versatile to be modified for any drug, it is expected to impact a number of treatment strategies.

Acknowledgement

I would like to acknowledge the guidance and encouragement of my advisors Dr. Mark Byrne and Dr. Jacek Wower. I also want to extend my heart felt gratitude to my committee Dr. Christopher Roberts, Dr. Elizabeth Lipke, Dr. Valery Petrenko, and my outside reader Dr. Terry Brandebourg, for their patience and extraordinary support. I want to acknowledge Alabama Commission of Graduate Research for funding this project

I would like to thank all the members of Byrne group Matthew Eggert, Amanda Paine, Matthew McBride, Kayla Pate, James Kazsmarek, Ricky Whitener, and Jessica Larsen. I especially want to thank Arianna Tieppo, Charles White, Vishal Salian and Helena Kurniawan for being so helpful and making my PhD period a memorable time. Would also like to thank Dr. Iwona Wower for all the valuable advice, and my collaborators Dr. Edward Davis, Dr. Alexander Simonian and Dr. Elizabeth Lipke. I appreciate the help of Shantanu Pradhan with cellular studies. A very special thanks to my two best friends Surya and Phani for being my iron pillars and making this happen for me. I could not have done it without their encouragement and support.

I would like to thank my parents Ambika and Mohana Sundaram for their unconditional love, support, and encouragement. They are the apple of my eye, and I dedicate this work to them. Lastly, I want to thank my sister Priya and my brother Kumar for caring and loving me always.

Table of Contents

List of Tables

List of Figures

Chapter 1. Introduction

In the last few decades, there has been enormous developments in the field of medicine. Entirely new classes of therapeutics have been discovered for the treatment of various human diseases and disorders. However, in medicine, the success and failure of a therapy is often not the use of a drug itself but how the drug is being used. At present, about 95% of the new therapeutics and the potential therapeutics have poor pharmacokinetics and biopharmaceutical properties[1]. Therefore there is a need for the development of a delivery systems that can improve the therapeutic index and pharmacokinetics of the drug.

Creating a targeting drug delivery carrier is an integral component of the overall process of drug delivery. Drug delivery systems have already had a great impact on medical technology, greatly improving the performance of existing and enabling the use of new therapeutics. At present, however, the performance of these drug delivery system are constrained by several technological barriers[2]. With the discovery of anti-sense oligonucleotides and small interfering RNA technologies, delivery of therapeutics into the cell has become a necessity. The carriers need to be targeted with high specificity to the cells of interest with little to no off-targeting effects. Thus, new technologies and approaches are needed to develop systems that can reduce the amount of drug used, target the drug to the affected tissues, and improve compliance by reducing the chances of missing in a dose.

Over the last four decades, researchers have concentrated their work in developing a sound technical background for drug delivery systems with a motive to use them for the targeted delivery of therapeutics in the clinic. Along with targeted delivery, it is highly desirable to control the rate of release of the therapeutic in the site of action for an extended period of time. With such a control over drug delivery, lower side effects, little to no off-targeting of drug, and non-toxic drug concentrations can be achieved. With the rapid discovery of potent small molecules as drugs, such delivery systems holds immense promise in improving various complex therapy regimes including chemotherapy.

Increasing the therapeutic index of a delivered compound by selectively delivering it to target areas is a goal that has many obstacles. For example, some non-biological materials used for developing drug delivery systems are toxic and also trigger strong inflammatory reactions. The movement of the drug and the carrier can be restricted by the natural biological barriers. Once inside the target cells, drug carriers are immediately subjected to lysosomal degradation which reduces the availability of the drug inside the cell. Thus, the design of multi-functional, non-toxic drug carriers, capable of targeted and multiple drug delivery to cells with controlled release mechanisms, which bypass normal physiological barriers such as endosomal degradation, is a significant unmet need yet to be realized.

This dissertation is focused on developing a delivery carrier for targeted, dynamic, and controlled release of drug for an extended period of time using gold nanoparticles (AuNps) and DNA. Nucleic acids have been researched extensively to explore their potential as therapeutics, diagnostics materials, and biosensors. Various classes of nucleic acids and their application in the field of medicine along with their challenges are discussed

in detail in chapters 2 and 3. The other component of our delivery carrier is gold nanoparticles which has been a delivery platform of interest since the past two decades because of it non-toxic gold core, ease of preparation of monodispersed particles, ease of functionalization of small molecules, and efficient cellular uptake. Various drug delivery platforms researched and in clinical trials at present along with their advantages and disadvantages are discussed in chapter 4.

Using gold nanoparticles and a particular class of nucleic acids called aptamers, we have developed a nano-delivery carrier for the antibiotic drug neomycin. Aptamers have the ability to bind to small molecules such as drug, amino acids, and cells with high affinity in their three dimensional structure. They have been found as an excellent cell targeting moiety, and have been extensively researched to be used in drug delivery as targeting entity. For the first time, we have used the ability of aptamers in binding drug to control the release of drug from the nano-carrier. The synthesis and characterization of the nano-carrier are described in chapter 5. The ability of our nano-carrier in releasing the drug for an extended period of time using temperature and drug binding affinity modulations are presented in chapter 6.

Much of the present work in the field of drug delivery is concentrated in developing an efficient delivery carrier for cancer therapeutics. Major reasons for such a concentration of work is due to the fact that, cancer is the cause of death of 8.2 million people around the world according to the world cancer report 2014, and chemotherapeutics are neither specific nor targeted, thereby causing toxicity to normal cells even under optimal conditions. Therefore, there is a demand and necessity to develop a delivery carrier that can reduce the non-specific toxicity of the drug and target therapeutics to the tumor. Using

gold nanoparticles and DNA, we developed a novel nano-carrier for the targeted delivery of anti-cancer drug daunomycin. The synthesis and characterization of nano-carrier for daunomycin along with the proof of its ability to release the drug for an extended period of time, and its potential to be taken in by the cells and induce cancer cell death better than the drug alone is presented in chapter 7.

The results presented in this dissertation conclusively demonstrate the value of creative and novel delivery platform for dynamic and controlled delivery of drug for an extended period of time.

1.1. References

1. Koo OM, Rubinstein I, Onyuksel H. Role of nanotechnology in targeted drug delivery and imaging: a concise review. Nanomedicine: Nanotechnology, Biology and Medicine. 2005;1: 193-212.

2. LaVan DA, McGuire T, Langer R. Small-scale systems for in vivo drug delivery. Nature Biotechnology. 2003;21: 1184-1191.

Chapter 2. Different Classes of Nucleic Acids in Medicine

Nucleic acids (NAs) are the most important biological molecules that act as storage and transfer units of genetic information. Since the milestone discoveries of catalytic ribonucleic acids (RNA) in late 1980's and RNA interference in 1990's, NAs have evolved as versatile and dynamic molecules that regulate the genes in all living organisms. This and further breakthrough work in the field of NAs lead to the emergence of numerous types of NAs such as ribozymes, RNA interference, antisense oligonucleotides, and aptamers. These classes of nucleic acids, capable of selectively modulating gene expression and protein function at the deoxyribonucleic acid (DNA), RNA, and protein levels, have produced a major revolution in the field of medicine. In this chapter, all these different classes of NAs are described, and aptamers are discussed in detail along with their various applications.

2.1. Ribozymes

Ribozymes are catalytic RNA that function as enzymes, even in the complete absence of proteins, for RNA cleavage and ligation reactions. They have great potential as therapeutics due to their enzymatic activity and ability to cleave deleterious RNA or repair cellular mutant RNAs. Ribozymes naturally have the ability to specifically recognize and modify their target RNAs. The substrate recognition domain of ribozymes can also be

artificially engineered to stimulate site-specific cleavage in *cis* (the same nucleic acid strand) or *trans* (a non-covalently linked nucleic acid)[1]. Since their discovery in 1988[2], ribozymes have been widely used to silence gene expression. The hammerhead catalytic ribozyme motif has been successfully used to silence genes in bacteria, flies, plant, amphibians, and mammals[3]. Although there are numerous ribozymes, most of the therapeutic ribozymes are derived from either hammerhead or hairpin motifs.

The ribozyme catalytic core has two major functions. First, it destabilizes the substrate strand to twist the phosphodiester bond into cleavable conformation. Second, it assists in positioning of divalent cation that stimulates the catalytic activity of the ribozyme[4]. Over the past decades, ribozymes have been intensely studied to be used as therapeutic agents for potential, fatal, and devastating viral infections. This work was quite successful, and today ribozyme technology is available for specific inhibition of many human viral diseases including HIV[5].

To use ribozymes as therapeutics, several parameters have to be resolved. The binding of ribozyme to RNA is a crucial step, and it largely determines the activity of the ribozyme in vivo. Thus, it is very important to choose the correct target mRNA. It has been suggested that targeting the mRNA of a protein downstream of mutated gene product may result in more effective inhibition than targeting the mutated gene sequence. However, this could lead to decrease in specificity. It is equally important to select a suitable binding site on mRNA as the efficiency of the ribozyme is dictated by the sequence and accessibility of the target site due to the secondary and tertiary structure of the mRNA[6]. Experimental procedures such as nuclease mapping, chemical probing, and RNA folding computer programs are used to determine the accessible sites, but both the procedures have their own

limitations. Thus, selecting the right mRNA binding site is a crucial and difficult task. The length of the ribozyme's hybridizing arm must have a balance between providing specificity to the sequence while allowing product dissociation[7, 8]. The cell free system experiments suggest that asymmetric arms may be more effective than symmetric arms in balancing these two activities[9]. This might not be really true in a cellular system.

In an attempt to improve the ribozyme technology, researchers developed a multi-unit ribozyme which can target different sites within the same mRNA. This type of ribozyme was shown to be more efficient than the traditional ribozymes in targeting HIV and BCR/ABL mRNAs[10, 11]. Chemical modifications are commonly used in the therapeutic ribozymes to ensure longer lifetime of ribozyme molecules. The first clinical trial of synthetic ribozyme therapeutic was published in 2005 for the treatment of renal cancer (Angiozyme)[12]. Currently, there are several hammer head ribozymes in clinical trial[13, 14] **(Table 2.1)**. The delivery of ribozyme into the cells constitutes another major challenge in ribozyme technology, which will be addressed in a later section.

2.2. Antisense Oligonucleotides

Better understanding of diseases at the molecular level, such as molecular interactions on the level of proteins, led to the development of new therapeutics called antisense oligonucleotides (ASON). They bind to mRNA molecules of disease related protein and thereby specifically inhibit that protein synthesis. The concept of using synthetic oligonucleotide as a potential therapeutic was proposed by Zamecnik and Stepheson in 1978[15]. In 1998, the first antisense drug Vitravene was approved by the food and drug administration (FDA), and many more are in clinical trials at present **(Table 2.2)**.

This approach takes advantage of the basic, well understood rules of Watson-Crick base pairing by which single stranded nucleic acid interacts with the complementary nucleic acid to form a double stranded helix. Antisense technology is very advantageous as the short oligonucleotides can be easily synthesized and can be made resistant to enzymes by chemical modification ensuring the long lasting of the drug.

ASONs can inhibit translation of mRNA by various mechanisms. They can hybridize to mRNA at ribosomal binding site and arrest their translation[16]. The target site on mRNA is either AUG codon or untranslated region at the 5' terminal[17]. They can also activate RNase H, enzyme that cleaves the RNA strand in a RNA-DNA duplex[16], and thereby interrupt translation. Moreover, they can also target splicing site and inhibit production of matured mRNA or target capping and polyadenylation site to destabilize mRNA[17].

Though this technology is promising, it suffers from some major drawbacks such as difficulty in selection of the target site on mRNA, and designing of antisense oligonucleotide. In vivo, antisense technology is bound to the base pairing accessibility of mRNA target site. A better target site can be selected by understanding the 3D structure of the target RNA. Various modeling software can be used, but discerning the structures that target RNA adopts in vivo is still very difficult[18]. Another option is to test the accessibility of mRNA site by oligonucleotide hybridization in vitro, but this method has also met with limited success[19]. Therefore, the most effective method is to screen a large number of oligonucleotides that bind to different sites on mRNA, including the 5' and 3' untranslated region, initiation codon site, coding region, and identify a set of optimal target sites. But

this experimental procedure is very expensive and highly time consuming. Thus, an easy, economical and efficient method for identifying the target site is yet to be discovered.

Designing the effective ASON is another major challenge of antisense technology. Many algorithms and software have been developed to theoretically design the effective antisense oligonucleotides[20, 21]. Unfortunately, all of them fail to predict non-canonical interactions in RNA structure. The base composition and sequence of the antisense oligonucleotide are very important as they determine the specificity and affinity for its target RNA[22]. Oligonucleotides having palindromic sequence, which could form stable secondary structure, usually fail to serve well as antisense oligonucleotide as the secondary structure formation would compete with its binding to mRNA[23]. Oligonucleotides with GGGG sequence can induce cell proliferation and immune responses, and also have different cellular uptake, pharmacokinetics and in vivo distribution from the other oligonucleotides[24, 25]. Oligonucleotide containing the two-base sequence CpG (where p stands for phosphate) can activate B cells and natural killer cells as they can be identified as bacterial DNA by the body[26, 27]. These aspects makes the designing of an ASON a difficult and time consuming task. Even if a very suitable ASON is designed for a given mRNA, the method cannot be generalized for designing ASON to inhibiting other mRNA targets.

2.3. RNA Interference

RNA interference (RNAi) is a naturally occurring gene silencing process that uses small RNAs to mediate post-transcriptional/transcriptional gene silencing in eukaryotic

cells[28-31]. The RNAi pathways are guided by small RNAs such as small interference RNA (siRNA), micro RNA (miRNA), and PIWI interacting RNA (piRNA). It was in 1998 when Fire *et al*., discovered the ability of double stranded RNA to silence gene expression in worms that the technique attained great attention[32]. The RNAi mechanism was initially believed to function only in plants and worms, but in 2001 Tuschi and coworkers[33] demonstrated the sequence specific gene knock-down in mammalian cells by siRNA. Soon after, McCaffery *et al*., demonstrated the first use of siRNA in mice for treating hepatitis C[34]. This work opened the possibility of using the RNAi technology to cure human disease. Since then billions of dollars have been invested on developing siRNAs for therapeutic application. This technology is poised for delivering ground breaking developments in the field of medicine.

In the naturally occurring RNAi process in the eukaryotic cells, the RNAi is activated in the presence of a long double stranded (ds) RNA, and it's cleaved into multiple 21-23 nucleotide long siRNA by the enzyme Dicer. While in an induced RNAi, siRNA can be directly synthesized and introduced into the cell. Unlike long pieces (>30 nucleotide) of dsRNA, synthesized siRNA does not trigger the immune responses or cause shutdown of cellular protein expression by interacting with intracellular RNA receptors[35]. When inside the cytoplasm of the cell, the siRNA incorporates into a protein complex called RNA-induced silencing complex (RISC)[36]. The Argonaute 2 (AGO2) protein, a multifunctional protein present in the RISC, unwinds the siRNA and cleaves the sense or passenger strand[36, 37]. Then the antisense strand in the activated RISC interacts with mRNA complimentary to the antisense strand and degrades it[38]. The cleavage of mRNA generally takes places between 10^{th} and 11^{th} nucleotide from the 5' end of antisense RNA[39]. Later,

the activated RISC moves to the next mRNA and propagates gene silencing. The siRNA therapeutic effect prolongs for 3-7 days in a rapidly dividing cell and for several days in non-dividing cells[40, 41] **(Figure 2.1)**.

In contrast to siRNA, miRNA mediate the translation repression and transcriptional degradation of the imperfectly complementary target. The endogenous RNAs with a stem loop or short hairpin structure are encoded and processed in nuclease, and transported to cytoplasm as pre-miRNA where it is furthered shortened by Dicer to produce imperfectly matched double stranded miRNA. Similar to siRNA, miRNA forms RISC which is activated by AGO2 but the passenger strands are released and not cleaved. If the RNA duplex loaded on RISC has imperfect sequence complementary, the sense (passenger) strand is unwound leaving the matured miRNA bound to RISC. The miRNA binds to mRNA leading to direct translational repression or mRNA degradation by P-bodies[42] **(Figure2.2)**.

The synthetic siRNAs makes the natural RNAi pathway consistent and predictable. Thus, they are very attractive as therapeutics. As they enter the pathway after the Dicer step, they are less likely to interfere with gene regulation by endogenous miRNAs[35]. The efficiency of the synthetic siRNA is determined by its sequence rather than the mRNA. Dharmacon, the leading player in siRNA design market listed 8 criteria for effective siRNA design such as (i) low G/C nucleotide content, (ii & iii) sense strand having same sequence as mRNA target, i.e to have 3 or more A/U nucleotide at the 3' terminal, avoiding internal repeat that could form secondary structure, (iv) having an A at position 3, (v) U at position 10, (vi & vii) A or U at 19, and (viii) absence of G at position 13[43].

RNAi technique has many advantages over the classical genetic screening techniques. It is a forward genetics screen using a reverse genetic technique where the function of the target gene is inferred when silenced. The sequences of all the identified genes are known and thus the mutations can be easily identified. As the recovery of the gene mutants are not necessary, RNAi allows more sophisticated analysis of data[44]. Unlike classical genetic studies, the genome of the organism remains untouched during the RNAi process. Moreover, 75% of the mRNA transcripts can be efficiently knocked down by this technique. Over the decade, considerable work has been done on developing siRNA therapeutics for various human disease targets including cancer[45-47]. At present, siRNA therapeutics for Pachyonychia Congenita, Subfoveal Choroidal Neovascularization (CNV), Chronic Myeloid Leukemia (CML) and many other human diseases are undergoing different phases of clinical trials[14, 48] **(Table 2.3)**.

2.4. Aptamers

Aptamers are single stranded (ss) nucleic acid molecules (RNA/DNA) which can fold into complex three dimensional structures[49-52] and form binding pockets and clefts for specific binding to target molecules[53-55] via hydrogen bonds, van der Walls interactions, or base stacking interactions. These molecules have properties comparable to antibodies and are considered as alternatives to the long established antibody-based products for diagnostic and therapy[56, 57]. Aptamers exhibit similar molecular recognition characteristics to antibodies, but they can recognize minor structural differences between the target and their related molecules. They are different from other nucleic acid therapeutics because

they do not directly affect the steps preceding protein function, instead they modulate the function of their target proteins by binding to them directly.

2.4.1. History

The first aptamer was found by Craig Turek while trying to understand the nature of the translational operator with in bacteriophage T4 gene 43 mRNA in 1990[58]. In an attempt to recognize a NA that binds T4 DNA polymerase, Turek mutated the 8 nucleotide-long hairpin loop of the bacteriophage mRNA (that binds T4 DNA polymerase and repress the further polymerase synthesis[59]) and produced 65,536 individual species. The high-affinity nucleic acid ligands for T4 DNA polymerase from the mutated NA pool was isolated by an experimental protocol called as *S*ystematic *E*volution of *L*igands by *EX*ponential Enrichment (SELEX). The experiment yielded two sequences with high affinity. One was the wild type sequence found in the bacteriophage mRNA, and the other was a mutant varied at four positions from the wild-type. Those 8 sequences were the focus of the first SELEX experiment. Turek choose to name the ligands as "nucleic acid antibodies" (antibodies made of nucleic acids). But latter they were named as "aptamers", derived from the word aptus; the Greek word meaning "to fit", by Dr. Andy Ellington and Dr. Jack Szostak and became widely used.

The randomized domain of the 8-nucleotide RNA molecule by Turek was shortly expanded to a 30 to 40-nucleotide RNA by Jellinek[60]. Since the first SELEX experiment, considerable progress has been achieved in the field, and aptamers with very high binding affinity and specificity for hundreds of target molecules such as metal ions, amino acids,

peptides, nucleic acid, proteins, antibodies, drug molecules, organic molecules, and cells have been discovered.

2.4.2. SELEX

The SELEX procedure is comprised of cycles of sequential steps. The process is initiated by synthesizing large oligoribonucleotide pools containing as many as 10^{16} different sequences. The generated random oligoribonucleotide strands are incubated with the immobilized ligand, and the non-binding sequences are removed while retaining the binding sequence bound to the ligand. The separation of non-binding sequences is achieved by membrane based filter assay, chromatography, or capillary electrophoresis[61-64]. The binding sequences from the pool are amplified using polymerase chain reaction (PCR) to generate several copies of each binding oligoribonucleotide. The amplified oligoribonucleotide pool is then used to perform the next SELEX selection cycle. The selection and amplification steps are repeated until functional molecules -- RNA aptamers -- dominate the oligoribonucleotide population. In order to increase the resistance of generated aptamer towards degradation by nucleases, various chemical modified nucleoside triphosphate derivatives, which are not present in natural nucleic acids, can be incorporated[65-67]. Aptamers selected from this chemically-modified pool of RNA molecules can be completely resistant to nucleases, and the additional functional group can lead to ligands with novel physical and chemical properties. The number of iterations of the SELEX process required to isolate an aptamer depends on the stringency imposed to each round as well as on the affinity of interaction between the target and the aptamer.

Typically, 6 – 18 iteration cycles of selection and amplification have to be performed to generate a suitable aptamer. These experiments could take months when performed manually. Thus, over the last few years, considerable work has been done in automating the SELEX procedure[68, 69]. Using the automated SELEX, aptamers for multiple targets can now be selected and characterized within few days.

Isolating aptamers against cell-surface receptors presents challenges, such as replication of the native conformation and glycosylation pattern of the extracellular region of the protein, when performing selection in vitro with recombinant proteins. Recently, multiple groups have reported selection using living cells as the target to identify cell- and receptor-specific aptamers[70-73]. As they can bind to proteins in their native configuration on the cell surface[74-76], these aptamers can not only block cell surface receptors but can also be exploited for the delivery of a variety of therapeutic agents into the cell. Since the first SELEX experiment, aptamers for hundreds of target molecules and cells have been discovered and investigated[77-81]. The majority of them are listed in the aptamer database maintained by the Ellington Laboratory[W1].

2.4.3. Applications

Aptamer technology has many advantages. Aptamers can be produced in vitro by chemical synthesis with very good accuracy and reproducibility, and they are very stable for long-term storage. They can be modified with various functional groups, and they can be reversibly denatured and regenerated. Thus, aptamer technology stands as a potential tool for wide spread applications in biomedical, biotechnology, and molecular biology.

2.4.3.1. Diagnostic Assays

Aptamers have been proven to be a very potential diagnostic tool. They inevitably rival antibodies, which are still the ubiquitous reagents in the field of diagnostics. Soon after the discovery of aptamers in 1990, they were found to be a versatile diagnostic assay tools and capable of replacing monoclonal antibodies[82]. Similar to antibodies, aptamers have been used in wide range of assays such as ELISA[83], Western Blot analysis[84, 85], flow cytometry[86], in vivo imaging[87], and microarrays[88, 89]. The aptamer based assays are easy to perform and do not require extensive washes and separations.

In 1996, Drolet *et al.,* used aptamer that binds vascular endothelial growth factor (VEGF) protein in enzyme-linked immunosorbent format assay (ELISA)-like format assay[83]. This work demonstrated that aptamers provide comparable results to antibodies, and thereby proved the effectiveness of aptamers in diagnostic applications. Following that study, a number of researchers reported the successful use of aptamers binding L-selectin, tenascin-c, and thyroid transcription factor 1 (TTF1) in aptamer-based ELISA. Latter, an ingenious approach to improve the efficiency of an enzyme linked aptamer-based diagnostic system was developed by using aptamer molecules as both detection element and the template for amplification reaction[90-92]. This process involves two aptamers targeting two distinct epitopes of the protein complex which upon binding come into close proximity, such that the free 3' and 5' ends of the aptamers can be ligated by a complementary splint oligonucleotide. The resulting ligand product is amplified with two primers specific for each aptamer. This approach demonstrated a 1000 fold increase in sensitivity compared to conventional ELISA[90]. This technology has further advanced to

the triple binder proximity ligation assay (3PLA) which uses three recognition events for improved sensitivity and specificity[93].

Another aptamer based solution phase assay was developed using aptamers that generate fluorescent signals upon structural rearrangement[94-96]. This technique is also called aptamer beacons, and it is very efficient for the real-time monitoring of the aptamer-target binding. The fluorescence of the fluorophore attached DNA aptamer is quenched by the complimentary DNA labeled with the quencher in the absence of target molecules. When the system is exposed to a target, the DNA aptamers bind to target molecules releasing the quencher labeled DNA, and a fluorescent signal is generated. Using this method, detection of target molecules as little as 10 ng [97] and with picomolar sensitivity [98] has been reported. Recently, Zhu *et al.,* developed a sandwich ELISA based on aptamers for diagnosing pulmonary tuberculosis (PTB) using a high affinity aptamer antibody for MPT64. This method was found to have potential clinical value with high sensitivity and a detection limit of 2.5 mg/L. Clinical validation proved that this ELISA is a reliable method for serological diagnostics of PTB and could be used for clinical diagnostic purposes[99].

Aptamers were also used for Western Blot analysis[84, 85]. These aptamers were proven to be feasible enough for specific detection even in crude cell lysates [84, 85]. They were able to bind denatured proteins with much less non-specific binding. Aptamers are generally expected to recognize the three dimensional structure rather than a specific peptide epitope. As the target protein denatures during the SDS-PAGE, it is not clear whether the protein refolds into its structure or if the aptamer recognizes the epitopes like antibodies.

2.4.3.2. Biosensors

Aptamers have the property of binding target molecules with high affinity, and therefore, they can be used as capture ligands in affinity columns for purification of proteins, as well as in biosensors. They can be synthesized chemically with a functional group attached to their 3' or 5' end, and immobilized on carrier materials.

Aptamers covalently labeled by single or double fluorophores at appropriate positions can be employed for determination of targets. The dyes such as fluoroscene (FAM, FITC), rhodamines (TRITC, TAMRA), and cyanines (Cy3, Cy5) are commonly used for labeling aptamers. Roming *et al.,* demonstrated the use of aptamers in affinity chromatography-based purification of recombinant L-selectin Ig fusion protein from a complex cell medium[84]. The anti-L-selectin ssDNA aptamers were immobilized on a solid support, and used to purify L-selectin from Chinese hamster ovary cell medium. This aptamer capturing method resulted in a 1,500 fold enriched purification with 83% recovery, and almost 100% homogeneity. Later publications described the aptamer-based purification of various proteins such as thyroid transcription factor 1[85], tenascin-c[100], and pigpen[70]. Michaud *et al*., demonstrated the use of aptamer that specifically selects enantiomers as solid support during HPLC[101, 102]. They developed a chiral stationary phase (CSP) for the separation of enantiomers of peptides and small molecules which was then extended for use during HPLC[101, 102]. Unlike antibodies, aptamers do not require denaturing elution conditions which would result in loss of protein function. Thus, aptamers are demonstrated to be a viable tool for affinity-based separation applications.

Another prominent application of aptamers is as biosensors. In 1998, Potyrailo *et al*., reported the use of aptamers for biosensor applications[103]. In this study, fluorescently labeled anti-thrombin DNA aptamers were covalently immobilized on glass, and they were demonstrated to detect as little as 0.7 pmol of thrombin in a 140 pL volume by changes in the evanescent-wave-induced fluorescence anisotropy of the immobilized aptamer. The detection precision was higher than 4% RSD in a range of 0-200 nM, and the sensor could detect in less than 10 minutes. Similar to this, the Archemix Corporation reported a chip-based biosensor for multiplex analysis of proteins. They demonstrated specific detection of cancer-associated proteins like vascular endothelial factor, basic fibroblast growth factor, and more[104]. Lee *et al.,* used the thrombin detection system to develop a fiber optic microarray biosensor[105]. The anti-thrombin DNA aptamer was immobilized on silica beads and distributed in a micro-well on the distal tip of an imaging fiber. Thrombin-aptamer interactions were then visualized with a modified epi-fluorescence microscope system by imaging fiber interconnection. Recently, a magnetic microparticle conjugated DNA aptamer biosensor was developed for the detection of adenosine in 30% serum[106]. The system consists of aptamer, modified at 5' end with fluorescein, hybridized to the complimentary DNA with a quencher attached to its 3' end. Adenosine binding to the aptamer changes its configuration resulting in the displacement of quencher DNA and recovery of fluorescence.

Major problems with fluorescent detection of the target using aptamers are detection sensitivity, and the influence of fluorophore on the aptamer-target binding affinity. Jhaveri *et al.,* showed that the sensitivity of the target detection can be highly improved by having fluorescently labeled nucleosides adjacent to the binding site[107]. The

intensity of fluorescence of the aptamer on target binding was found to be very high when the fluorophore was attached close to target binding site. Another method to obtain an enhanced fluorescent signal was demonstrated by Yamana *et al.,*[108] by using bis-pyrene label which can be chemically synthesized by covalent linkage of two pyrene monomers. The label was intercalated (bound in between adjacent base pairs) as a non-nucleoside to the aptamer near the binding site. On target binding, the conformation switch of the aptamer formed an excimer by bringing the pyrenes to a proximity status, thereby resulting in a relatively better fluorescent intensity. However, with these modifications near the binding site, the aptamer-target affinity decreased. This drawback has been overcome by Merino *et al.* They detected AMP, tyrosinamide and arginiamide with aptamers modified with 2'-ribose-linked fluorophore close to the binding site by attaching to a certain nucleoside[109]. Following this, Katilius *et al.,* reported an increased fluorescence signal in detection of human r-thombin, immunoglobulin E, and platelet-derived growth factor B using respective aptamers in which the binding specific bases were displaced by fluorescent base analogues such as 2'-aminopurine[110]. Both the modification methods had only little effects on aptamer-target binding affinity.

Aptamer-based biosensors can be efficiently re-used. Kirby *et al.,* immobilized aptamer-based biosensor on beads, and then introduced them into micro-machine chips[111] **(Figure 2.3)**. The chips were used to detect protein 'ricin' in both capture and sandwich assays with high sensitivity. Even after repetitive denaturing of the sensor surface with urea, the sensor produced stable signals of anti-ricin aptamer beads with comparable intensity. Latter, a similar chip-based microsphere array for the detection of nucleic acid was developed by Ali *et al.,*[112]. A quartz crystal-based biosensor for detection of human

IgE was developed by Liss *et al.,*[113]. It was found to detect as low as 0.5 nmol/L of IgE equivalent to the antibody method. They were able to immobilize aptamers in a dense and well-oriented manner, and, thereby, they obtained 10 fold higher detection range. Later, the surface acoustic wave detector developed by Schlensog *et al.,* was proven to be 40-fold more sensitive than the quartz crystal sensor[114].

Another new fluorphore that can be used for the purpose with aptamers for biosensors is quantum dots (QDs). The semiconductor nanocrystal QDs were found to have highly stable and tunable photoluminescence comparable to many organic dyes. Since the emission wavelength is size dependent, the interference of fluorescence in biological matrix can be avoided using size controlled QDs at near infrared emission. Aptamer functionalized QDs have been successfully applied to detect thrombin and *Bacillus thuringiensis* spores[115, 116]. Using two QDs with different emission spectra, Liu *et al.,* developed an apamer-linked QD nanostructure which can detect adenosine and cocaine in one pot[117]. Gold nanoparticles were incorporated in this nanostructure as quencher **(Figure 2.4).** In the presence of target molecules, the nanostructure disassembled and resulted in increased emission from the quantum dots. This system allows a simultaneous colorimetric and fluorescence detection of multiple targets in one container. Recently, Zheng *et al.,* developed an aptamer-based and gold nanoparticle enhanced quartz crystal microbalance (QCM) biosensor for the detection of small molecules[118]. The QCM crystals were first modified using thiolated linker DNA which are partly complementary to the detection part containing adenosine aptamer. In the presence of adenosine, the aptamers binds to adenosine and folds into a complex structure precluding the reporter part carrying AuNps to combine with the coiled detection part **(Figure 2.5)**. Therefore, even low concentration

of adenosine caused a large frequency change. This aptamer-based sensor has a detection limit of 65nM and exhibits several excellent characteristics such as high sensitivity, selectivity, good stability, and reproducibility.

Photoaptamer which has at least one photoreactive nucleotide such as 5-azidouracil, 8-azidoadenine, 8-azidoguanine, 4-thiouracil, 5-bromouracil, 5-iodouracil, and 5-iodocytosine can bind covalently to target protein molecules on exposure to UV radiation. Using these photoaptamers, Petach *et al.,* developed an improved aptamer-based microarray technology[88]. Due to the strong covalent bond between the aptamer and the protein molecule, the microarray can be safely exposed to harsh washing conditions to remove background and non-specific binding of protein without disturbing the bound proteins. Thus, the obtained results revealed superior signal to noise ratio, hence very low concentration of proteins can be visualized by common protein staining methods.

2.4.3.3. Therapeutics

Aptamers have enormous potential as therapeutic agents. For an aptamer to be a therapeutic agent, it must bind to the target protein and specifically inhibit its function without any harmful side effects. Some of the traditional therapeutic agents like erythromycin and Tamiflu, used to treat skin disease and flu respectively, fits into the cleft on the surface of the target molecule and form an intricate network of stabilizing interactions in their course of therapeutic action[119]. Instead, aptamers bind to the crevice of the target protein and fold to form a cleft which acts as a receptor site for the protruding part of the target protein. Due to the multiple contacts between the protein and the aptamer,

they form tighter and more specific bonds than the therapeutic molecules. Most of the aptamers have a common mechanism of action. They bind the target protein with high affinity (dissociation constant in the nanomolar range) and block the interaction of that protein with another endogenous proteins, and thereby disrupt the protein:protein interaction as a competitive inhibitor[120].

The use of aptamers as therapeutic agents was first demonstrated in 1990 by Sullenger and colleagues. This ground breaking work demonstrated the inhibition of HIV viruses replication by RNA decoys (with the same sequence as TAR RNA of HIV) by sequestering all available Tat protein in the infected cells[121]. This finding was based on an obvious function of therapeutic aptamer of binding to the RNA/DNA binding proteins by mimicking the protein target sequence and act as decoys to inhibit binding of disease causing proteins. Subsequent study on TAR RNA decoy revealed that the structural element in TAR dictates the binding and inhibition of HIV-tat [122]**.** Following the principle of TAR aptamer, a RNA decoy aptamer that mimics the Rev Response Element (RRE) of HIV-1 was identified[123]**.** HIV replication was inhibited by >90% in the cells expressed with tRNA-RRE. In phase I clinical trials, the tRNA-RRE was transduced into the bone marrow of HIV-1 pediatric patient using a rectoviral vector[123, 124]. The results revealed low level of the transduced decoy gene in patient after 1 year, because of low level of gene transfer and no other adverse effect [124]. More TAR decoys capable of inhibiting HIV replications have been identified[94, 125, 126]. Browning *et al.,* identified a TAR decoy RNA that effectively recognizes HIV-1 and HIV-2-tat isoforms, thus enhancing its therapeutic ability[125].

Proliferation of cardiac and vascular cells are the major cause for cardiovascular diseases such as cardiac intimal hyperplasia, cardiac hypertrophy and atherosclerosis[127,

[128]. Transcription factor E2F is essential for regulating cellular proliferation[128]. A 14 nucleotide dsDNA decoy containing E2F binding sequence was constructed and tested in rats for its ability to inhibit E2F activity. The test results confirmed excellent inhibition of E2F along with 8 weeks post-transfection following a single administration of the aptamer[129]. Latter, the DNA decoy was tested on humans to limit hyperplasia in bypass vein graft by delivering the aptamer into infranguinal vein graft by ex vivo pressure-mediated transfection[130, 131]. Impressive results of fewer graft occlusions, revisions, or major stenosis were observed at 12 months with the DNA aptamer compared to untreated group[131]. Two more RNA aptamer capable of preventing E2F from binding to its cognate DNA response element have been identified using SELEX[132, 133]. The 2'-fluoro-modified RNA aptamer developed by Giangrande *et al.,* targets the E2F isoforms E2F1 and E2F3 without affecting the E2F isoform implicated in vascular smooth muscle cell (VSMC) differentiation and growth arrest (E2F4). Latter the authors demonstrated that the aptamer was effective at blocking VSMC proliferation only in the presence of E2F4 activity[133].

Nuclear factor κ-B (NF- κ–B) is a transcription factor that activates genes involved in inflammation and a molecule that involves ischemia-reperfusion injuries seen in most myocardial infarcation[134]. It is also essential in HIV-1 gene expression and apoptosis[134, 135]. A dsDNA aptamer for NF- κ-B found in nature was evaluated in several animal models as an inhibitor of NF- κ-B activity. In a rat model, the aptamer expressed tremendous results with improved recovery, lower percentage of neutrophil adhesion to endothelial cells, and a lower level of interleukin. The aptamer showed promises in phase I/II clinical trials for the treatment of eczema/ atopic dermatitis. Several other RNA aptamers for NF– κ-B were identified in vitro by SELEX[136, 137 138]. These aptamers are yet to be

extended to clinical trials. As NF-κ-B is a key regulatory factor in many human diseases, these aptamers have greater probability of becoming a powerful tool for treating many human pathologies.

In order to test the performance of aptamers as an anti-tumour agents, Nair *et al.,* isolated a RNA aptamer capable of binding cytotoxic T cell antigen-4 (CTLA-4) by SELEX. The antigen CTLA-4 inhibits the activation of T cell by cofactor CD28, and thereby impedes T cell in mounting an immune response against tumors. The isolated aptamer was found to bind to CTLA-4 with a K_D of 10 nM, and enhance T cell proliferation more effectively than antibody CTLA-4 inhibitor. The inhibition of CTLA-4 would promote T cell activity to generate an antitumor immune response[139]. A tetrameric derivative of the aptamer was constructed of a dsDNA scaffold to increase the efficiency of the aptamer activity. This tetrameric aptamer exhibited greater inhibitory capacity for CTLA-4 than the monomeric aptamer both in cell culture and in vivo[140].

Other aptamers that can be used as anti-cancer therapeutics are antisoma (AS1411) and tenascin-C aptamer (TTA1). AS1411 is a guanine rich oligonucleotide class of aptamer which forms G-quartets and exhibit anti-proliferative activity[141]. Aptamers capable of anti-proliferative activity were found to bind nucleolin, a protein that is often over expressed in cancer cells and has various functions. Inhibition of nucleolin activity by binding of AS1411 affects a variety of signaling pathways, including NF-κ-B[142] and Bcl-2[143]. The performance of AS1411 in clinical trials are discussed in detail in chapter 3.

Tenascin-C is expressed on many types of solid tumors, such as glioblastoma, breast, lung, and colorectal cancers. Aptamer for tenasin-C (TTA1) was identified using

cell-based SELEX, and is extensively modified to increase stability[71, 144]. The aptamer was observed to be rapidly taken up by cells in the preclinical studies[145].

Aptamers have been identified for several blood-clotting factors, such as von Willerbrand factor, thrombin, factor VII, and factor IXa[146-151]. The major goal of these aptamers is to prevent coagulation during acute cardiovascular procedure. Some of them, like NU172, ARC183, ARC1779 are being evaluated in different phases of clinical trials (discussed in chapter 3). Many aptamers have been identified so far for immune modulation[152-156], anti-angiogenesis[157, 158], anti-inflamation[159-161], cell surface signaling receptor[162-164]. Presently, many aptamers are in different levels of clinical development and are discussed in detail in chapter 3.

2.5. Toxicology of Therapeutic Nucleotides

Among all the classes of therapeutic oligonucleotides, the toxicological properties of ASOs have been extensively studied and published. Less information is available on the toxicology of the other classes of oligonucleotides such as siRNA, aptamers, and other partially or completely nucleic acid-based molecules. Compared to antisense oligonucleotides (ASOs), other NA therapeutics remain as an unpredicted class from toxicological point of view. When preparing a therapeutic NA, it is important to understand the toxicity of ASOs, but it is not appropriate to assume that they possess the same properties. Aptamers and siRNA differ from ASOs in sequence, structure, and modification. However, one can expect that some findings about the toxicology of ASOs may be applicable to aptamers and other NA therapeutics. There are three major

oligonucleotide class effects that have been widely described in the literature: polyanion effects, stimulation of innate immunity, and tissue accumulation of oligonucleotide material. These three effects are not the only toxicities produced by oligonucleotides but are the most important and dominating phenomena which have to be considered before preparing any oligonucleotide therapeutic.

High concentrations of oligonucleotide and nonspecific, off-target protein interactions can trigger the polyanionic effect. It includes activation of the alternative path of complement (C') induced by interaction of ASOs with factor H, a regulatory protein which prevents the alternative path of C'[165]. It also results in a pseudo hypersensitivity response and inhibition of the blood coagulation pathway, which leads to prolonged coagulation and clotting times[166]. The polyanionic effect is unique to monkeys and usually is not observed in rodent and human studies. In monkeys, activation of C' protein typically lead to cardiovascular syndrome characterized by hypotension and tachycardia, and in some severe cases to cardiovascular collapse and death[120]. The risk of activation of the alternative path for C' by ASOs can be reduced by slow or continuous IV infusion of ASOs, which substantially lowers the maximum plasma concentration[166].

Another acute, blood-level dependent effect of oligonucleotides is anticoagulation. It is attributed to low affinity interactions of oligonucleotides with a tenase complex of coagulation (factor IXA, factor VIIIa, phospholipid and calcium), which inhibit its functions and result in measurable prolongation of coagulation time. This effect has been observed with a number of phosphorothioate oligonucleotides and is independent of the oligonucleotide sequence[167]**.** It has been described mainly in non-human primates as a laboratory observation rather than a functionally relevant clinical effect[120, 166, 168].

Stimulation of the immune response by oligonucleotides has been extensively investigated. This effect is observed predominantly in rodents as a result of the interaction of CpG motif of ssDNA with Toll-Like Receptor 9 (TLR 9)[120]. RNA-based molecules were observed to stimulate other TLRs (TLR 3, 7 and 8) and produce similar immunostimulatory effects. These immune stimulations can cause undesired effects such as hyperplasmia in lymphoid organs and mononuclear cell infiltration in nonlymphoid organs[169].

The most frequently observed change in the histomorphology of the tissue resulting from repeated administration of the oligonucleotide was its accumulation in tissues. The accumulated oligonucleotides form basophilic granules, and they are found in the cytoplasm of renal proximal tubular epithelial cells, in reticuloendothelial cells in lymph nodes, and in the liver. It is hypothesized that oligonucleotides filtered by the glomerulus are reabsorbed from the tubular lumen into proximal epithelial cells resulting in oligonucleotide accumulation in those cells[166, 170]. The accumulation is dose-related and is generally not associated with adverse effects in the cells unless they are present in very high concentrations. A higher concentration of basophilic granules within the renal proximal tubular epithelium can cause its degeneration and measurable organ dysfunction[169].

There is very limited toxicological information available for aptamers. When aptamers were tested in International Conference on Harmonizaton (ICH) - recommended genotoxicity studies the results were always observed to be negative for evidence of genotoxic effects. During the general toxicity studies, the most consistent observation was the accumulation of aptamers in mononuclear phagocytes. The most commonly affected tissues are the liver, spleen, and lymph nodes, but almost any tissue with resident or

infiltrating macrophages can be affected. This observation is dependent on dosage and time. Vacuolation of tissue macrophages has been previously observed with other PEGylated aptamers and ASOs[171]. While unPEGylated aptamers were administered, basophilic granules were observed but not vacuolation. The vacuolation and the basophilic granules, when not accompanied with any other change in the cell, are generally not considered as an adverse effect and are reversible upon cessation of the administration of drug. Generally, a partial resolution is observed after 4 weeks of drug-free recovery period, and a complete resolution is observed after 13 weeks[120].

A slight decrease in red blood cell mass along with a slight decrease in red cell reticulocytes has sometimes been observed in rats after repeated administration of high doses of therapeutic aptamers. Plasma volume expansion and a commensurate decrease in plasma compartment were sometimes observed with daily infusion of high doses of 40 kDa PEGylated aptamer (i.e., greater than 140 mg/kg/day oligonucleotide weight). The polyanionic effect observed with ASOs was found to be infrequent and negligible with the aptamer, most likely due to the absence of phosphorothiate substitutions in the aptamer[120]**.** Overall, the general toxicity profile of the aptamers was found to be favorable for the administration of drug with minimal-toxicity.

2.6. References

1. Scherer LJ, Rossi JJ. Approaches for the Sequence-Specific Knockdown of mRNA. Nature Biotech. 2003;21: 1457-1465.

2. Cech TR. Ribozymes and Their Medical Implications. The Journal of the American Medical Association. 1988;260: 3030-3034.

3. Rossi JJ. Therapeutic Applications of Catalytic Antisense RNAs (Ribozymes). Ciba Foundation Symposium 209 - Oligonucleotides as Therapeutic Agents: John Wiley & Sons, Ltd., 2007:195-206.

4. Pley HW, Flaherty KM, McKay DB. Three-Dimensional Structure of A Hammerhead Ribozyme. Nature. 1994;372: 68-74.

5. James HA, Gibson I. The Therapeutic Potential of Ribozymes. Blood. 1998;91: 371-382.

6. Xing Z, Whitton JL. Ribozymes Which Cleave Arenavirus Rnas: Identification of Susceptible Target Sites and Inhibition By Target Site Secondary Structure. Journal of. Virology. 1992;66: 1361-1369.

7. Herschlag D. Implications of Ribozyme Kinetics For Targeting The Cleavage of Specific RNA Molecules In Vivo: More Isn't Always Better. Proceedings of the National Academy of Sciences. 1991;88: 6921-6925.

8. Sioud M. Effects of Variations In Length Of Hammerhead Ribozyme Antisense Arms Upon The Cleavage Of Longer RNA Substrates. Nucleic Acids Research. 1997;25: 333-338.

9. Tabler M, Homann M, Tzortzakaki S, Sczakiel G. A Three-Nucleotide Helix I is Sufficient For Full Activity of A Hammerhead Ribozyme: Advantages of an Asymmetric Design. Nucleic Acids Research. 1994;22: 3958-3965.

10. Atkinsu D, Gerlach WL. Artificial Ribozyme and Antisense Gene Expression in Saccharomyces Cerevisiae. Antisense Research and Development. 1994;4: 109-117.

11. Atkins D, Patrikakis M, Izant JG. The ade6 Gene of the Fission Yeast as a Target for Antisense and Ribozyme RNA-Mediated Suppression. Antisense Research and Development. 1995;5: 295-305.

12. Kobayashi H, Gail Eckhardt S, Lockridge J, et al. Safety and Pharmacokinetic Study of RPI.4610 (Angiozyme), an Anti-VEGFR-1 Ribozyme, in Combination with Carboplatin and Paclitaxel in Patients with Advanced Solid Tumors. Cancer Chemotherapy and Pharmacology. 2005;56: 329-336.

13. Mulhbacher J, St-Pierre P, Lafontaine DA. Therapeutic Applications Of Ribozymes and Riboswitches. Current Opinion in Pharmacology. 2010;10: 551-556.

14. Burnett John C, Rossi John J. RNA-Based Therapeutics: Current Progress and Future Prospects. Chemistry & Biology. 2012;19: 60-71.

15. Zamecnik PC, Stephenson ML. Inhibition of Rous sarcoma Virus Replication and Cell Transformation by a Specific Oligodeoxynucleotide. Proceedings of the National Academy of Sciences of the United States of America. 1978;75: 280-284.

16. Uhlmann E, Peyman A. Antisense Oligonucleotides: A New Therapeutic Principle. Chemical Reviews. 1990;90: 543-584.

17. Smith L, Andersen KB, Hovgaard L, Jaroszewski JW. Rational Selection of Antisense Oligonucleotide Sequences. European Journal of Pharmaceutical Sciences. 2000;11: 191-198.

18. Patzel V, Sczakiel G. Theoretical Design of Antisense RNA Structures Substantially Improves Annealing Kinetics And Efficacy In Human Cells. Nature Biotechnology. 1998;16: 64-68.

19. Matveeva O, Felden B, Tsodikov A, et al. Prediction of Antisense Oligonucleotide Efficacy by in Vitro Methods. Nature Biotechnology. 1998;16: 1374-1375.

20. Lehmann MJ, Patzel V, Sczakiel G. Theoretical Design of Antisense Genes with Statistically Increased Efficacy. Nucleic Acids Research. 2000;28: 2597-2604.

21. Kretschmer-Kazemi Far R, Nedbal W, Sczakiel G. Concepts to Automate the Theoretical Design Of Effective Antisense Oligonucleotides. Bioinformatics. 2001;17: 1058-1061.

22. Freier SM, Altmann K-H. The Ups and Downs of Nucleic Acid Duplex Stability: Structure-Stability Studies on Chemically-Modified DNA:RNA Duplexes. Nucleic Acids Research. 1997;25: 4429-4443.

23. Agrawal S, Kandimalla ER. Antisense Therapeutics: Is It As Simple As Complementary Base Recognition? Molecular Medicine Today. 2000;6: 72-81.

24. Agrawal S, Tan W, Cai Q, Xie X, Zhang R. In Vivo Pharmacokinetics of Phosphorothioate Oligonucleotides Containing Contiguous Guanosines. Antisense and Nucleic Acid Drug Development. 1997;7: 245-249.

25. Galbraith WM, Hobson WC, Giclas PC, Schechter PJ, Agrawal S. Complement Activation and Hemodynamic Changes Following Intravenous Administration of Phosphorothioate Oligonucleotides in the Monkey. Antisense Research and Development. 1994;4: 201-206.

26. Davis HL, Weeranta R, Waldschmidt TJ, Tygrett L, Schorr J, Krieg AM. CpG DNA Is a Potent Enhancer of Specific Immunity in Mice Immunized with Recombinant Hepatitis B Surface Antigen. The Journal of Immunology. 1998;160: 870-876.

27. Zhao Q, Temsamani J, Iadarola PL, Jiang Z, Agrawal S. Effect of Different Chemically Modified Oligodeoxynucleotides on Immune Stimulation. Biochemical Pharmacology. 1996;51: 173-182.

28. Chang S-S, Zhang Z, Liu Y. RNA Interference Pathways in Fungi: Mechanisms and Functions. Annual Review of Microbiology. 2012;66: 305-323.

29. Cogoni C, Macino G. Homology-Dependent Gene Silencing in Plants and Fungi: A Number of Variations on The Same Theme. Current Opinion in Microbiology. 1999;2: 657-662.

30. Catalanotto C, Azzalin G, Macino G, Cogoni C. Transcription: Gene Silencing in Worms and Fungi. Nature. 2000;404: 245-245.

31. Plasterk RHA, Ketting RF. The Silence of the Genes. Current Opinion in Genetics & Development. 2000;10: 562-567.

32. Fire A, Xu S, Montgomery MK, Kostas SA, Driver SE, Mello CC. Potent and Specific Genetic Interference by Double-Stranded RNA in Caenorhabditis Elegans. Nature. 1998;391: 806-811.

33. Elbashir SM, Harborth J, Lendeckel W, Yalcin A, Weber K, Tuschl T. Duplexes of 21-nucleotide RNAs mediate RNA interference in cultured mammalian cells. Nature. 2001;411: 494-498.

34. McCaffrey AP, Meuse L, Pham T-TT, Conklin DS, Hannon GJ, Kay MA. Gene expression: RNA interference in adult mice. Nature. 2002;418: 38-39.

35. Grimm D, Streetz KL, Jopling CL, et al. Fatality in Mice Due to Oversaturation of Cellular Microrna/Short Hairpin RNA Pathways. Nature. 2006;441: 537-541.

36. Rand TA, Ginalski K, Grishin NV, Wang X. Biochemical Identification of Argonaute 2 As The Sole Protein Required for RNA-Induced Silencing Complex Activity. Proceedings of the National Academy of Sciences of the United States of America. 2004;101: 14385-14389.

37. Matranga C, Tomari Y, Shin C, Bartel DP, Zamore PD. Passenger-Strand Cleavage Facilitates Assembly of siRNA into Ago2-Containing RNAi Enzyme Complexes. Cell. 2005;123: 607-620.

38. Ameres SL, Martinez J, Schroeder R. Molecular Basis for Target RNA Recognition and Cleavage by Human RISC. Cell. 2007;130: 101-112.

39. Rand TA, Petersen S, Du F, Wang X. Argonaute2 Cleaves the Anti-Guide Strand of siRNA during RISC Activation. Cell. 2005;123: 621-629.

40. Bartlett DW, Davis ME. Insights into the Kinetics of Sirna-Mediated Gene Silencing From Live-Cell and Live-Animal Bioluminescent Imaging. Nucleic Acids Research.34: 322-333.

41. Whitehead KA, Langer R, Anderson DG. Knocking Down Barriers: Advances in Sirna Delivery. Nature Reviews Drug Discovery. 2009;8: 129-138.

42. De Fougerolles A, Vornlocher H-P, Maraganore J, Lieberman J. Interfering with Disease: A Progress Report on Sirna-Based Therapeutics. Nature Reviews Drug Discovery. 2007;6: 443-453.

43. Reynolds A, Leake D, Boese Q, Scaringe S, Marshall WS, Khvorova A. Rational siRNA Design for RNA Interference. Nature Biotechnology. 2004;22: 326-330.

44. Boutros M, Ahringer J. The Art and Design of Genetic Screens: RNA Interference. Nature Review Genetics. 2008;9: 554-566.

45. Ptasznik A, Nakata Y, Kalota A, Emerson SG, Gewirtz AM. Short Interfering RNA (Sirna) Targeting the Lyn Kinase Induces Apoptosis in Primary, and Drug-Resistant, BCR-ABL1(+) Leukemia Cells. Nature Medicine. 2004;10: 1187-1189.

46. Kim SH, Jeong JH, Lee SH, Kim SW, Park TG. Local and Systemic Delivery of VEGF Sirna Using Polyelectrolyte Complex Micelles for Effective Treatment Of Cancer. Journal of Controlled Release. 2008;129: 107-116.

47. Xia C-F, Zhang Y, Zhang Y, Boado R, Pardridge W. Intravenous siRNA of Brain Cancer with Receptor Targeting and Avidin–Biotin Technology. Pharmaceutical Research. 2007;24: 2309-2316.

48. Clinical trail. gov USNIoH. http://clinicaltrials.gov/ct2/results?term=siRNA.

49. Gold L, Polisky B, Uhlenbeck O, Yarus M. Diversity of Oligonucleotide Functions. Annual Review of Biochemistry. 1995;64: 763-797.

50. Patel DJ. Structural Analysis of Nucleic Acid Aptamers. Current Opinion in Chemical Biology. 1997;1: 32-46.

51. Hermann T, Patel DJ. Adaptive Recognition by Nucleic Acid Aptamers. Science. 2000;287: 820-825.

52. Patel DJ, Suri AK. Structure, Recognition and Discrimination in RNA Aptamer Complexes with Cofactors, Amino Acids, Drugs and Aminoglycoside Antibiotics. Reviews in Molecular Biotechnology. 2000;74: 39-60.

53. Famulok M, Jenne A. Oligonucleotide Libraries - Variatio Delectat. Current Opinion in Chemical Biology. 1998;2: 320-327.

54. Famulok M, Mayer G. Aptamers as Tools in Molecular Biology and Immunology. Current Topics in Microbiology and Immunology. 1999;243: 123-136.

55. Hesselberth J, Robertson MP, Jhaveri S, Ellington AD. In Vitro Selection of Nucleic Acids for Diagnostic Applications. Reviews in Molecular Biotechnology. 2000;74: 15-25.

56. Joyce GF. In Vitro Evolution of Nucleic Acids. Current Opinion in Structural Biology. 1994;4: 331-336.

57. Wilson DS, Szostak JW. In Vitro Selection of Functional Nucleic Acids. Annual Review of Biochemistry. 1999;68: 611-647.

58. Tuerk C, Gold L. Systematic Evolution of Ligands by Exponential Enrichment: RNA Ligands to Bacteriophage T4 DNA Polymerase. Science. 1990;249: 505-510.

59. Andrake M, Guild N, Hsu T, Gold L, Tuerk C, Karam J. DNA Polymerase of Bacteriophage T4 is an Autogenous Translational Repressor. Proceedings of the National Academy of Sciences. 1988;85: 7942-7946.

60. Jellinek D, Lynott CK, Rifkin DB, Janjić N. High-affinity RNA Ligands to Basic Fibroblast Growth Factor Inhibit Receptor Binding. Proceedings of the National Academy of Sciences. 1993;90: 11227-11231.

61. Mallikaratchy P, Stahelin RV, Cao Z, Cho W, Tan W. Selection of DNA Ligands for Protein Kinase C-[Small Delta]. Chemical Communications. 2006: 3229-3231.

62. Drabovich AP, Berezovski M, Okhonin V, Krylov SN. Selection of Smart Aptamers by Methods of Kinetic Capillary Electrophoresis. Analytical Chemistry. 2006;78: 3171-3178.

63. Mosing RK, Mendonsa SD, Bowser MT. Capillary Electrophoresis-SELEX Selection of Aptamers with Affinity for HIV-1 Reverse Transcriptase. Analytical Chemistry. 2005;77: 6107-6112.

64. Berezovski M, Drabovich A, Krylova SM, et al. Nonequilibrium Capillary Electrophoresis of Equilibrium Mixtures: A Universal Tool for Development of Aptamers. Journal of the American Chemical Society. 2005;127: 3165-3171.

65. Eaton BE, Pieken WA. Ribonucleosides and RNA. Annual Review of Biochemistry. 1995;64: 837-863.

66. Eaton BE. The Joys of In Vitro Selection: Chemically Dressing Oligonucleotides to Satiate Protein Targets. Current Opinion in Chemical Biology. 1997;1: 10-16.

67. Brody EN, Gold L. Aptamers as Therapeutic and Diagnostic Agents. Reviews in Molecular Biotechnology. 2000;74: 5-13.

68. Cox JC, Ellington AD. Automated Selection of Anti-Protein Aptamers. Bioorganic & Medicinal Chemistry. 2001;9: 2525-2531.

69. Eulberg D, Buchner K, Maasch C, Klussmann S. Development of an Automated In Vitro Selection Protocol to Obtain RNA-Based Aptamers: Identification of A Biostable Substance P Antagonist. Nucleic Acids Research. 2005;33: e45.

70. Blank M, Weinschenk T, Priemer M, Schluesener H. Systematic Evolution of a DNA Aptamer Binding to Rat Brain Tumor Microvessels. Journal of Biological Chemistry. 2001;276: 16464-16468.

71. Daniels DA, Chen H, Hicke BJ, Swiderek KM, Gold L. A Tenascin-C Aptamer Identified by Tumor Cell SELEX: Systematic Evolution of Ligands by Exponential enrichment. Proceedings of the National Academy of Sciences. 2003;100: 15416-15421.

72. Cerchia L, Ducongé F, Pestourie C, et al. Neutralizing Aptamers from Whole-Cell SELEX Inhibit the RET Receptor Tyrosine Kinase. PLoS Biology. 2005;3: 697-704.

73. Shamah SM, Healy JM, Cload ST. Complex Target SELEX. Accounts of Chemical Research. 2008;41: 130-138.

74. Cerchia L, Giangrande P, McNamara J, Franciscis V. Cell-Specific Aptamers for Targeted Therapies. Nucleic Acid and Peptide Aptamers, 2009:59-78.

75. Ray P, White RR. Aptamers for Targeted Drug Delivery. Pharmaceuticals. 2010;3: 1761-1778.

76. Zhou J, Rossi J. Cell-Specific Aptamer-Mediated Targeted Drug Delivery. Oligonucleotides. 2011;21: 1-10.

77. Burgstaller P, Famulok M. Isolation of RNA Aptamers for Biological Cofactors by In Vitro Selection. Angewandte Chemie International Edition. 1994;33: 1084-1087.

78. Kiga D, Futamura Y, Sakamoto K, Yokoyama S. An RNA Aptamer to the Xanthine/Guanine Base with A Distinctive Mode of Purine Recognition. Nucleic Acids Research. 1998;26: 1755-1760.

79. Lin C, Katilius E, Liu Y, Zhang J, Yan H. Self-Assembled Signaling Aptamer DNA Arrays for Protein Detection. Angewandte Chemie. 2006;118: 5422-5427.

80. Li Z, Huang P, He R, et al. Aptamer-Conjugated Dendrimer-Modified Quantum Dots for Cancer Cell Targeting and Imaging. Materials Letters. 2010;64: 375-378.

81. Wang Y, Rando RR. Specific Binding of Aminoglycoside Antibiotics to RNA. Chemistry & Biology. 1995;2: 281-290.

82. Jayasena SD. Aptamers: An Emerging Class of Molecules that Rival Antibodies in Diagnostics. Clinical Chemistry. 1999;45: 1628(1623).

83. Drolet DW, Moon-McDermott L, Roming TS. An Enzyme-Linked Oligonucleotide Assay. Nature. 1996;14: 1021-1025.

84. Romig TS, Bell C, Drolet DW. Aptamer Affinity Chromatography: Combinatorial Chemistry Applied to Protein Purification. Journal of Chromatography B: Biomedical Sciences and Applications. 1999;731: 275-284.

85. Murphy MB, Fuller ST, Richardson PM, Doyle SA. An Improved Method for the In Vitro Evolution of Aptamers and Applications In Protein Detection and Purification. Nucleic Acids Research. 2003;31: e110.

86. Davis KA, Abrams B, Lin Y, Jayasena SD. Staining of Cell Surface Human CD4 with 2′-F-Pyrimidine-Containing RNA Aptamers for Flow Cytometry. Nucleic Acids Research. 1998;26: 3915-3924.

87. Charlton J, Sennello J, Smith D. In Vivo Imaging of Inflammation Using an Aptamer Inhibitor of Human Neutrophil Elastase. Chemistry & Biology. 1997;4: 809-816.

88. Petach H, Gold L. Dimensionality is the Issue: Use of Photoaptamers in Protein Microarrays. Current Opinion in Biotechnology. 2002;13: 309-314.

89. Bock C, Coleman M, Collins B, et al. Photoaptamer Arrays Applied to Multiplexed Proteomic Analysis. Proteomics. 2004;4: 609-618.

90. Fredriksson S, Gullberg M, Jarvius J, et al. Protein Detection Using Proximity-Dependent DNA Ligation Assays. Nature Biotechnology. 2002;20: 473-477.

91. Famulok M. Bringing Picomolar Protein Detection into Proximity. Nature Biotechnology. 2002;20: 448-449.

92. Söderberg O, Leuchowius K-J, Kamali-Moghaddam M, et al. Proximity Ligation: A Specific and Versatile Tool for the Proteomic Era. Genetic Engineering. 2007:85-93.

93. Schallmeiner E, Oksanen E, Ericsson O, et al. Sensitive Protein Detection Via Triple-Binder Proximity Ligation Assays. Nature Methods. 2007;4: 135(133).

94. Yamamoto R, Katahira M, Nishikawa S, Baba T, Taira K, Kumar PKR. A Novel RNA Motif that Binds Efficiently and Specifically to the Tat Protein of HIV and Inhibits the Trans-Activation by Tat of Transcriptionin Vitro And in Vivo. Genes to Cells. 2000;5: 371.

95. Yamamoto R, Kumar PKR. Molecular Beacon Aptamer Fluoresces in the Presence of Tat Protein of HIV-1. Genes to Cells. 2000;5: 389.

96. Hamaguchi N, Ellington A, Stanton M. Aptamer Beacons for the Direct Detection of Proteins. Analytical Biochemistry. 2001;294: 126-131.

97. Vicens MC, Sen A, Vanderlaan A, Drake TJ, Tan W. Investigation of Molecular Beacon Aptamer-Based Bioassay for Platelet-Derived Growth Factor Detection. ChemBioChem. 2005;6: 900-907.

98. Heyduk E, Heyduk T. Nucleic Acid-Based Fluorescence Sensors for Detecting Proteins. Analytical Chemistry. 2005;77: 1147-1156.

99. Zhu C, Liu J, Ling Y, et al. Evaluation of the clinical value of ELISA based on MPT64 antibody aptamer for serological diagnosis of pulmonary tuberculosis. BMC Infectious Diseases. 2012;12: 96.

100. Dion AD, Chen H, Hicke BJ, Swiderek KM, Gold L. A Tenascin-C Aptamer Identified by Tumor Cell SELEX: Systematic Evolution of Ligands by Exponential Enrichment. Proceedings of the National Academy of Sciences. 2003;100: 15416-15421.

101. Michaud M, Jourdan E, Ravelet C, et al. Immobilized DNA Aptamers as Target-Specific Chiral Stationary Phases for Resolution of Nucleoside and Amino Acid Derivative Enantiomers. Analytical Chemistry. 2004;76: 1015-1020.

102. Michaud M, Jourdan E, Villet A, Ravel A, Grosset C, Peyrin E. A DNA Aptamer as a New Target-Specific Chiral Selector for HPLC. Journal of the American Chemical Society. 2003;125: 8672-8679.

103. Potyrailo RA, Conrad RC, Ellington AD, Hieftje GM. Adapting Selected Nucleic Acid Ligands (Aptamers) to Biosensors. Analytical Chemistry. 1998;70: 3419-3425.

104. McCauley TG, Hamaguchi N, Stanton M. Aptamer-based Biosensor Arrays for Detection and Quantification of Biological Macromolecules. Analytical Biochemistry. 2003;319: 244-250.

105. Lee M, Walt DR. A Fiber-Optic Microarray Biosensor Using Aptamers as Receptors. Analytical Biochemistry. 2000;282: 142-146.

106. Huang P-JJ, Liu J. Flow Cytometry-Assisted Detection of Adenosine in Serum with an Immobilized Aptamer Sensor. Analytical Chemistry. 2010;82: 4020-4026.

107. Jhaveri SD, Kirby R, Conrad R, et al. Designed Signaling Aptamers that Transduce Molecular Recognition to Changes in Fluorescence Intensity. Journal of the American Chemical Society. 2000;122: 2469-2473.

108. Yamana K, Ohtani Y, Nakano H, Saito I. Bis-Pyrene Labeled DNA Aptamer as an Intelligent Fluorescent Biosensor. Bioorganic & Medicinal Chemistry Letters. 2003;13: 3429-3431.

109. Merino EJ, Weeks KM. Facile Conversion of Aptamers into Sensors Using a 2‘-Ribose-Linked Fluorophore. Journal of the American Chemical Society. 2005;127: 12766-12767.

110. Katilius E, Katiliene Z, Woodbury NW. Signaling Aptamers Created Using Fluorescent Nucleotide Analogues. Analytical Chemistry. 2006;78: 6484-6489.

111. Kirby R, Cho EJ, Gehrke B, et al. Aptamer-Based Sensor Arrays for the Detection and Quantitation of Proteins. Analytical Chemistry. 2004;76: 4066-4075.

112. Ali MF, Kirby R, Goodey AP, et al. DNA Hybridization and Discrimination of Single-Nucleotide Mismatches Using Chip-Based Microbead Arrays. Analytical Chemistry. 2003;75: 4732-4739.

113. Liss M, Petersen B, Wolf H, Prohaska E. An Aptamer-Based Quartz Crystal Protein Biosensor. Analytical Chemistry. 2002;74: 4488-4495.

114. Schlensog MD, Gronewold TMA, Tewes M, Famulok M, Quandt E. A Love-Wave Biosensor Using Nucleic Acids as Ligands. Sensors and Actuators B: Chemical. 2004;101: 308-315.

115. Choi JH, Chen KH, Strano MS. Aptamer-Capped Nanocrystal Quantum Dots: A New Method for Label-Free Protein Detection. Journal of the American Chemical Society. 2006;128: 15584-15585.

116. Ikanovic M, Rudzinski W, Bruno J, et al. Fluorescence Assay Based on Aptamer-Quantum Dot Binding to Bacillus Thuringiensis Spores. Journal of Fluorescence. 2007;17: 193-199.

117. Liu J, Lee JH, Lu Y. Quantum Dot Encoding of Aptamer-Linked Nanostructures for One-Pot Simultaneous Detection of Multiple Analytes. Analytical Chemistry. 2007;79: 4120-4125.

118. Zheng B, Cheng S, Liu W, Lam MH-W, Liang H. Small Organic Molecules Detection Based on Aptamer-Modified Gold Nanoparticles-Enhanced Quartz Crystal Microbalance with Dissipation Biosensor. Analytical Biochemistry. 2013;438: 144-149.

119. Tu D, Blaha G, Moore PB, Steitz TA. Structures of MLSBK Antibiotics Bound to Mutated Large Ribosomal Subunits Provide a Structural Explanation for Resistance. Cell. 2005;121: 257-270.

120. Bouchard PR, Hutabarat RM, Thompson KM. Discovery and Development of Therapeutic Aptamers. Annual Review of Pharmacology and Toxicology. 2010;50: 237-257.

121. Sullenger BA, Gallardo HF, Ungers GE, Gilboa E. Overexpression of TAR Sequences Renders Cells Resistant to Human Immunodeficiency Virus Replication. Cell. 1990;63: 601-608.

122. Sullenger BA, Gallardo HF, Ungers GE, Gilboa E. Analysis of Trans-Acting Response Decoy RNA-Mediated Inhibition Of Human Immunodeficiency Virus Type 1 Transactivation. Journal of Virology. 1991;65: 6811-6816.

123. Lee TC SB, Gallardo HF, Ungers GE, Gilboa E. Overexpression of RRE-Derived Sequences Inhibits HIV-1 Replication in CEM Cells. The New Biologists. 1992;4: 66-74.

124. Kohn DB, Bauer G, Rice CR, et al. A Clinical Trial of Retroviral-Mediated Transfer of arev-Responsive Element Decoy Gene Into CD34+Cells From the Bone Marrow of Human Immunodeficiency Virus-1–Infected Children. Blood. 1999;94: 368-371.

125. Browning CM, Cagnon L, Good PD, Rossi J, Engelke DR, Markovitz DM. Potent Inhibition of Human Immunodeficiency Virus Type 1 (HIV-1) Gene Expression and Virus Production by an HIV-2 Tat Activation-Response RNA Decoy. Journal of Virology. 1999;73: 5191-5195.

126. Michienzi A, Li S, Zaia JA, Rossi JJ. A Nucleolar TAR Decoy Inhibitor Of HIV-1 Replication. Proceedings of the National Academy of Sciences. 2002;99: 14047-14052.

127. Hunter T. Braking the Cycle. Cell. 1993;75: 839-841.

128. Nevins JR. E2F: A Link Between the Rb Tumor Suppressor Protein and Viral Oncoproteins. Science. 1992;258: 424-429.

129. Morishita R, Gibbons GH, Horiuchi M, et al. A Gene Therapy Strategy Using A Transcription Factor Decoy of the E2F Binding Site Inhibits Smooth Muscle Proliferation In Vivo. Proceedings of the National Academy of Sciences. 1995;92: 5855-5859.

130. Mann MJ, Gibbons GH, Hutchinson H, et al. Pressure-Mediated Oligonucleotide Transfection of Rat and Human Cardiovascular Tissues. Proceedings of the National Academy of Sciences. 1999;96: 6411-6416.

131. Mann MJ, Whittemore AD, Donaldson MC, et al. Ex-Vivo Gene Therapy Of Human Vascular Bypass Grafts With E2F Decoy: The Prevent Single-Centre, Randomised, Controlled Trial. The Lancet. 1999;354: 1493-1498.

132. Ishizaki J, Nevins JR, Sullenger BA. Inhibition of Cell Proliferation by an RNA Ligand that Selectively Blocks E2F Function. Nature Medicine. 1996;2: 1386-1389.

133. Giangrande PH, Zhang J, Tanner A, et al. Distinct Roles of E2F Proteins in Vascular Smooth Muscle Cell Proliferation and Intimal Hyperplasia. Proceedings of the National Academy of Sciences. 2007;104: 12988-12993.

134. Verma IM, Stevenson JK, Schwarz EM, Van Antwerp D, Miyamoto S. Rel/NF-Kappa B/I Kappa B Family: Intimate Tales of Association And Dissociation. Genes and Developments. 1995;9: 2723-2735.

135. Beg AA, Baltimore D. An Essential Role for NF-κB in Preventing TNF-α-Induced Cell Death. Science. 1996;274: 782-784.

136. Lebruska LL, Maher LJ. Selection and Characterization of an RNA Decoy for Transcription Factor NF-κB. Biochemistry. 1999;38: 3168-3174.

137. Cassiday LA, Maher LJ. Yeast Genetic Selections to Optimize RNA Decoys for Transcription Factor NF-κB. Proceedings of the National Academy of Sciences. 2003;100: 3930-3935.

138. Wurster SE, Maher LJ. Selection and Characterization of anti-NF-κB p65 RNA Aptamers. RNA. 2008;14: 1037-1047.

139. Nair SK, Heiser A, Boczkowski D, et al. Induction of Cytotoxic T Cell Responses and Tumor Immunity Against Unrelated Tumors Using Telomerase Reverse Transcriptase RNA Transfected Dendritic Cells. Nature Medicine. 2000;6: 1011-1017.

140. Santulli-Marotto S, Nair SK, Rusconi C, Sullenger B, Gilboa E. Multivalent RNA Aptamers That Inhibit CTLA-4 and Enhance Tumor Immunity. Cancer Research. 2003;63: 7483-7489.

141. Bates PJ, Kahlon JB, Thomas SD, Trent JO, Miller DM. Antiproliferative Activity of G-rich Oligonucleotides Correlates with Protein Binding. Journal of Biological Chemistry. 1999;274: 26369-26377.

142. Girvan AC, Teng Y, Casson LK, et al. AGRO100 Inhibits Activation Of Nuclear Factor-κB (NF-κB) by Forming A Complex with NF-κB Essential Modulator (NEMO) and Nucleolin. Molecular Cancer Therapeutics. 2006;5: 1790-1799.

143. Soundararajan S, Chen W, Spicer EK, Courtenay-Luck N, Fernandes DJ. The Nucleolin Targeting Aptamer AS1411 Destabilizes Bcl-2 Messenger RNA in Human Breast Cancer Cells. Cancer Research. 2008;68: 2358-2365.

144. Hicke BJ, Marion C, Chang Y-F, et al. Tenascin-C Aptamers Are Generated Using Tumor Cells and Purified Protein. Journal of Biological Chemistry. 2001;276: 48644-48654.

145. Hicke BJ, Stephens AW, Gould T, et al. Tumor Targeting by an Aptamer. Journal of. Nuclear. Medicine. 2006;47: 668-678.

146. Bock LC, Griffin LC, Latham JA, Vermaas EH, Toole JJ. Selection of Single-Stranded DNA Molecules that Bind and Inhibit Human Thrombin. Nature. 1992;355: 564-566.

147. Rusconi. C. P YA, Lyerly. H. K , Lawson. J. H , Sullenger.B .A. Blocking the Initiation of Coagulation By RNA Aptamers To Factor VIIa. Thrombosis and Haemostasis. 2000;84: 841-848.

148. White. R RC, Scaedino.E, Wolberg. A, Lawson.J, Hoffman.M, Sullenger.B. Generation of Species Cross-Reactive Aptamers Using "Toggle" SELEX. Molecular Therapy. 2001;4: 567-573.

149. Rusconi CP, Scardino E, Layzer J, et al. RNA Aptamers as Reversible Antagonists of Coagulation Factor IXa. Nature. 2002;419: 90-94.

150. Müller J, Wulffen B, Pötzsch B, Mayer G. Multidomain Targeting Generates a High-Affinity Thrombin-Inhibiting Bivalent Aptamer. ChemBioChem. 2007;8: 2223-2226.

151. Oney S, Nimjee SM, Layzer J, et al. Antidote-Controlled Platelet Inhibition Targeting von Willebrand Factor with Aptamers. Oligonucleotides. 2007;17: 265-274.

152. Lee SW, Sullenger BA. Isolation of a Nuclease-Resistant Decoy RNA That Selectively Blocks Autoantibody Binding to Insulin Receptors on Human Lymphocytes. The Journal of Experimental Medicine. 1996;184: 315-324.

153. Seo, Seon H, Lee SW. In Vitro Selection of the 2'-Fluoro-2'-Deoxyribonucleotide Decoy RNA Inhibitor of Myasthenic Autoantibodies. Journal of Microbiology and Biotechnology. 2000;10: 707-713.

154. Lee S-W, Sullenger BA. Isolation of a Nuclease-Resistant Decoy RNA that Can Protect Human Acetylcholine Receptors from Myasthenic Antibodies. Nature Biotechnology. 1997;15: 41-45.

155. Wiegand T, Williams P, Dreskin S, Jouvin M, Kinet J, Tasset D. High-Affinity Oligonucleotide Ligands to Human Ige Inhibit Binding to Fc Epsilon Receptor I. Journal of Immunology. 1996;157: 221-230.

156. Kubik M, Bell C, Fitzwater T, Watson S, Tasset D. Isolation and Characterization of 2'-fluoro-, 2'-amino-, and 2'-fluoro- /amino-Modified RNA Ligands to Human IFN-gamma that Inhibit Receptor Binding. Journal of Immunology. 1997;159: 259-267.

157. Ruckman J, Green LS, Beeson J, et al. 2′-Fluoropyrimidine RNA-based Aptamers to the 165-Amino Acid Form of Vascular Endothelial Growth Factor (VEGF165). Journal of Biological Chemistry. 1998;273: 20556-20567.

158. White RR, Shan S, Rusconi CP, et al. Inhibition of Rat Corneal Angiogenesis by A Nuclease-Resistant RNA Aptamer Specific for Angiopoietin-2. Proceedings of the National Academy of Sciences. 2003;100: 5028-5033.

159. Smith D, Kirschenheuter GP, Charlton J, Guidot DM, Repine JE. In Vitro Selection of RNA-Based Irreversible Inhibitors of Human Neutrophil Elastase. Chemistry & Biology. 1995;2: 741-750.

160. Charlton J, Kirschenheuter GP, Smith D. Highly Potent Irreversible Inhibitors of Neutrophil Elastase Generated by Selection from a Randomized DNA−Valine Phosphonate Library. Biochemistry. 1997;36: 3018-3026.

161. Green LS, Jellinek D, Jenison R, Östman A, Heldin C-H, Janjic N. Inhibitory DNA Ligands to Platelet-Derived Growth Factor B-Chain. Biochemistry. 1996;35: 14413-14424.

162. Chen C-hB, Chernis GA, Hoang VQ, Landgraf R. Inhibition of Heregulin Signaling by an Aptamer that Preferentially Binds to the Oligomeric Form of Human Epidermal Growth Factor Receptor-3. Proceedings of the National Academy of Sciences. 2003;100: 9226-9231.

163. Ohuchi SP, Ohtsu T, Nakamura Y. Selection of RNA Aptamers Against Recombinant Transforming Growth Factor-[Beta] Type III Receptor Displayed on Cell Surface. Biochimie. 2006;88: 897-904.

164. Sennino B, Falcón BL, McCauley D, et al. Sequential Loss of Tumor Vessel Pericytes and Endothelial Cells after Inhibition of Platelet-Derived Growth Factor B by Selective Aptamer AX102. Cancer Research. 2007;67: 7358-7367.

165. Henry SP, Giclas PC, Leeds J, et al. Activation of the Alternative Pathway of Complement by a Phosphorothioate Oligonucleotide: Potential Mechanism of Action. Journal of Pharmacology. 1997;281: 810-816.

166. Farman CA, Kornbrust DJ. Oligodeoxynucleotide Studies in Primates: Antisense and Immune Stimulatory Indications. Toxicologic Pathology. 2003;31: 119-122.

167. Sheehan JP, Lan H-C. Phosphorothioate Oligonucleotides Inhibit the Intrinsic Tenase Complex. Blood. 1998;92: 1617-1625.

168. Ireson CR, Kelland LR. Discovery and Development of Anticancer Aptamers. Molecular Cancer Therapeutics. 2006;5: 2957-2962.

169. Henry SP, Kim TW, Stickland KK, Zanardi TA, Fey RA, Levin AA. Toxicological Properties Of 2'-O-Methyoxyethyl Chimeric Antisense Inhibitors In Animal And Man. Antisense Drug Technology. 2008: 327-364

170. Monteith DK, Horner MJ, Gillett NA, et al. Evaluation of the Renal Effects of an Antisense Phosphorothioate Oligodeoxynucleotide in Monkeys. Toxicologic Pathology. 1999;27: 307-317.

171. Bendele A, Seely J, Richey C, Sennello G, Shopp G. Short Communication: Renal Tubular Vacuolation in Animals Treated with Polyethylene-Glycol-Conjugated Proteins. Toxicological Sciences. 1998;42: 152-157.

2.7. Web References

W1. The Ellington Lab, 2004, Aptamer Database. Available from URL: http://aptamer.icmb.utexas.edu/index.php [accessed Januvary 2, 2014].

Ribozyme Therapeutic	Sponsor	Medical Condition	Current Status
Angiozyme	Merck-Sirna	Renal Cancer	Awaiting Phase III
Heptazyme	Merck-Sirna	HCV	Phase II terminated
MY-2	UCSD	HIV	Awaiting Phase II
RRz1	Johnson & Johnson	HIV	Awaiting Phase II
OZ1	Janssen-Cilag Pty Ltd, UCLA	HIV	Phase II
CCR5 ribozyme	City of Hope, Benitec	HIV	Phase 0
L-TR/Tat-neo	City of Hope	HIV	Awaiting Phase III

Table 2.1. Ribozymes in Clinical Trials

Antisense Oligo Therapeutic	Sponsor	Medical Condition	Current Status
AVI-4658	Imperial College London	Duchenne Muscular Dystrop	Awaiting Phase III
LErafAON-ETU	Insys Therapeutics Inc	Neoplasms	Awaiting Phase II
EZN-2968	National Institute of Cancer	Neoplasms with Liver Metastases	Awaiting Phase II
Liposomal Grb-2	Bio-Path Holdings, Inc.	Acute Myeloid Leukemia	Phase I Ongoing
OGX-427	Vancouver Coastal Health	Bladder Cancer	Phase I Recruiting
SB010	Sterna Biologicals GmbH & Co. KG	Asthma	Phase II Ongoing
VEGF-Antisense Oligonucleotide	USC/Norris Comprehensive Cancer Center	Mesothelioma	Phase II Withdrawn

Table 2.2. Antisense Oligonucleotides in Clinical Trial

siRNA Therapeutic	Sponsor	Medical Condition	Current Status
Bevasiranib	Opko Health	Age related Macular Degeneration	Phase III terminated
AGN-745	Allergan/ Sirna	Age related Macular Degeneration	Phase II terminated
PF-655	Quark/ Pfizer	Age related Macular Degeneration	Awaiting Phase III
QPI- 1007	Quark Pharma.	Non-arteritic Anterior Ischemic Optic Neuropath	Phase II ongoing
TD101	Transderm/ IPCC	Pachyonychia Congenita	Awaiting Phase II
SYL040012	Sylentis	Ocular Hyper Tension	Awaiting Phase III
SYL1001	Sylentis	Dry Eye Syndrome	Phase II ongoing
ALN-RSV01	Alnylam/ Cubist	Respiratory Syncytial Viru Infections	Awaiting Phase III
siG12D LODER	Silenseed	Pancreatic Cancer	Phase II ongoing
Atu027	Silence Therapeutics	Advanced Solid Tumors	Phase II ongoing
I5NP	Quark Pharma	Delayed Graft Function an Acute Kidney Injury	Phase II ongoing
CALAA-01	Calando Pharma	Solid Tumors	Phase I terminated
FANG Vaccine	Grandalis Inc	Solid Tumors	Phase II ongoing

Table 2.3. siRNA Therapeutics in Clinical Trials

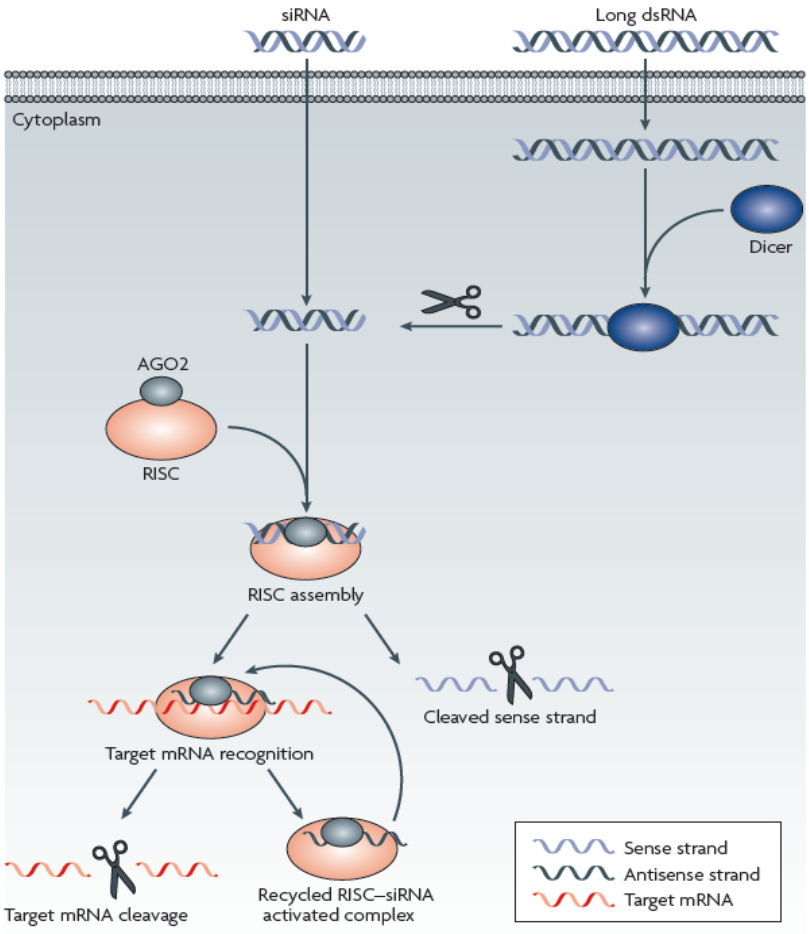

Figure 2.1. The Mechanism of RNA Interference. Long double-stranded RNA (dsRNA) is introduced into the cytoplasm, where it is cleaved into small interfering RNA (siRNA) by the enzyme Dicer. Alternatively, siRNA can be introduced directly into the cell. The siRNA is then incorporated into the RNA-induced silencing complex (RISC), resulting in the cleavage of the sense strand of RNA by argonaute 2 (AGO2). The activated RISC–siRNA complex seeks out, binds to and degrades complementary mRNA, which leads to the silencing of the target gene. The activated RISC–siRNA complex can then be recycled for the destruction of identical mRNA targets. (Used with permission from reference 41)

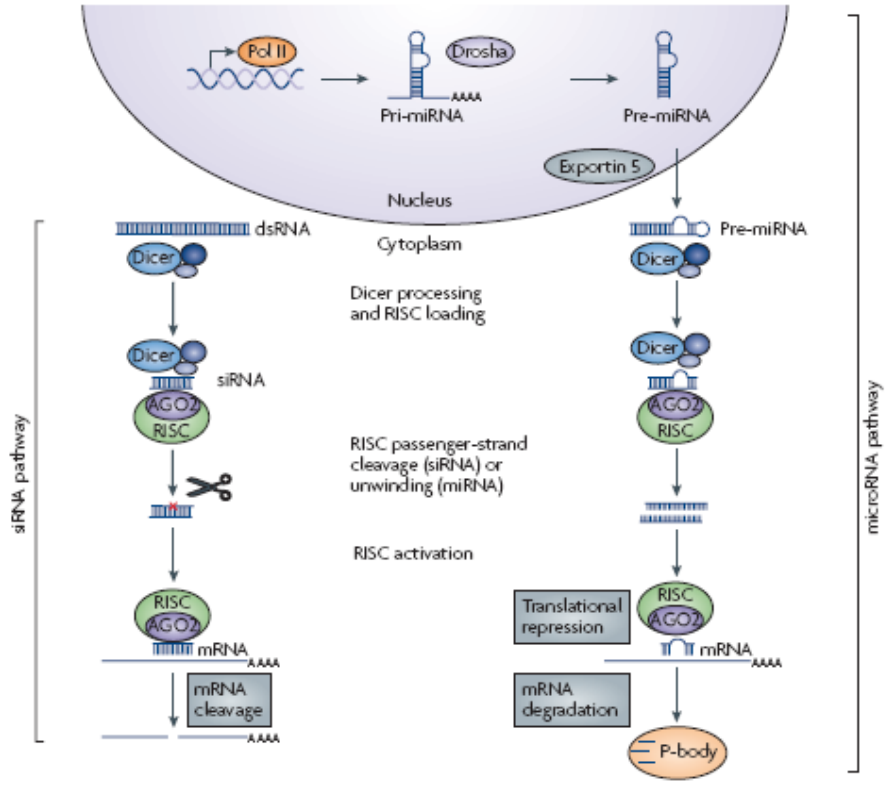

Figure 2.2. Mechanism of RNA Interference in Mammalian Cells. The microRNA pathway begins with endogenously encoded primary microRNA transcripts (pri-miRNAs) that are transcribed by RNA polymerase II (Pol II) and are processed by the Drosha enzyme complex to yield precursor miRNAs (pre-miRNAs). These precursors are then exported to the cytoplasm by exportin 5 and subsequently bind to the Dicer enzyme complex. When the RNA duplex loaded onto RISC has imperfect sequence complementarity, the passenger (sense) strand is unwound leaving a mature miRNA bound to active RISC. The mature miRNA recognizes target sites in the mRNA, leading to direct translational inhibition. (Used with permission from reference 42).

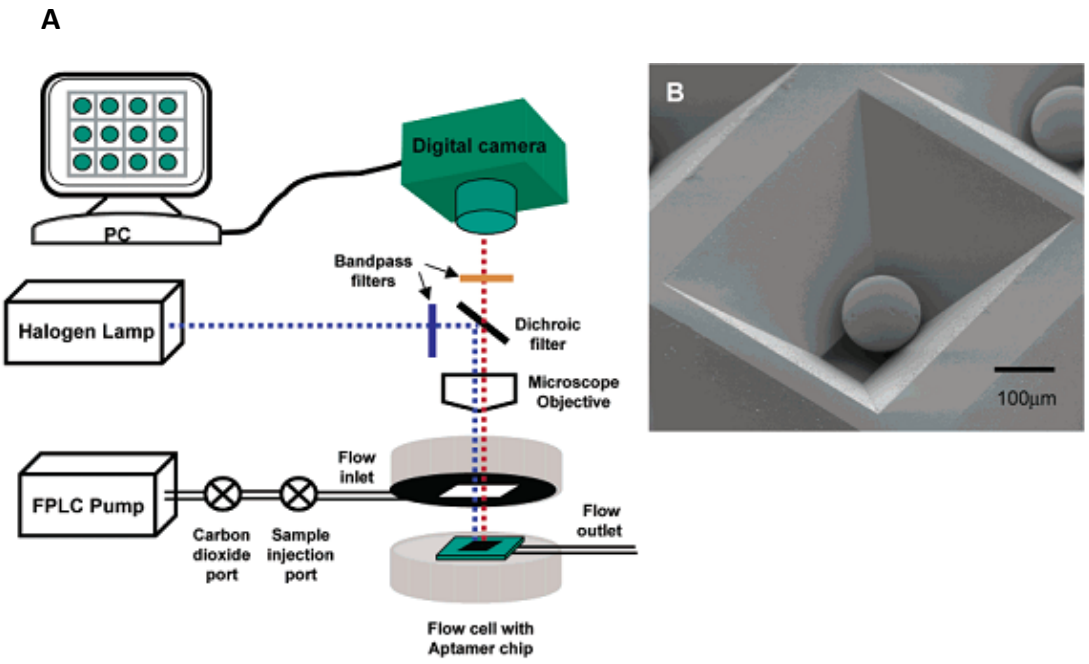

Figure 2.3. Aptamer Chip Detection System. (A) The electronic tongue setup contains a fluid delivery system, fluorescence microscope, digital camera, flow cell in which the aptamer chip will be loaded, and computer for data analysis. (B) Close-up look at a bead in a rectangular-shaped micromachined well of the aptamer chip. (Used with permission from reference 111).

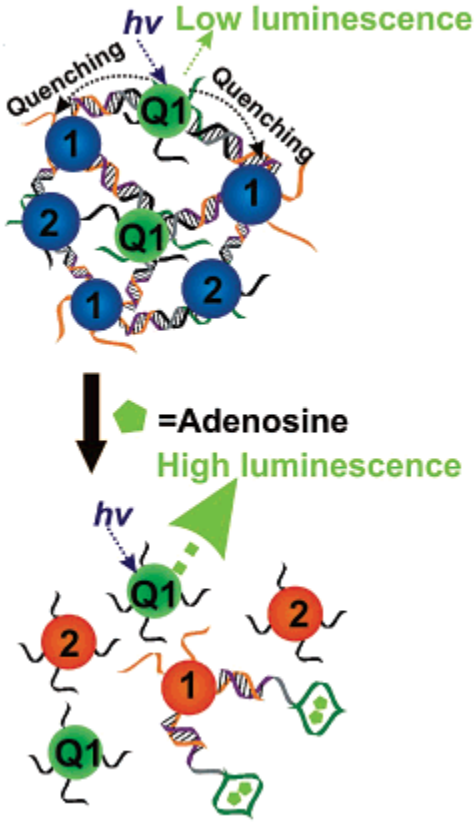

Figure 2.4. Assembly of Quantum Dots, Gold Nanoparticles and Nucleic Acids. (A) Gold nanoparticles 1, 2, and quantum dot Q1 were assembled by an adenosine aptamer DNA, resulting in quenched QD emission. Addition of adenosine disassembled the aggregates with increased QD emission observed. (Used with permission from reference 117)

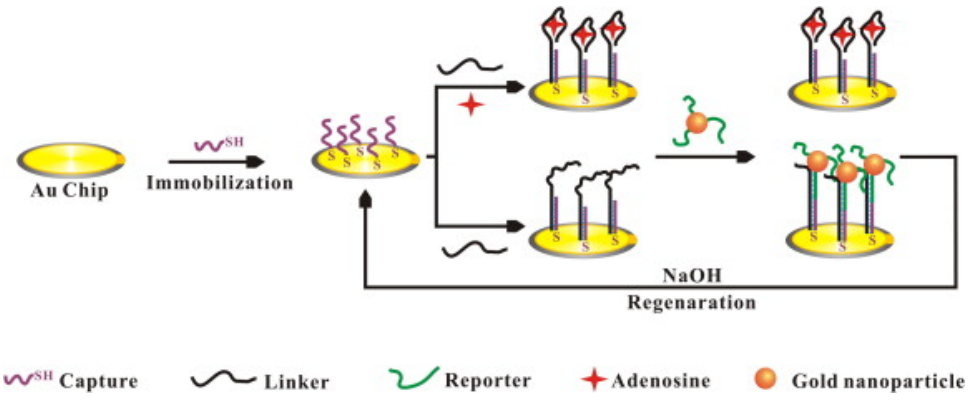

Figure 2.5. Schematic Representation of QCM Biosensor. Adenosine detection.by aptamer using AuNPs as amplification element (Used with permission from reference 118)

Chapter 3. Aptamer Therapeutics in Clinical Trials and Their Challenges

As described in the previous chapter, aptamers are tools that have strong potential for wide spread application in various fields. One of the very exciting and promising application of aptamers are their use as therapeutics. For an aptamer to be a therapeutic agent it must bind to the target protein and specifically inhibit its function without any harmful side effects. Aptamers bind to the crevice of the target protein and fold to form a cleft which acts as a receptor site for the protruding part of the target protein. Due to its multiple contacts with the protein, aptamers form very tight and specific bonds with the protein. Most of the aptamers have a common mechanism of action. They bind the target protein with high affinity (e.g. dissociation constants can be in the nanomolar range) and block the interaction of that protein with other endogenous proteins, and thereby disrupting the protein:protein interaction as competitive inhibitor.

In this chapter, the therapeutic aptamers that are currently in different stages of clinical trials are presented with a summary of their performance in the trials. Furthermore, the various challenges of aptamer therapeutics are discussed.

3.1 Introduction

Ribonucleic acids (RNA) are emerging as important drug targets and versatile therapeutic agents because they can adopt complex three-dimensional structures capable

of expressing many enzymatic activities and regulate the flow of genetic information from DNA to proteins. Advances in nucleic acid synthesis and the development of in vitro selection methods to discover protein-binding oligonucleotides led to the development of a new class of nucleic acids called aptamers. RNA aptamers fold into complex structures[1-4] with pockets and clefts for specific binding of target molecules[5-7]. These smart molecules can be selected from a large pool of random sequence oligonucleotides based on their ability to bind a target molecule such as metals, small organic compounds, proteins, viruses, and living cells. The selection of aptamers, also known as SELEX (*S*ystematic *E*volution of *L*igands by *EX*ponential Enrichment), was developed in 1990 in three laboratories[8-10].

RNA aptamers can be produced in vitro with a high degree of accuracy and reproducibility. Frequently, aptamers are chemically modified to increase their resistance to degradation by nucleases and improve their storage stability[11]. The most widely used chemical modifications are nucleotides with fluoro or O-methyl groups at the 2' position of their sugar moiety[12]. Most of the therapeutic aptamers are incorporated with more than one of these chemically modified nucleotides for increased stability.

The use of aptamers as therapeutic agents was first demonstrated in 1990 by Sullenger and colleagues[13]. Unlike antisense oligonucleotides, siRNAs, and miRNAs, aptamers can modulate the functions of their target proteins. Many of them act as competitive inhibitors that bind to the target proteins and block their interactions with other macromolecules. As expected, these aptamers display a relatively simple and predictable concentration-effect, both in vitro and in vivo[11]. Only a very few aptamers function as agonists. This category includes the aptamers isolated for the extracellular domain of

human epidermal growth factor receptor 3 and the aptamer isolated against isoleucyl tRNA synthetase[14, 15].

Although the doors for using aptamers as therapeutics were opened in 1990, it took 15 years for the first therapeutic aptamer to be used in clinical therapy. As of now, Macugen is the only FDA approved therapeutic aptamer available in the market. Presently, aptamers for treating macular degeneration, choroidal neovascularization, intravascular thrombus, acute coronary syndrome, von Willebrand factor related disorder, von Hippel-Lindau syndrome, angiomas, acute myeloid leukemia, renal cell carcinoma, non-small cell lung cancer, and thrombotic thrombocytopenic purpura are in different stages of clinical development[16] **(Table 3.1)**. Thus, the future is indeed bright as more therapeutic aptamers make their way to the clinic.

3.2. Aptamer Therapeutics for Macular Degeneration and Macular Edema

3.2.1. Pegaptanib (Macugen®)

Pegaptanib (Eyetech Inc and Pfizer) is a 27 ribonucleotide RNA aptamer **(Figure 3.1A)**. It is used to treat age-related macular degeneration (AMD), a medical condition which causes vision loss in older adults due to retinal damage. The stability of this aptamer is increased by transcriptionally modifying it with 2'-fluoro pyrimidines and 2'-O-methyl purines, and equipping it with a 3'-3'-linked deoxythymidine terminal cap[17]. To prolong its bioavailability, a 40 kDa polyethylene glycol (PEG) moiety is added to the 5' end of the aptamer[17] **(Figure 3.2A)**. Pegaptanib targets vascular endothelial growth factor (VEGF), a

signal protein that stimulates vasculogenesis and angiogenesis and prevents choroidal neovascularization[18, 19] **(Figure 3.2B)**. For AMD treatment, a 0.3 mg/eye pegaptanib dose is administered once every 6 weeks by intraviteral injections.

Although Pegaptanib sold well after FDA approval, it soon lost its marketability to the antibodies Lucentis and Avastin. Pegaptanib was selected to specifically target $VEGF_{165}$ isoform and does not bind to $VEGF_{121,}$ while the antibodies Lucentis and Avastin targets both $VEGF_{165}$ and $VEGF_{121}$. However, it was later discovered that some VEGF activity is necessary for the maintenance of normal blood vessel and retinal neurons[20, 21] , and selective inhibition of $VEGF_{165}$ may still be a useful option for long term treatment of AMD[16].

Recently, a phase IV clinical trial (NCT00354445) has been completed[22], which assessed the efficacy of Pegaptanib as maintenance therapy after induction therapy in patients with neovascular age-related macular degeneration (NV-AMD). The study was performed on 568 patients with subfoveal NV-AMD who had undergone one to three induction treatments approximately 30 to 120 days before the study. Patients were given Pegaptanib doses of 0.3 mg/eye every 6 weeks for 48 weeks as maintenance therapy; with follow-up to week 54. About 86% of the patients completed one year of Pegaptanib treatment. In the final assessment, the mean visual acuity (VA) improvement during induction therapy was observed to be well preserved, and the post-induction center point thickness of the retina was found to be stable. The study showed that Pegaptanib may have particular relevance to patients with systemic co-morbidities who require long term anti-VEGF therapy for NV-AMD.

Pegaptanib was also found effective in treating diabetic macular edema (DME), a leading cause of blindness in the United States. DME is a medical condition in which the retina swells due to leaking of fluid from blood vessels within the macula, the center portion of retina. A phase II trial (NCT00040313) conducted on 172 patients with best-corrected visual acuity (VA) ranging from 20/50 to 20/320 was completed in 2005[23]. Patients were treated with either intravitreous Pegaptanib (0.3 mg, 1 mg, 3 mg) or a sham injection on day 1, week 6, and week 12. If required, additional injections and/or focal photocoagulation were given for another 18 weeks. Final assessments on week 36 showed that the median VA was improved to 20/50 with 0.3 mg Pegaptanib and to 20/63 with sham injections ($p = 0.04$). The mean central retinal thickness was decreased by 68 μm with 0.3 mg Pegaptanib, versus an increase of 4 μm with sham ($p = 0.02$). All Pegaptanib doses were well tolerated, and visual improvements occurred in 73% of the patients compared to 51% in the sham group. Overall, the phase II trial showed the potential efficiency of 0.3 mg Pegaptanib in treating DME and the need for further studies.

Following the phase II trial, a multicenter, randomized, sham control comparative phase II/III trial of DME (NCT00605280) was completed in 2010 with 260 and 207 patients in one and two years, respectively, at 56 global sites [24,w1]. The patients received 0.3 mg Pegaptanib injections or sham injections every 6 weeks for a total of 9 injections in year one. In year two, patients received injections as often as 6 weeks based on pre-specified criteria. Up to three focal or grid laser treatments per year were permitted beginning at week 18. In the primary efficiency endpoint of the study, 37% of patients treated with Pegaptanib were found to gain two lines (10 ETDRS letters) in 54 weeks compared to 20% of patients who received the sham procedure. In year one, the VA of

patients treated with Pegaptanib was increased to an average of 5.2 letters compared with 1.2 letters with sham treatment ($p < 0.05$). At the end of year two, patients receiving Pegaptanib had gained an average of 6.1 letters, compared with 1.3 letters for patients who received the sham procedure ($p < 0.01$). These findings indicate that intravitreal Pegaptanib is effective in the treatment of DME and supports a positive safety profile in patients. A Phase III trial (NCT01100307) was completed recently[w2] and the results of the study is yet to be published.

A number of pre-clinical studies showed that Pegaptanib can also be used to efficiently treat proliferative diabetic retinopathy (PDR). In late 2008, a phase I trial that compared the efficacy of intravitreal Pegaptanib (IVP) with panretinal laser photocoagulation (PRP) in the treatment of active PDR was completed[25]. In this study, 20 patients with active PDR were evenly and randomly assigned to receive treatment in one eye either with IVP (0.3 mg) every 6 weeks for 30 weeks, or with a PRP laser. The final assessment of this study measured regression of retinal neovascularisation (NV), changes from baseline in best-corrected visual acuity (BCVA), and foveal thickness. In 90% of eyes treated with IVP, the retinal NV showed regression by week 3. Complete regression was observed in 100% of the IVP eyes by week 12 and was maintained through week 36. In the PRP laser-treated group, two eyes demonstrated complete regression, two showed partial regression, and four showed persistent active PDR at the end of week 36. The mean change in BCVA was +5.8 letters in Pegaptanib-treated eyes compared to +26.0 letters in PRP-treated eyes. Only mild to moderate transient ocular adverse events were reported with Pegaptanib. The data on the phase II and III trials are not available, and Pegaptanib is

currently under phase IV trials evaluating the safety of extended doses of Pegaptanib in the treatment of PDR.

Presently, Pegaptanib is being evaluated in the clinic for treating ischaemic diabetic macular edema (MIDME), phase IV ((NCT01175070)[W3], uveitis (pilot study (NCT00790803)[W4]), choroidal neovascularisation secondary to pathologic myopia (pilot study (NCT01218230)[W5]), and iris neovascularization (phase I (NCT00295828)[W6]). Research is also being conducted to collect information on adverse drug effects on the long term use of Pegaptanib for subfoveal choroidal neovascularization (phase IV (NCT00845273)[W7]).

3.2.2. E10030 (Fovista^{TM})

A major limitation of anti-VEGF agents used to treat wet AMD is the lack of regression of the new vessels which are responsible for vision loss. In order to overcome this limitation, Ophthotech Corp developed the E10030 (Fovista^{TM}) aptamer which binds to platelet-derived growth factor (PDGF) that regulates the recruitment and maturation of pericytes, a type of cell found in central nervous system[W8] **(Figure 3.3)**. E10030 is a PEGylated, 29 nucleotide-long aptamer with seven 2'-fluoro pyrimidines and five 2'-*O*-methyl purines. In pre-clinical models, E10030 successfully induced neovascular regression when administered in combination with anti-VEGF agents[26]. A phase I (NCT00569140), single ascending dose trial was conducted to evaluate intravitreal combination therapy of E10030 and anti-VEGF agent ranibizumab (Lucentis, Genentech). The study included 22 patients at multiple sites with subfoveal choroidal

neovascularization (CNV). The patients were given 0.03, 0.3, 1.5, 3 mg of E10030 in combination with 0.5 mg of ranibizumab, once a month for 3 months. At week 12, all the patients demonstrated significant neovascular regression, and 59% of the patients had an increase in visual acuity. The mean center-point retinal thickness, which was 395 µm at baseline, decreased to 251µm at week 4, 231µm at week 8, and 229µm at week 12[W9]. In addition, 91% of the patients in the combination study demonstrated partial regression of CNV lesions compared to 16% of the patients with anti-VEGF monotherapy[27,W10]. Furthermore, no adverse drug effects were observed in anti-PDGF and anti-VEGF combination study. This study proved that the AMD treatment with anti-VEGF agent is more effective when combined with E10030. Recently, Ophthotech released the results of the phase II trial of E10030 (NCT01089517) in combination with ranibizumab. In this study, 449 patients with wet AMD were randomly assigned to receive 0.3 mg E10030 in combination with 0.5 mg ranibizumab, or 1.5 mg E10030 in combination with 0.5 mg ranibizumab, or sham in combination with 0.5 mg ranibizumab, once every 4 weeks for 24 weeks. Patients receiving 1.5 mg E10030 in combination with 0.5 mg ranibizumab were observed to have 62 % better vision gain than the patients treated with only ranibizumab. The enhanced visual outcome of the combination treatment over the monotherapy was observed to be demonstrated at every monthly time point[W11]**.** Recently in September 2013, Opthotech corp initiated a phase III trial (NCT01944839) to evaluate the safety and efficiency of Fovista in combination with lucentis. The study is currently recrutting patients and is expected to be completed by July 2016[W12].

3.2.3. ARC1905

ARC1905 (Ophthotech Corp) is a 39 nucleotide **(Figure 3.1B)**, PEGylated aptamer capped at the 3'-terminus with an inverted nucleotide[28]. It selectively binds to complement component 5 (C5), which is pro-inflammatory and is found in crystalline deposits under the retina in dry AMD. Inhibition of C5 prevents the formation of the key terminal fragments responsible for tissue pathology (C5a), and the membrane attack complex (MAC). Thus, ARC1905 can be a therapeutic to both dry and wet AMD while sparing the immunoprotective functions of the complement system. The phase I clinical trial of ARC1905 (NCT00709527) for wet AMD in combination with multiple doses of ranibizumab by intravitreal injection was completed in March 2011. In this study, a subgroup of 43 patients, who did not receive any anti-VEGF treatment previously, received 6 injections of ARC1905 in combination with anti-VEGF treatment. At every data point, there was an increase in the mean visual acuity from the baseline. After 24 weeks, there was a 13.6 letter improvement in the mean visual acuity in the patients receiving 0.3 mg of ARC1905, and 11.7 letter and 15.3 letter increment in patients treated with 1 mg and 2 mg of ARC1905. Based on these results, Opthotech initiated a phase I clinical trial (NCT00950638) to examine the safety and tolerability of ARC1905 in subjects with dry AMD which was completed in November 2013 (data not available yet).

3.3. Therapeutic Aptamers for Hemostasis

3.3.1. RB006

RB006 is a 34 nucleotide aptamer that binds to factor IXa[29] **(Figure 3.1C)**. It is a part of the anti-coagulant system REG1 (Regado Biosciences, Inc.) which includes RB006 and its complementary oligonucleotide (antidote, RB007). RB006 is a PEGylated aptamer with an inverted nucleotide at the 3' terminus to reduce 3'-exonuclease-mediated degradation. It selectively blocks the factor VIIa/IXa catalyzed conversion of factor X to factor Xa, an important step in prothrombin assembly and thrombin generation **(Figure 3.4)**. RB007 is a 17-mer oligonucleotide fully 2'-*O*- methyl substituted, complimentary to the portion of RB006 that binds effectively to factor IXa **(Figure 3.1C)**.

The REG1 system underwent three phase I clinical trials. The phase Ia trial was to determine the safety profile and characterize the pharmacodynamic responses in healthy human volunteers (NCT00113997). It was a subject-blinded, dose-escalation, placebo-controlled study of 85 healthy volunteers, who received drug or placebo followed by antidote or placebo after 3 hours. The subjects were randomly enrolled in the three arms of the study (Arm 1: Placebo+Antidote, Arm 2: Drug+Antidote, Arm3: Drug+Placebo)**.** The doses of RB006 were fixed to 15, 30, 60 and 90 mg to provide a high margin of safety to the study subjects. The doses of RB007 were twice that of RB006 (30, 60,120, and 180 mg) which were 4-fold the minimal amount of RB007 required to neutralize RB006. No significant bleeding was observed in the subjects. An episode of transient bleeding occurred in one subject receiving 30 mg of RB006. The symptoms were resolved rapidly

and no further effects were observed. Overall, both the drug and the antidote were well tolerated[30].

The phase Ib trial was completed to evaluate the safety, tolerability, and pharmacodynamic profile of REG1 in a randomized, double-blinded, placebo-controlled study on 50 patients with coronary artery disease[31]. Among the enrolled 50 patients, half the patients had an episode of myocardial infarction at least once, 80% received prior precutaneous coronary intervention, and 34% received prior coronary artery bypass. Patients were randomly divided into three groups (drug plus antidote, drug plus placebo, placebo plus placebo), and each group was subdivided into four subgroups and given four different dose levels of RB006 (15, 30, 50, and 75 mg) and RB007 (30, 60, 100, and 150 mg). Minor bleeding, in the form of intravenous-site hematomas, was observed in five cases, and transient cutaneous reactions were observed in two patients at 8 and 15 minutes after injection of 30 mg RB006 and 100 mg RB007, respectively. Stool occult blood tests were positive for the patients receiving 75 mg RB006 followed by 150 mg RB007 at 48 hours, although the test was negative for at 24 hrs and 7 days. Also, mild dizziness was reported in one of the patients five minutes after receiving a 75 mg dose of RB006. Except for the four patients who received high intermediate or high doses of RB006, the hematologic measurement and serum chemistries, including electrolytes, creatinine, and blood urea nitrogen, remained stable through seven days. A dose dependent increase of the activated partial thromboplastin time (aPTT) was observed with RB006. The median aPTTs at 10 minutes after the single intravenous bolus of 15, 30, 50, and 75 mg RB006 were 29.2, 34.6, 46.9, and 52.2 seconds, respectively, and RB007 was found to reverse the aPTT to baseline approximately within one minute with no rebound increase through 7

days[31]. Overall, no serious adverse events or major bleeding was observed in any patient throughout the 7 day trial both the drug and the antidote were found to be well tolerated.

The phase Ic clinical trial evaluated the multiple repeated dose safety, intra-individual pharmacodynamics, reproducibility, and the grade active reversibility of REG1[32]. The study involved 39 healthy volunteers, randomly divided into three groups to receive three consecutive, weight-adjusted, drug-antidote treatment cycles or double placebo. The treatment cycles included an intravenous bolus of 0.75 mg/kg RB006, followed by descending dose of RB007 from 1.5 mg/kg to 0.094 mg/kg 60 minutes later. Post-randomized clinical assessment and coagulation measurements were performed for the next 14 days, and highly reproducible aPTT results were observed with the repeated dose of RB006 (with low intrasubject variability). Highly reproducible dose-dependent aPTT levels were also observed with repeated doses of RB007. Neither major bleeding nor other serious side effects were observed.

After collecting the preliminary phase I results on safety, pharmacodynamics, and reproducibility at multiple doses, REG1 underwent a phase IIa clinical trial to determine whether it was feasible and safe to use the REG1 anticoagulation system instead of the current standard of care (i.e. unfractionated heparin treatment) during percutaneous coronary intervention (PCI) in subjects with coronary artery disease (CAD)[33] (NCT00715455). The study involved a roll-in group (two patients) and 24 patients divided into two groups (partial reversal group and complete reversal group). Each group was randomized 5:1 to receive REG1 and unfractionated heparin (UFH), respectively. The roll-in group was included in the study to optimize the timing and performance of the study related procedure, and this group was not included in final data analysis. All the patients in

group 1 and group 2 were pretreated with aspirin and clopidogrel. In group 1, RB006 was partially reversed by RB007 (0.2:1 RB007:RB006) immediately after PCI and completely reversed (1.8:1 RB007:RB006) after 4 hours. In group 2, RB006 was completed reversed by RB007 (2:1 RB007:RB006) after PCI followed by sheath removal. The patients assigned to receive UFH were given an intravenous bolus of 60 to 70 U/kg and the sheaths were removed 4 hours after PCI. All cases were successful, with final thrombolysis in myocardial infarction grade 3 flow and no angiographic thrombotic complications. Partial reversal of RB006 provided controlled step-down in anticoagulation after PCI with a definite sheath removal whereas complete reversal of RB006 allowed sheath removal immediately after PCI, both without complication. This revealed that REG1 can be safely used instead of UFH during the PCI procedure.

Later, a phase IIb study (RADAR, NCT00932100) was carried out to evaluate the safety and efficacy of the REG1 anticoagulation system in acute coronary syndrome (ACS) patients undergoing cardiac catheterization[34]. The use of RB006 was investigated in 800 patients with ACS undergoing early cardiac catherization. To validate the dose selection and stability of anticoagulants, 33 patients underwent studies to assess RB006 pharmacokinetic and pharmacodynamic. RB006 was administered intravenously at a dose of 1 mg/kg and rapidly achieved high plasma concentrations, prolonged aPTT by three fold, and maintained near complete inhibition of factor IX activity in patients. The effects of the drug remained stable from the time of drug administration through completion of catherization. Until now, the results with REG1 have been very positive, and this aptamer therapeutic is currently waiting for phase III trials.

Recently, the results of the RB006 phase Ia study, to assess the safety, tolerability, pharmacokinetic and pharmacodynamic responses of RB006 when administrated subcutaneously, have been published[35]. This study enrolled 36 healthy volunteers in 5 cohorts. Cohort 1, 1A, 2, 3 and 4 consisted of 6, 4, 6, 6, 8 patients respectively. Patients in cohorts1 and 1A received 0.5mgkg^{-1}; cohort2 received 1.0mgkg^{-1}; cohort3 received 3.0mgkg^{-1}; and cohort4 received 2.0mgkg^{-1}. Two subjects in cohorts 1 and 3 were randomized to receive placebo, and subjects in cohort4 were equally randomized to receive single-dose or multi-dose of anivamersen. The maximum relative activated partial thromboplastin time and time needed to achieve this in patients in cohorts 1, 1A, 2 and 3 were 1.18 at 2days, 1.16 at 2days, 1.27 at 3days, and 1.85 at 2days, respectively. The calculated mean half-life and mean residence times of pegnivacogin were 6.12days and 9.6days, respectively. Overall, the aptamer was well tolerated and provided dose-proportional anticoagulation for several days after a single subcutaneous dose, with complete, although transient, reversal by its control agent.

3.3.2. ARC1779

ARC1779 (Archemix Corp) is a 39 nucleotide, PEGylated DNA/RNA aptamer **(Figure 3.1D)** that binds to the A1 domain of activated von Willebrand factor (vWF) and inhibits the binding of the domain to platelet receptor glycoprotein Ib[36] **(Figure 3.5)**. It reduces platelet adhesion and aggregation, and thereby reduces thrombus formation in arterial beds. It is a potential therapeutic for acute coronary syndromes, von Willebrand disease, and vWF-related platelet disorders. It has potential therapeutic benefits in PCI due

to its ability to readily reverse the action by binding to a complementary sequence of oligonucleotides.

After many successful laboratory studies, ARC 1779 was evaluated on healthy humans to study its safety, pharmacokinetics, and pharmacodynamics in 2006[37]. This small-scale phase I study (NCT00432770) was a randomized, double-blind, placebo-controlled study involving 47 healthy volunteers. The subjects were randomized into two sections (5:1) to receive either intravenous bolus of ARC1779 (part A) or placebo (NaCl injection of 0.9%; part B). The subjects in part A (n = 41) were enrolled in cohorts with 6 subjects in each cohort, who received 0.05, 0.1, 0.3, 0.6, or 1.0 mg/kg doses of ARC1779. The drug was diluted to a maximal concentration of 3.7 mg/mL and administrated as slow intravenous bolus over 15 minutes. The pharmacokinetics profile of ARC1779 showed a low degree of inter-individual variability, a simple dose proportionality of exposure, a distribution into the plasma component of the central compartment, an apparent half-life of elimination on the order of 2 to 3 hours, and a predominantly non-renal route of clearance. Overall, the drug was well-tolerated with no deaths, and no serious adverse effects or premature withdrawal due to adverse effects.

Following the phase I study, Archemix initiated a phase II study of ARC1779 in patients with acute myocardial infarction (MI) undergoing PCI (NCT00507338). However, the study was terminated for unknown reasons. Similarly, phase II studies of ARC1779 in patients with thrombotic microangiopathy (NCT00726544) and in patients undergoing carotid endarterectomy (NCT00742612) were terminated due to slow enrollment. However, a phase II study of ARC1779 in patients with von Willebrand factor-related platelet function disorders (NCT00632242) was completed in 2008. This pilot clinical

study evaluated the effectiveness of ARC1779 in comparison to and in conjunction with the drug desmopressin[38]. The patients were given desmopressin alone, desmopressin with ARC1779, and ARC1779 alone. Infusion of desmopressin induces the release of large amounts of VWF and hyperactive multimers from endothelial cells, causing transient thrombocytopenia in patients with VWF type 2B because of the formation of platelet agglutinates. ARC1779, when administered alone, increased the VWF antigen concentration and the amount of platelets over 8-12 hours, and normalized the VWF ristocetin cofactor activity (VWF: RCo). The infusion of ARC1779, together with desmopressin, enhanced the desmopressin-induced maximal increase in all parameters, and the increase persisted for at least 12 hours. When ARC1779 was injected before desmopressin, the depletion of platelets caused by desmopressin was prevented. This study concluded that ARC1779 is indeed effective in increasing the amount of platelet formation, and it can potentially be used as an anti-bleeding drug for VWD patients.

3.3.3. NU172

NU172 is a 26-nucleotide, unmodified and uncapped oligonucleotide developed by Nuvelo and ARCA Biopharma. It prevents fibrinogen cleavage of α-thrombin through its contact and reaction with exosite I, the secondary binding site on the protein, and thereby inhibits blood protein thrombin. A pre-clinical trial conducted in 2006 and 2007 found that NU172 was a good candidate for rapid anticoagulation with sufficiently quick return to hemostatic blood-clotting conditions upon removal, providing a sigmoidal concentration-response curve in the graph of initial clot formation versus time[39]. A phase Ia “proof-of-

concept" trial, completed in April 2008, showed that NU172 was able to exhibit coagulation and anticoagulation in a very efficient manner after one bolus-style dose, while exerting no harmful effects on the patient[W13]. The trial was conducted on healthy volunteers, in which the rate of anticoagulation, measured by activated clotting time (ACT), was found to be directly related to the size of the bolus dose administered. For example, the 2 mg/kg dose of the aptamer was able to achieve its estimated ACT of 400 seconds. Upon removal, the ACT quickly returned to its baseline values[W13,W14].

In August 2008, the results of phase Ib trails revealed that NU172 was successful in quickly and safely reversing the process of anticoagulation with one bolus-style dose. This trial was administered on 24 normal, male volunteers who were initially given a 2 mg/kg bolus-style dose of NU172 followed by increasing infusion doses for four hours. The trial was divided into four cohorts, all of which showed direct correlations between dose-dependency and increases in anticoagulation times, which was verified through measurements of the ACT, prothrombin time (PT), and aPPT. The maximum infusion dose rate given was 6.0 mg/kg/hr, which gave average ACTs of 373 to 414 seconds (an upsurge of three times the baseline), average PTs of 56 to 92 seconds (an increase of five times the baseline), and average aPPTs of 130 to 178 seconds (an increase of five times the baseline), all of which were maintained during the length of the entire infusion. Upon termination of infusion, coagulation parameters quickly returned to normal, which was expected due to the brief plasma half-life of NU172 found in the phase Ia trial. NU172 is currently waiting on phase II clinical trials (NCT00808964) with the hope that it will eventually be certified as a short-term anticoagulant for invasive medical procedures, specifically coronary artery bypass graft surgery and percutaneous interventions[W14].

3.3.4. ARC19499

ARC19499 is an aptamer therapeutic developed to treat hemophilia, a rare genetic blood clotting disorder. Deficiency of coagulation factor VII and factor IX causes hemophilia A and B, respectively, which results in deficient blood coagulation via the intrinsic pathway. ARC19499 binds to tissue factor pathway inhibitor (TFPI), which negatively regulates the extrinsic coagulation pathway, thereby enabling clot initiation via the extrinsic pathway[40, 41]. The phase I/II trial of ARC19499 (NCT01191372) was initiated by Archemix in August 2010 and terminated in April 2013 for unknown reason[W15].

3.4. Therapeutic Aptamers for Cancer

3.4.1. AS1411

AS1411 (Antisoma, PLC), previously known as AGRO100, is an aptamer that binds to the external domain of the membrane protein nucleolin, a protein over-expressed on the surface of cancer cells that normally plays a role in survival, growth and proliferation, nuclear transport, and transcription of the cell[42] **(Figure 3.6)**. Inhibition of nucleolin activity by binding of AS1411 affects a variety of signaling pathways, including NF-κ-B[43] and Bcl-2[44]. AS1411 was the first nucleic acid-based aptamer approved for phase I clinical testing for the treatment of different types of cancer in humans and is also the first-in-class drug known to specifically target nucleolin.

The phase I study of this aptamer (NCT00881244) was initiated in September 2003 at James Graham Brown Cancer Center of the University of Louisville in Kentucky, sponsored by Aptamera Inc[45, 46]. It enrolled 17 patients with advanced cancers, in cohorts of 3 per dose. The treatment started with a dose of 1 mg/kg/day AS1411 administered as continuous intravenous (IV) infusion for 4 days. The patients were observed for 28 days after therapy. If no toxicity was observed after 28 days, the dose was increased to 10 mg/kg/day over 7 days. Each patient was given 1 to 2 cycles of the drug. The results indicate that AS1411 was very well tolerated with no adverse effects. Moreover, eight patients had stable disease after two months of treatment until 9 months, and one patient with metastatic renal cell carcinoma (RCC) maintained a near complete response after more than 6 months of therapy. These results appear promising, particularly for RCC.

With early clinical data supporting the safety and tolerability of AS1411, Antisoma, PLC started an extended and dose escalated phase I study in 2005 with the goal of finding an optimal biological dose in patients with RCC and non-small cell lung cancer (NSCLC)[47]. The study was restricted to patients with advanced RCC and NSCLC, who were divided into groups, and AS1411 was administered to the groups at dose levels of 5.5, 11, 22 and 40mg/kg as a continuous intravenous infusion over 7 days. The results indicated no serious toxicity and were very promising in patients with RCC. Out of five RCC patients, one patient maintained near complete response for 18 months after the treatment, and three patients had stable disease (SD).

On the basis of these findings, Antisoma initiated phase II studies on patients with acute myeloid leukemia (AML)[48] and metastatic RCC (NCT00512083)[49]. The phase II study with AML patients enrolled 71 subjects and randomized them into three groups.

Group 1 (n=22) received 10 mg/kg/day AS1411 as continuous IV on days 1-7 plus 1.5 g/m^2/ twice daily cytarabine (HiDAC), brand names Cytosar-U, Tarabine PFS, Depocyt, AraC, on days 4-7. Group 2 (n=26) received 40 mg/kg/day AS1411 on days 1-7 plus HiDAC (similar dosage as group 1). Group 3 (n=23) received 1.5 g/m^2/ twice daily HiDAC alone for 4 days. The results were encouraging with enhanced anti-leukemic activity. Both 10 and 40 mg/kg/day doses of AS1411 along with HiDAC were found to be very tolerable. And, some patients responding to the drug showed substantial survival duration. The aptamer is currently under phase II b trials to treat AML[50].

The phase II study of AS1411 with RCC patients enrolled 35 patients. Among them 33 patients were given two complete 28 day cycles of 40 mg/kg/day of AS1411 for 1-4 days. Three percent of the patients showed partial response (PR) and 60% showed stable disease (SD). No adverse toxicity was observed and progressive-free survival was comparable to that with active agents in the refractory setting. Further studies are required to determine the optimal dosing and scheduling for this aptamer therapeutic.

3.4.2. NOX-A12

NOX-A12 (Noxxon Pharma) is a 45 nucleotide long, Spiegelmer aptamer **(Figure 3.1E).** Spiegelmers are L-RNA aptamers based on synthetic mirror-image oligonucleotides. They are highly selective for their particular pharmacological targets and potent inhibitors of target function. They provide a combined benefit of a small molecule drug and a biopharmaceutical, and they do not become metabolized or hybridized with original nucleic acids within the cell. They possess high resistance to nuclease mediated

degradation as the natural nucleases only recognize D-nucleic acids and not L-nucleic acids[51]. Spiegelmers are extremely non-immunogenic and do not trigger the cell's immune response.

NOX-A12 targets and blocks stroma cell-derived factor-1 (SDF-1 (CXCL12)), a chemokine intermediate that promotes stem cell migration to the bone marrow and plays a role in vasculogenesis, tumor growth, and metastasis[W16, W17]. NOX-A12 is linked to a 40 kDa PEG at the 3' end. Being composed of L-nucleotides, the NOX-A12 aptamer is highly resistant to degradation by abundant nucleases and does not need to be chemically modified. Moreover, as Spiegelmers have only weak, if any, immunogenic potential[52], NOX-A12 is likely to benefit from a "stealth effect".

NOX-A12 was selected from the library of D-RNA using a mirror image target (D-amino acid), and it was then synthesized as L-RNA to bind the wild-type target (L-amino acid). NOX-A12 was developed for use with autologous hematopoietic stem cell transplants and has therapeutic potential for multiple myelomas and non-Hodgkin's lymphoma.

A phase I trial (NCT00976378) was conducted in October 2009 on 48 healthy patients[W18] in order to determine the safety and tolerability of aptamer dosages, and its pharmacokinetic and pharmacodynamic profiles showed that the mobilization of white blood cells and CD34+ cells was directly related to the dosage of NOX-A12 administered[W19]. Pharmacokinetically, it was measured to have a very long half-life of thirty-seven hours. NOX-A12's particular blockage of SDF-1 forces tumor cells to become more susceptible to chemotherapy and, thus, makes this treatment more successful than current treatments [W19]. The results of this study were recently presented at an American

Society of Hematology (ASH) conference in December 2011. The phase II study in patients with Chronic Lymphocytic Leukemia has been started in December 2011 and is now recruiting participants. Similarly, another phase II trial to evaluate the safety and efficacy of NOX A12 alone, and in combination with a background therapy of bortezomib and dexamethasone (VD) chemotherapy in previously treated patients with multiple myeloma (MM), has been started in January 2012 and is currently recruiting participants.

3.5. Therapeutic Aptamers for Diabetes Mellitus

3.5.1. NOX-E36

NOX-E36 is also a Spiegelmer aptamer created by the company Noxxon that targets the Monocyte Chemoattractant Protein 1 (MCP-1 (CCL2))[W20] (Noxxon Pharma, Spiegelmer® NOX-E36). It is a 40-nucleotide long L-RNA **(Figure 3.1F)** linked to 40 kDa PEG. This aptamer has a slightly longer pharmacokinetic half-life of fifty hours and was developed as a possible future treatment option for type II diabetes mellitus, nephropathy, and lupus nephritis. A phase I trial (NCT00976729) was conducted on 72 people in May 2009[W21], in which two double-blind trial groups were given either increasing doses of NOX-E36 or placebo, or a single dose of NOX-E36 or placebo[W22]. The results of this study were positive; namely, an increase in dosage of NOX-E36 resulted in the production of fewer peripheral blood monocytes, the most common immune cells to carry MCP-1[W23]. In 2010, Noxxon initiated a phase Ib trial of NOX-E36 to evaluate its effect on type II diabetes mellitus (NCT01085292) and renal impairment (NCT01372124). The results are not yet

published. Recently, in June 2012, Noxxon announced the treatment of the first patient with diabetic nephropathy, a progressive kidney disease which causes end stage renal diseases, in Phase IIa trial of NOX-E36 (NCT01547897). The study is planned to be conducted with 75 patients with Type II diabetes mellitus and albuminuria for a period of 12 days. It will be a multicentered and double blinded study with 50 patients receiving 0.5mg/kg of NOX-E36 subcutaneously, and the rest of the patients receiving placebo. All the patients in the study will be receiving standard care for hypertension, hyperglycemia, and dyslipidemia[W24].

3.6. Challenges of Aptamer Therapeutics

Aptamer therapeutics are administered in vivo by intravenous (IV), subcutaneous (SC), or intravitreal (IVT) methods[11]. Based on earlier work with oligonucleotides, other routes involving inhalation, mucosal, dermal, or intrathecal delivery are feasible, but they have not been demonstrated to date with aptamers. The targets of most aptamer therapeutics are surface proteins of cells present in the blood or interstitial fluids, and thus aptamers are required to remain in these compartments for extended period of time. In these media, aptamers are subjected to nuclease-mediated degradation, rapid renal filtration, and rapid biodistribution from the plasma compartment into the tissues[11]. Though these hurdles are generally true for all oligonucleotide classes, the specific challenges vary depending on the class. Thus, for an aptamer to be a therapeutic, its structural stability must be increased, and the rate of renal clearance must be decreased **(Table 3.2)**.

3.6.1. Nucleases Mediated Degradation

When unmodified RNA aptamers enter the cell, they are rapidly degraded by nucleases, and the released nucleosides are metabolized through the endogenous purine and pyrimidine metabolism pathways[11]. Their half-life in the blood can be as short as two minutes, but it can be extended by incorporating nucleotides modified at sugar moieties or internucleotide phosphodiester linkages[53]. The most widely used modifications are nucleotides with fluoro or O-methyl groups at the 2' position of their sugar moiety. These modifications significantly enhance the pharmacokinetic profiles of aptamers in vivo. An excellent review by Keefe and Cload discusses the use of various modified nucleotides in aptamers[54].

Modifications involving 2'-fluoro and 2'-O-methyl groups can be incorporated into aptamers before or after the SELEX process using the mutant T7 RNA polymerase[55, 56]. However, additional characterization tests are required as post-selection modifications can alter critical properties of the aptamer. Capping of oligonucleotide termini protects the aptamers from degradation by exonucleases and, thereby, increases their stability. This is frequently achieved by attaching a nucleotide via a 3'-3'phosphodiester bond[12].

Exquisite protection against nucleotides are provided by locked nucleic aptamers (LNA), and Spiegelmers. LNA nucleotides contain a methyl bridge connecting the 2'-O to the 4'-C of the sugar moiety. It increases the stability of the base pairing and enhances the nucleases resistance by locking the ribose in the 3' endo conformation[57]. Replacing D-ribose with L-ribose yields unnatural L-nucleotides, and chemical polymerization of L-nucleotides results in Spiegelmers. Being a mirror image of natural oligonucleotide,

Spiegelmers are highly resistant to degradation by nucleases[51]. They were first synthesized by Furste and co-workers[58], and many Spiegelmer aptamers are presently undergoing clinical trials.

3.6.2. Rapid Renal Clearance

The molecular mass of an aptamer ranges from 5 to 15 kDa. Though the low molecular weight allows economical chemical synthesis and better target accessibility of the aptamer, it facilitates rapid elimination from the body by renal clearance. The bioavailability of the aptamer can be extended by increasing the molecular weight of the aptamer. This can be accomplished by conjugating aptamers to cholesterol or polyethylene glycol (PEG). PEGylation has been extensively used with proteins, peptides, small molecules, and oligonucleotides as a strategy for slowing down renal clearance and extending circulation half-lifetime[11, 59]. For example, the circulation half-life of a 40 kDa PEG-aptamer conjugate was found to be longer than a 20 kDa PEG-aptamer conjugate[60]. With 2'-fluoro/2'-O-methly and 40 kDa PEG modification, the circulation half-life of an aptamer in Sprague-Dawley rats was increased from 0.5 hours to 12 hours. Also, Burmeister et al. showed that the circulation half-life of an aptamer can be extended to 23 hours by fully modifying with 2'-O-methyl and conjugating with 40 kDa PEG[61].

3.6.3. Large Scale Production

With the growing market for therapeutic oligonucleotides, there is the demand for efficient and cost effective manufacturing of oligonucleotides addressing the critical parameters such as raw material availability, production yield, cost, reproducibility, purity, and consistency during process scale up. Higher yield, greater purity, and lower production costs are driving factors for the development of new oligonucleotide synthesis technology. Purity of the raw material is very important in the manufacturing process as it reduces the lot-to-lot variation and greatly increases consistency. Large scale chromatography columns are used for raw material purification. The production yield and purity of oligonucleotides also depends on the liquid reagent used in each step of the solid-phase synthesis cycle[W25]. For a given reactor column volume in the solid-phase oligonucleotide synthesis method, increasing the solid support nucleoside loading, dimensional stability and synthesis efficiency can significantly enhance synthesis economy. The most widely used solid supports are controlled porosity glass (CPG) and low cross-linked polystyrene (PS). CPS has a unique combination of rigidity, well-defined pore structure and dimensional stability in organic solvent, but the loading capacity is limited by the density and the distribution of surface silanol groups. While PS can be loaded with initial nucleoside amounts higher than conventional CPG, but they expand and so the solvent and the column loading must be limited. In order to increase the efficiency of the solid support synthesis method, a hybrid support based on CPG (HybCPG) has been developed[W26]. A very thin (~50Å), highly functionalized polymer coating based on polystyrene on CPG aids in higher ligand loading than conventional CPG since the ligand loading no longer depends on the surface silanol

distribution. The pore size and the pore volume of HybCPG can be specifically tailored for each application to maximize the product purity [W26].

Another major challenge in the production of therapeutic oligonucleotides is to incorporate modifications during the production process, ensuring the necessary quality and yield of the end-product. An important consideration is to incorporate the modification to the oligonucleotide while on solid support. The post-synthesis means of conjugation can be used if the modification group is not amenable to or is unstable to the synthesis condition. Thus, the most frequently used modifications are thiol-, amine-, and aldehyde modifications. To conjugate these modifications, chemistry originated from protein modifications has been used. Recently, pericyclic reactions have been used as the reagents, and the conditions are very mild with high yield and little to no side products [W25].

3.7. Conclusions

Therapeutic aptamers will facilitate economical and versatile treatments for a variety of disorders. In this chapter, aptamers undergoing clinical trials for the treatment of diverse medical conditions including macular degeneration, choroidal neovascularization, intravascular thrombus, acute coronary syndrome, von Willebrand factor related disorder, von Hippel-Lindau syndrome (VHL), angiomas, acute myeloid leukemia, renal cell carcinoma, non-small cell lung cancer, and thrombotic thrombocytopenic purpura are discussed. While presenting the mechanism of aptamers' action, the therapeutic potential of each aptamer are highlighted, and also major challenges facing manufacturing and utilization of therapeutic aptamers are considered. Increased availability and lower costs of

raw materials have significantly reduced costs of manufacturing chemically modified aptamers. Advances in chemical strategies for incorporating modified nucleotides and producing mirror image oligonucleotides (Spiegelmers) dramatically improved aptamer resistance to nuclease-mediated degradation. Conjugation of the aptamers to various delivery vehicles (e.g. high molecular weight PEG and cholesterol) effectively mitigates rapid renal clearance. At present, ten aptamers have been subjected to clinical trials. As investment in therapeutic aptamers is constantly increasing, it is projected that clinical testing of this class of drugs will significantly accelerate in the next two years. Of particular interest are aptamers able to bind to proteins on the cell surface which can block cell surface receptors and also be used for the delivery of a variety of therapeutic agents into the cell. Together, the above mentioned developments promise to bring significant changes to the field of medicine by facilitating personalized, controlled, and on-demand delivery of therapeutic agents and reducing side effects inherent to many traditional therapies.

3.8. References

1. Gold L, Polisky B, Uhlenbeck O, Yarus M. Diversity of Oligonucleotide Functions. Annual Review of Biochemistry. 1995;64: 763-797.

2. Hermann T, Patel DJ. Adaptive Recognition by Nucleic Acid Aptamers. Science. 2000;287: 820-825.

3. Patel DJ. Structural Analysis of Nucleic Acid Aptamers. Current Opinion in Chemical Biology. 1997;1: 32-46.

4. Patel DJ, Suri AK. Structure, Recognition And Discrimination in RNA Aptamer Complexes with Cofactors, Amino Acids, Drugs and Aminoglycoside Antibiotics. Reviews in Molecular Biotechnology. 2000;74: 39-60.

5. Famulok M, Jenne A. Oligonucleotide Libraries - Variatio Delectat. Current Opinion in Chemical Biology. 1998;2: 320-327.

6. Famulok M, Mayer G. Aptamers as Tools in Molecular Biology and Immunology. Current Topics in Microbiology and Immunology. 1999;243: 123-136.

7. Hesselberth J, Robertson MP, Jhaveri S, Ellington AD. In Vitro Selection of Nucleic Acids for Diagnostic Applications. Reviews in Molecular Biotechnology. 2000;74: 15-25.

8. Tuerk C, Gold L. Systematic Evolution of Ligands by Exponential Enrichment: RNA Ligands to Bacteriophage T4 DNA Polymerase. Science. 1990;249: 505-510.

9. Ellington AD, Szostak JW. In Vitro Selection of RNA Molecules That Bind Specific Ligands. Nature. 1990;346: 818-822.

10. Robertson DL, Joyce GF. Selection in Vitro of an RNA Enzyme that Specifically Cleaves Single-Stranded DNA. Nature. 1990;344: 467-468.

11. Bouchard PR, Hutabarat RM, Thompson KM. Discovery and Development of Therapeutic Aptamers. Annual Review of Pharmacology and Toxicology. 2010;50: 237-257.

12. Beigelman L, Matulic-Adamic J, Haeberli P, et al. Synthesis and Biological Activities of A Phosphorodithioate Analog of 2′, 5′-Oligoadenylate. Nucleic Acids Research. 1995;23: 3989-3994.

13. Sullenger BA, Gallardo HF, Ungers GE, Gilboa E. Overexpression of TAR Sequences Renders Cells Resistant to Human Immunodeficiency Virus Replication. Cell. 1990;63: 601-608.

14. Chen C-hB, Chernis GA, Hoang VQ, Landgraf R. Inhibition of Heregulin Signaling by an Aptamer that Preferentially Binds To The Oligomeric Form of Human Epidermal Growth Factor Receptor-3. Proceedings of the National Academy of Sciences. 2003;100: 9226-9231.

15. Hale SP, Schimmel P. Protein Synthesis Editing by A DNA Aptamer. Proceedings of the National Academy of Sciences. 1996;93: 2755-2758.

16. Gold L, Janjic N, Jarvis T, et al. Aptamers and the RNA World, Past and Present. Cold Spring Harbor Perspectives in Biology. 2010.

17. Ng EWM, Adamis AP. Anti-VEGF Aptamer (Pegaptanib) Therapy for Ocular Vascular Diseases. Annals of the New York Academy of Sciences. 2006;1082: 151-171.

18. Jellinek D, Green LS, Bell C, Janjic N. Inhibition of Receptor Binding by High-Affinity RNA Ligands to Vascular Endothelial Growth Factor. Biochemistry. 1994;33: 10450-10456.

19. Ng EWM, Shima DT, Calias P, Cunningham ET, Guyer DR, Adamis AP. Pegaptanib, A Targeted Anti-VEGF Aptamer For Ocular Vascular Disease. Nature Review of Drug Discovery. 2006;5: 123-132.

20. Nishijima K, Ng Y-S, Zhong L, et al. Vascular Endothelial Growth Factor-A Is a Survival Factor for Retinal Neurons and a Critical Neuroprotectant during the Adaptive Response to Ischemic Injury. The American Journal of Pathology. 2007;171: 53-67.

21. Saint-Geniez M, Kurihara T, Sekiyama E, Maldonado AE, D'Amore PA. An Essential Role for RPE-Derived Soluble VEGF in the Maintenance Of The Choriocapillaris. Proceedings of the National Academy of Sciences. 2009;106: 18751-18756.

22. Friberg TR, Tolentino M, Group ftLS. Pegaptanib Sodium as Maintenance Therapy in Neovascular Age-Related Macular Degeneration: The LEVEL Study. British Journal of Ophthalmology. 2010.

23. Group MDRS. A Phase II Randomized Double-Masked Trial of Pegaptanib, an Anti–Vascular Endothelial Growth Factor Aptamer, for Diabetic Macular Edema. Ophthalmology. 2005;112: 1747-1757.

24. Sultan MB, Zhou D, Loftus J, Dombi T, Ice KS. A Phase 2/3, Multicenter, Randomized, Double-Masked, 2-Year Trial of Pegaptanib Sodium for the Treatment of Diabetic Macular Edema. Ophthalmology. 2011;118: 1107-1118.

25. González VH, Giuliari GP, Banda RM, Guel DA. Intravitreal Injection of Pegaptanib Sodium for Proliferative Diabetic Retinopathy. British Journal of Ophthalmology. 2009;93: 1474-1478.

26. Jo N, Mailhos C, Ju M, et al. Inhibition of Platelet-Derived Growth Factor B Signaling Enhances the Efficacy of Anti-Vascular Endothelial Growth Factor Therapy in Multiple Models of Ocular Neovascularization. The American Journal of Pathology. 2006;168: 2036-2053.

27. Zarbin MA, Rosenfeld PJ. Pathway-Based Therapies For Age-Related Macular Degeneration: An Integrated Survey Of Emerging Treatment Alternatives. Retina. 2010;30: 1350-1367.

28. Ricklin D, Lambris JD. Complement-Targeted Therapeutics. Nature Biotechnology. 2007;25: 1265-1275.

29. Nimjee SM, Rusconi CP, Harrington RA, Sullenger BA. The Potential of Aptamers as Anticoagulants. Trends in Cardiovascular Medicine. 2005;15: 41-45.

30. Dyke CK, Steinhubl SR, Kleiman NS, et al. First-in-Human Experience of an Antidote-Controlled Anticoagulant Using RNA Aptamer Technology. Circulation. 2006;114: 2490-2497.

31. Chan MY, Cohen MG, Dyke CK, et al. Phase 1b Randomized Study of Antidote-Controlled Modulation of Factor IXa Activity in Patients With Stable Coronary Artery Disease. Circulation. 2008;117: 2865-2874.

32. Chan MY, Rusconi CP, Alexander JH, Tonkens RM, Harrington RA, Becker RC. A Randomized, Repeat-Dose, Pharmacodynamic and Safety Study of an Antidote-Controlled Factor IXa Inhibitor. Journal of Thrombosis & Haemostasis. 2008;6: 789-796.

33. Cohen MG, Purdy DA, Rossi JS, et al. First Clinical Application of an Actively Reversible Direct Factor IXa Inhibitor as an Anticoagulation Strategy in Patients Undergoing Percutaneous Coronary Intervention / Clinical Perspective. Circulation. 2010;122: 614-622.

34. Povsic TJ, Wargin WA, Alexander JH, et al. Pegnivacogin Results In Near Complete FIX Inhibition in Acute Coronary Syndrome Patients: RADAR Pharmacokinetic and Pharmacodynamic Substudy. European Heart Journal. 2011;32: 2412-2419.

35. Vavalle JP, Rusconi CP, Zelenkofske S, Wargin WA, Alexander JH, Becker RC. A Phase 1 Ascending Dose Study Of A Subcutaneously Administered Factor IXa Inhibitor and its Active Control Agent. Journal of Thrombosis and Haemostasis. 2012;10: 1303-1311.

36. Keefe AD, Pai S, Ellington A. Aptamers as Therapeutics. Nature Review of Drug Discovery. 2010;9: 537-550.

37. Gilbert JC, DeFeo-Fraulini T, Hutabarat RM, et al. First-in-Human Evaluation of Anti–von Willebrand Factor Therapeutic Aptamer ARC1779 in Healthy Volunteers. Circulation. 2007;116: 2678-2686.

38. Jilma B, Paulinska P, Jilma-Stohlawetz P, Gilbert JC, Hutabarat R, Knöb P. A Randomised Pilot Trial of the Anti-Von Willebrand Factor Aptamer ARC1779 in Patients with Type 2b Von Willebrand Disease. Thrombosis and Haemostasis. 2010;104: 563–570.

39. Waters E, Richardson J, Schaub R, Kurz J. Effect of NU172 and Bivalirudin on Ecarin Clotting Time in Human Plasma and Whole Blood-Posters. Journal of Thrombosis and Haemostasis. 2009;7: 367.

40. Gilbert GE, Mast AE. Curbing an Inhibitor for Hemostasis. Blood. 2011;117: 5277-5278.

41. Waters EK, Genga RM, Schwartz MC, et al. Aptamer ARC19499 Mediates A Procoagulant Hemostatic Effect By Inhibiting Tissue Factor Pathway Inhibitor. Blood. 2011;117: 5514-5522.

42. Bates PJ, Laber DA, Miller DM, Thomas SD, Trent JO. Discovery and Development of the G-Rich Oligonucleotide AS1411 as A Novel Treatment for Cancer. Experimental and Molecular Pathology. 2009;86: 151-164.

43. Girvan AC, Teng Y, Casson LK, et al. AGRO100 Inhibits Activation of Nuclear Factor-Kb (NF-Kb) by Forming A Complex with NF-κB Essential Modulator (NEMO) and Nucleolin. Molecular Cancer Therapeutics. 2006;5: 1790-1799.

44. Soundararajan S, Chen W, Spicer EK, Courtenay-Luck N, Fernandes DJ. The Nucleolin Targeting Aptamer AS1411 Destabilizes Bcl-2 Messenger RNA in Human Breast Cancer Cells. Cancer Research. 2008;68: 2358-2365.

45. Laber DA, Choudry MA, Taft BS, et al. A Phase I Study of AGRO100 in Advanced Cancer. ASCO Meeting Abstracts. 2004;22: 3112.

46. Laber DA, Sharma VR, Bhupalam L, Taft B, Hendler FJ, Barnhart KM. Update on the First Phase I Study of AGRO100 in Advanced Cancer. ASCO Meeting Abstracts. 2005;23: 3064.

47. Laber DA, Taft BS, Kloecker GH, Bates PJ, Trent JO, Miller DM. Extended Phase I Study of AS1411 in Renal and Non-Small Cell Lung Cancers. ASCO Meeting Abstracts. 2006;24: 13098.

48. Rizzieri D, Stockerl-Goldstein K, Wei A, Herzig RH, Erlandsson F, Stuart RK. Long-Term Outcomes Of Responders in a Randomized, Controlled Phase II Trial of Aptamer AS1411 in AML. ASCO Meeting Abstracts. 2010;28: 6557.

49. Rosenberg JE, Drabkin HA, Lara P, et al. A Phase II, Single-Arm Study Of AS1411 in Metastatic Renal Cell Carcinoma (RCC). ASCO Meeting Abstracts. 2010;28: 4590.

50. Stuart RK, Wei A, Lewis ID, Estey E, Erlandsson F, Schiller GJ. A Multicenter Dose-Finding Randomized Controlled Phase IIb Study of the Aptamer AS1411 in Patients with Primary Refractory or Relapsed AML. ASCO Meeting Abstracts. 2010;28: TPS279.

51. Eulberg D, Klussmann S. Spiegelmers: Biostable Aptamers. ChemBioChem. 2003;4: 979-983.

52. Wlotzka B, Leva S, Eschgfäller B, et al. In Vivo Properties of an Anti-Gnrh Spiegelmer: aan Example of An Oligonucleotide-Based Therapeutic Substance Class. Proceedings of the National Academy of Sciences. 2002;99: 8898-8902.

53. Griffin L, Tidmarsh G, Bock L, Toole J, Leung L. In Vivo Anticoagulant Properties of A Novel Nucleotide-Based Thrombin Inhibitor and Demonstration of Regional Anticoagulation in Extracorporeal Circuits. Blood. 1993;81: 3271-3276.

54. Keefe AD, Cload ST. SELEX with Modified Nucleotides. Current Opinion in Chemical Biology. 2008;12: 448-456.

55. Chelliserrykattil J, Ellington AD. Evolution of a T7 RNA Polymerase Variant That Transcribes 2[Prime]-O-Methyl RNA. Nature Biotechnology. 2004;22: 1155-1160.

56. Huang Y, Eckstein F, Padilla R, Sousa R. Mechanism of Ribose 2‘-Group Discrimination by an RNA Polymerase. Biochemistry. 1997;36: 8231-8242.

57. Schmidt KS, Borkowski S, Kurreck J, et al. Application of Locked Nucleic Acids to Improve Aptamer In Vivo Stability and Targeting Function. Nucleic Acids Research. 2004;32: 5757-5765.

58. Kluszmann S, Nolte A, Bald R, Erdmann VA, Furste JP. Mirror-image RNA that binds D-adenosine. Nature Biotechnology. 1996;14: 1112-1115.

59. Brody EN, Gold L. Aptamers as Therapeutic and Diagnostic Agents. Reviews in Molecular Biotechnology. 2000;74: 5-13.

60. Healy JM, Lewis SD, Kurz M, et al. Pharmacokinetics and Biodistribution of Novel Aptamer Compositions. Pharmaceutical Research. 2004;21: 2234-2246.

61. Burmeister PE, Lewis SD, Silva RF, et al. Direct In Vitro Selection of a 2′-O-Methyl Aptamer to VEGF. Chemistry and Biology. 2005;12: 25-33.

3.9. WEB REFERENCES

W1. Eyetech Inc., 2010. Phase 3 Study Presented at World Ophthalmology Congress Evaluates Investigational Use of Macugen in Patients with Diabetic Macular Edema. Available from URL: http://www.marketwire.com/press-release/phase-3-study-presented-world-ophthalmology-congress-evaluates-investigational-use-macugen-1271620.htm [accessed July 8, 2012]

W2. NIH, 2013, A Phase 3 Study to Compare the Safety and Efficiency of 0.3 MG Pegaptanib Sodium To Sham Injection In Patients With Diabetic Magular Edema. Available from URL: http://clinicaltrials.gov/ct2/show/NCT01100307?term=NCT01100307&rank=1 [accessed December 16, 2013].

W3. NIH, 2010a, Intravitreal Macugen for Ischaemic Diabetic Macular Oedema (MIDME). Available from URL: http://clinicaltrials.gov/ct2/show/NCT01175070?term=macugen&rank=2 [accessed June 16, 2012].

W4. NIH, 2008a, Pegaptanib Therapy in Uveitis. Available from URL: http://clinicaltrials.gov/ct2/show/NCT00790803?term=macugen&rank=15 [accessed June 16, 2012].

W5. NIH, 2010c, Intravitreal Pegaptanib in Treatment of Choroidal Neovascularisation Secondary to Pathologic Myopia. Available from URL: http://clinicaltrials.gov/ct2/show/NCT01218230?term=macugen&rank=18 [accessed July 3, 2012].

W6. NIH, 2006, A Pilot Study for the Treatment of Iris Neovascularization With Macugen. Available from URL: http://clinicaltrials.gov/ct2/show/NCT00295828?term=macugen&rank=10 [accessed July 3, 2012].

W7. NIH, 2008b, Long-Term Use Of Pegaptanib In Patients For Subfoveal Choroidal Neovascularization Secondary To Age-Related Macular Degeneration. Available from URL: http://clinicaltrials.gov/ct2/show/NCT00845273?term=macugen&rank=20 [accessed June 16, 2012].

W8. Ophthotech, 2012a, Fovista™ (E10030) - Anti-PDGF. Available from URL: http://www.ophthotech.com/products/e10030/ [accessed July 5, 2012].

W9. Retina Today Archive, 2009a Neovascular Regression and Improved Visual Acuity Achieved With Combined Anti-PDGF/Anti-VEGF Therapy. Available from URL: http://bmctoday.net/retinatoday/2009/06/article.asp?f=0609NEWS_01.php [accessed July 3, 2012].

W10. Retina Today Archive, Cousins SW, 2009b. Intravitreal Anti-VEGF and Anti-PDGF Combination Therapy. Available from URL: http://bmctoday.net/retinatoday/2009/10/article.asp?f=1009_12.php [accessed July 5, 2012].

W11. Ophthotech, 2012b, Ophthotech's Novel Anti-PDGF Combination Agent Fovista™ Demonstrated Superior Efficacy over Lucentis® Monotherapy in Large Controlled Wet AMD Trial. Available from URL: http://www.ophthotech.com/ophthotechs-anti-pdgf-fovista-superior-efficacy-phase2b/ [accessed July 3, 2012].

W12. NIH, 2013, A Phase 3 Safety and Efficiency of Fovista Intravenous Administration In Combination With Lucentis Compared to Lucentis Monotherapy. Available from URL: http://clinicaltrials.gov/ct2/show/NCT01944839?term=NCT01944839&rank=1 [accessed December 16, 2013].

W13. Fierce Healthcare, 2008, Nuvelo Announces Positive Proof-of-Concept Data With Anticogulant NU172 Available from URL: http://www.fiercehealthcare.com/press-releases/nuvelo-announces-positive-proof-concept-data-anticogulant-nu172 [accessed June 9, 2012].

W14. Wikinivest, 2009, NUVO NU172. Available from URL: http://www.wikinvest.com/stock/Nuvelo_%28NUVO%29/Nu172 [accessed July 5, 2012].

W15. NIH, 2010b, First-in-human and proof-of-mechanism study of ARC19499 administered to hemophilia patients. Available from URL: http://clinicaltrials.gov/ct2/show/NCT01191372 [accessed Januvary 4, 2012].

W16. Noxxon Pharma, 2010a, NOXXON Announces the Completion of the First-in-Human Clinical Trial with Spiegelmer® NOX-A12. Available from URL: http://www.noxxon.com/downloads/pressrel/100503_NOXXON_Announces_the_Completion_of_the_First-in-Human_Clinical_Trial_with_Spiegelmer_NOX-A_12.pdf [accessed July 4, 2012].

W17. Noxxon Pharma, 2010b, Noxxon initiates multiple dose phase I clinical trail of SDF-1inhibitor NOX-A12. Available from URL: http://www.noxxon.com/downloads/pressrel/2010-09-22_NOXXON_INITIATE_MULTIPLE_DOSE_PHASE_I_CLINICAL_TRIAL_OF_SDF-1_INHIBITOR_NOX-A12.pdf [accessed July 3, 2012].

W18. NIH, 2009a, NOX-A12 first-in-human (FIH) study. Available from URL: http://www.clinicaltrials.gov/ct2/show/NCT00976378 [accessed Januvary 4, 2012].

W19. Noxxon Pharma, 2011, Noxxon's SDF-1 inhibitor NOX-A12 completes Phase I : Preclinical data in models of hematological tumors to be presented at ASH conference. Available from URL: http://www.noxxon.com/downloads/pressrel/2011-12-12_NOXXONs_SDF-1_inhibitor_NOX-A12_completes_Phase_I.pdf [accessed July 5, 2012].

W20. Noxxon Pharma, Spiegelmer® NOX-E36. Available from URL: http://www.noxxon.com/index.php?option=com_content&view=article&id=60&Itemid=98 [accessed July 3, 2012].

W21. NIH, 2009b, NOX-E36 first-in-human (FIH) study. Available from URL: http://www.clinicaltrials.gov/ct2/show/NCT00976729 [accessed Januvary 4, 2012].

W22. Noxxon Pharma, 2009, Noxxon Announces Initiation of First Clinical Trial with a Spiegelmer®. Available from URL: http://www.noxxon.com/downloads/pressrel/090608_NOXXON_Announces_Initiation_of_First_Clinical_Trial_with_a_Spiegelmer.pdf [accessed July 4, 2012].

W23. Noxxon Pharma, 2010c, NOXXON to initiate phase Ib clinical trail of MCP-1 inhibitor NOX-E36: Study to include healthy volunteers and diabetic patients. Available from URL: http://www.noxxon.com/downloads/pressrel/100707-noxxon_to_initiate_phase_ib_clinical_trial_of_mcp-1_inhibitor_nox-e36.pdf [accessed July 4, 2012].

W24. Noxxon Pharma, 2012, NOXXON Initiates Phase IIa of anti-CCL2/MCP-1 Spiegelmer® NOX-E36 for Treatment of Diabetic Nephropathy. Available from URL: http://www.noxxon.com/downloads/pressrel/2012-06-19_NOXXON_Initiates_Phase_IIa_of_Spiegelmer_NOX-E36.pdf . [accessed July 3, 2012].

W25. Genetic engineering & biotechnology news (GEN), 2012a, Redefining oligonucleotid production. Available from URL: http://www.genengnews.com/gen-articles/redefining-oligonucleotide-production/4065/ [accessed September 20, 2012].

W26. Genetic engineering & biotechnology news (GEN), 2012b, Solid-phase support for oligo synthesis. Available from URL: http://www.genengnews.com/gen-articles/solid-phase-supports-for-oligo-synthesis/4096/ [accessed September 20, 2012].

Aptamer Therapeutic	Sponsor	Medical Condition	Current Status
Pegaptanib/Macugen	Eyetech Inc/Pfitzer	Age related macular degeneration/ Diabeti macular edema/ proliferative diabetic retinopathy	In market
E10030	Opthotech Corp	Neovascular age related macular degeneration	Phase III
ARC1905	Opthotech Corp	Neovascular age related macular degeneration	Phase I
RB006	Regado Biosciences, Inc	Coronary artery disease	Awaiting Phase III
ARC1779	Archimex Corp	von Willebrand's disease	Awaiting Phase III
NU172	Nuvelo/ARCA Biopharma	Coronary artery disease	Phase II
ARC19499	Archimex	Hemophilia	Phase I/II terminated
AS1411	Antisoma PLC	Renal cell carcinoma/ Non-small cell lung cancer	Awaiting Phase III
NOX-A12	Noxxon Pharma	Tumor	Phase II, recruiting patients
NOX-E36	Noxxon Pharma	Type II diabetes mellitus/ Renal impairmer nephropathy/ lupus nephritis	Phase IIa

Table 3.1. Current Status of the Aptamer Therapeutics Undergoing Clinical Trails

Challenge	Solutions
Rapid Renal Clearance	Attachment of high molecular weight poly ethylene glycol or cholesterol
Nucleases Mediated Degradation	Incorporation of protective groups at 2'-O-position of ribose sugar
Production Yield	Incorporation of the protective groups Increased yield through large scale manufacturing, flow through technology, and more efficient and novel solid phase synthesis
Cost of Production	Recent price reduction due to lowered cost of raw material, various types of building blocks Expected to reduce further through more efficient large scale manufacturing
Toxicity	Minimal toxicity with selected aptamers More toxicity studies are required

Table 3.2. Challenges of Aptamer Therapeutics

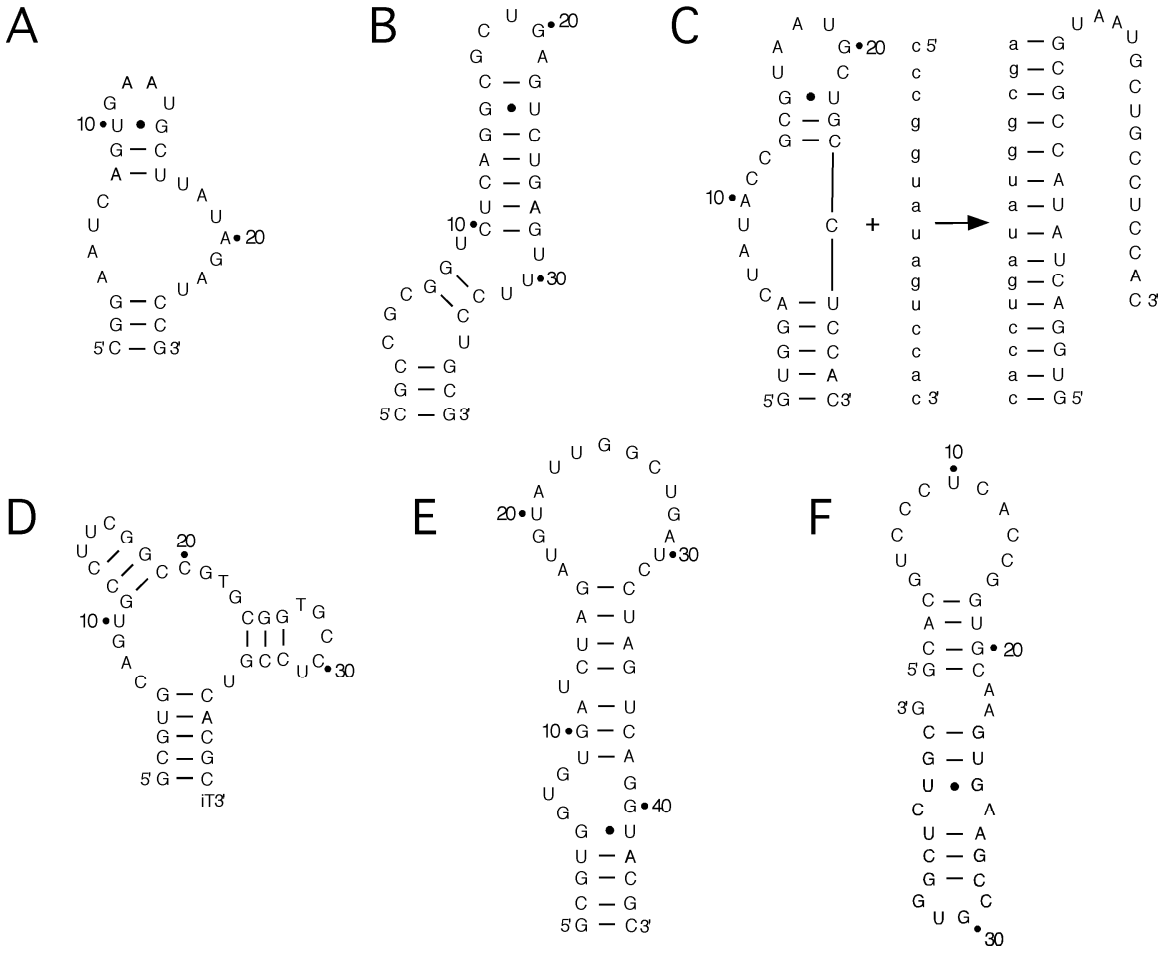

Figure 3.1. Secondary Structure. A: Pegaptanib; B: ARC1905; C:RB006/007; D: ARC-1779; E: NOX-A12 and F: NOX-E36.

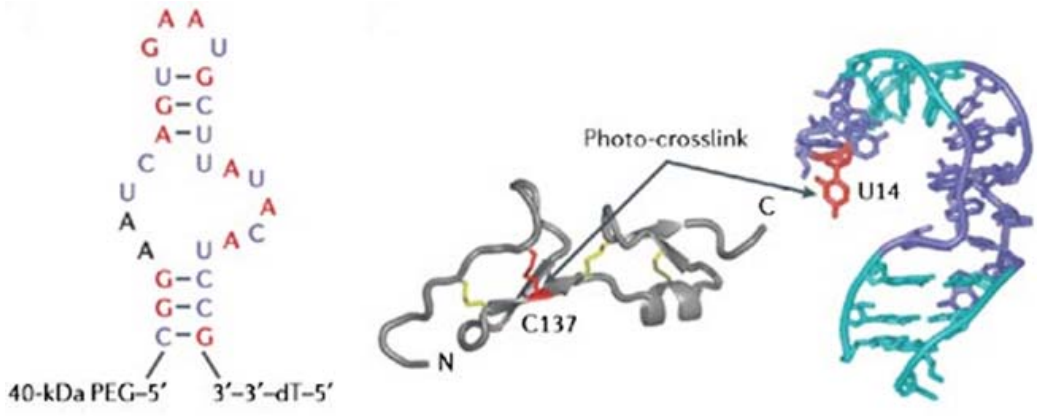

A **B**

Figure 3.2. Sequence, Structure and Interaction Site of Pegaptanib. (A) Secondary structure of Pegaptanib with 2'-O-methylated nucleotides in red, 2'- fluoro pyramidines in blue, 40 kDa PEG attached to the 5'end, and 3'-dT attached to the 3' end of the aptamer. (B) Interaction between the cysteine-137 (C137) of the heparin binding domain of $VEGF_{165}$ and uridine-14 (U14) of pegaptanib, indicated in red (used with permission from reference 19).

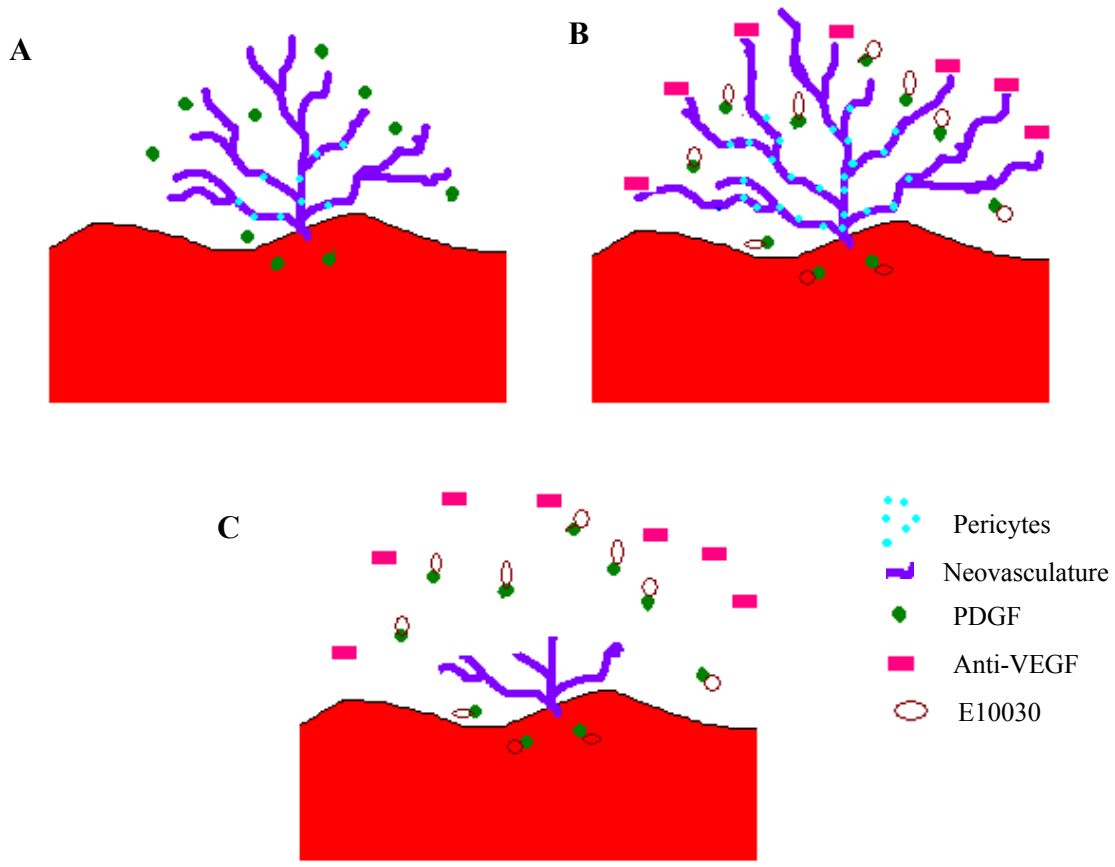

Figure.3.3. **Co-administration of Anti-VEGF Agent and E10030**. (A) PDGF molecules regulates the recruitment and regulation of pericytes (mural cell) which secrets growth factors. Increased expression of PDGF in neovascular tissue results in increased secretion of growth factors such as VEGF. (B) The anti-VEGF agents attack VEGF and not the pericytes. Thus neovascular tissue is resistant to regression during anti-VEGF therapy. E10030 strongly binds to PDGF and strips the pericyte. (C) Combination therapy of E10030 and anti-VEGF induces significant neovascular regression. (Adapted from reference W11).

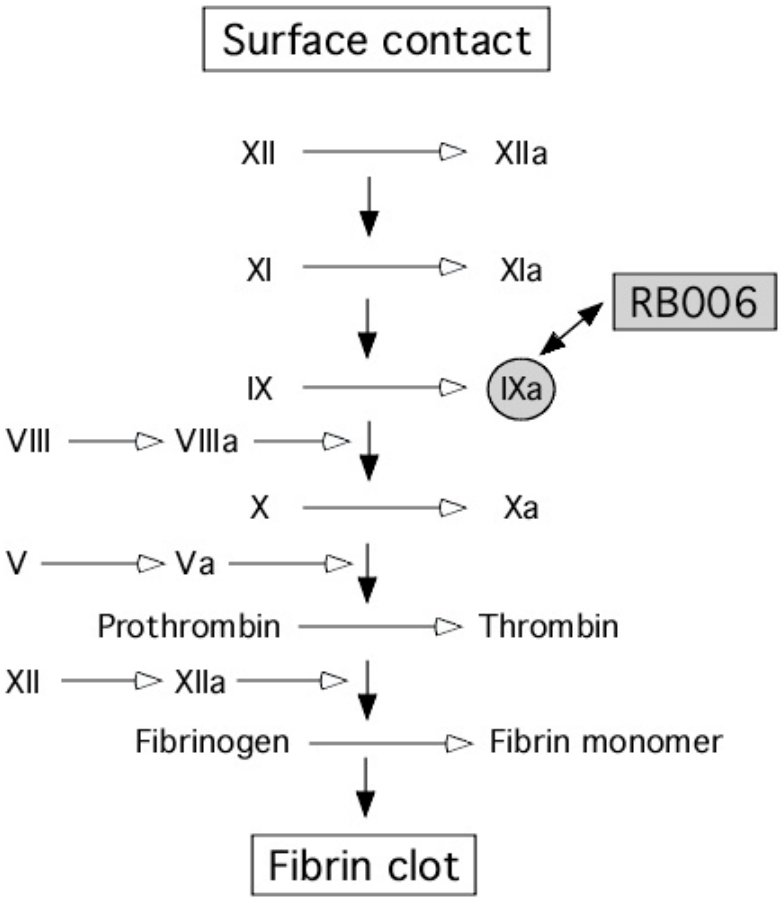

Figure 3.4. Coagulation Model. RB006 binds to the factor IXa and blocks the factor VIIIa/IXa-catalyzed conversion of factor X to factor Xa, a pivotal step in generation of thrombin which is essential for conversion of fibrinogen to fibrin monomer. The anticoagulant effect of RB006 can be reversed by binding of RB007, an oligonucleotide complimentary to RB006, to RB006.

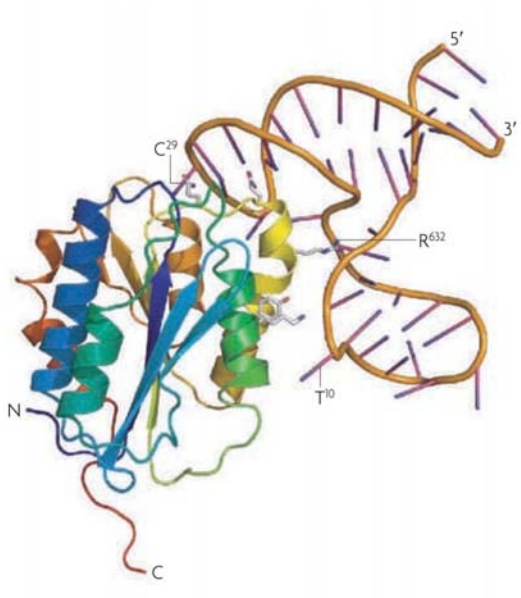

Figure 3.5. Three Dimensional Structure of ARC1779. Binding of all-DNA parent of ARC1779 to the A1 domain of von-Willebrand factor (used with permission from reference 36).

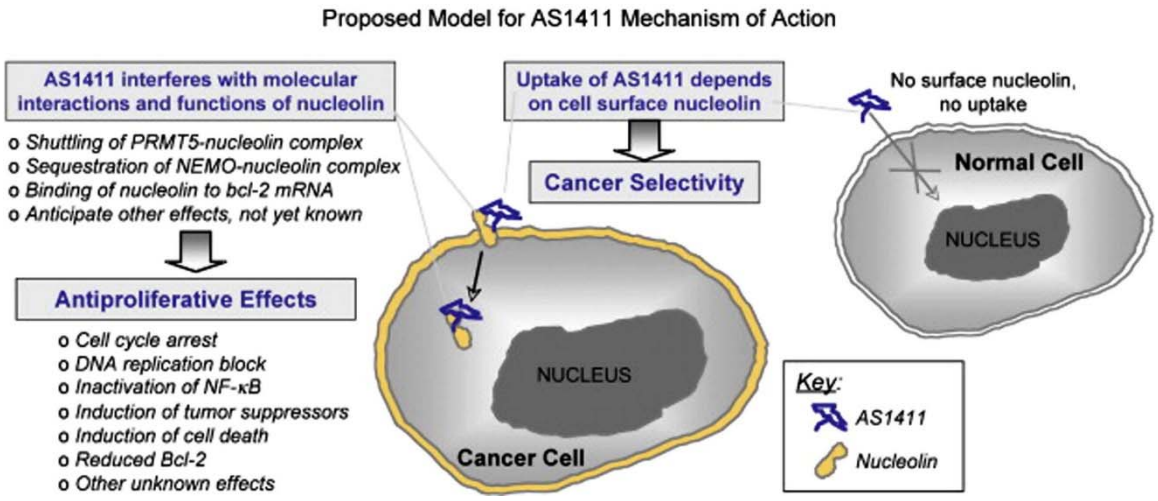

Figure 3.6. Proposed Model for AS1411 Mechanism of Action. Cellular uptake of AS1411 depends upon the cell surface nucleolin over expressed on cancer cells. Thus, AS1411 are specifically internalized by malignant cells and not by normal cells. Binding of AS1411 to nucleolin, which plays a major role in many cancer-associated pathways, disrupts its normal function and causes pleiotropic antiproliferation (used with permission from reference 42).

Chapter 4. Nano-Carrier Materials for Drug and Nucleic Acid Delivery

In vivo, drug molecules and genes have the disadvantage of low bioavailability, and rapid renal clearance. Thus there is a significant need to develop a delivery carrier that is capable of effectively delivering the drug to diseased cells. An effective delivery system should protect the therapeutic from in vivo biological elements, and provide efficient delivery into target cells. It should be biocompatible, biodegradable, and should not raise immune responses in host. The system must be capable of avoiding rapid hepatic or renal clearance, and provide tissue specific distribution. Once inside the cell via endocytosis, the system should promote releases of the therapeutic into cytoplasam. More importantly, the delivery system must be capable of overcoming the series of biological hurdles it has to face in vivo **(Figure 4.1)**. When administered in to the blood stream, the delivery system has to first overcome phagocytosis. The phagocytosis cells such as macrophages and monocytes protect the body against the bacteria, viruses, and fungi by removing the foreign material from the body. Unfortunately, these cells have the tendency of identifying the nanomedicines and drug delivery vehicles as harmful foreign material, and will attempt to clear them out[1]. After escaping the phagocytosis, the delivery system has to overcome the vascular endothelial barrier. Generally, molecules larger than 5 nm in diameter do not readily cross the capillary endothelial, and remain in the circulation until removed by renal system. Although, entries of larger molecules upto 200 nm in diameter are allowed in by a few organs like liver, spleen and tumor cells[2]. Thus the size of the delivery vehicle has to

be decided considering the characteristics of the delivery site. After leaving the blood vessel, the carrier has to diffuse through extracellular matrix, a dense network of polysaccharides and fibrous proteins. Generally, the matrix resists the transport of macromolecules and nanoparticles which can increase their retention time and provide additional opportunity to the macrophages to clear them out[3]. Once inside the target cell, the particles have to escape the endosome and reach the cytoplasm of the cell. If the carriers remain in the endosome, they will be subjected to degradation in the endomembrane compartments of decreasing pH[4].

The properties of the delivery carrier affecting its performance are the size, surface charge, biocompatibility, and toxicity. Surface charge of the nanoparticle is one of the important factors that influences the way it reacts with the target cell. Theoretically, a positively charged particle facilitates cellular uptake by associating with the negatively charged cellular membrane. But in practice, positively charged particle induces complex formation, and interacts with the polyanionic nucleic acids as well as negatively charged serum proteins[5] in vivo. Covering the delivery vehicle with hydrophilic conjugates like PEG could subsidize the above mentioned problems. PEG conjugation can also prevent particle aggregation in the presence of serum[6].

Biodistribution of the nanoparticles depends on the size of the particle. To prevent rapid renal clearance, particles have to be at least of 50 kDa in size[7]. However, clearance of larger molecular weight material typically requires them to be biodegradable. In case of delivering a therapeutic to tumor site, directed delivery can be obtained by adjusting the size of the nanoparticle according to the pore size of the leaky vasculature of tumor cells[8, 9]. Targeted delivery can also be obtained by conjugating targeting ligands such as aptamers

and antibodies to delivery vehicle[10, 11]. Another major aspect to be taken into consideration is the toxicity of the carrier in vivo. Even the most efficacious delivery agent cannot be used if it renders unacceptable level of toxicity or activates the immune system. Use of biodegradable materials can help in reducing cytotoxicity.

Over the past couple of decades, nanocarriers have received much attention due to their surface properties, and their ability to conjugate various functional groups. In this chapter, we discuss the various nanoparticle materials that have been used to construct nano delivery carriers for therapeutics. A focus is made on liposomes, polymeric materials, quantum dots, and gold nanoparticles for drug and gene delivery.

4.1. Liposomes

Liposomes are composed of lipid or phospholipid molecules containing a hydrophilic head region and hydrophobic tail region that have aggregated together to form an enclosed bilayer particle with an aqueous center and lipid membrane. They offer the ability to deliver both hydrophilic drugs (in the aqueous center) and lipid-soluble drugs (within the bilayer structure). This sort of therapeutic loading does not occupy surface functionality groups that may further be used to attach targeting ligands and/or biocompatibility agents such as PEG, chitosan, silk-fibroin, and polyvinyl alcohol (PVA)[12]. Liposomes have been receiving attention as therapeutic carriers for over 40 years, and have been explored as carriers for anticancer drugs, antifungal drugs, analgesics, gene therapies, and vaccines[13].

Liposome mediated gene delivery is one of the earliest strategies used to introduce exogenous genetic material into host cells. The physical and chemical properties of liposomal nanoparticles can be easily optimized for delivering nucleic acids as they can be created with single or multiple lipids. The capability of various liposomes in delivering nucleic acids are being explored since 1970. Some of the cationic lipids that have been used for delivering of both DNA and RNA into cells are DOTMA (N-[1-(2,3-dioeyloxy)propyl)-N,N,N- trimethylammonium chloride) [14, 15], DOSPA (2,3-dioleyloxy-N-[2(sperminecaboxamido)ethyl]-N-N-dimethyl-1-propanaminium triluoroacetate)[16], DOTAP (1,2-dioeoyl-3-trimethylammonium-propane)[17] and DOGS (dioctadecylamido-glycylspermine)[18].

Cationic lipids basically contains three structural domains: a cationic head group, a hydrophobic portion, and a linker between two domains. Over these four decades, scientist have tried various combination of these lipid domains to formulate a liposome with high transfection and low toxicity. The hydroethyl derivatives of DOTMA[19], DOTAP[20], and tetradecylamine-based[21] lipids showed enhanced transfection efficiency compared to their methylammonim analogs. Furthermore, linear and branched headgroups, lipids with dendritic cationic headgroups have been observed to exhibit significantly higher gene transfer efficiency than the commercially available agents. PAMAM dentron-based headgroup was found to have enhanced transfection efficiency as a result of higher buffering capacity. Grafting of PEG chain onto PAMAM headgroup was observed to further improve the serum stability[22]. Recently, aminoglycoside lipoplexes have been successfully used for siRNA delivery and interference[23]. Furthermore, greater increase in transfection efficiency was demonstrated with the cationic peptide headgroup[24]. The

biodegradability and fusogenic capability of the liposome was probed by the use of cholesterol[25-27] and other steroids[28] in the hydrophobic tail-group. For all lipids used in gene transfection, hydrophobic and cationic portions are joined by several common linkers including amides, carbamates, esters and ethers. On manipulating the linking groups, scientist demonstrated that the transfection efficiency can be sufficiently increased by the use of pH sensitive linkers including vinyl ether[29], ketals[30], orthoether[31-33], acylhydrazone[34], as well as redox reactive groups[35-37].

In 2005, Jeff *et al*., developed a modified ethanol dialysis method to produce stable lipid particles in the size of 100-150 nm encapsulated with DNA[38]. These particles were named as Stable nucleic acid-lipid particles (SNALP). Later, Protiva Biotherapeutics formulated SNALP encapsulated with siRNA and tested in several models in vivo. siRNA-SNALP complexes have been successfully used to knockdown ApoB in the liver of monkey[39], inhibit HBV replication[40], combat Ebola virus and prevent haemorrahagic fever in guinea pigs[41]. Recently, Li *et al*., developed a lipid coated calcium phosphate (LCP) nanocarier with siRNA entrapped in the core for efficient delivery of siRNA[42]. After entering the cells, LCP would disassemble in the endosome due to low pH causing endosomal swelling and bursting, resulting in the release of entrapped siRNA.

Similar to nucleic acids, liposomes can also encapsulate drugs in a variety of fashion. There are multiple examples of liposomes with hydrophilic therapeutics encapsulated within the aqueous layer[42-44] and hydrophobic therapeutics entrapped within the lipid bilayer[45, 46]. Scientists have also produced stimuli-responsive liposomes to control the release of encapsulated drug in vivo in response to stimulus such as light, magnetism, temperature, ultrasonic waves, or a change in pH[12]. Lentacker *et al*., produced a liposomal

nanocarrier for doxorubicin. The nanocarrier is 147 nm in diameter, and is attached to a lipid microbubble (diameter ~ 2 μm) filled with perfluorobutane, C_4F_{10}, via conjugated biotin and avidin affinity[47]. The localization of therapeutic release in vitro was controlled by ultrasonic wave application, and the biotin molecules attached to the lipid surface via PEG rendered greater biocompatibility. This method of doxorubicin delivery resulted in statistically significant decreases in melanoma cell viability over other doxorubicin loaded liposomes. Recently, drug-targeting macrophages using liposomes were demonstrated by Etzerodt *et al*. Liposomes loaded with calcein were targeted to CD163, a hemoglobin scavenger receptor found in tissue resident macrophages, using CD163 binding monoclonal antibodies[48].

The first liposomal pharmaceutical product, Doxil was approved by US Food and Drug Administration (FDA) in 1995[49]. Doxil is successfully being used for treating solid tumor in patients with breast carcinoma as it significantly reduced cardiac toxicity of doxorubicin[49-51]. Currently, there are twelve liposomal based drug approved for clinical use and many more in different stages of clinical trial[52, 53] (Table 4.1 & 4.2). Though liposomes have demonstrated to be capable of efficiently delivering gene and drug, it has concerns regarding toxicity in vitro and in vivo[52, 54].

4.2. Polymers

Polymer carriers offer a high versatility in both structural and physiochemical properties. A major reason for this versatility is the wide variety of monomers that may be used to form the polymer architectures. Some of the commonly used structures as delivery

carrier includes polymersomes, dendrimers, and cyclodextrin-containing polymers (CDPs). Polymersomes are structurally similar to liposomes, but they are formed from amphiphilic block copolymers. Dendrimers are multi-branched polymer structures extending out from a core. CDPs are polymers that contain cyclodextrin molecules within the core structure or attached as side chains. Furthermore, certain polymers contain chemical groups that have the ability to adapt accordingly to the current environment resulting in a change of properties in the overall polymer itself. These polymers are referred to as responsive or "smart polymers". Some common environmental stimuli include pH, ionic strength, chemical agents, mechanical stress, temperature, electromagnetic radiation, and electric field.

Polymers used for drug delivery are generally classified into synthetic and natural polymers. Synthetic polymers include Poly-L-lysine (PLL), polyethylenimine (PEI), and polymethacrylate based macromolecules. Natural polymers include chitosan, cyclodextrin, and schizophyllan. The capability of PLL to form complex with DNA was demonstrated by Laemmli in 1975[55]. Subsequently, PLL was used for in vitro[56] and in vivo[57] gene transfers. Akinc and Langer determined the pH environment of PLL-DNA complex after cellular intake to be in-between 4 to 4.5, which indicate that most of the polyplex were contained in lysosomal trafficking pathway as opposed to being released into the cytoplasam[58]. Drugs like daunomycin can be attached to PLL using chemical spacers. Shen and Ryser utilized pH sensitive spacers such as N-cis- aconityl and N-maleyl to attach daunomycin to PLL[59]. The drug was triggered to release from the formulation with the pH change.

Despite the effective formation of complex with DNA and drug, PLL has major drawbacks of high toxicity and aggregation in serum solution[60, 61]. Incorporation of imidazole functionality into poly(lysine) chain reduced its toxicity sufficiently[62] , and copolmerization of PEG with PLL increased the serum stability[63]. In order to reduce the cytotoxicity and improve the release of DNA from the PLL-DNA complex, various biodegradable polylysine conjugates have been synthesized. Kim *et al*., synthesized ester-linked PLL-PEG multiblock copolymer with various ratios of histidine to improve the buffering capacity. This complex showed improved transfection and reduced cytotoxicity than the underivatized PLL along with the blood circulation time upto 3 days[64, 65].

PEI is another broadly studied delivery carrier for DNA, siRNA and wide range of oligonucleotides. It is often considered the gold standard for gene transfection. Since 1995, when PEI was demonstrated to successfully transfer oligonucleotide[66], it has been derivatized to improve the physiochemical and biological properties of polyplexes. It has been frequently used for various local siRNA delivery applications. PEI-siRNA complex was reported to selectively knockdown a pain receptor in rat when administered intrathecally[67]. Additionally, they also showed efficiency with intraperitoneal administration in the mouse model to reduce tumor growth by down regulation of human epidermal growth factor2[68]. PEI has been shown to induce cell death in a variety of cells through nercrosis and apoptosis[69, 70]. A copolymer of PEI, PEG and RGD peptide was found to inhibit simplex virus I in mice model[71, 72]. Though it showed better efficiency in delivering therapeutics, it has a major drawback of high toxicity. Strategies to reduce toxicity while retaining transfection efficiency by changing the structure of PEI agents are in development[73-75].

Natural cationic polymers such as chitosan, cyclodextrin and schizophyllan have been used as therapeutic delivery agents as they are nontoxic, biocompatible and biodegradable. Chitosan is one of the most prominent, naturally derived nonviral vectors for gene delivery. The chitosan-g-PLL polymer exihibited better DNA-binding ability, reduced cytotoxicity, and increased transfection efficiency compared to polylyisne and PEI[76]. It has been demonstrated to effectively deliver siRNA in vivo. Chitosan/siRNA nanoparticles were shown to knockdown endogeneously enhanced green fluorescent protein in bronchiole epithelial cells in mice[77]. Polyisohexylcyanoacrylate (PIHCA) nanoparticles coated with chitosan were safely used for intratumoral and intravenous delivery of RhoA-specific siRNA in mice without any toxic effect[78, 79]. Moreover, chitosan nano and microparticles were found to be very suitable for controlled release of drug molecules. Mitra *et al*., developed a chitosan encapsulated dextren-doxorubincin conjugate for targeted delivery to cancer cells[80]. Controlled release of clozapine from chitosan microparticles was demonstrated by Agnihothri *et al*.,[81]. Chitosan encapsulation of drugs hav improved therapeutic efficiency and reduced toxicity. Chitosan was also proved to have a great potential for pulmonary therapeutic delivery[82].

Cyclodextrin (CD) polymers can self-assemble with siRNA and form colloidal nanoparticle[83]. They have been used as siRNA delivery agent and has showed promising safety profile in non-human primate studies[84]. CD nanoparticle with targeting ligand transferrin and siRNA specific for EWS-FLI1 was found to successfully inhibit Ewing's sarcoma in mouse model with no evidence of toxicity or immune stimulation, when delivered systemically[85]. In addition, CD-transferin nanoparticles demonstrated efficacy in knocking down luciferase and ribonucleotide reductase genes in mice[86, 87]. A study on the

effect of CD-transferin nanoparticle on the immune system of cynomolgus monkeys by Heidel and coworker revealed that systemic dosage of targeted nanoparticle can be safely administrated multiple time in non-human primates[84]. CD nanoparticles are useful is targeting water insoluble drugs through oral or parental routes. Active components such as toxil and daunomycin are entrapped into the CD nanoparticle with loading ranging from 0.01 to 300 mg/g of nanoparticles. CD nanoparticles loaded with steroid drugs were developed by Dunchene *et al*.,[88]. In these nanoparticles, drugs were molecularly dispersed in alkyl chain hydrophobic domain and so were released very rapidly. Recent formulations of CD nanoparticles are combination of CD and modified alkyl chain dextran loaded with benzophenone and tamoxifen[89], CD and chitosan mixture nanoparticle incorporated with triclosan and furosemide for oral absorption[90], micelle-like core-shell nanospheres mediated by host–guest interactions[91]

Schizophyllan, a polysaccharide structure with potential antitumor effect, was found to bind NA through non-ionic hydrogen bond interaction[92]. Taking advantage of this ability, schizophyllan and various derivatives have been successfully used in vitro to promote CpG DNA in mammalian cell[93]. Following this schizophyllan-ovalbumin derivative complexed with CpG DNA was used to elicit antigen specific immune response in macrophage-like cell line[94]. Delivery efficiency of plasmid DNA was found to be higher with PEGylated cationic schizophyllan derivatives compared to PEI complexes[95].

4.3. Quantum Dots

Recently, quantum dots (QD) were found to be a potential gene delivery agent. In 2006, Burgess and coworkers first showed that plasmid DNA can be conjugated to QD for transfection studies[96]. Transfection study of the QD-DNA conjugate showed a maximum cellular uptake at 6 hrs. Within the cell, about 75% of the uptaken DNA was located in cytoplasam and 25% in nucleus. However, the amount of DNA in the nucleus increased with time, and after 10 hours almost 2/3 of the DNA was found in nucleus of the cell. Transfection studies of QD-DNA conjugate by Leong and Wang *et al*., showed that even after 24 hours of transfection, the complexes were found intact and localized around nucleus. After 48 hours, most of the complex were found to have released DNA[97-99]. QD was used by Bhatia *et al*., for intracellular trafficking of siRNA[98]. On conjugating the tumor targeting agent F3 peptide to QD-siRNA complex, tumor specific delivery of siRNA was attained with gene transfer promotion agent Lipofectamine 2000. In HeLa cell line, F3 peptide-QD-siRNA complex was found to knockdown ~ 29% of EGFP gene[100].

Along with therapeutic delivery, QD can also be used to image the cells. QD can be functionalized with a targeting ligand to obtain targeted drug delivery and selective cell imaging. Xie and co-workers developed a QD-aptamer conjugates to specifically recognize the mouse liver hepatoma cell line BNL 1ME A.7R.1 (MEAR)[101]. Cui *et al*., used QD-GBI-10 aptamer conjugate for specific targeting and imaging of U251 human glioblastoma cells[102]. Bagalkot *et al*., have used QD-aptamer conjugate with an anticancer drug, Doxorubicin (DOX), for prostate cancer imaging and therapy[103] **(Figure 4.2)**. The anti-prostate-specific membrane antigen (PSMA) aptamers were conjugated to QD, and Dox

was intercalated to the aptamer strands. The fluorescence of the QD and Dox were quenched by each other in the complex. Once delivered into the cell, Dox was gradually released from the system, resulting in recovery of QD and Dox fluorescence, providing a means of imaging target cells and monitoring drug delivery at the same time. Recently, Miko and coworkers developed a pH responsive QD-mucin1-aptamer-Dox (QD-MUC1-Dox) conjugate for the imaging and chemotherapy of ovarian cancer[104]. In this conjugate, Dox was attached to QD via a pH-sensitive hydrazine bond in order to provide stability of the complex for systemic circulation and drug release at acidic environment inside cancer cells. This QD-MUC1-Dox conjugate was found to have higher cytotoxicity and accumulation in ovarian tumor than free Dox and was successfully applied for in vivo imaging and treatment.

4.4. Gold Nanoparticles

Gold nanoparticles (AuNps) have recently emerged as an attractive candidate for delivery of small drug molecules or biomolecules, such as proteins, or RNA or DNA into target cells. Advantages of AuNps over polymeric nanoparticle gene delivery agents include (i) ease of preparation of mono-dispersed particles of size ranging from 1 to 150nm; (ii) non–toxicity of the gold core; (iii) easy functionalization of small molecules or nucleic acids via covalent or non-covalent interactions; and (iv) ability to release the attached drug at remote places using their photo-physical properties.

AuNps are viable nano-carriers as they possess the ability of cellular uptake[105, 106] and their surface can be easily modified for attachment of drug molecules. Drug or gene

molecules can be directly conjugated to AuNps via ionic or covalent bonding or by physical adsorption. Surface modification of AuNps plays an important role in conjugating the therapeutic molecules and in drug delivery. The nanoparticle surface can be modified with suitable conjugates to increase the circulation life time, target the drug molecule, and improve the stability of the nanoparticle and reduce cytotoxicity. One such modification that aids in improving the stability and increases the circulation life time of gold nanoparticles is the attachment of PEG. The hydrophilic nature of PEG prevents opsonization by steric hinderance, and thereby prevents the gold nanoparticles from RES clearance[107]. Several examples exist for the attachment of PEG and therapeutics to the surface of gold nanoparticles. These include: PEGylation and attachment of the anticancer platinum based therapeutic (oxaliplatin)[108], covalent attachment of PEG and PEG-tamoxifen for breast cancer therapy[109] and covalent attachment of a Pt(IV) oligonucleotide conjugate for various cancer therapeutics[110], attachment of anticancer drug doxorubicin via amino group[111], and many others.

One interesting application of gold nanoparticles for the delivery of a therapeutic includes the formation of biomimetic high density lipoprotein gold nanoparticles (HDL-AuNPs)[112, 113]. The HDL-AuNPs are formed by mixing aqueous solutions of AuNps with apolipoprotein A-1 (APOA1) to form an APOA1 wrapped AuNps. Two different phospholipids are then introduced, with one phospholipid head having an affinity for the AuNps and the other phospholipid protruding out of the surface to form a biomimetic HDL-AuNP[112]. Furthermore, cholesterylated antisense nucleic acids (Chol-NA) may be added via affinity of cholesterol attachment to the phospholipid bilayer[113]. This process and particles are shown in **Figure 4.3**. This therapeutic carrier has the possibility to deliver

nucleic acids to target cells that show specific uptake of HDL, and may be applied for diseases such as atherosclerosis, inflammation, and cancer.

Mirza and Shamshad demonstrated the conjugation of doxorubicin to AuNps via amino group by complexing to the citrate anion self-assembly on the surface of AuNps[111]. Kim *et al*., developed a delivery carrier for efficient release of drug inside cancer cells by entrapping a monolayer of hydrophobic drug on the surface of AuNps[114]. Another novel application of AuNps for drug delivery is the functionalization of the nanoparticle with an RNA aptamer that specifically targets prostate cancer cells and also loaded with doxorubicin[115]. An average of 615 ± 34 molecules of doxorubicin were loaded per nanoparticle of 29.4 ± 7.7 nm in diameter. Furthermore, the conjugated nanoparticles had cellular uptake three times more specific to targeted cells as opposed to untargeted cells. Recently, Sundaram *et al*., developed a nanocarrier by functionalizing gold nanoparticles with antibiotic drug neomycin via DNA aptamer, and demonstrated extended release of drug from the nanocarrier by temperature and affinity modulation[116]. Neomycin was bound to the DNA aptamer, and the aptamer-drug complex was conjugated to AuNps via a thiol-gold bond. Taking advantage of the temperature sensitivity of the DNA structure and the different binding affinity of neomycin to different aptamers, extended release of drug with varying rates from the nanocarrier was obtained.

Nucleic acids (NA) can be conjugated to AuNps by covalent or non-covalent interactions. In non-covalent binding method, DNAs are immobilized on AuNps by electrostatic interactions. Rotello and coworker demonstrated that the cationic quartenary amine coated AuNps can bind plasmid DNA [117, 118]. Amine surface groups are positively charged at physiological pH, and thus amine coated nanoparticles can interact with the

negatively charged nucleic acids. Additionally, this nanoparticle complex was shown to protect DNA from enzymatic digestion[119], and deliver DNA to 293T cells with a transfection efficiency ~ 8 folds greater than the commonly used cationic tranfection agent PEI[117]. The researchers have also demonstrated that the nanoparticle complex mediated gene delivery depends on the ratio of positively charged amine to the negatively charged phosphate of DNA, and also on the relative length of surface-bound uncharged thiol chain. Later on, Kilbavon *et al*., formed a hybrid AuNps-polymer transfection vector by coating AuNps surface with 2 kDa PEI[120]. This hybrid vector was found to successfully deliver plasmid DNA into monkey kidney (Cos-7) cells. The transfection efficiency was observed to vary with the PEI:gold molar ratio in the conjugate. The vector with the optimized ratio of PEI:gold was found to deliver plasmid into Cos-7 cells with an efficiency ~ 12 folds more than the polymer itself. Following this, Liu *et al*., developed a delivery vector by anchoring b-cyclodextrin on the periphery of oligo(ethylenediamino)-modified AuNps. This polymer-AuNps-DNA complex was found to successfully deliver plasmid DNA into breast cancer cell (MCF-7). Recently, lysine functionalized AuNps was demonstrated to deliver DNA plasmid with very high efficiency, and outperform a commercial vector by a factor of 28[121].

NA strands could be easily modified with thiol (-SH) and can be grafted on AuNps by thiol-gold covalent interactions. Many researchers worked on understanding the properties of DNA functionalized AuNps. An unusual ability of DNA-AuNps is their ability to bind complementary nucleic acids with a high affinity. The polyvalent particles exhibit binding constant as large as two orders of magnitude greater than the analogous molecular oligonucleotide of same sequence[122]. This property is likely due to dense

packing and high local concentration of oligonucleotide on the gold surface[123, 124]. Another important property of DNA-AuNps complex is their resistance to degradation by enzymes such as DNase I[125]**.** This phenomenon was experimentally proved to be due to (i) dense packing of oligonucleotide on AuNps which could lead to steric inhibition of enzyme binding and cleavage of DNA; (ii) high local ion concentration which screens the densely packed DNA, as it is known that high concentration of Na^+ ion reduces enzyme activity[126, 127]. This property of resistance to enzymatic degradation makes NA-AuNps complex a promising candidate for introducing nucleic acid into cells.

Furthermore, AuNps have also been demonstrated as potential siRNA delivery carrier. Lee *et al*., developed amine coated AuNps for the intracellular delivery of siRNA[128]. The positively charged AuNps could form stable electrostatic interactions with the negatively charged siRNA-PEG conjugates having cleavable disulfide linkages. The resulting nanostructure has a PEG protective layer preventing aggregation, there by promoting endocytosis. The nanostructure was observed to be efficiently internalized into human prostate carcinoma cells without severe cytotoxicity. Similarly, Anderson and coworkers developed poly-β-amino ester (PBAE) functionalized AuNps for siRNA delivery[129]. In this synthesis, the AuNps were modified with SH-PEG-NH_2 and the complex was functionalized with N-succinimidyl 3-(2pyridyldithio)propionate (SPDP). Then thiolated siRNA (antifirefly luciferase) was conjugated to SPDP-PEG-AuNps by displacing 2-pyridyldithio group of SPDP. A maximum of ~40 siRNA strands were conjugated per particle. The siRNA-SPDP-PEG-AuNps complex was then complexed with PBAE (**Figure 4.4)**. The resulting nanocomplex was demonstrated to selectively knockdown firefly luciferase expression in HeLa cells after incubating for 24 hours,

depending on the type and dosage of PBAEs. These nanocomplexes demonstrated better gene delivery efficiency than the commercially available liposome-based delivery carrier (Lipofectamine 2000, Invitrogen), without any significant toxicity. Recently, Tung and coworkers have developed a layer by layer assembly of protease degradable poly-L-lysine (PLL) and siRNA on AuNps[130]. The AuNp is coated with 4 layers of PLL and 3 layers of siRNA via charge-charge interactions. Slow degradation of PLL by proteases facilitated the gradual release of siRNA and extended gene silencing effect. Kong *et al*., developed a siRNA delivery complex by crosslinking thiolated siRNA using 5nm AuNPs via Au-S chemisorption. The crosslinked multimer was later complexed with linear polyethylenimine (L-PEI). The resultant complex possessed high enzymatic stability and exhibited much higher gene silencing of green fluorescent protein and vascular endothelial growth factor than naked siRNA. Along with the efficient gene silencing, the complex also demonstrated the ability to be visualized by micro-CT providing simultaneous gene silencing and imaging[131].

The cellular uptake of AuNps has been well studied by various research groups. Chan and coworkers determined the influence of particle size on cellular internalization[132]. Their study revealed that the time for which AuNps remain inside the cell is independent of size of the particle. The maximum number of AuNps of diameter 14, 50, and 74 nm internalized per HeLa cell were 3000, 6160, and 2988, respectively, which showed that the optimum size of the particle for maximum internalization is 50nm. Investigation on the cellular uptake mechanism of AuNps showed that the citrate-capped nanoparticle complexes with the positively charged proteins, such as transferrin, and enters the cell through clathrin-mediated endocytosis[133, 134].

Conjugation of ligands to AuNps has been shown to increase cellular uptake ability[135], alter intercellular localization[136], and impart cellular response affecting functionality[125]. For example, citrate coated AuNps functionalized with thiol modified DNA facilitated the cellular uptake of the particles. The number of particles internalized by cells depended on the cell type, concentration, incubation time, and most importantly on the density of DNA on the surface of AuNps. For about 60 DNA strands per particle, the cellular uptake can exceed 1 x 10^6AuNps per cell. It has been hypothesized that with the increase in DNA density, the ability to bind more protein increases, and thereby the cellular uptake increases[137]. The DNA density on AuNps in turn depends upon salt concentration, DNA concentration, and the radius of curvature of the particle[138].

Toxicity of AuNps has been extensively studied. In a study with the human dermal fibroblast, Pernodet *et al*., demonstrated that the presence of AuNps slowed the rate of cell proliferation, spreading, and adhesion. The cause for this effect was proven to be actin stress[139]. Another *in vitr*o study of lung fibroblasts demonstrated that the presence of AuNps decreased cell growth by oxidative damage[140]. Similar results have also been reported when similar particles were used in myeloma cells[141]. However, the acute and gross toxicity was not observed in any of these studies. Interestingly, the toxicity of AuNps has been found to depend on the size of the particle. AuNps of diameter 1.4 nm were found to be toxic, whereas 15 nm diameter AuNps were nontoxic, even up to 100 fold higher concentration. The toxicity of 1.4 nm AuNps was proven to be the result of necrosis[142]. The toxicity of ligand functionalized AuNps depend upon the ligand itself. No toxicity was observed with DNA functionalized AuNps[125].

4.5. Clinical Trial

Of all the nanocarriers discussed in this chapter, liposomes are the most developed and currently possess the greatest amount of clinical trials with some formulations currently in the market. This is probably due to the fact that the other materials discussed within this paper have not been investigated for the same duration and are relatively new in comparison. For this reason, polymer based materials, and AuNps should not be overlooked as nanomedicine delivery materials just because of the relatively low number of recent clinical trials.

Recent clinical trials are shown in Table 4.1. Some of the more promising trials include Genexol-PM, which is an amphiphilic diblock copolymer (PEG-(D,L-lactic acid)) forming a micelle that delivers Paclitaxel for various types of cancers. Clinical trials are currently in phase 4 using Genexol–PM for recurrent breast cancer and phase 3 for breast cancer. The liposomal formulation AmBiosome® consisting of the antifungal Amphotericin B is currently in phase 4 trials for fungal infections associated with acute leukemia and for central line fungal infections. ThermoDox, a thermally sensitive doxorubicin-loaded liposome is currently in phase 3 trials for hepatocellular carcinoma. Lastly, Caelyx, a doxorubicin HCL loaded liposome that is PEGylated, is currently in phase 4 trials for ovarian neoplasms.

Additionally, many trials are using a combinational therapy consisting of two different types of therapeutics. Increased efficacy from combination therapy may be due to the increased cellular uptake of one therapy combined with the superior endosomal escape mechanism of the other therapy, along with separate underlined mechanisms used by

various agents to attack cancer cells. A common combination utilizes one therapeutic that is effective at stopping the cell division cycle along with a therapeutic that is effective at causing carcinoma cell death, thus attacking current cells and stopping the cell proliferation cycle. Combined therapies from clinicaltrials.gov are listed in Table 4.2. The vast majority of combination therapies contain doxorubicin-loaded liposomes along with an adjacent therapeutic. The later phase trials for combined therapies include a phase 3 trial for ovarian cancer using PEGylated liposomal doxorubicin and EC145—an anticancer therapeutic and a phase 3 trial for Aspergillosis using AmBiosome® and anidulafungin.

4.6. Conclusions

All therapeutic agents optimally requires drug delivery and targeting mechanism to be delivered to the affected cells without reducing their therapeutic efficiency. An efficient delivery carrier would lead to a new era of medicine where drugs will have high bioavailability, less toxicity and high efficacy. Nanoparticles because of their versatility in structural and physiochemical properties, sustained release properties, biocompatibility with tissues appears to be very promising drug delivery system. In this chapter, we have discussed about various materials including liposomes, cationic polymers, quantum dots and AuNps as potential drug delivery nano-carriers. These nano-carriers are being actively researched with an interest to develop an efficient therapeutic delivery carrier through advances in both material/structural design and cellular targeting. Although liposome is the only material that is being intensively researched in clinical level, other nano-carrier materials discussed in this chapter also holds great potential that cannot be overlooked.

Thus we can safely say that in the next decade more nano-carrier other than liposomes will be making their way into clinical trials, and very soon we might land on a nano-carrier that could bring a huge change into the current treatment regime.

4.7. References

1. Alexis F, Pridgen E, Molnar LK, Farokhzad OC. Factors Affecting the Clearance and Biodistribution of Polymeric Nanoparticles. Molecular Pharmaceutics. 2008;5: 505-515.

2. Whitehead KA, Langer R, Anderson DG. Knocking Down Barriers: Advances in siRNA Delivery. Nature Reviews Drug Discovery. 2009;8: 129-138.

3. Zámeènik J, Vargová L, Homola A, Kodet R, Syková E. Extracellular Matrix Glycoproteins and Diffusion Barriers in Human Astrocytic Tumours. Neuropathology & Applied Neurobiology. 2004;30: 338-350.

4. Di Guglielmo GM, Le Roy C, Goodfellow AF, Wrana JL. Distinct Endocytic Pathways Regulate TGF-[Beta] Receptor Signalling And Turnover. Nature Cell Biology. 2003;5: 410-421.

5. Torchilin VP, Levchenko TS, Rammohan R, Volodina N, Papahadjopoulos-Sternberg B, D'Souza GGM. Cell Transfection In Vitro and In Vivo with Nontoxic TAT Peptide-Liposome–DNA Complexes. Proceedings of the National Academy of Sciences. 2003;100: 1972-1977.

6. Auguste DT, Furman K, Wong A, et al. Triggered Release of siRNA from Poly(ethylene glycol)-Protected, pH-Dependent Liposomes. Journal of Controlled Release. 2008;130: 266-274.

7. Rappaport J, Hanss B, Kopp JB, et al. Transport of Phosphorothioate Oligonucleotides in Kidney: Implications for Molecular Therapy. Kidney Int. 1995;47: 1462-1469.

8. McNamara JO, Andrechek ER, Wang Y, et al. Cell Type-Specific Delivery of siRNAs with Aptamer-siRNA Chimeras. Nature Biotechnology. 2006;24: 1005-1015.

9. Takei Y, Kadomatsu K, Yuzawa Y, Matsuo S, Muramatsu T. A Small Interfering RNA Targeting Vascular Endothelial Growth Factor as Cancer Therapeutics. Cancer Research. 2004;64: 3365-3370.

10. Song E, Zhu P, Lee S-K, et al. Antibody Mediated In Vivo Delivery of Small Interfering RNAs via Cell-Surface Receptors. Nature Biotechnology. 2005;23: 709-717.

11. Peer D, Park EJ, Morishita Y, Carman CV, Shimaoka M. Systemic Leukocyte-Directed siRNA Delivery Revealing Cyclin D1 as an Anti-Inflammatory Target. Science. 2008;319: 627-630.

12. Mufamadi MS, Pillay V, Choonara YE, et al. A Review on Composite Liposomal Technologies for Specialized Drug Delivery. Journal of drug delivery. 2011; 1-19.

13. Lian T, Ho RJY. Trends and Developments in Liposome Drug Delivery Systems. Journal of Pharmaceutical Sciences. 2001;90: 667-680.

14. Felgner PL, Gadek TR, Holm M, et al. Lipofection: A Highly Efficient, Lipid-Mediated DNA-Transfection Procedure. Proceedings of the National Academy of Sciences. 1987;84: 7413-7417.

15. Malone RW, Felgner PL, Verma IM. Cationic Liposome-Mediated RNA Transfection. Proceedings of the National Academy of Sciences. 1989;86: 6077-6081.

16. Gebeyehu G, Jessee JA, Ciccarone VC, Nelson PH, Chytil A. Cationic Lipids. In: Patent US, editor. United States: Life Technology.Inc, 1994.

17. Stamatatos L, Leventis R, Zuckermann MJ, Silvius JR. Interactions of Cationic Lipid Vesicles with Negatively Charged Phospholipid Vesicles and Biological Membranes. Biochemistry. 1988;27: 3917-3925.

18. Behr JP, Demeneix B, Loeffler JP, Perez-Mutul J. Efficient Gene Transfer into Mammalian Primary Endocrine Cells with Lipopolyamine-Coated DNA. Proceedings of the National Academy of Sciences. 1989;86: 6982-6986.

19. Bennett MJ, Aberle AM, Balasubramaniam RP, Malone JG, Malone RW, Nantz MH. Cationic Lipid-Mediated Gene Delivery to Murine Lung: Correlation of Lipid Hydration with in Vivo Transfection Activity. Journal of Medicinal Chemistry. 1997;40: 4069-4078.

20. Felgner JH, Kumar R, Sridhar CN, et al. Enhanced Gene Delivery and Mechanism Studies with A Novel Series of Cationic Lipid Formulations. Journal of Biological Chemistry. 1994;269: 2550-2561.

21. Majeti BK, Karmali PP, Reddy BS, Chaudhuri A. In Vitro Gene Transfer Efficacies of N,N-Dialkylpyrrolidinium Chlorides: A Structure−Activity Investigation. Journal of Medicinal Chemistry. 2005;48: 3784-3795.

22. Takahashi T, Hirose J, Kojima C, Harada A, Kono K. Synthesis of Poly(amidoamine) Dendron-Bearing Lipids with Poly(ethylene glycol) Grafts and Their Use for Stabilization of Nonviral Gene Vectors. Bioconjugate Chemistry. 2007;18: 1163-1169.

23. Desigaux L, Sainlos M, Lambert O, et al. Self-Assembled Lamellar Complexes Of siRNA With Lipidic Aminoglycoside Derivatives Promote Efficient siRNA Delivery and Interference. Proceedings of the National Academy of Sciences. 2007;104: 16534-16539.

24. Prata CAH, Zhang X-X, Luo D, McIntosh TJ, Barthelemy P, Grinstaff MW. Lipophilic Peptides for Gene Delivery. Bioconjugate Chemistry. 2008;19: 418-420.

25. Guy-Caffey JK, Bodepudi V, Bishop JS, Jayaraman K, Chaudhary N. Novel Polyaminolipids Enhance the Cellular Uptake of Oligonucleotides. Journal of Biological Chemistry. 1995;270: 31391-31396.

26. Choi JS, Lee EJ, Jang HS, Park JS. New Cationic Liposomes for Gene Transfer into Mammalian Cells with High Efficiency and Low Toxicity. Bioconjugate Chemistry. 2001;12: 108-113.

27. Aissaoui A, Oudrhiri N, Petit L, et al. Progress in Gene Delivery by Cationic Lipids : Guanidinium-Cholesterol-Based Systems as an Example. Current Drug Targets. 2002;3: 1.

28. Fujiwara T, Hasegawa S, Hirashima N, Nakanishi M, Ohwada T. Gene Transfection Activities of Amphiphilic Steroid-Polyamine Conjugates. Biochimica et Biophysica Acta (BBA) - Biomembranes. 2000;1468: 396-402.

29. Boomer J, Thompson D, Sullivan S. Formation of Plasmid-Based Transfection Complexes with an Acid-Labile Cationic Lipid: Characterization of In Vitro and In Vivo Gene Transfer. Pharmaceutical Research. 2002;19: 1292-1301.

30. Zhu M-Z, Wu Q-H, Zhang G, Ren T, Liu D, Guo Q-X. Synthesis and Evaluation of Cationic Lipids Bearing Cholesteryl Groups for Gene Delivery In Vitro. Bulletin of the Chemical Society of Japan. 2001;75: 2207-2213.

31. Zhu J, Munn RJ, Nantz MH. Self-Cleaving Ortho Ester Lipids: A New Class of pH-Vulnerable Amphiphiles. Journal of the American Chemical Society. 2000;122: 2645-2646.

32. Choi JS, MacKay JA, Szoka FC. Low-pH-Sensitive PEG-Stabilized Plasmid−Lipid Nanoparticles: Preparation and Characterization. Bioconjugate Chemistry. 2003;14: 420-429.

33. Chen H, Zhang H, McCallum CM, Szoka FC, Guo X. Unsaturated Cationic Ortho Esters for Endosome Permeation in Gene Delivery. Journal of Medicinal Chemistry. 2007;50: 4269-4278.

34. Aissaoui A, Martin B, Kan E, et al. Novel Cationic Lipids Incorporating an Acid-Sensitive Acylhydrazone Linker: Synthesis and Transfection Properties. Journal of Medicinal Chemistry. 2004;47: 5210-5223.

35. Tang F, Hughes JA. Introduction of a Disulfide Bond into a Cationic Lipid Enhances Transgene Expression of Plasmid DNA. Biochemical and Biophysical Research Communications. 1998;242: 141-145.

36. Byk G, Wetzer B, Frederic M, et al. Reduction-Sensitive Lipopolyamines as a Novel Nonviral Gene Delivery System for Modulated Release of DNA with Improved Transgene Expression. Journal of Medicinal Chemistry. 2000;43: 4377-4387.

37. Chittimalla C, Zammut-Italiano L, Zuber G, Behr J-P. Monomolecular DNA Nanoparticles for Intravenous Delivery of Genes. Journal of the American Chemical Society. 2005;127: 11436-11441.

38. Jeffs LB, Palmer LR, Ambegia EG, Giesbrecht C, Ewanick S, MacLachlan I. A Scalable, Extrusion-Free Method for Efficient Liposomal Encapsulation of Plasmid DNA. Pharmaceutical Research. 2005;22: 362-372.

39. Zimmermann TS, Lee ACH, Akinc A, et al. RNAi-Mediated Gene Silencing in Non-Human Primates. Nature. 2006;441: 111-114.

40. Morrissey DV, Lockridge JA, Shaw L, et al. Potent and Persistent In Vivo Anti-HBV Activity of Chemically Modified siRNAs. Nature Biotechnology. 2005;23: 1002-1007.

41. Geisbert TW, Hensley LE, Kagan E, et al. Postexposure Protection of Guinea Pigs against a Lethal Ebola Virus Challenge Is Conferred by RNA Interference. Journal of Infectious Diseases. 2006;193: 1650-1657.

42. Li J, Chen Y-C, Tseng Y-C, Mozumdar S, Huang L. Biodegradable Calcium Phosphate Nanoparticle with Lipid Coating for Systemic siRNA Delivery. Journal of Controlled Release. 2010;142: 416-421.

43. Villares GJ, Zigler M, Wang H, et al. Targeting Melanoma Growth and Metastasis with Systemic Delivery of Liposome-Incorporated Protease-Activated Receptor-1 Small Interfering RNA. Cancer Research. 2008;68: 9078-9086.

44. Katanasaka Y, Ishii T, Asai T, et al. Cancer Antineovascular Therapy with Liposome Drug Delivery Systems Targeted to BiP/GRP78. International Journal of Cancer. 2010;127: 2685-2698.

45. Williams J, Lansdown R, Sweitzer R, et al. Nanoparticle Drug Delivery System for Intravenous Delivery of Topoisomerase Inhibitors. Journal of Controlled Release. 2003;91: 167-172.

46. Tang J, Wei H, Liu H, et al. Pharmacokinetics and Biodistribution of Itraconazole in Rats and Mice Following Intravenous Administration in A Novel Liposome Formulation. Drug Delivery. 2010;17: 223-230.

47. Lentacker I, Geers B, Demeester J, De Smedt SC, Sanders NN. Design and Evaluation of Doxorubicin-containing Microbubbles for Ultrasound-triggered Doxorubicin Delivery: Cytotoxicity and Mechanisms Involved. Molecular Therapy. 2009;18: 101-108.

48. Etzerodt A, Maniecki MB, Graversen JH, Moller HJ, Torchilin VP, Moestrup SK. Efficient Intracellular Drug-Targeting Of Macrophages Using Stealth Liposomes Directed

to the Hemoglobin Scavenger Receptor CD163. Journal of Controlled Release. 2012;160: 72-80.

49. Perez AT, Domenech GH, Frankel C, Vogel CL. Pegylated Liposomal Doxorubicin (Doxil®) for Metastatic Breast Cancer: The Cancer Research Network, Inc., Experience. Cancer Investigation. 2002;20: 22-29.

50. O'Shaughnessy JA. Pegylated Liposomal Doxorubicin in the Treatment of Breast Cancer. Clinical Breast Cancer. 2003;4: 318-328.

51. Symon Z, Peyser A, Tzemach D, et al. Selective Delivery of Doxorubicin to Patients with Breast Carcinoma Metastases by Stealth Liposomes. Cancer. 1999;86: 72-78.

52. Rust DM, Jameson G. The Novel Lipid Delivery System of Amphotericin B: Drug Profile and Relevance to Clinical Practice. Oncology Nursing Forum. 1998;25: 35-48.

53. Chang H-I, Yeh M-K. Clinical Development of Liposome-Based Drugs: Formulation, Characterization, and Therapeutic Efficacy. International Journal of Nanomedicine. 2012;7: 49.

54. Akhtar S, Benter IF. Nonviral Delivery of Synthetic siRNAs In Vivo. The Journal of Clinical Investigation. 2007;117: 3623-3632.

55. Laemmli UK. Characterization of DNA Condensates Induced by Poly(ethylene oxide) andPpolylysine. Proceedings of the National Academy of Sciences. 1975;72: 4288-4292.

56. Wu GY, Wu CH. Receptor-Mediated in Vitro Gene Transformation by A Soluble DNA Carrier System. Journal of Biological Chemistry. 1987;262: 4429-4432.

57. Wu GY, Wu CH. Receptor-Mediated Gene Delivery and Expression In Vivo. Journal of Biological Chemistry. 1988;263: 14621-14624.

58. Akinc A, Langer R. Measuring The pH Environment of DNA Delivered using Nonviral Vectors: Implications for Lysosomal Trafficking. Biotechnology and Bioengineering. 2002;78: 503-508.

59. Shen W-C, Ryser HJP. Cis-aconityl Spacer between Daunomycin and Macromolecular Carriers: A Model of pH-Sensitive Linkage Releasing Drug from a Lysosomotropic Conjugate. Biochemical and Biophysical Research Communications. 1981;102: 1048-1054.

60. Choi YH, Liu F, Kim J-S, Choi YK, Jong Sang P, Kim SW. Polyethylene Glycol-Grafted Poly--Lysine as Polymeric Gene Carrier. Journal of Controlled Release. 1998;54: 39-48.

61. Liu G, Molas M, Grossmann GA, et al. Biological Properties of Poly-l-lysine-DNA Complexes Generated by Cooperative Binding of the Polycation. Journal of Biological Chemistry. 2001;276: 34379-34387.

62. Putnam D, Gentry CA, Pack DW, Langer R. Polymer-Based Gene Delivery with Low Cytotoxicity by A Unique Balance of Side-Chain Termini. Proceedings of the National Academy of Sciences. 2001;98: 1200-1205.

63. Wolfert MA, Schacht EH, Toncheva V, Ulbrich K, Nazarova O, Seymour LW. Characterization of Vectors for Gene Therapy Formed by Self-Assembly of DNA with Synthetic Block Co-Polymers. Human Gene Therapy. 1996;7: 2123-2133.

64. Bikram M, Ahn C-H, Chae SY, Lee M, Yockman JW, Kim SW. Biodegradable Poly(ethylene glycol)-co-poly(l-lysine)-g-histidine Multiblock Copolymers for Nonviral Gene Delivery. Macromolecules. 2004;37: 1903-1916.

65. Bikram M, Lee M, Chang C-W, Janát-Amsbury M-M, Kern SE, Kim SW. Long-Circulating DNA-Complexed Biodegradable Multiblock Copolymers for Gene Delivery: Degradation Profiles and Evidence of Dysopsonization. Journal of Controlled Release. 2005;103: 221-233.

66. Boussif O, Lezoualc'h F, Zanta MA, et al. A Versatile Vector for Gene and Oligonucleotide Transfer into Cells in Culture and In Vivo: Polyethylenimine. Proceedings of the National Academy of Sciences. 1995;92: 7297-7301.

67. Tan PH, Yang LC, Shih HC, Lan KC, Cheng JT. Gene Knockdown with Intrathecal siRNA of NMDA Receptor NR2B Subunit Reduces Formalin-Induced Nociception in the Rat. Gene Therapy. 2004;12: 59-66.

68. Urban-Klein B, Werth S, Abuharbeid S, Czubayko F, Aigner A. RNAi-Mediated Gene-Targeting Through Systemic Application of Polyethylenimine (PEI)-Complexed siRNA in Vivo. Gene Therapy. 2004;12: 461-466.

69. Boeckle S, von Gersdorff K, van der Piepen S, Culmsee C, Wagner E, Ogris M. Purification of Polyethylenimine Polyplexes Highlights the Role of Free Polycations in Gene Transfer. The Journal of Gene Medicine. 2004;6: 1102-1111.

70. Hunter AC. Molecular Hurdles in Polyfectin Design and Mechanistic Background to Polycation Induced Cytotoxicity. Advanced Drug Delivery Reviews. 2006;58: 1523-1531.

71. Kim B, Tang Q, Biswas PS, et al. Inhibition of Ocular Angiogenesis by siRNA Targeting Vascular Endothelial Growth Factor Pathway Genes: Therapeutic Strategy for Herpetic Stromal Keratitis. The American journal of pathology. 2004;165: 2177-2185.

72. Schiffelers RM, Storm G. ICS-283: a System for Targeted Intravenous Delivery of siRNA. Expert Opinion on Drug Delivery. 2006;3: 445-454.

73. Richards Grayson A, Doody A, Putnam D. Biophysical and Structural Characterization of Polyethylenimine-Mediated siRNA Delivery In Vitro. Pharmaceutical Research. 2006;23: 1868-1876.

74. Thomas M, Lu JJ, Ge Q, Zhang C, Chen J, Klibanov AM. Full Deacylation of Polyethylenimine Dramatically Boosts its Gene Delivery Efficiency and Specificity to Mouse Lung. Proceedings of the National Academy of Sciences. 2005;102: 5679-5684.

75. Werth S, Urban-Klein B, Dai L, et al. A Low Molecular Weight Fraction Of Polyethylenimine (PEI) Displays Increased Transfection Efficiency of DNA and siRNA in Fresh or Lyophilized Complexes. Journal of Controlled Release. 2006;112: 257-270.

76. Mintzer MA, Simanek EE. Nonviral Vectors for Gene Delivery. Chemical Reviews. 2008;109: 259-302.

77. Howard KA, Rahbek UL, Liu X, et al. RNA Interference in Vitro and in Vivo Using a Chitosan/siRNA Nanoparticle System. Molecular Therapy. 2006;14: 476-484.

78. De Martimprey H, Bertrand J-R, Fusco A, et al. siRNA Nanoformulation Against the Ret/PTC1 Junction Oncogene is Efficient in an In Vivo Model of Papillary Thyroid Carcinoma. Nucleic Acids Research. 2008;36: e2.

79. Pillé JY, Li H, Blot E, et al. Intravenous Delivery of Anti-RhoA Small Interfering RNA Loaded in Nanoparticles of Chitosan in Mice: Safety and Efficacy in Xenografted Aggressive Breast Cancer. Human Gene Therapy. 2006;17: 1019-1026.

80. Mitra S, Gaur U, Ghosh PC, Maitra AN. Tumour Targeted Delivery of Encapsulated Dextran–Doxorubicin Conjugate Using Chitosan Nanoparticles as Carrier. Journal of Controlled Release. 2001;74: 317-323.

81. Agnihotri SA, Aminabhavi TM. Controlled Release of Clozapine Through Chitosan Microparticles Prepared by a Novel Method. Journal of Controlled Release. 2004;96: 245-259.

82. Okamoto H, Nishida S, Todo H, Sakakura Y, Iida K, Danjo K. Pulmonary Gene Delivery by Chitosan–PDNA Complex Powder Prepared by a Supercritical Carbon Dioxide Process. Journal of Pharmaceutical Sciences. 2003;92: 371-380.

83. Davis ME, Pun SH, Bellocq NC, et al. Self-Assembling Nucleic Acid Delivery Vehicles via Linear, Water-Soluble, Cyclodextrin-Containing Polymers. Current Medicinal Chemistry. 2004;11: 179-197.

84. Heidel JD, Yu Z, Liu JY-C, et al. Administration in Non-Human Primates of Escalating Intravenous Doses of Targeted Nanoparticles Containing Ribonucleotide Reductase

Subunit M2 siRNA. Proceedings of the National Academy of Sciences. 2007;104: 5715-5721.

85. Hu-Lieskovan S, Heidel JD, Bartlett DW, Davis ME, Triche TJ. Sequence-Specific Knockdown of EWS-FLI1 by Targeted, Nonviral Delivery of Small Interfering RNA Inhibits Tumor Growth in a Murine Model of Metastatic Ewing's Sarcoma. Cancer Research. 2005;65: 8984-8992.

86. Bartlett DW, Su H, Hildebrandt IJ, Weber WA, Davis ME. Impact of Tumor-Specific Targeting on the Biodistribution and Efficacy of Sirna Nanoparticles Measured by Multimodality In Vivo Imaging. Proceedings of the National Academy of Sciences. 2007;104: 15549-15554.

87. Bartlett DW, Davis ME. Impact of Tumor-Specific Targeting and Dosing Schedule on Tumor Growth Inhibition After Intravenous Administration of siRNA-Containing Nanoparticles. Biotechnology and Bioengineering. 2008;99: 975-985.

88. Laza-Knoerr A, Gref R, Couvreur P. Cyclodextrins for Drug Delivery. Journal of Drug Targeting. 2010;18: 645-656.

89. Gref R, Amiel C, Molinard K, et al. New Self-Assembled Nanogels Based on Host–Guest Interactions: Characterization and Drug Loading. Journal of Controlled Release. 2006;111: 316-324.

90. Maestrelli F, Garcia-Fuentes M, Mura P, Alonso MJ. A New Drug Nanocarrier Consisting of Chitosan and Hydoxypropylcyclodextrin. European Journal of Pharmaceutics and Biopharmaceutics. 2006;63: 79-86.

91. Zhang J, Ma PX. Polymeric Core–Shell Assemblies Mediated by Host–Guest Interactions: Versatile Nanocarriers for Drug Delivery. Angewandte Chemie International Edition. 2009;48: 964-968.

92. Tabata K, Ito W, Kojima T, Kawabata S, Misaki A. Ultrasonic Degradation of Schizophyllan, an Antitumor Polysaccharide Produced by Schizophyllum Commune Fries. Carbohydrate Research. 1981;89: 121-135.

93. Mizu M, Koumoto K, Anada T, et al. A Polysaccharide Carrier for Immunostimulatory CpG DNAs To Enhance Cytokine Secretion‖. Journal of the American Chemical Society. 2004;126: 8372-8373.

94. Shimada N, Ishii KJ, Takeda Y, et al. Synthesis and in Vitro Characterization of Antigen-Conjugated Polysaccharide as a CpG DNA Carrier. Bioconjugate Chemistry. 2006;17: 1136-1140.

95. Nagasaki T, Hojo M, Uno A, et al. Long-Term Expression with a Cationic Polymer Derived from a Natural Polysaccharide: Schizophyllan. Bioconjugate Chemistry. 2004;15: 249-259.

96. Srinivasan C, Lee J, Papadimitrakopoulos F, Silbart LK, Zhao M, Burgess DJ. Labeling and Intracellular Tracking of Functionally Active Plasmid DNA with Semiconductor Quantum Dots. Molecular Therapy. 2006;14: 192-201.

97. Ho Y-P, Chen HH, Leong KW, Wang T-H. Evaluating the Intracellular Stability And Unpacking of DNA Nanocomplexes by Quantum Dots-FRET. Journal of Controlled Release. 2006;116: 83-89.

98. Chen AA, Derfus AM, Khetani SR, Bhatia SN. Quantum Dots to Monitor RNAi Delivery and Improve Gene Silencing. Nucleic Acids Research. 33: e190.

99. Chen HH, Ho Y-P, Jiang X, Mao H-Q, Wang T-H, Leong KW. Quantitative Comparison of Intracellular Unpacking Kinetics of Polyplexes by a Model Constructed From Quantum Dot-FRET. Molecular Therapy. 2008;16: 324-332.

100. Derfus AM, Chen AA, Min D-H, Ruoslahti E, Bhatia SN. Targeted Quantum Dot Conjugates for siRNA Delivery. Bioconjugate Chemistry. 2007;18: 1391-1396.

101. Zhang J, Jia X, Lv X-J, Deng Y-L, Xie H-Y. Fluorescent Quantum Dot-Labeled Aptamer Bioprobes Specifically Targeting Mouse Liver Cancer Cells. Talanta. 2010;81: 505-509.

102. Li Z, Huang P, He R, et al. Aptamer-Conjugated Dendrimer-Modified Quantum Dots for Cancer Cell Targeting and Imaging. Materials Letters. 2010;64: 375-378.

103. Bagalkot V, Zhang L, Levy-Nissenbaum E, et al. Quantum Dot−Aptamer Conjugates for Synchronous Cancer Imaging, Therapy, and Sensing of Drug Delivery Based on Bi-Fluorescence Resonance Energy Transfer. Nano Letters. 2007;7: 3065-3070.

104. Savla R, Taratula O, Garbuzenko O, Minko T. Tumor Targeted Quantum Dot-Mucin 1 Aptamer-Doxorubicin Conjugate for Imaging And Treatment of Cancer. Journal of Controlled Release. 2011;153: 16-22.

105. Connor EE, Mwamuka J, Gole A, Murphy CJ, Wyatt MD. Gold Nanoparticles Are Taken Up by Human Cells but Do Not Cause Acute Cytotoxicity. Small. 2005;1: 325-327.

106. Male KB, Lachance B, Hrapovic S, Sunahara G, Luong JHT. Assessment of Cytotoxicity of Quantum Dots and Gold Nanoparticles Using Cell-Based Impedance Spectroscopy. Analytical Chemistry. 2008;80: 5487-5493.

107. Dobrovolskaia MA, Aggarwal P, Hall JB, McNeil SE. Preclinical Studies To Understand Nanoparticle Interaction with the Immune System and Its Potential Effects on Nanoparticle Biodistribution. Molecular Pharmaceutics. 2008;5: 487-495.

108. Brown SD, Nativo P, Smith J-A, et al. Gold Nanoparticles for the Improved Anticancer Drug Delivery of the Active Component of Oxaliplatin. Journal of the American Chemical Society. 2010;132: 4678-4684.

109. Dreaden EC, Mwakwari SC, Sodji QH, Oyelere AK, El-Sayed MA. Tamoxifen−Poly(ethylene glycol)−Thiol Gold Nanoparticle Conjugates: Enhanced Potency and Selective Delivery for Breast Cancer Treatment. Bioconjugate Chemistry. 2009;20: 2247-2253.

110. Dhar S, Daniel WL, Giljohann DA, Mirkin CA, Lippard SJ. Polyvalent Oligonucleotide Gold Nanoparticle Conjugates as Delivery Vehicles for Platinum(IV) Warheads. Journal of the American Chemical Society. 2009;131: 14652-14653.

111. Mirza AZ, Shamshad H. Preparation and Characterization of Doxorubicin Functionalized Gold Nanoparticles. European Journal of Medicinal Chemistry. 2011;46: 1857-1860.

112. Thaxton CS, Daniel WL, Giljohann DA, Thomas AD, Mirkin CA. Templated Spherical High Density Lipoprotein Nanoparticles. Journal of the American Chemical Society. 2009;131: 1384-1385.

113. McMahon KM, Mutharasan RK, Tripathy S, et al. Biomimetic High Density Lipoprotein Nanoparticles For Nucleic Acid Delivery. Nano Letters. 2011;11: 1208-1214.

114. Kim CK, Ghosh P, Pagliuca C, Zhu Z-J, Menichetti S, Rotello VM. Entrapment of Hydrophobic Drugs in Nanoparticle Monolayers with Efficient Release into Cancer Cells. Journal of the American Chemical Society. 2009;131: 1360-1361.

115. Kim D, Jeong YY, Jon S. A Drug-Loaded Aptamer−Gold Nanoparticle Bioconjugate for Combined CT Imaging and Therapy of Prostate Cancer. ACS Nano. 2010;4: 3689-3696.

116. Sundaram P, Wower J, Byrne ME. A Nanoscale Drug Delivery Carrier Using Nucleic Acid Aptamers for Extended Release of Therapeutic. Nanomedicine: Nanotechnology, Biology and Medicine. 2012;8: 1143-1151.

117. Sandhu KK, McIntosh CM, Simard JM, Smith SW, Rotello VM. Gold Nanoparticle-Mediated Transfection of Mammalian Cells. Bioconjugate Chemistry. 2001;13: 3-6.

118. McIntosh CM, Esposito EA, Boal AK, Simard JM, Martin CT, Rotello VM. Inhibition of DNA Transcription Using Cationic Mixed Monolayer Protected Gold Clusters. Journal of the American Chemical Society. 2001;123: 7626-7629.

119. Han G, Martin CT, Rotello VM. Stability of Gold Nanoparticle-Bound DNA toward Biological, Physical, and Chemical Agents. Chemical Biology & Drug Design. 2006;67: 78-82.

120. Thomas M, Klibanov AM. Conjugation to Gold Nanoparticles Enhances Polyethylenimine's Transfer of Plasmid DNA into Mammalian Cells. Proceedings of the National Academy of Sciences. 2003;100: 9138-9143.

121. Ghosh PS, Kim C-K, Han G, Forbes NS, Rotello VM. Efficient Gene Delivery Vectors by Tuning the Surface Charge Density of Amino Acid-Functionalized Gold Nanoparticles. ACS Nano. 2008;2: 2213-2218.

122. Lytton-Jean AKR, Mirkin CA. A Thermodynamic Investigation into the Binding Properties of DNA Functionalized Gold Nanoparticle Probes and Molecular Fluorophore Probes. Journal of the American Chemical Society. 2005;127: 12754-12755.

123. Jin R, Wu G, Li Z, Mirkin CA, Schatz GC. What Controls the Melting Properties of DNA-Linked Gold Nanoparticle Assemblies? Journal of the American Chemical Society. 2003;125: 1643-1654.

124. Long H, Kudlay A, Schatz GC. Molecular Dynamics Studies of Ion Distributions for DNA Duplexes and DNA Clusters: Salt Effects and Connection to DNA Melting. The Journal of Physical Chemistry B. 2006;110: 2918-2926.

125. Rosi NL, Giljohann DA, Thaxton CS, Lytton-Jean AKR, Han MS, Mirkin CA. Oligonucleotide-Modified Gold Nanoparticles for Intracellular Gene Regulation. Science. 2006;312: 1027-1030.

126. Pan CQ, Lazarus RA. Engineering Hyperactive Variants of Human Deoxyribonuclease I by Altering Its Functional Mechanism. Biochemistry. 1997;36: 6624-6632.

127. Shack J, Bynum BS. Determination of the Interaction of Deoxyribonucleate and Magnesium Ions by Means of a Metal Ion Indicator. Nature. 1959;184: 635-636.

128. Lee SH, Bae KH, Kim SH, Lee KR, Park TG. Amine-Functionalized Gold Nanoparticles as Non-Cytotoxic and Efficient Intracellular siRNA Delivery Carriers. International Journal of Pharmaceutics. 2008;364: 94-101.

129. Lee J-S, Green JJ, Love KT, Sunshine J, Langer R, Anderson DG. Gold, Poly(β-amino ester) Nanoparticles for Small Interfering RNA Delivery. Nano Letters. 2009;9: 2402-2406.

130. Lee SK, Han MS, Asokan S, Tung C-H. Effective Gene Silencing by Multilayered siRNA-Coated Gold Nanoparticles. Small. 2011;7: 364-370.

131. Kong WH, Bae KH, Hong CA, Lee Y, Hahn SK, Park TG. Multimerized siRNA Cross-linked by Gold Nanoparticles. Bioconjugate Chemistry. 2011;22: 1962-1969.

132. Chithrani BD, Ghazani AA, Chan WCW. Determining the Size and Shape Dependence of Gold Nanoparticle Uptake into Mammalian Cells. Nano Letters. 2006;6: 662-668.

133. Yang P-H, Sun X, Chiu J-F, Sun H, He Q-Y. Transferrin-Mediated Gold Nanoparticle Cellular Uptake. Bioconjugate Chemistry. 2005;16: 494-496.

134. Chithrani BD, Chan WCW. Elucidating the Mechanism of Cellular Uptake and Removal of Protein-Coated Gold Nanoparticles of Different Sizes and Shapes. Nano Letters. 2007;7: 1542-1550.

135. Cho EC, Xie J, Wurm PA, Xia Y. Understanding the Role of Surface Charges in Cellular Adsorption versus Internalization by Selectively Removing Gold Nanoparticles on the Cell Surface with a I2/KI Etchant. Nano Letters. 2009;9: 1080-1084.

136. Tkachenko AG, Xie H, Coleman D, et al. Multifunctional Gold Nanoparticle−Peptide Complexes for Nuclear Targeting. Journal of the American Chemical Society. 2003;125: 4700-4701.

137. Giljohann DA, Seferos DS, Patel PC, Millstone JE, Rosi NL, Mirkin CA. Oligonucleotide Loading Determines Cellular Uptake of DNA-Modified Gold Nanoparticles. Nano Letters. 2007;7: 3818-3821.

138. Hill HD, Millstone JE, Banholzer MJ, Mirkin CA. The Role Radius of Curvature Plays in Thiolated Oligonucleotide Loading on Gold Nanoparticles. ACS Nano. 2009;3: 418-424.

139. Pernodet N, Fang X, Sun Y, et al. Adverse Effects of Citrate/Gold Nanoparticles on Human Dermal Fibroblasts. Small. 2006;2: 766-773.

140. Li JJ, Zou L, Hartono D, Ong CN, Bay BH, Lanry Yung LY. Gold Nanoparticles Induce Oxidative Damage in Lung Fibroblasts In Vitro. Advanced Materials. 2008;20: 138-142.

141. Bhattacharya R, Patra CR, Verma R, Kumar S, Greipp PR, Mukherjee P. Gold Nanoparticles Inhibit the Proliferation of Multiple Myeloma Cells. Advanced Materials. 2007;19: 711-716.

142. Pan Y, Neuss S, Leifert A, et al. Size-Dependent Cytotoxicity of Gold Nanoparticles. Small. 2007;3: 1941-1949.

Delivery Material	Drug Name	Phase	Condition	Therapeutic Delivered	Details	ClinicalTrials.gov Indentifier
CDP	CRLX101	1 & 2	Cancer Solid Tumor	CPT	CPT conjugated to linear CDP	NCT00333502
CDP	CALAA-01	1	Cancer Solid Tumor	siRNA	CDP self-assembled with siRNA containing AD-PEG and AD-PEG-Tf	NCT00689065
CDP	CRLX101	1	Advanced or metastatic stomach, gastroesophageal, or esophageal cancer	camptothecin	Camptothecin conjugated to linear CDP	NCT01612546
Drug Polymer Conjugate	XMT-1001	1	Advanced Cancer Solid Tumor	CPT	CPT tethered to PHF	NCT00455052
amphiphilic diblock copolymer forming micelle	Genexol-PM	4	Recurrent Breast Cancer	Paclitaxel	PEG-b-poly-(D,L-lactic acid)	NCT00912639
amphiphilic diblock copolymer forming micelle	Genexol-PM	2	Non Small Cell Lung Cancer	Paclitaxel	PEG-b-poly-(D,L-lactic acid)	NCT01023347
amphiphilic diblock copolymer forming micelle	Genexol-PM	2	Advance Pancreatic Cancer	Paclitaxel	PEG-b-poly-(D,L-lactic acid)	NCT00111904
amphiphilic diblock copolymer forming micelle	Genexol-PM	3	Breast Cancer	Paclitaxel	PEG-b-poly-(D,L-lactic acid)	NCT00876486
Polymeric nanoparticles	docetaxel-PNP	1	Advanced Solid Malignancies	Docetaxel	Unspecified	NCT01103791
Drug Polymer Conjugate	Paclitaxel poliglumex	2	Prostate Cancer	Paclitaxel	Poly-L-glutamic acid conjugated to paclitaxel	NCT00459810
Drug Polymer Conjugate	Paclitaxel poliglumex	1 & 2	Head and neck cancer	Paclitaxel	Poly-L-glutamic acid conjugated to paclitaxel	NCT00660218
AuNP	CYT-6091	1	Unspecified Adult Solid Tumor	TNF	TNF-bound colloidal gold	NCT00356980
PEG-liposome	Kogenate FS	1	Hemophilia A	Recombinant factor VIII	Liposome composed of POPC and MPEG2000 DSPE	NCT00629837
PEG-liposome	Nancort	2	Multiple Sclerosis	Prednisolone	PEG-liposomal prednisolone sodium phosphate	NCT01039103
liposome	DOTAP:Chol-fus1	1	Non Small Cell Lung Cancer	Plasmid for FUS1 protein to induce apoptosis	DOTAP and cholesterol at 1:1 molar ratio with plasmid for FUS1 protein	NCT00059605
liposome	LErafAON-ETU	1	Neoplasms	Antisense oligonucleotide	Positively charged synthetic cardiolipin liposome entrapping antisense oligonucleotide	NCT00100672
liposome	LEP-ETU	1	Neoplasms	Paclitaxel	Paclitaxel entrapped within liposome	NCT00100139
liposome	liposomal alendronate	2	Coronary Artery Stenosis	Alendronate	Liposomal alendronate	NCT00739466
liposome	NX 211	2	Fallopian Tube, Ovarian, and Peritoneal Cavity Cancer	Lurtotecan	Lurtotecan liposome	NCT00010179

liposome	AmBisome®	4	Fungal infection associated with acute leukemia	Amphotericin B	Liposomal amphotericin B	NCT00386997
liposome	LEP-ETU	1	Neoplasms	Paclitaxel	Paclitaxel entrapped within liposome	NCT00080418
liposome	long-circulating liposomal prednisolone disodium phosphate	2	Rheumatoid Arthritis	Prednisolone	Liposomal prednisolone	NCT00241982
liposome	MBP-426	1	Cancer	Oxaliplatin	Liposomal oxaliplatin	NCT00355888
liposome	LEM	1	Tumors	Mitoxantrone	Liposomal encapsulated mitoxantrone	NCT00024492
liposome	Liposomal Doxorubicin HCl	1	Ovarian Carcinoma	Doxorubicin	Liposomal Doxorubicin HCl	NCT00862355
liposome	LE-DT	2	Pancreatic Cancer	Doxetaxel	Liposome Entrapped Docetaxel	NCT01186731
liposome	LE-DT	2	Prostate Cancer	Doxetaxel	Liposome Entrapped Docetaxel	NCT01188408
liposome	Liprostin	2	Peripheral Vascular Disease	Prostaglandin E1	Liposomal Prostaglandin E1	NCT00053716
liposome	AmBisome®	4	Central Line Fungal Infections	amphotericin B	Liposomal amphotericin B	NCT00936910
liposome	LE-DT	1	Solid Tumors	Doxetaxel	Liposome Entrapped Docetaxel	NCT01151384
liposome	ThermoDox	3	Hepatocellular Carcinoma	Doxorubicin	Thermally sensitive liposomal Doxorubicin	NCT00617981
liposome	BAY79-4980	2	Hemophilia A	Recombinant factor VIII	Liposomal recombinant factor VIII	NCT00623727
polymeric micelle	Lipotecan	1	Advanced Solid Tumors	TLC388 HCl (camptothecin analog)	Formulation is Proprietary	NCT00747474
liposome	VSLI	1	Malignant Melanoma	Vincristine	Liposomal Vincristine	NCT00145041
liposome	L-BLP25	2	Lung Neoplasms, Non-Small Cell Lung Carcinoma	BLP25	Liposomal vaccine	NCT00157309
liposome	L-BLP25	2	Lung Neoplasms, Non-Small Cell Lung Carcinoma	BLP25	Liposomal vaccine	NCT00157196
PEG-liposome	Caelyx	4	Ovarian Neoplasms	Doxorubicin	PEGylated liposomal Doxorubicin HCl	NCT00727961
liposome	RGI-2001	1 & 2	GvHD prevention in patients with Hematological Malignancies Undergoing AHSCT	RGI-2001	α-galactosylceramide liposomal formulation	NCT01379209
liposome	Lipovaxin-MM	1	Melanoma	Lipovaxin-MM (anti-cancer vaccine)	3-nitrlotriacetic acid linked to DTDA liposome with histidine tagged targeting ligands or antigens	NCT01052142
liposome	PNT2258	1	Cancer, Lymphoma, Prostate, Melanoma	PNT100 (24-mer oligonucleotide)	PNT100 encapsulated in liposome	NCT01191775

Table 4.1. Recent Clinical Trials for Nano-Carrier. Data obtained from clinicaltrials.gov.

Delivery Material	Drug Name	Phase	Condition	Therapeutic Delivered	Details	ClinicalTrials.gov Identifier
liposome	Cisplatin and Liposomal Doxorubicin	1	Advanced Cancer	Cisplatin and doxorubicin	Combo therapy of cisplatin and liposomal doxorubicin	NCT00507962
liposome	AmBisome®	2 & 3	Aspergillosis	Anidulafungin and amphotericin B	Combo therapy of anidulafungin and liposomal amphotericin B	NCT00037206
PEG-liposome	DVD-R	2	Relapsed/ Refractory Multiple Myeloma	Dexamethasone, bortezomib, doxorubicin, and lenalidomide	Combo therapy of dexamethasone, bortezomib, liposomal doxorubicin, and lenalidomide	NCT01160484
PEG-liposome	PLD	2	Fallopian Tube, Ovarian, and Peritoneal Neoplasms	Carboplatin, doxorubicin, and bevacizumab	Combo therapy of carboplatin, DOXIL (doxorubicin HCl loaded liposomes), and bevacizumab	NCT00698451
liposome	JNS002 and bortezomib	1	Multiple Myeloma	Doxorubicin and bortezomib	Combo therapy of JNS002 (doxorubicin HCL liposome) and bortezomib	NCT01371227
PEG-liposome	Topotecan and DOXIL	1	Small Cell Lung, Pancreatic, Head and Neck, Gastric, and Esophageal Cancers	Topotecan and doxorubicin	Combo therapy of topotecan and PEGylated liposomal doxorubicin	NCT00252889
PEG-liposome	Farletuzumab, carboplatin and PEG-liposomal doxorubicin	1	Epithelial Ovarian Cancer	Farletuzumab, carboplatin, and doxorubicin	Combo therapy of farletuzumab, carboplatin and PEGylated liposomal doxorubicin	NCT01004380
liposome	DOXIL and rituximab	2	Lymphoma	Doxorubicin and rituximab	Combo therapy of DOXIL and rituximab	NCT00392990
PEG-liposome	bortezomib, liposomal doxorubicin, vorinostat	1	Multiple Myeloma and Plasma Cell Neoplasm	bortezomib, doxorubicin, and vorinostat	Combo therapy of bortezomib, PEG-liposomal doxorubicin, and vorinostat	NCT00744354
liposome	Liposomal doxorubicin and bevacizumab	2	Kaposi's Sarcoma	Doxorubicin and bevacizumab	Combo therapy of liposomal Doxorubicin and Bevacizumab	NCT00923936
PEG-liposome	Docetaxel and caelyx	2	Ovarian Cancer	Docetaxel, carboplatin and doxorubicin	Combo therapy of docetaxel/carboplatin or docetaxel/caelyx (PEGylated liposomal doxorubicin)	NCT00758732
liposome	Seliciclib and liposomal doxorubicin	1	Breast Cancer	Doxorubicin and seliciclib	Combo therapy of seliciclib and liposomal doxorubicin	NCT01333423
PEG-liposome	NGR-hTNF and PEGylated liposomal doxorubicin	2	Ovarian Cancer	NGR-hTNF	Combo therapy of NGR-hTNF	NCT01358071
liposome	LY573636 and liposomal doxorubicin	1	Solid Tumors	LY573636 and doxorubicin	Combo therapy of LY573636 (anticancer agent) and liposomal doxorubicin	NCT01214668
PEG-liposome	EC145 and PEGylated liposomal doxorubicin	3	Ovarian Cancer	EC145 and doxorubicin	Combo therapy of EC145 and PEGylated liposomal doxorubicin	NCT01170650
liposome	bortezomib, dexamethasone, and liposomal doxorubicin	2	Multiple Myeloma	bortezomib, doxorubicin, and dexamethasone	Combo therapy of bortezomib, liposomal doxorubicin, and dexamethasone	NCT00366106

liposome	TL32711 and liposomal doxorubicin	1 & 2	Cancer	TL32711 (apoptosis inducer) and doxorubicin	Combo therapy of liposomal doxorubicin and TL32711	NCT01188499
amphiphilic diblock copolymer forming micelle	Genexol-PM	1	Ovarian Cancer	Paclitaxel & Carboplatin	PEG-b-poly-(D,L-lactic acid) plus Carboplatin	NCT00877253
Drug Polymer Conjugate	AP5346	Not Stated	Head and Neck Cancer	AP5346 and oxaliplatin	Diaminocyclohexane platinum moiety linked to hydroxypropylmethacrylamide	NCT00415298
amphiphilic diblock copolymer forming micelle	Genexol-PM	1 & 2	Ovarian Cancer	Paclitaxel and carboplatin	Combo therapy of Genexol-PM and Carboplatin	NCT00886717

Table 4.2. Recent Clinical Trials for Combination Therapies Incorporating Nano-Carrier. Data obtained from clinicaltrials.gov.

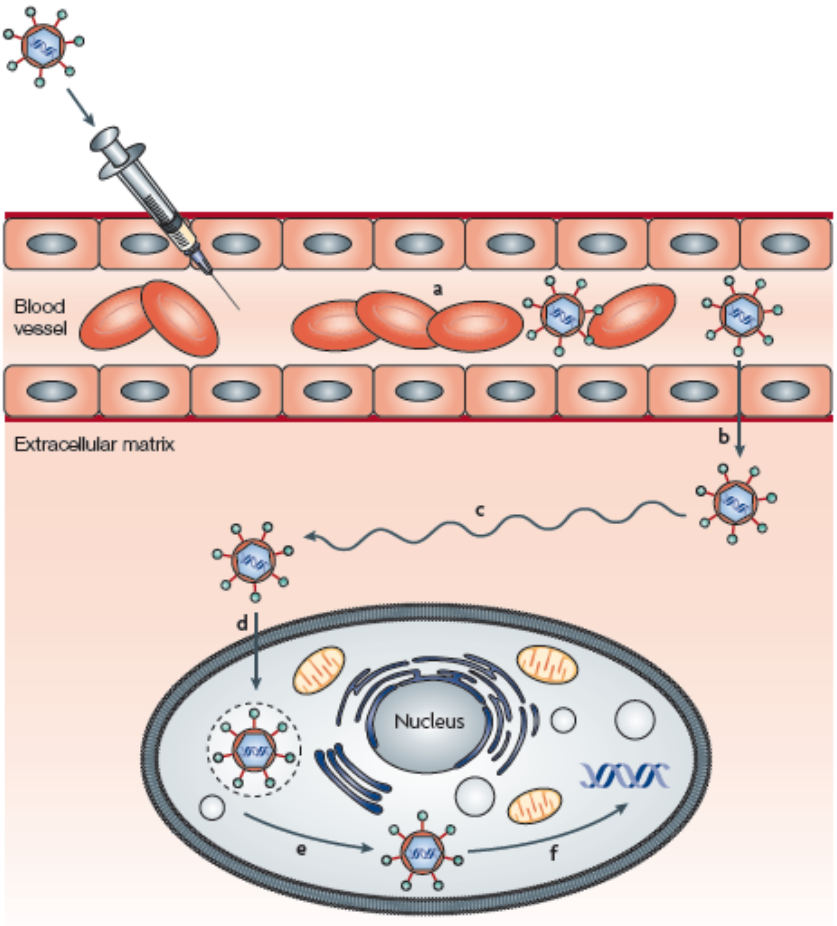

Figure 4.1. Physiological Barriers to the Systemic Delivery of Small Interfering RNA (siRNA) Nanoparticles. An injected nanoparticle must avoid filtration, phagocytosis and degradation in the bloodstream (**a**); be transported across the vascular endothelial barrier (**b**); diffuse through the extracellular matrix (**c**); be taken up into the cell (**d**); escape the endosome (**e**); and unpackage and release the siRNA to the RNA interference (RNAi) machinery (**f**). (used with permission from reference 2)

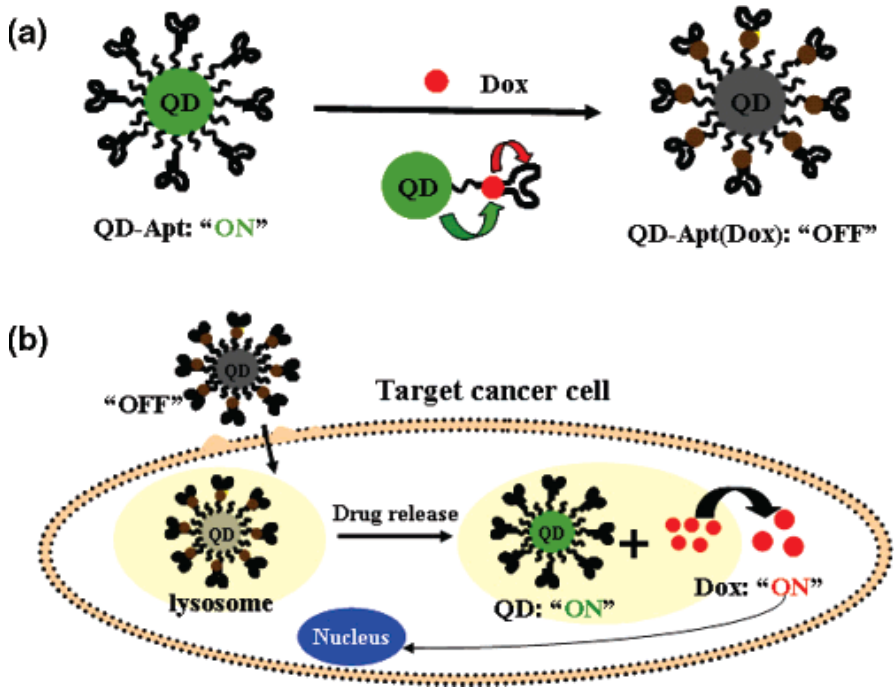

Figure 4.2. QD-Aptamer-DOX Complex. (a) Schematic illustration of QD-Apt(Dox) system. The A10 PSMA aptamers are functionalized on the surface of QD followed by intercalation of Dox within the aptamer results in the formation of the QD-Apt(Dox). The fluorescence of the QD is quenched by Dox while simultaneously the fluorescence of Dox is quenched by intercalation within the A10 PSMA aptamer resulting in the "OFF" state. (b) Schematic illustration of specific uptake of QD-Apt(Dox) conjugates into target cancer cell through PSMA mediate endocytosis. The release of Dox from the QD-Apt(Dox) conjugates induces the recovery of fluorescence from both QD and Dox ("ON" state), thereby sensing the intracellular delivery of Dox. (used with permission from reference 103)

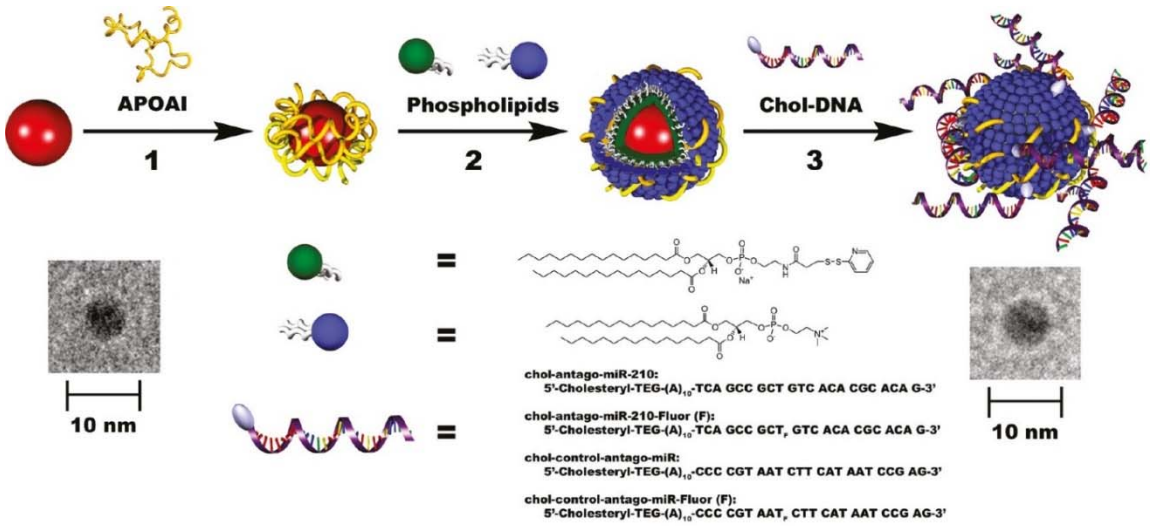

Figure 4.3. Formation of Chol-DNA-HDL AuNP (used with permission from reference 113)

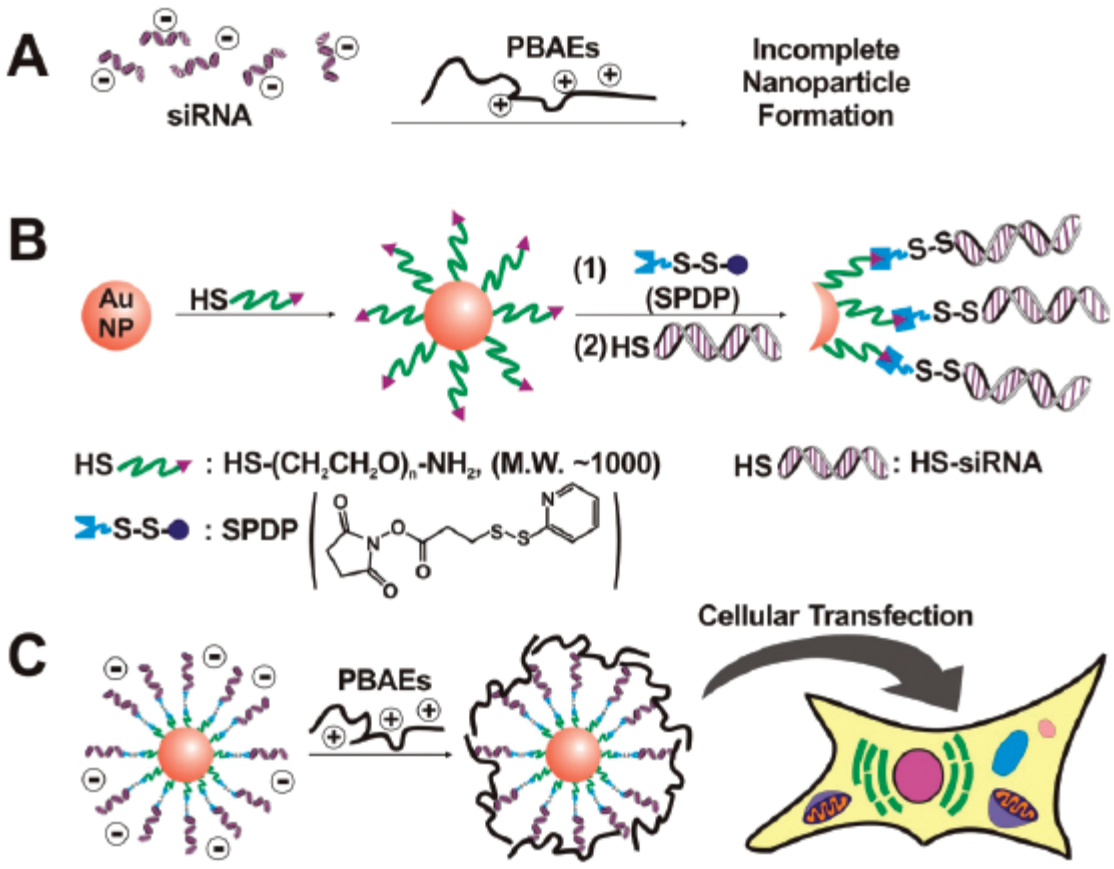

Figure 4.4. Formation of AuNp, siRNA and Polymer Complex. (A) The scheme illustratin incomplete nanoparticle formation of siRNA combined with PBAEs. (B) The synthesis of siRNA-modified AuNPs (siRNA-AuNPs) with a disulfide linkage. (C) The complexation of siRNA-AuNPs with PBAEs followed by cellular transfection (used with permission from reference 129)

Chapter 5. Development and Characterization of a Novel Bio-Hybrid Nano-Carrier for On-Demand and Controlled Release of Drugs

In this chapter, the design and characterization of a biohybrid nano-carrier is presented which utilizes the versatile properties of nucleic acids for programmable and on-demand drug release. Nucleic acid aptamers that bind small molecules in their three dimensional structure was discovered in 1990. The major hypothesis in this work was that the covalent incorporation of drug binding aptamers on gold nanoparticles (AuNps) could produce a novel nano-scale drug delivery device platform capable of tissue-specific and controlled release of therapeutics with very high sensitivity. Aptamers can be used as excellent drug release control moieties due to their controllable drug binding ability, and exquisite response to various physiological triggers. Such a delivery device would be amenable to wide variety of triggers which can be used to tailor the release of drug with strict control.

Our drug delivery nano-carrier consists of 15 nm gold nanoparticles (AuNps) functionalized with drug binding DNA aptamers via single stranded (ss) DNA anchor. The presence of anchor DNA makes the nano-carrier flexible to be reprogrammed with various aptamers. The factors affecting the conjugation of single stranded (ss) DNA on gold nanoparticles was investigated to find the optimal conditions for maximum loading of DNA on AuNps. In order to develop the nano-carrier for antibiotic drug neomycin, a DNA aptamer for neomycin was formulated by translating the sequence of the RNA aptamer to DNA, and tested its drug binding affinity using surface plasmon resonance. The drug

binding DNA aptamers were conjugated to AuNps using ss DNA as anchors. Also, various methods of conjugating aptamers and drugs to AuNps were investigated to identify the method that yielded the maximum loading of the drug. This novel biohybrid platform designed using the principles of molecular biology was hypothesized to be capable of controlled release of drug for extended period of time.

5.1. Scientific Rationale

While development of new drugs are very crucial to combat various disorders, it is equally important to deliver those drugs to the correct site in the body and control the release of therapeutics inside the diseased cells for an extended period of time. Such control over drug delivery would improve the efficiency of the therapy, reduce the frequency of drug administration, and thereby improve the standard of living of the patients. Presently, targeted and controlled delivery of drug is one of the biggest challenges of modern medicine. Thus, it is very important to develop an efficient delivery carrier that can deliver the drug specifically to diseased tissues as well as keep releasing the drug inside the cells for a long period of time. Nano-delivery carriers made of synthetic polymers and metals hold immense potential in the development of such a delivery carrier. In this chapter, we discuss the synthesis and characterization of one such nano-carrier that is capable of controlled release of drug for extended periods of time, and can be easily modified to deliver any drug as well as multiple drugs.

Nucleic acid aptamers are emerging as versatile therapeutic agents and important drug targets. Broadly, aptamers are nucleic acids that can bind specifically to target

molecules with high affinity. They can form complex three dimensional structures and bind small molecules such as drug molecules, nucleic acids, peptides, and proteins. In addition to being able to bind small molecules, aptamers can also be designed to release them in response to an external trigger. This makes aptamers very attractive for controlled therapeutic delivery. These novel "smart" molecules can be selected from random pools of both RNA and DNA molecules based on their ability to bind target molecules. Our strategy is to exploit the aptamer's response to different physical and physiological triggers to produce controlled and extended drug release profiles.

With nucleic acid aptamers as our release control moiety, we decided to use AuNps as the delivery platform. AuNps are attractive candidates for drug delivery due to their non-toxic core, tunable surface properties, and efficient cellular uptake. We investigated the potential of aptamer conjugated gold nanoparticles as a biohybrid drug delivery platform capable of programmed and controlled drug release. This aptamer and gold based nano-carrier when functionalized with a targeting ligand could produce an injectable nano-carrier capable of tissue-specific and controlled drug delivery.

5.2. Materials and Methods

In this section, the materials and methods for synthesis and characterization of novel biohybrid drug delivery platform for the antiobiotic drug neomycin are described. All nucleic acid sequences used were custom designed to minimize secondary structure formation except the aptamers. Some of the nucleic acids used were labeled with radioactive nucleotide or fluorescent tag to test their loading on gold nanoparticles.

5.2.1. Materials

Gold nanoparticles of 15 nm diameter (AuNPs) were purchased from Tedpella (Redding, CA). Modified and unmodified oligonucleotides were synthesized by Operon Biotechnologies. NAP-5 columns (Sephadex G-25 DNA grade) were purchased from G.E. Healthcare (Piscatiway, NJ). Sterile, 6 well clear multiple well plates and 384 well low flange solid black microplates were obtained from Corning, Inc. (Corning NY). Polyester sealing films were purchased from VWR International (West Chester, PA), and drop dialysis membranes (13 mm, 0.025 μm) were obtained from Millipore (Billerica, MA). Neomycin sulfate (analytical standard) and Neomycin-TMR were purchased from Sigma-Aldrich (St. Louis, MO) and Echelon Biosciences, Inc. (Salt Lake City, UT), respectively. All other chemicals were molecular biology grade and unless specified, were from Sigma-Aldrich (St. Louis, MO). All radiochemicals were purchased from ICN Biochemicals, Inc.

5.2.2. Methods. Conjugation of Single Stranded Alkanethiol Oligonucleotide to AuNps

The anchor oligonucleotide (NAN-ANC) with thiol group at 5'end (**Figure 5.1**) was suspended in TE buffer to 1 mM final concentration. To cleave the disulfide functionality on the oligonucleotide, 4 μL of NAN-ANC was incubated in 0.18 M phosphate buffer solution (PB) at a pH of 7.2 with 0.1 M dithiothreitol (DTT) for 3 hrs at 37^{o}C, followed by desalting within a NAP-5 column according to the manufacturer's specifications. Desalted oligonucleotides were concentrated to ~ 20 μL using an Integrated

Speed Vac System (Savant Instrument, Inc.) and then 1 mL of AuNps (15 nm, $1.4x10^{12}$ particles / mL) and 1 μL of 10% SDS solution were added. The mixture was vortexed for 16 hours at room temperature. The PB was added until a final concentration of 0.01 M was achieved, and then the oligonucleotide/AuNps solution was incubated at room temperature for 2 hrs. Aliquots of 10 μL of 5 M NaCl solution were added to the oligonucleotide/AuNps solution. The mixture was sonicated for 10 seconds using a sonic dismembrator (Fisher Scientific) and incubated for 20 minutes at room temperature after every addition of NaCl. This process was repeated to a final concentration of 0.4 M NaCl. The oligonucleotide/AuNps solution was then vortexed for 24 hrs at room temperature. The solution was centrifuged 3 times for 40 minutes each time at 13,000 rpm to remove unbound oligonucleotides. The oligonucleotide conjugated AuNps pellet was resuspended in a 10 mM PB and 0.2 M NaCl solution (PBS; pH 7).

[γ–^{32}P]-labeled NAN-ANC was prepared according to the protocol developed by Fedor and Uhlenbeck[34]. The amount of radioactivity was quantified by Cerenkov counting using a LKE Wallac scintillation counter. The mean diameter of oligonucleotides conjugated AuNps was studied using Dynamic Light Scattering (DLS) instrument (PSS-NICOMP).

5.2.3. Methods. Attaching Neomycin Binding DNA Aptamer to AuNps

DNA aptamers were bound to AuNps using two different approaches; pre-hybridization and post-hybridization (**Figure 5.2A and 5.2B)**. In the pre-hybridization approach, a 65 μL hybridization reaction mixture containing NAN-ANC (2 nmoles) and

fluorophore (fluorescein, ^{6}Fam) modified NAN-NEO (2 or 4 nmoles), 0.18 M PB and 0.1 M DTT (pH 7.2) were incubated at 37^{o}C for 3 hrs. Complexes of hybridized NAN-ANC and NAN-NEO (NAN-NEO:NAN-ANC) were desalted on a NAP-5 column, concentrated using a Speed Vac to ~ 20 µL and conjugated to AuNps as per NAN-ANC conjugation procedure, described previously.

In the post-hybridization approach, 2 nmoles of NAN-ANC was conjugated to AuNps. Then, 2 or 4 nmoles of ^{6}Fam modified NAN-NEO was added. The mixture was heated for 10 minutes at 70^{o}C, cooled at room temperature for 2 minutes and on ice for 2 minutes, vortexed for 24 hrs at room temperature. Unbound NAN-NEO strands were removed by centrifugation for 40 minutes at 13,000 rpm. The NAN-NEO:NAN-ANC complex conjugated AuNps pellet was resuspended in PBS.

To remove the DNA from the AuNps, aptamer bound AuNps were incubated for 16-20 hours in 0.05 M DTT. Removed DNA strands were separated from AuNps by centrifugation for 30 min at 13,000 rpm. Supernatant was measured for ^{6}Fam fluorescence in a Synergy multimode microplate reader (BioTek) at 494 nm and 518 nm, excitation and emission wavelength, respectively. All the steps in these experiments were carried out in dark to prevent quenching of fluorescence.

5.2.4. Methods. Neomycin-DNA Aptamer Binding Studies.

Surface Plasmon Resonance (SPR, TA instruments) was used to characterize the interactions between neomycin and the DNA aptamer. Prior to the experiment, each Spreeta sensor chip (Texas Instruments) was pre-conditioned with pirannah solution for 5

minutes, washed with water and absolute ethanol, and then was plasma cleaned for 5 minutes. The system was initially equilibrated with Hepes buffer (HBS; 35mM HEPES/NaOH, 100mM NaCl; pH 7). The DNA aptamers were attached to the sensor chip via thiol-gold bond by continuous circulation of 2 μM solution of NAN-NEO:NAN-ANC complex in HBS for 16 hours. Non-covalently bound DNA was washed from the surface by circulating HBS until stabilization. The DNA-attached sensor chip was then equilibrated with a neomycin binding buffer (NBB; 50mM Tris/Cl, 5 mM MgCl, 150 mM NaCl; pH 7.4). Then 0.05 μM solution of neomycin sulfate in NBB was allowed to flow through the system until saturation occurred, which took approximately 20 minutes. Non-specifically adsorbed neomycin was washed by circulating NBB until stabilization. Then, the surface was regenerated (i.e., bound neomycin was removed without affecting the structure of NAN-NEO:NAN-ANC complex) by passing water at a temperature of 41°C for 5 minutes followed by circulation of NBB to bring back the signal to the equilibrated position **(Figure AI.1)**. The binding of neomycin and the regeneration of surface were repeated for different concentrations of neomycin sulfate (0.075 – 2 μM).

5.2.5. Method. Binding of Neomycin to Aptamer Conjugated AuNps

Binding of neomycin to DNA aptamer conjugated AuNps was accomplished in two approaches: pre- and post-binding (**Figure 5.2C and 5.2D**). Hybridization reaction mixture (65 μL) containing NAN-ANC (2 nmoles) and NAN-NEO (2 nmoles), 0.18 M PB and 0.1 M DTT (pH 7.2) were incubated at 37°C for 3 hrs. NAN-NEO:NAN-ANC complexes were then desalting on NAP-5 column and concentrating to ~ 20 μL using a Speed Vac.

In pre-binding approach, Neomycin-TMR (0.2 nmoles) suspended in 20 µL of NBB was added to the NAN-NEO:NAN-ANC complexes and incubated on ice for 30 minutes for binding. Then the neomycin:NAN-NEO:NAN-ANC complexes were conjugated to AuNps as per NAN-ANC conjugation procedure. In the post-binding approach**,** NAN-NEO:NAN-ANC complexes were conjugated to AuNps as per NAN-ANC conjugation procedure. Neomycin-TMR (0.2 nmoles) suspended in 20 µL NBB was then added and allowed to stand on ice for 1 hour. The samples were vortexed for 16 hrs at room temperature and centrifuged for 30 minutes at 10,000 rpm to remove excess neomycin. The neomycin:NAN-NEO:NAN-ANC complexes conjugated AuNps pellet was resuspended in PBS.

The neomycin:NAN-NEO:NAN-ANC was removed from the AuNps by incubating for 16-20 hours in 0.05 M DTT. The samples were then centrifuged for 30 minutes at 13,000 rpm. Supernatant was measured for fluorescence of Neomycin-TMR in a Synergy multimode microplate reader at 555 nm and 580 nm, excitation and emission wavelength, respectively. All the steps involving Neomycin-TMR in these experiments were carried out in dark to prevent quenching of fluorescence.

5.3. Results and Discussion

We designed a nano-delivery carrier that consists of AuNps and neomycin-binding DNA aptamer, NAN-NEO (**Figure 5.1**). As the aptamer is attached to AuNp through an ss DNA anchor, this carrier can be readily reprogrammed for delivery of other drugs. The anchor DNA is covalently conjugated to AuNp via the thiol group attached to its 5’ end by

forming thiol-gold covalent bond. To minimize non-specific interactions between AuNp and DNA anchor, the latter has a $(dT)_4$ spacer.

The anchor DNA was conjugated to AuNps via thiol-gold covalent bond. This reaction is affected by salt and DNA concentration. Salt screens the negative charges on the DNA and prevents repulsion between the DNA strands[1, 2]. We measured conjugation of SH-derivatized NAN-ANC to 15 nm AuNps at 0 to 1.5 M NaCl and 1 to 4 μM DNA concentrations. The [γ–^{32}P]-labeled NAN-ANC was used to monitor progress of the conjugation reaction. We demonstrated that the maximum number (101 ± 8) of NAN-ANC (19 nucleotide long) strands were attached at 0.4 M NaCl (**Figure 5.3A).** Further increases in salt concentration inhibited conjugation of NAN-ANC strands to AuNps.

Previously, Mirkin and coworkers showed that the conjugation of the 25 nucleotide long DNA to 15 nm AuNps increased until 0.7 M NaCl and then leveled off [1, 2]. Our data suggests that the optimum salt concentration for loading of 19 nucleotide long DNA strands is 0.4 M and after which the loading decreases. These differences suggest that salt requirements for conjugation of DNA to AuNps are affected by the length and most likely the sequence of DNA strands. This suggestion is supported by earlier studies which demonstrated that the relative adsorption affinity of nucleotide bases to gold is A > C > G > T [3, 4]. Nucleic acid chains of high density of nucleotide A do not lead to the most efficient loading on the surface of AuNps due to multiple point adsorption on the particle surface. Poly(dT) spacers lead to significantly less multiple point adsorption resulting in higher DNA loading[5].

Then, we investigated the effect of DNA concentration on conjugation of NAN-ANC to AuNps at various salt concentrations (0.1, 0.2, 0.3 and 0.4 M). The number of

NAN-ANC conjugated per particle increased with the increase in DNA concentration until 4 μM at all salt concentrations (**Figure 5.3B**). With the increase in DNA concentration in the reaction mixture, the number of DNA molecules available for binding increases thereby DNA loading increases. For DNA concentration above 4 μM, the AuNps were observed to aggregate.

The aggregation of AuNps with any increase in DNA concentration above 4 μM could most probably be due to the presence of charged hydrogen molecules cleaved from the S-H group, attached to anchor DNA, after formation of gold-thiol bond. The nature of the thiol-gold bond and the fate of the hydrogen atom in the thiol group after binding are still controversial[6-8]. A number of descriptions for the nature of the S-H bond are available within the literature but the most probable explanation for our data is that partially charged hydrogen molecules exist within our solution. As AuNps aggregate in the presence of cations and oligo cations[9], the presence of positively charged hydrogen molecules above a threshold limit could cause aggregation of AuNps. At the optimal salt (0.4 M) and DNA (4 μM) concentrations, maximum loading of 101 ± 8 ssDNA strands per 15 nm AuNps was obtained.

Orientation of DNA conjugated to AuNps depends on the number of DNA strands attached to the AuNp. DNA bases have specific adsorption affinity to gold[3, 4] which can potentially influence the orientation of the DNA attached to AuNPs. When a low number of DNA strands are attached to AuNps, due to the availability of free surface area and the adsorption affinity of the bases, DNA could bend or partially wrap around the AuNp. When more thiol modified DNA strands are available for binding, as the energy gained from thiol-gold bond formation favors attachment of DNA via thiol-gold bond[10, 11], the DNA

number density on the AuNps increases. Finally, when many DNA strands are immobilized on AuNps, due to unavailability of free surface area and repulsion forces between adjacent DNA strands, the DNA strands are hypothesized to adopt a stretched conformation.

We investigated the orientation of NAN-ANC conjugated to AuNps with different DNA concentration by measuring the mean diameter using dynamic light scattering (DLS), and the obtained results **(Figure 5.4A)** supports out hypothesis. With the increase in concentration of NAN-ANC in the reaction mixture, the mean diameter of the NAN-ANC conjugated AuNps increased to a maximum value of 30.43 ± 2 nm at 1 μM NAN-ANC in the reaction mixture, after which it remained constant. The constant mean diameter after 1 μM NAN-ANC in the reaction mixture suggest that after a particular DNA number density the DNA strands remain in stretched conformation for any further increase in DNA loading.

To understand the change in DNA conformation with length of DNA when immobilized on AuNps, we designed NAN-ANC-20MER, NAN-ANC-30MER, NAN-ANC-40MER, NAN-ANC-50MER DNA complexes which are 20, 30, 40 and 50 nucleotides long **(Figure 5.4B**). The DNA complexes were conjugated to AuNps by the pre-hybridization method (**Figure 5.2A**) with 4 μM DNA and 0.4 M salt concentration, and the mean diameters were measured using DLS. The measured mean diameter were compared to the theoretical mean diameter (**Figure 5.4C)**, calculated by adding twice the length of DNA to the diameter of AuNps. The length of DNA strands were calculated by assuming that nucleotides are separated by 4 Å. The calculated mean diameters corresponded to the measured mean diameters for AuNps functionalized with 20 and 30 nucleotide long DNA strands and were higher than the measured mean diameters for

AuNps functionalized with 40 and 50 nucleotide long DNA strands. This suggests that smaller DNA molecules (30 bases or less) immobilized on AuNps adopt a fully stretched conformation, while longer DNA molecules adopt a partially coiled conformation. Similar results were obtained by Alivisatos and coworkers[11] on investigating the length dependent orientation of DNA on AuNps by gel electrophoresis.

To construct the drug delivery carrier, we investigated different approaches. The NAN-NEO aptamer was attached to AuNp via NAN-ANC using either the pre-hybridization or the post-hybridization approach. The non-covalent Watson-Crick base paring determines specificity and affinity of interactions between the aptamer and DNA anchor. In pre-hybridization approach, the NAN-NEO was hybridized to NAN-ANC to form the NAN-NEO:NAN-ANC complex which was then conjugated to AuNp **(Figure 5.2A)**. In post-hybridization approach, NAN-NEO was hybridized to NAN-ANC already conjugated to AuNp **(Figure 5.2B).**

We used ^{6}Fam fluorophore modified NAN-NEO to monitor the aptamer loading to AuNps. DNA aptamer loading was tested using both the approaches with 1:1 and 1:2 NAN-ANC to NAN-NEO ratio (**Figure 5.5A**). As the presence of AuNps would quench the fluorescence of the fluorophores[12], the loading of aptamer on AuNps was quantified by removing the NAN-NEO:NAN-ANC complexes from AuNps and then measuring the fluorescence of ^{6}Fam. Better loading of aptamer to AuNps was obtained using the pre-hybridization approach, 35 ± 9 and 37 ± 6 aptamers per AuNps with 1:1 and 1:2 NAN-ANC to NAN-NEO ratios, respectively, compared to the post-hybridization approach. Less aptamer loading with the post-hybridization could be due to various reasons. The most suitable explanation would be that a tight NAN-ANC arrangement on AuNps inhibits

hybridization of NAN-NEO to NAN-ANC. As the loading with 1:1 and 1:2 NAN-ANC to NAN-NEO ratios were almost the same, all the NAN-NEO:NAN-ANC:AuNps complexes for other experiments were prepared using the pre-hybridization approach with 1: 1 NAN-ANC to NAN-NEO ratio.

Later, we investigated the binding of neomycin to the DNA aptamer NAN-NEO. Neomycin belongs to the family of aminoglycoside antibiotics that display activity against Gram-positive and Gram-negative bacteria. It binds to the A site of the 16S ribosomal RNA[13, 14] and disturbs protein synthesis within bacteria. Neomycin interacts with RNA through both electrostatic interactions and hydrogen bonds. Initially, it was assumed that neomycin bound specifically only to double stranded RNA. Later it was found that neomycin can bind to a wide variety of duplex and triplex nucleic acids with an A-type conformation[15] including RNA triplex[16], RNA-DNA hybrid triplex[17], RNA duplex[18], A form DNA duplex[19], RNA aptamers[20], and DNA tetraplex[21]. A variety of RNA aptamers for neomycin have been discovered by in vitro selection, and their binding mechanisms have been well studied[14, 20, 22]. RNA aptamers that bind neomycin adopt a stem-loop structure. The loop has a consensus GNRNA sequence (where N is any nucleotide and R is purine), and the stem contain a stretch of at least three G:U wobble pairs[20]. NMR studies revealed that neomycin binds to the major grove of the G:U rich segment by hydrogen bonding and is capped over by the looped out purine[22].

In this study, for the first time, we have demonstrated that neomycin can also bind to the DNA molecule having same sequence as the RNA aptamer. Demonstrating the binding of neomycin to DNA aptamer is important since RNA is less resilient to enzyme degradation, more liable to modifications by in-vivo biological agents, and has higher

production cost than DNA. We characterized this process using SPR. We calculated the change in response units (RU) with binding of neomycin and then converted RU to molarity by using the instrument standard of 1RU equal to 1 picogram per cm^2. Using the Lineweaver-Burk equation (Equation 1), we calculated the dissociation constant (K_D) (**Figure 5.5B**).

$$\frac{1}{RU} = \frac{K_D}{RU_{\max}} \frac{1}{[\text{Neo}]} + \frac{1}{RU_{\max}} \qquad [1]$$

Our SPR analysis showed that the K_D for neomycin-DNA aptamer binding is 98.101 nM, which is very close to the published value of K_D for neomycin-RNA aptamer interaction (100 nM)[14, 41].

The binding of neomycin to AuNps was accomplished in two different ways. In the pre-binding approach, neomycin was bound to hybridized NAN-NEO:NAN-ANC complex and then the neomycin:NAN-NEO:NAN-ANC complexes were conjugated to AuNps **(Figure 5.2C).** In the post-binding approach, the NAN-NEO:NAN-ANC complexes were conjugated to AuNps using the pre-hybridization approach and then neomycin was bound to it **(Figure 5.2D).**

We used neomycin-TMR, a fluorescent antibiotic derivative, to follow this process. The loading was quantified by removing the neomycin:NAN-NEO:NAN-ANC complex from AuNps and measuring the fluoresce of Neomycin-TMR to prevent fluorescence quenching due to AuNps[12]. The number of neomycin molecules bound to each AuNp with the pre- and post-binding approaches were 20 ± 2 and 11 ± 4 molecules, respectively. The difference in the neomycin loading with two approaches could be explained through the formulation procedure. In the pre-binding approach, neomycin was dispersed with DNA in

a very small solvent volume (~ 50 μL), allowing high contact between the drug and the drug binding site of the aptamer. However, in the post-binding approach, aptamers conjugated AuNps were suspended in larger volumes of solvent (1mL) and on adding neomycin the probability of the drug finding the binding site decreased. Therefore, the neomycin:NAN-NEO:NAN-ANC:AuNps complex for all further neomycin studies were prepared by pre-binding method.

From the above described loading of aptamer and the drug experiments, we observed that dimensions of DNA complexes affected the DNA number density on AuNps. When 2 nmoles of NAN-ANC was present in the conjugation reaction mixture, 50 ± 5 NAN-ANC were conjugated per AuNps. While, when 2 nmoles of NAN-NEO:NAN-ANC complexes and neomycin:NAN-NEO:NAN-ANC complexes were present in the reaction mixture, 35 ± 8 and 20 ± 2 strands were attached per AuNps, respectively. This is most likely because, with the increase in dimensions of the DNA complex, the space required to stabilize its structure increases, thereby loading per particle decreases.

5.4. Conclusions

In this chapter, the synthesis, characterization and optimization of a novel nano-delivery carrier which utilizes the versatile properties of nucleic acid for programmable and on-demand drug release was described. The drug delivery carrier consisted of 15 nm gold nanoparticles (AuNps) functionalized with drug binding DNA aptamers via single stranded (ss) anchor DNA. The presence of anchor DNA makes the nano carrier flexible to be reprogrammed with various aptamers.

The factors affecting the loading of ss DNA such as salt concentration and DNA concentration were investigated, and the optimal binding conditions were found to be 0.4 M NaCl and 4 μM DNA. Under the optimum binding conditions a maximum of 101±8 anchor DNA strands were conjugated per particle. The orientation of DNA conjugated to AuNps was studied, by measuring the mean diameter of the AuNps functionalized with different concentration of DNA, using DLS. The results suggest that when less number of DNA are functionalized on AuNps: the DNA tend to bend or partially wrap around the AuNps, but when higher numbers of DNA are functionalized on AuNps: the DNA adopts a stretched conformation due to repulsion forces of adjacent DNA. DNA of different lengths adopt different conformations when conjugated to AuNps. Shorter DNA (≤ 30 nucleotide) adopts a stretched conformation while the longer DNA (> 30 nucleotide) adopts a partially coiled conformation.

The binding of neomycin, an antibiotic drug, to RNA aptamers were previously well studied. Even the binding of neomycin to a variety of A type nucleic acids such as DNA and RNA duplexes, triplexes, tetraplexes and hybrid duplexes were studied. In this chapter, we describe the first ever study investigating the binding of neomycin to the DNA molecule with the same sequence as the RNA aptamer. The Kd of the neomycin:DNA aptamer was found to be 98.101 nM which is very close to the Kd of the RNA aptamer (100 nM). Thus, we have produced a DNA aptamer for neomycin which is more resilient to enzyme degradation and has lower cost of production than the RNA aptamer

Neomycing DNA aptamers were conjugated to AuNps by two different methods: pre-hybridization and post-hybridization. The loading of aptamer to AuNps was higher with the pre-hybridization than post-hybridization. Similarly, the drug was loaded onto

AuNps by pre-binding and post-binding methods, and the loading of drug was observed to be higher with pre-binding than post-binding method. On binding DNA-aptamer:drug complexes to AuNps a maximum of 22 neomycin molecules were bound per AuNp.

5.5. References

1. Hurst SJ, Lytton-Jean AKR, Mirkin CA. Maximizing DNA Loading on a Range of Gold Nanoparticle Sizes. Analytical Chemistry. 2006;78: 8313-8318.

2. Hill HD, Millstone JE, Banholzer MJ, Mirkin CA. The Role Radius of Curvature Plays in Thiolated Oligonucleotide Loading on Gold Nanoparticles. ACS Nano. 2009;3: 418-424.

3. Kimura-Suda H, Petrovykh DY, Tarlov MJ, Whitman LJ. Base-Dependent Competitive Adsorption of Single-Stranded DNA on Gold. Journal of the American Chemical Society. 2003;125: 9014-9015.

4. Demers LM, Östblom M, Zhang H, Jang N-H, Liedberg B, Mirkin CA. Thermal Desorption Behavior and Binding Properties of DNA Bases and Nucleosides on Gold. Journal of the American Chemical Society. 2002;124: 11248-11249.

5. Storhoff JJ, Elghanian R, Mirkin CA, Letsinger RL. Sequence-Dependent Stability of DNA-Modified Gold Nanoparticles. Langmuir. 2002;18: 6666-6670.

6. Hasan M, Bethell D, Brust M. The Fate of Sulfur-Bound Hydrogen on Formation of Self-Assembled Thiol Monolayers on Gold: 1H NMR Spectroscopic Evidence from Solutions of Gold Clusters. Journal of the American Chemical Society. 2002;124: 1132-1133.

7. Nuzzo RG, Zegarski BR, Dubois LH. Fundamental Studies of the Chemisorption of Organosulfur Compounds on Gold(111). Implications for Molecular Self-Assembly on Gold Surfaces. Journal of the American Chemical Society. 1987;109: 733-740.

8. Grönbeck H, Curioni A, Andreoni W. Thiols and Disulfides on the Au(111) Surface: The Headgroup−Gold Interaction. Journal of the American Chemical Society. 2000;122: 3839-3842.

9. Shipway AN, Lahav M, Gabai R, Willner I. Investigations into the Electrostatically Induced Aggregation of Au Nanoparticles. Langmuir. 2000;16: 8789-8795.

10. Steel AB, Levicky RL, Herne TM, Tarlov MJ. Immobilization of Nucleic Acids at Solid Surfaces: Effect of Oligonucleotide Length on Layer Assembly. Biophysical Journal. 2000;79: 975-981.

11. Parak WJ, Pellegrino T, Micheel CM, Gerion D, Williams SC, Alivisatos AP. Conformation of Oligonucleotides Attached to Gold Nanocrystals Probed by Gel Electrophoresis. Nano Letters. 2002;3: 33-36.

12. Jennings TL, Singh MP, Strouse GF. Fluorescent Lifetime Quenching near d = 1.5 nm Gold Nanoparticles: Probing NSET Validity. Journal of the American Chemical Society. 2006;128: 5462-5467.

13. Moazed D, Noller HF. Interaction of Antibiotics with Functional Sites In 16S Ribosomal RNA. Nature. 1987;327: 389-394.

14. Recht MI, Fourmy D, Blanchard SC, Dahlquist KD, Puglisi JD. RNA Sequence Determinants for Aminoglycoside Binding to an A-site rRNA Model Oligonucleotide. Journal of Molecular Biology. 1996;262: 421-436.

15. Arya DP, Xue L, Willis B. Aminoglycoside (Neomycin) Preference Is for A-Form Nucleic Acids, Not Just RNA: Results from a Competition Dialysis Study. Journal of the American Chemical Society. 2003;125: 10148-10149.

16. Arya DP, Coffee RL, Willis B, Abramovitch AI. Aminoglycoside−Nucleic Acid Interactions: Remarkable Stabilization of DNA and RNA Triple Helices by Neomycin. Journal of the American Chemical Society. 2001;123: 5385-5395.

17. Arya DP, Coffee RL, Charles I. Neomycin-Induced Hybrid Triplex Formation. Journal of the American Chemical Society. 2001;123: 11093-11094.

18. Chen Q, Shafer RH, Kuntz ID. Structure-Based Discovery of Ligands Targeted to the RNA Double Helix. Biochemistry. 1997;36: 11402-11407.

19. Robinson H, Wang AH-J. Neomycin, Spermine and Hexaamminecobalt(III) Share Common Structural Motifs in Converting B- to A-DNA. Nucleic Acids Research. 1996;24: 676-682.

20. Wallis MG, von Ahsen U, Schroeder R, Famulok M. A Novel RNA Motif for Neomycin Recognition. Chemistry & Biology. 1995;2: 543-552.

21. Kypr J, Fialová M, Chládková J, Tůmová M, Vorlíčková M. Conserved Guanine-Guanine Stacking in Tetraplex and Duplex DNA. European Biophysics Journal. 2001;30: 555-558.

22. Jiang L, Majumdar A, Hu W, Jaishree TJ, Xu W, Patel DJ. Saccharide-RNA Recognition in a Complex Formed Between Neomycin B and an RNA Aptamer. Structure. 1999;7: 817-827.

NAN-ANC Anchor

5′-(SH)TTTTAT**GGTTTACAATATT**-3′
3′-**CCAAATGTTATAA**CCTGATTTGAAGAGCGGGTCAGG-5′

NAN-NEO Aptamer

Figure 5.1. **Design of Programmable Carrier for Neomycin Delivery**. The DNA aptamer (NAN-NEO) attaches to the ssDNA anchor (NAN-ANC) by forming 13 Watson-Crick base-pairs. Bold letters denote base paired nucleotides.

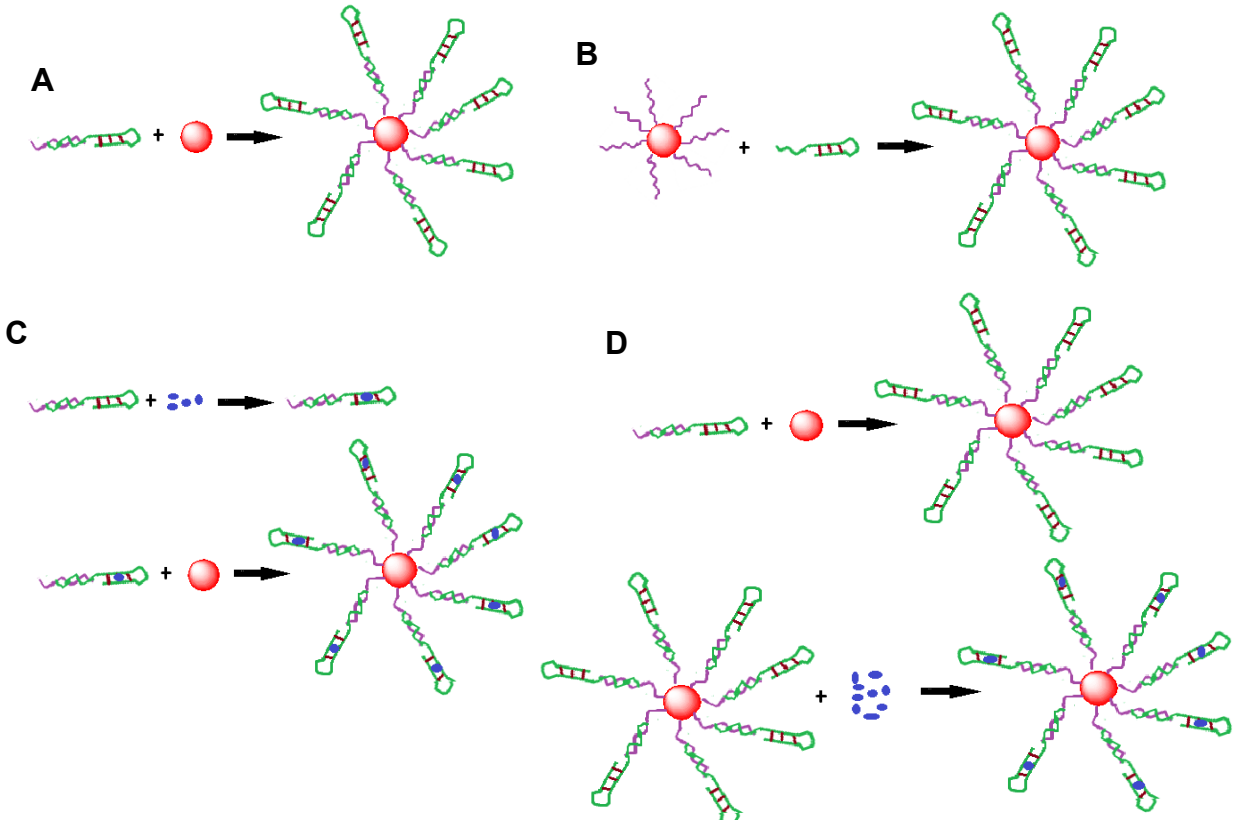

Figure 5.2. **Assembly of the Programmable Carrier for Neomycin Delivery.** Schematic illustration of the pre-hybridization approach (A), the post-hybridization approach (B) for the conjugation of DNA anchor to AuNps. Schematic illustration of binding of neomycin to AuNps by pre-binding approach (C), and post-binding approach (D).

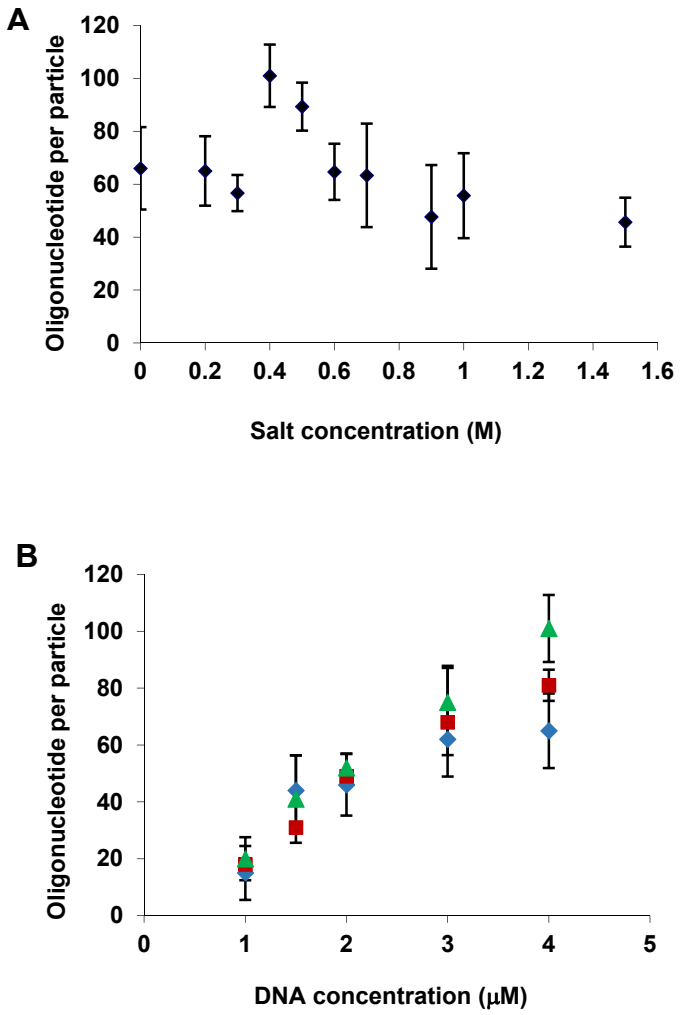

Figure 5.3. **Conjugation of SH-derivatized NAN-ANC Strands to 15 nm AuNps as a Function of Salt and DNA Concentration.** (A) Number of NAN-ANC attached per AuNps at different salt concentration with a constant NAN-ANC concentration (4 μM) in the reaction mixture. (B) Increasing number of DNA/AuNps with DNA concentration at (♦) 0.2 M, (■) 0.3 M, (▲) 0.4 M salt concentrations. N=3.

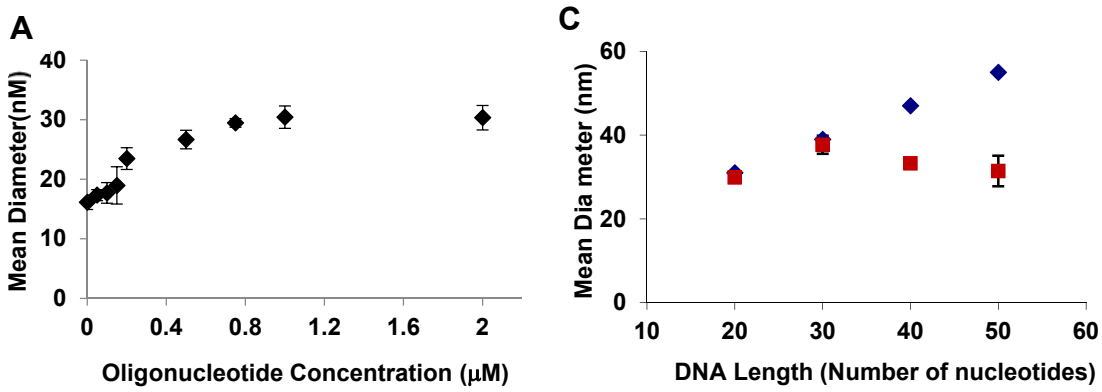

B NAN-ANC-20MER

5′-(SH) TTTTATGGTTTACAATATTT -3′

NAN-ANC-30MER

5′-(SH) TTTTAT**GGTTTACAATATT** -3′
3′-**CCAAATGTTATAA**CACACACACAA

NAN-ANC-40MER

5′-(SH) TTTTAT**GGTTTACAATATT** -3′
3′-**CCAAATGTTATAA**CACACACACACACACACACAA

NAN-ANC-50MER

5′-(SH) TTTTAT**GGTTTACAATATT** -3′
3′-**CCAAATGTTATAA**ACACACACACACACACACACACACACAA-5′

Figure 5.4. **Characterization of DNA on AuNps.** (A) Change in mean diameter of the DNA conjugated AuNps with number of DNA in reaction mixture. (B) 20, 30, 40 and 50 nucleotide long DNA complexes. (C) Deviation between (■) measured and (♦) theoretical mean diameters of AuNps functionalized with DNA of various lengths. N=3.

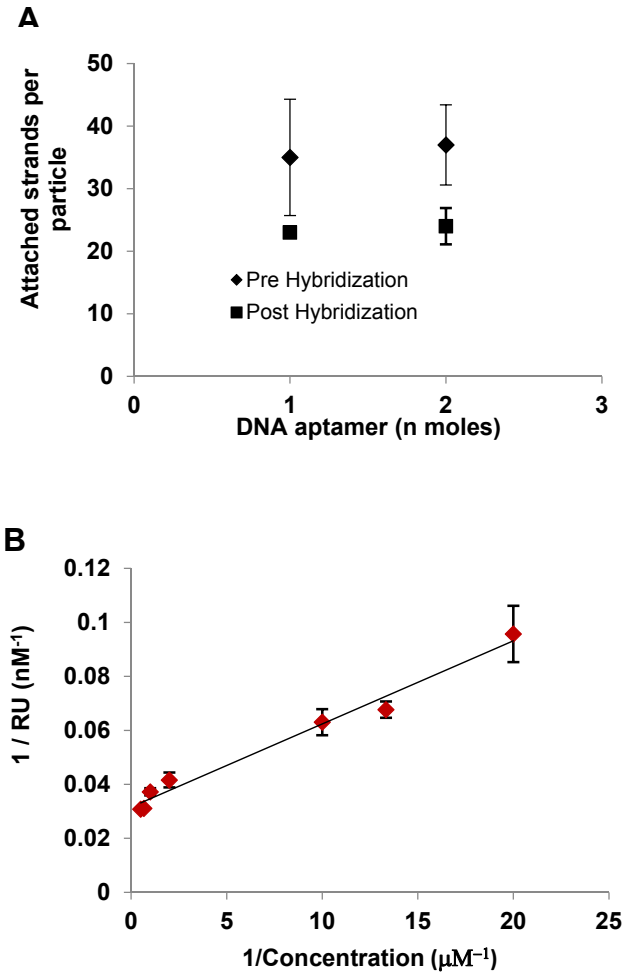

Figure 5.5: Neomycin Loading and Association Constant. (A) Comparison of (♦) pre and (■) post-hybridization methods of conjugating DNA aptamers to AuNps (B) Lineweaver-Burk plot to calculate the binding constant (K_D) of neomycin to DNA aptamer. K_D= 98.101 nM. N=3.

Chapter 6. Dynamic and Controlled Release of Neomycin from the Biohybrid Nano-Carrier by Temperature and Affinity Modulation

Aptamers are single-stranded nucleic acid molecules (RNA/DNA) which can fold into complex three dimensional structure[1-4] and form binding pockets and clefts for specific binding to target molecules[5-7] via hydrogen bonding, van der Walls forces, or base stacking interactions. Aptamers, with their ability to bind various molecules with high affinity, are being explored as potential devices for targeted and controlled drug delivery. The interest in aptamers as modules for drug delivery increased in the last ten years as various methods have been developed to increase their stability and protect them from ubiquitous nucleases[8]. In this section, we discuss examples demonstrating the applications of aptamers in drug delivery.

Using cell-SELEX, where live cells are used to select aptamers, aptamers that can specifically bind to various cells have been discovered. Such aptamers are used to target chemotherapeutic drugs for the treatment of cancer. Aptamers that specifically bind to a ligand, which is over expressed on the surface of the cancer cells, with high affinity can be complexed with the chemotherapeutic drugs or the drug carrier enabling cell-specific delivery of the drug. A simple aptamer-drug delivery system can be formed by conjugating the drug molecule to the aptamer by non-covalent or covalent interactions. In a study by Bangalkot *et al*., anti-cancer drug doxorubicin (DOX) was intercalated into A10 2'-fluoropyrimidine RNA aptamer capable of specific binding to the prostate-specific membrane antigen (PSMA)[9]. The cellular uptake of the aptamer-DOX conjugate was not

enhanced compared to the free DOX but the uptake was more specific to PSMA expressing cells. Shieh *et al*., conjugated a photosensitive agent (TMPyP4) to AS1411, aptamer that specifically binds to nucleon over expressed on the cancer cell membrane, to delivery TMPyP4 to breast cancer cells (MCF-7)[10]. The aptamer-TMPyP4 exhibited higher accumulation of the drug in MCF-7 cells than in M10 normal endothelial cells. And also, after the photodynamic treatment, the damage was higher in MCF-7 cells than in M10 cells. Anti-cancer drugs can also be conjugated to aptamers via covalent interactions by using chemical modifications that form stable ester, amide, and disulfide bonds. In a recent study, DOX was modified with hydrazone and conjugated to sgc8c aptamer which specifically binds to the protein tyrosine kinase 7 on CCRF-CEM cells[11]. Once inside the endosome of the cancer cell, the hydrazone linkage cleaves due to low pH resulting in drug release. The cytotoxicity in the CCRF-CEM cells due to the aptamer-DOX complex was about 6.7 fold more than that in the control cells without protein tyro kinase 7. Though these aptamer-drug conjugates were found to target the drug efficiently, the small molecular weight of these conjugates can lead to rapid renal clearance in vivo, and, thus, they may not be very efficient drug delivery devices.

Aptamers are also being investigated to be used in the interface of nanotechnology and medicine by developing aptamer-nanoparticle conjugates that can be used for targeted delivery of drugs to affected cells. Kim *et al*., developed an aptamer conjugated gold nanoparticle (AuNps) nano-carrier for targeted delivery of DOX[12]. The PSMA aptamer with an extended double stranded portion, capable of intercalating daunomycin, was conjugated to AuNps. This nano-carrier had cellular uptake with approximately three times more specificity to targeted cells as opposed to untargeted cells. In another study, Luo *et*

al., developed aptamer functionalized AuNps for the targeted and light controlled delivery of DOX[13]. DOX was intercalated to the DNA with repeated sequence (hpDNA), which along with the cell specific aptamer was conjugated to AuNps. The cell specific uptake of the nano-carrier was aided by the aptamer, and the release of DOX from the conjugate was controlled by the exposure to the resonating wave length corresponding to AuNps. Recently, Gao *et al*., developed a thrombin aptamer-functionalized, TBA-tethered, lipid-coated, mesoporous silica nanoparticles as an extra and intercellular anticancer nano-carrier[14]. The nano-carrier was loaded with anticancer drug docetaxel in the lipid vessicle. This nano-carrier, with the specific antithrombin characteristics of the aptamer-suppressed Hela cell growth by extracellular distribution of PAR-1, and it also caused effective cytotoxicity by releasing docetaxel in the cytoplasam.

Aptamers can also be used to control drug release from the delivery carrier. This phenomenon is demonstrated with the aptamer-fucntionalized hydrogel delivery carrier for protein drugs. The ability of the aptamers to bind a target molecule or complimentary oligonucleotide was used to release the drug from the hydrogels crosslinked or conjugated with aptamers. Hydrogels crosslinked with DNA aptamers dissolved in the presence of the target molecule due to competitive binding of target molecule to aptamer, and the embedded drug[15] was released. In a series of studies, the Wang group demonstrated that by incorporating aptamers with a specific binding affinity for the protein drug into a hydrogel, the release of protein from the hydrogel can be controlled and prolonged. Acrylamide-bisacrylamide hydrogel incorporated with aptamer for platelet derived growth factor BB (PDGF-BB) was found to decrease the rate of release of the protein from 70% to 10% in the initial 24 hours and to 6% in the next 120 hours[16]. In another study, they demonstrated

that the release of PGDF-BB from the aptamer functionalized hydrogel can be controlled and made pulsatile with a complementary oligonucleotide (CO) that can break the aptamer-protein interaction by competitive binding[17]. Complementary oligonucleotide binds to the aptamer and breaks the aptamer-protein interaction resulting in protein release. Thus, the release of protein was controlled by controlling the concentration of CO. Using this concept, Battig *et al*., demonstrated the controlled release of multiple proteins from the aptamer-conjugated hydrogel with CO[18]. This concept of controlling the drug release in the presence of CO was also investigated on aptamer modified liposomes[19]. Liposomes encapsulated with cisplatin were functionalized with AS1411 DNA aptamer that can specifically bind to nucleolin overexpressed on the cancer cell membrane. The cellular uptake of this liposomal carrier by the cancer cells was demonstrated to be controlled by the presence of CO to the AS1411 aptamer. The CO binds to the aptamer and disrupts the structure of the aptamer required to bind to the cancer cell membrane, resulting in cessation of cellular uptake. Drug release from aptamer can be obtained using various modulations. Taking advantage of aptamer response to enzymatic and affinity modulations, Venkatesh et al. demonstrated controlled release of HIV-1 mRNA degrading deoxyribozyme[20]. Recently, an in situ injectable hydrogel functionalized with aptamers was developed for the controlled release of proteins[21]. This aptamer-functionalized hydrogel prolonged the release of protein from the hydrogel, and also the drug release was controlled by adjusting the affinity of the aptamer.

This concept of controlling the release of drug from the aptamer by exploiting the binding characteristics of the aptamer has not been explored in detail. In an attempt to prove that such control over drug delivery with the DNA aptamers can be obtained from

nanoparticles as small as 15 nm, we developed a nano-carrier for a model drug neomycin and demonstrated controlled release of the drug using temperature and affinity modulation

6.1. Scientific Rationale

We developed a novel drug delivery carrier by functionalizing DNA aptamers on gold nanoparticles for extended and controlled drug release. The DNA aptamer protects the therapeutic against modification and degradation by cellular and/or extracellular factors, facilitates specific high-affinity binding of the drug to the carrier, and provides multiple opportunities for modulation of drug release. These modulations include aptamer-therapeutic affinity modulation, physical modulation, enzymatic modulation, and stability modulation[22]. This make the aptamer a very attractive candidate to be used for drug delivery.

With physical modulation, a change in temperature can alter the aptamer-drug binding by disrupting the non-covalent interactions or significantly altering the nucleic acid tertiary structure, leading to drug release. Depending on the way the carrier is designed, melting of NA strands can also lead to release of therapeutic with or without the aptamer. Enzymatic modulation can also be used when nucleotide sequences recognized by specific exonucleases/endonucleases can be incorporated in the conjugating complex of nucleic acid aptamer, so that release of therapeutics can be tissue/cell specific depending on the presence or absence of the particular enzymes. The enzyme can act either as a programmable modulator or as an on-demand one-time release triggering agent. Also,

various resistances of nucleic acids to ubiquitous nucleases can be used to program susceptibility to degradation and structural stability, and thereby program drug release.

We hypothesized that these release control methods or the combination of them would provide an exquisite control over the therapeutic release profile of significant therapeutic payloads. By covalently incorporating single or multiple nucleic acid aptamers into delivery constructs, the release of single or multiple therapeutic release could be elegantly controlled in a number of ways, and also when incorporating a spectrum of affinities for a particular therapeutic agent, the aptamer with lower affinity for the therapeutic agent would release it more readily than the aptamer with higher affinity for the therapeutic agent.

In this chapter, we describe how well the drug release from DNA aptamers functionalized AuNps nano-carrier can be controlled and modulated. We report the controlled release of an antibiotic drug, neomycin, from the nano-carrier with temperature and drug binding affinity modulations.

6.2. Materials and Methods

In this section, we describe the materials and methods for synthesis of nano-carrier for extended release of neomycin, and describe the methods of controlled drug release from the nano-carrier.

6.2.1. Materials. Gold nanoparticles of 15 nm diameter (AuNPs) were purchased from Ted Pella (Redding, CA). Modified and unmodified oligonucleotides were synthesized by

Operon Biotechnologies. NAP-5 columns (Sephadex G-25 DNA grade) were purchased from G.E. Healthcare (Piscatiway, NJ). Sterile, 6 well clear multiple well plates and 384 well low flange solid black microplates were obtained from Corning, Inc. (Corning NY). Polyester sealing films were purchased from VWR International (West Chester, PA), and drop dialysis membranes (diameter: 13 mm, pore size: 0.025 μm) were obtained from Millipore (Billerica, MA). Neomycin sulfate (analytical standard) and Neomycin-TMR were purchased from Sigma-Aldrich (St. Louis, MO) and Echelon Biosciences, Inc. (Salt Lake City, UT), respectively. All other chemicals were molecular biology grade and unless specified, were from Sigma-Aldrich (St. Louis, MO).

6.2.2. Methods. Preparation of Neomycin Nano-carrier

Hybridization reaction mixture (65 μL) containing NAN-ANC (2 nmoles) and NAN-NEO (2 nmoles), 0.18 M phosphate buffer solution (PB; pH 7.2) and 0.1 M dithiothreitol (DTT) were incubated at 37^{o}C for 3 hours. NAN-NEO:NAN-ANC complexes were then desalted on NAP-5 column and concentrated to ~ 20 μL using a Speed Vac. Neomycin-TMR (0.2 nmoles) suspended in 20 μL of neomycin binding buffer (NBB) was added to the NAN-NEO:NAN-ANC complexes and incubated on ice for 30 minutes for binding. And then 1 mL of AuNps (15 nm, $1.4x10^{12}$ particles / mL) and 1 μL of 10% SDS solution were added. The mixture was vortexed for 16 hours at room temperature. The PB was added until a final concentration of 0.01 M was achieved, and then the neomycin:NAN-NEO:NAN-ANC/AuNps solution was incubated at room temperature for 2 hours. Aliquots of 10 μL of 5 M NaCl solution were added to the neomycin:NAN-

NEO:NAN-ANC/AuNps solution. The mixture was sonicated for 10 seconds using a sonic dismembrator (Fisher Scientific) and incubated for 20 minutes at room temperature after every addition of NaCl. This process was repeated to a final concentration of 0.4 M NaCl. The neomycin:NAN-NEO:NAN-ANC/AuNps solution was then vortexed for 24 hours at room temperature. The solution was centrifuged 3 times for 40 minutes each time at 13,000 rpm to remove unbound oligonucleotides and neomycin. The neomycin:NAN-NEO:NAN-ANC complexes conjugated AuNps pellet was resuspended in a 10 mM PB and 0.2 M NaCl solution (PBS; pH 7).

Neomycin nano-carrier with NAN-NEO mutants were also prepared similarly by replacing 2 nmoles of NAN-NEO with 2 nmoles of A13G-NAN-NEO or T17CT18C-NAN-NEO. Nano-carrier with combination of aptamer and mutant was prepare by adding 1:1 and 1:2 nmoles of NAN-NEO and mutant (A13G-NAN-NEO or T17CT18C-NAN-NEO) in the reaction mixture, and the nano-carrier was resuspended in DI water after centrifugation wash.

6.2.3. Methods. Dynamic In-vitro Release Studies

Neomycin bound aptamer (neomycin:NAN-NEO:NAN-ANC) or aptamer mutants (neomycin:A13G-NAN-NEO:NAN-ANC and neomycin:T17CT18C-NAN-NEO:NAN-ANC) conjugated AuNps were prepared as per protocol. A 100 µL aliquot of the sample was pipetted on a drop dialysis membrane floating on 10 mL of PBS in a clear 6 well plate. To minimize evaporation losses, the well plate was covered with adhesive polyester sealing films. After 10 minutes, the sample was pipetted from the membrane and corrected for any

volume loss due to evaporation by adding corresponding volume of PBS. The DNA aptamers were removed from AuNps by incubating in 0.05 M DTT for 16 hours at room temperature, centrifuged for 30 minutes at 13,000 rpm, and then the supernatant was measured for fluorescent Neomycin-TMR. The experiment was repeated for different dialysis times (30, 60, 120, 240, 480, 720, and 1,440 minutes) and at different temperatures (3 ± 1, 22 ± 1, and 40 ± 1^{o}C)

6.3. Results and Discussion

We hypothesized that the release of drug from the synthesized nano-carrier can be obtained by disrupting the non-covalent complexation between neomycin and the aptamer using temperature as an external stimuli. Hydrogen bonds between DNA strands are continuously formed and broken, and the average lifetime of a hydrogen bond decreases with increasing temperature. Taking advantage of this phenomenon, we obtained a temperature triggered release of neomycin from the NAN-NEO conjugated nano-carrier **(Figure 6.1)** for an extended period of 24 hours at 3 ± 1, 22 ± 1, and 40 ± 1^{o}C. We observed that the release rate of neomycin from the AuNps carriers increased with temperature. An average of 30 ± 3%, 72 ± 4 % and 87 ± 6% of bound neomycin was released at 3 ± 1, 22 ± 1 and 40 ± 1^{o}C, respectively, after 24 hours with no burst release **(Figure 6.1)**.

These temperatures were chosen to prove our hypothesis that drug release from the nano-carirer with increase in temperature is due to disruption of hydrogen bonds holding the three dimensional structure of the aptamer. The temperatures 3^{o}C and 22^{o}C corresponds to storage and room temperatures, respectively, and 40^{o}C is approximately the highest

temperature to release drugs inside the body without damaging the cells. The degradation temperature of the aptamer:anchor bond is ~53^{o}C (calculated using the DNAmelt web server) and thiol gold bond is ~80^{o}C[23], which clearly suggests that at 40^{o}C majority of bound neomycin is released and not the aptamer or the anchor.

To demonstrate that the extended release of neomycin was not due to diffusion limitations within the experiment, another experiment was conducted with a concentration spike of neomycin onto a dialysis membrane in well plate containing buffer. Diffusion of neomycin was very quick and the concentration curve differed drastically from the release curves (**Figure 6.1**). The free neomycin diffused within 15 minutes which proved that the extended release of drug from the nano-carrier was due to complexation of neomycin to the aptamer. Thus, control of release can be attributed to the strength of the non-covalent interactions between the aptamer and drug.

Besides temperature, the release of drug from the nano-carrier can be triggered using various other modulations such as binding affinity as well as specific and non-specific enzymes. We assumed that at a given temperature different drug release profiles can be obtained with aptamers having different drug binding affinity. We hypothesized that the aptamer with lower affinity for the therapeutic agent will release its ligand more readily than the aptamer with higher affinity for the therapeutic agent. In order to create aptamers with different binding affinity for neomycin, we produced two mutants of NAN-NEO (**Figure 6.2A**; aptamer with a high neomycin binding affinity; K_d= 98.101 nM) by changing one and two nucleotides at the drug binding site of the aptamer. By changing the adenine at the 13th position in NAN-NEO to guanine we produced A13G-NAN-NEO aptamer mutant **(Figure 6.2B)**, and by changing the thymine at the 17th and 18th position

in NAN-NEO to cytosine we produced T17CT18C-NAN-NEO aptamer mutants **(Figure 6.2C)**. These three aptamers, due to their difference in the sequence which implies a difference in their three dimensional structure, bind neomycin with different affinities. Release of neomycin from nano-carrier functionalized with these aptamers having different drug binding affinities were studied to evaluate the relationship between drug binding affinity and rate of drug release **(Figure 6.3)**. NAN-NEO aptamer conjugated nano-carrier **(Figure 6.2A)**, which binds the drug with a high affinity, released the drug relatively slowly, and the amount of drug released from the carrier increased steadily for up to 24 hours. The two nucleotide modified mutant (T17CT18C-NAN-NEO; **Figure 6.2C**) conjugated nano-carrier produced a burst release of 30% of the bound drug in the initial 10 minutes followed by a continuous and steady increase in the drug release which stabilized at 12 hours. The mutant with one nucleotide different from the aptamer (A13G-NAN-NEO**; Figure 6.2B**) produced a burst release of 40% of the bound drug in 10 minutes followed by a steep increase to 70% in 1 hour and then stabilized **(Figure 6.3)**.

The drug release from NAN-NEO, the aptamer with the highest drug binding affinity, conjugated nano-carrier increased steadily with time. While, the aptamer mutant A13G-NAN-NEO, with the lowest drug binding affinity, conjugated nano-carrier released 70% of the bound drug within 1 hour and then stabilized. The nature of drug release from the aptamer mutant T17CT18C- NAN-NEO is hypothesized to be due to two drug binding sites on the aptamer mutant with one low and another high binding affinity. The low binding affinity site can explain the 30% burst release followed by a slightly increasing release until 2 hours, and the high binding affinity site can explain the continuously increasing drug release profile from 2 to 24 hours. The high binding affinity site having an

affinity higher than that of NAN-NEO can explain the cumulative release being less than that of the NAN-NEO conjugated nano-carrier from 4 to 24 hours. These results prove that the drug release from the nano-carrier can be controlled by changing the drug binding affinity of the functionalized aptamer. It also supports our hypothesis that the aptamer with higher affinity would release the drug in a consistently increasing profile for a longer period of time, and the aptamers with lower affinity would release the drug very fast.

Similar to the release of drug from the aptamer conjugated nano-carrier, the drug release from the mutants are also temperature dependent. We studied the extended release of neomycin from the mutant-aptamer conjugated nano-carriers at different temperatures (**Figure 6.4**). The release was observed for a period of 24 hours at 3 ± 1, 22 ± 1, and 40 ± 1^{o}C. The drug release profile of the aptamer mutants shows that with the increase in temperature there is an increase in the amount of drug release at every time point. After 24 hours, an average of 21 ± 5%, 64 ± 2%, 77 ± 3% of the bound drug was released from T17CT18C-NAN-NEO conjugated nano-carrier at 3 ± 1, 22 ± 1 and 40 ± 1^{o}C, respectively, with a 30% initial burst release at 22 ± 1 and 40 ± 1^{o}C. Similarly, 33 ± 7%, 70 ± 5, 85 ± 4% of the bound drug was released from A13G-NAN-NEO conjugated nano-carrier at 3 ± 1, 22 ± 1 and 40 ± 1^{o}C, respectively, with a 40% initial burst release at 22 ± 1 and 40 ± 1^{o}C. This experiment proved that the combination of affinity and temperature modulation can extend the range of control over drug release. The temperature 3 ± 1^{o}C was found to be a good storage temperature for the aptamer, and the aptamer mutant conjugated nano-carrier, with less than 30% of the bound drug being released from it. On comparing the release profiles of NAN-NEO, A13G-NAN-NEO, T17CT18C- NAN-NEO conjugated nano-carriers at 40 ± 1^{o}C, we inferred that at higher temperatures, close to the melting

temperature of the aptamer, drug binding affinity difference does not vary the release pattern as much as at lower temperatures **(Figure 6.5)**. At temperature very close to the melting point of the aptamer, all the hydrogen bonds between the drug and the aptamer are expected to be distorted and almost 100% drug is expected to be released. Thus, at 40 ± 1^{o}C the drug binding affinity does not play a significant role in varying the drug release profile **(Figure 6.5)**. While at temperature less than the melting temperature (i.e., 22 ± 1^{o}C) very significant difference in the drug release profile with the drug binding affinity was observed **(Figure 6.3)**.

After understanding how well the drug release from the nano-carrier can be controlled and modulated with temperature and drug binding affinity, we investigated the control that could be obtained by conjugating multiple aptamers with different binding affinity onto the nano-carrier. The release profile from the nano-carrier with 1:1 and 1:2 combination of NAN-NEO and T17CT18C-NAN-NEO conjugated nano-carrier **(Figure 6.6)** were compared with the release profiles of NAN-NEO conjugated nano-carrier **(Figure 6.7)** and T17CT18C-NAN-NEO conjugated nano-carrier **(Figure 6.8)**. The release of neomycin from the nano-carrier functionalized with 1:1 combination of NAN-NEO and T17CT18C-NAN-NEO was found to be similar to that from the NAN-NEO conjugated nano-carrier. The drug release from the nano-carrier functionalized with 1:2 combination of NAN-NEO and T17CT18C-NAN-NEO was found to be similar to the release from the NAN-NEO conjugated nano-carrier until 2 hours and then was similar to the release from T17CT18C-NAN-NEO conjugated nano-carrier from 4 to 24 hours. The release of neomycin after 8 hours from the nano-carrier with the 1:1 combination of NAN-NEO and T17CT18C-NAN-NEO was higher than NAN-NEO nano-carrier, and 1:2 combination was

lesser than T17CT18C-NAN-NEO nano-carrier. This data proves that it is possible to further modulate the drug release from the nano-carrier by having a combination of aptamers with different binding affinity on the nano-carrier.

Similar study with 1:1 and 1:2 combination of NAN-NEO and A13G-NAN-NEO **(Figure 6.9)** demonstrated that the release of neomycin from the nano-carrier with 1:1 combination of aptamer and mutant had an initial burst release of 35% similar to that of A13G-NAN-NEO conjugated nano-carrier **(Figure 6.10)**, but later the release increased very slowly and stabilized at around 55%. The 1:2 combination of NAN-NEO and A13G-NAN-NEO conjugated nano-carrier released neomycin in a steadily increasing manner similar to NAN-NEO **(Figure 6.11)**, but the drug release at every time point was much lower than that from the NAN-NEO conjugated nano-carrier. The reason behind this decrease in the release from the nano-carrier functionalized with 1:1 and 1:2 combinations of NAN-NEO and A13G-NAN-NEO is not clear. A suitable and plausible explanation is that NAN-NEO and A13G-NAN-NEO forms additional complex with each other, and the complex holds the drug much stronger than the aptamer itself.

6.4. Conclusions

In this chapter, we have described the methods by which the drug release from the aptamer conjugated nano-carrier can be controlled and modulated. DNA aptamers are sensitive to various physical and enzymatical triggers. By taking advantage of this characteristic of aptamers, we demonstrated the controlled release of drug from aptamer functionalized AuNps with temperature and drug binding affinity modulations.

Aptamer binds the drug molecules in their complex three dimensional structure stabilized by hydrogen bonds and electrostatic interactions. The hydrogen bonds in the three dimensional structure of the aptamer are continuously broken and reformed, and the average lifetime of a hydrogen bond decreases with increasing temperature. Taking advantage of this phenomenon, we demonstrated different drug release profiles for the NAN-NEO conjugated nano-carrier at different temperatures (3 ± 1, 22 ± 1, and 40 ± 1^{o}C). The release rate of neomycin from the AuNps carriers increased with temperature. At 40 ± 1^{o}C, which is close to the melting temperature of the aptamer, maximum amount of bound drug was released demonstrating that with an hyperthermal treatment (medical treatment involving increase in the body temperature) maximum amount of drug can be release in vivo. At 3 ± 1^{o}C, only about 25% of the bound drug was released proving that the nano-carrier can be safely stored at this temperature without releasing much of the bound drug.

We also proved that the drug release from the nano-carrier can be modulated by varying the drug binding affinity of the aptamer. By changing one and two nucleotides at the drug binding site of NAN-NEO, aptamer that binds neomycin with a high affinity (Kd = 98.101 nM), we produced two mutants (A13G-NAN-NEO and T17CT18C-NAN-NEO) with different affinities to neomycin. The one nucleotide changed mutant (A13G-NAN-NEO) which binds the drug with the least affinity released about 70% of the bound drug within 1 hour, while the drug release from NAN-NEO (high affinity aptamer) was relatively slow and steadily increasing over time. This study confirmed that the aptamer with lower affinity would readily release the drug than the aptamer with higher affinity. On the other hand, drug release profile from the two nucleotide modified mutant (T17CT18C-NAN-NEO) inferred the presence multiple drug binding site on it. Two drug

binding sites, one with a low affinity and the other with an affinity higher than NAN-NEO would explain the release profile from T17CT18C-NAN-NEO conjugated nano-carrier. Thus, proving that the drug release from the DNA aptamer conjugated nano-carrier can be precisely modulated using spectrum of aptamers with different binding affinity to the drug.

The drug release from the aptamer mutants were also observed to be temperature dependent. At temperature close to the melting temperature of the aptamer ($40 \pm 1^{o}C$), all the hydrogen bonds in the aptamer structure are expected to be distorted resulting in maximum drug release. Thus, at this temperature, the drug release is independent of the variations in drug binding affinity. Moreover, we demonstrated that the drug release can be further modulated by functionalizing a combination of aptamers with different binding affinities on the nano-carrier.

Thus, we produced a proof of concept as to how well the drug release from the nano-carrier can be controlled by using DNA aptamers as drug release control moiety. Furthermore, we demonstrated that the drug release can be precisely modulated by varying the drug binding affinity of the aptamer conjugated to the nano-carrier, and by conjugating multiple aptamer with different drug binding affinity on the nano-carrier. Thus, drug delivery using aptamer conjugated nano-carrier can be a very versatile approach to modulated drug delivery according to the treatment regime.

6.5. References

1. Gold L, Polisky B, Uhlenbeck O, Yarus M. Diversity of Oligonucleotide Functions. Annual Review of Biochemistry. 1995;64: 763-797.

2. Patel DJ. Structural Analysis of Nucleic Acid Aptamers. Current Opinion in Chemical Biology. 1997;1: 32-46.

3. Hermann T, Patel DJ. Adaptive Recognition by Nucleic Acid Aptamers. Science. 2000;287: 820-825.

4. Patel DJ, Suri AK. Structure, Recognition and Discrimination in RNA Aptamer Complexes with Cofactors, Amino Acids, Drugs and Aminoglycoside Antibiotics. Reviews in Molecular Biotechnology. 2000;74: 39-60.

5. Famulok M, Jenne A. Oligonucleotide Libraries - Variatio Delectat. Current Opinion in Chemical Biology. 1998;2: 320-327.

6. Famulok M, Mayer G. Aptamers as Tools in Molecular Biology and Immunology. Current Topics in Microbiology and Immunology. 1999;243: 123-136.

7. Hesselberth J, Robertson MP, Jhaveri S, Ellington AD. In Vitro Selection of Nucleic Acids for Diagnostic Applications. Reviews in Molecular Biotechnology. 2000;74: 15-25.

8. Aurup H, Williams DM, Eckstein F. 2'-Fluoro and 2-Amino-2'-Deoxynucleoside 5'-Triphosphates as Substrates for T7 RNA Polymerase. Biochemistry. 1992;31: 9636-9641.

9. Bagalkot V, Farokhzad OC, Langer R, Jon S. An Aptamer–Doxorubicin Physical Conjugate as a Novel Targeted Drug-Delivery Platform. Angewandte Chemie International Edition. 2006;45: 8149-8152.

10. Shieh Y-A, Yang S-J, Wei M-F, Shieh M-J. Aptamer-Based Tumor-Targeted Drug Delivery for Photodynamic Therapy. ACS Nano. 2010;4: 1433-1442.

11. Huang Y-F, Shangguan D, Liu H, et al. Molecular Assembly of an Aptamer–Drug Conjugate for Targeted Drug Delivery to Tumor Cells. ChemBioChem. 2009;10: 862-868.

12. Kim D, Jeong YY, Jon S. A Drug-Loaded Aptamer−Gold Nanoparticle Bioconjugate for Combined CT Imaging and Therapy of Prostate Cancer. ACS Nano. 2010;4: 3689-3696.

13. Luo Y-L, Shiao Y-S, Huang Y-F. Release of Photoactivatable Drugs from Plasmonic Nanoparticles for Targeted Cancer Therapy. ACS Nano. 2011;5: 7796-7804.

14. Gao L, Cui Y, He Q, Yang Y, Fei J, Li J. Selective Recognition of Co-assembled Thrombin Aptamer and Docetaxel on Mesoporous Silica Nanoparticles against Tumor Cell Proliferation. Chemistry. 2011;17: 13170-13174.

15. Yang H, Liu H, Kang H, Tan W. Engineering Target-Responsive Hydrogels Based on Aptamer−Target Interactions. Journal of the American Chemical Society. 2008;130: 6320-6321.

16. Soontornworajit B, Zhou J, Shaw MT, Fan T-H, Wang Y. Hydrogel Functionalization with DNA Aptamers for Sustained PDGF-BB Release. Chemical Communications. 2010;46: 1857-1859.

17. Soontornworajit B, Zhou J, Wang Y. A Hybrid Particle-Hydrogel Composite for Oligonucleotide-Mediated Pulsatile Protein Release. Soft Matter. 2010;6: 4255-4261.

18. Battig MR, Soontornworajit B, Wang Y. Programmable Release of Multiple Protein Drugs from Aptamer-Functionalized Hydrogels via Nucleic Acid Hybridization. Journal of the American Chemical Society. 2012;134: 12410-12413.

19. Cao Z, Tong R, Mishra A, et al. Reversible Cell-Specific Drug Delivery with Aptamer-Functionalized Liposomes. Angewandte Chemie International Edition. 2009;48: 6494-6498.

20. Venkatesh S, Wower J, Byrne ME. Nucleic Acid Therapeutic Carriers with On-Demand Triggered Release. Bioconjugate Chemistry. 2009;20: 1773-1782.

21. Soontornworajit B, Zhou J, Zhang Z, Wang Y. Aptamer-Functionalized In Situ Injectable Hydrogel for Controlled Protein Release. Biomacromolecules. 2010;11: 2724-2730.

22. Venkatesh S, Wower J, Byrne ME. Drug Delivery Systems and Methods. In: LLP HaO, editor. United States of America, 2008.

23. Civit L, Fragoso A, O'Sullivan CK. Thermal Stability of Diazonium Derived and Thiol-Derived Layers on Gold for Application in Genosensors. Electrochemistry Communications. 2010;12: 1045-1048.

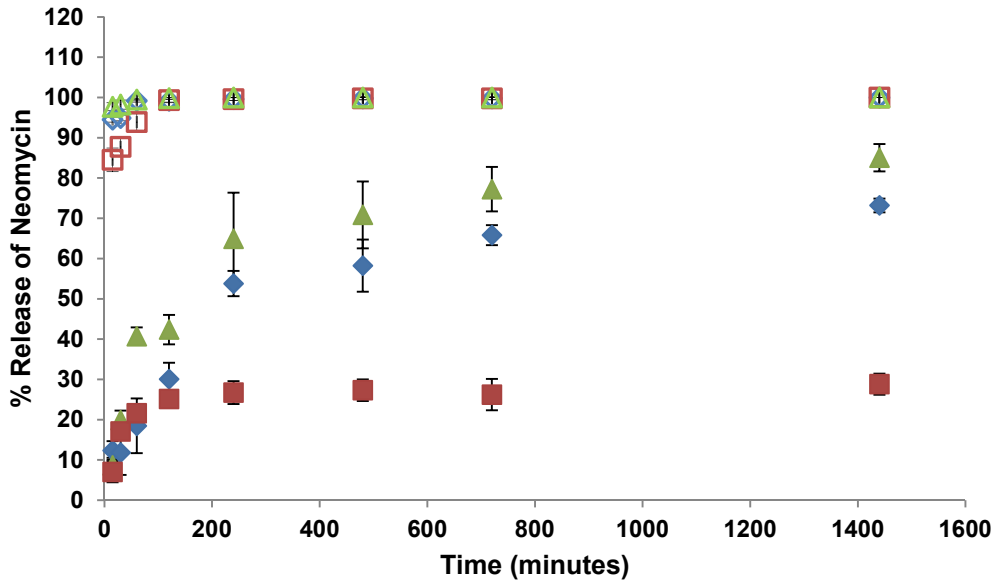

Figure 6.1. Dynamic Tunable, Extended Release of Neomycin from NAN-NEO Conjugated Nano-Carrier. The release of neomycin from the carrier at (■)3 ± 1°C, (♦)22 ± 1°C ,(▲) 40 ± 1°C are shown along with a concentration spike of neomycin onto a dialysis membrane in well plate containing only buffer (□) 3±1, (◊) 22±1, (Δ) 40±1°C. N = 3.

A

NAN-ANC Anchor

5′-(SH)TTTTAT**GGTTTACAATATT**-3′
3′-**CCAAATGTTATAA**CCTGATTTGAAGAGCGGGTCAGG-5′

NAN-NEO Aptamer

B

NAN-ANC Anchor

5′-(SH)TTTTAT**GGTTTACAATATT**-3′
3′-**CCAAATGTTATAA**CCTGATTTGAGGAGCGGGTCAGG-5′

A13G-NAN-NEO Aptamer mutant

C

NAN-ANC Anchor

5′-(SH)TTTTAT**GGTTTACAATATT**-3′
3′-**CCAAATGTTATAA**CCTGACCTGAAGAGCGGGTCAGG-5′

T17CT18C-NAN-NEO Aptamer mutant

Figure 6.2. Design of Programmable Carrier for Neomycin Delivery. (A) The DNA aptamer (NAN-NEO) attaches to the ssDNA anchor (NAN-ANC) by forming 13 Watson-Crick base-pairs. Bold letters denote base paired nucleotides. (B) Similar complexing with A13G-NAN-NEO aptamer mutant with one point mutation at the 13th position (marked in red). (C) Nano-carrier DNA complex with T17CT18C-NAN-NEO aptamer mutant with two point mutation at 17th and 18th nucleotide position (marked in red).

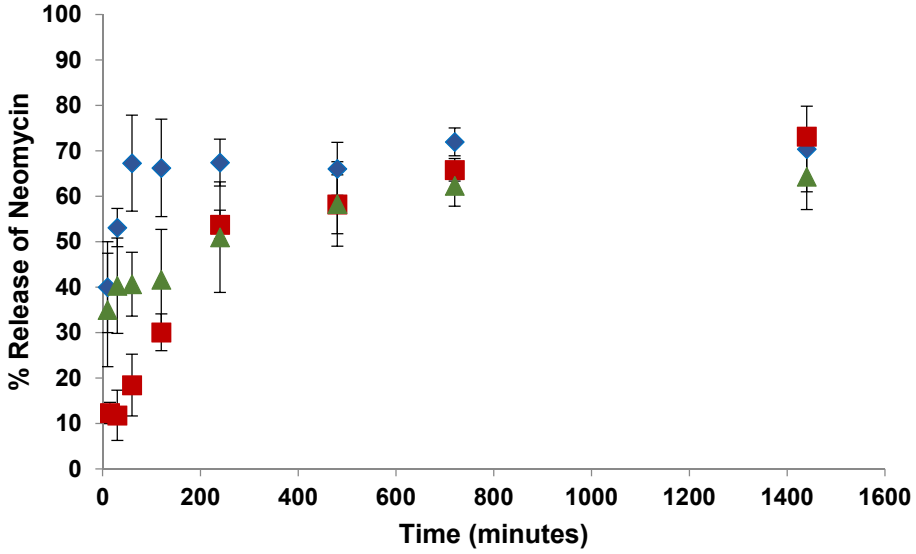

Figure 6.3. Affinity Modulated, Dynamic, Extended Release of Neomycin from Nanoscale Drug Delivery Carriers. The release of neomycin at 22 ± 1°C from (■) NAN-NEO conjugated nano-carrier, (♦) A13G-NAN-NEO conjugated nano-carrier, and (▲) T17CT18C-NAN-NEO conjugated nano-carrier. N = 3.

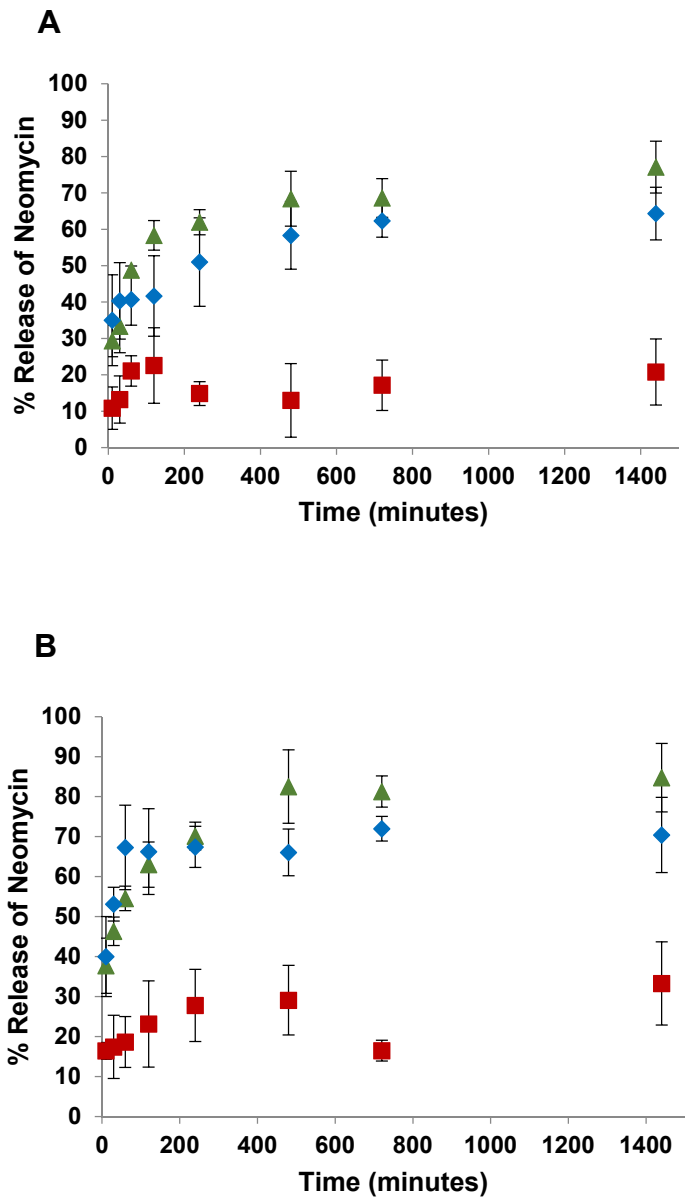

Figure 6.4. Temperature Dependent Dynamic, Extended Release of Neomycin from Nanoscale Drug Delivery Carriers. Neomycin release from (A) T17CT18C-NAN-NEO conjugated nano-carrier, and (B) A13G-NAN-NEO conjugated nano-carrier at (■) 3 ± 1°C, (♦) 22 ± 1°C, (▲) 40 ± 1°C. N = 3.

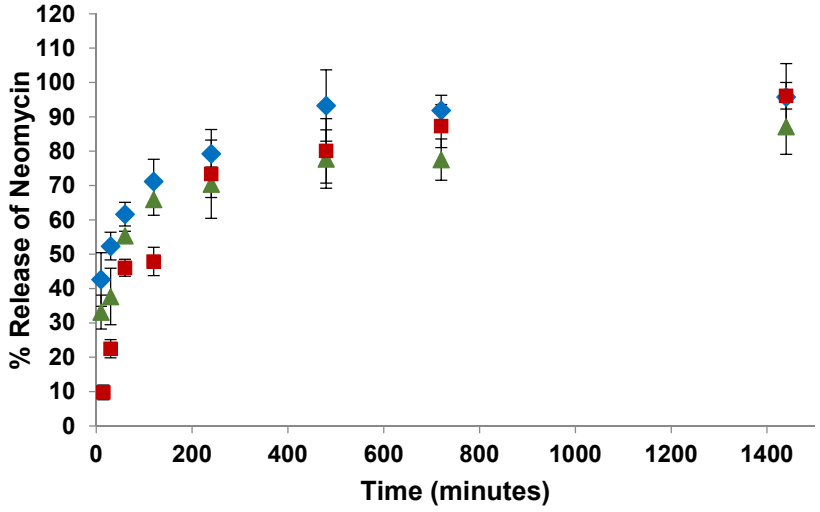

Figure 6.5. Affinity Modulated, Dynamic, Extended Release of Neomycin from Aptamer and Aptamer Mutants Nanoscale Drug Delivery Carriers. Release of neomycin from (■) NAN-NEO conjugated nano-carrier, (♦) A13G-NAN-NEO conjugated nano-carrier, and (▲) T17CT18C-NAN-NEO conjugated nano-carrier, at 40 ± 1ºC. N = 3.

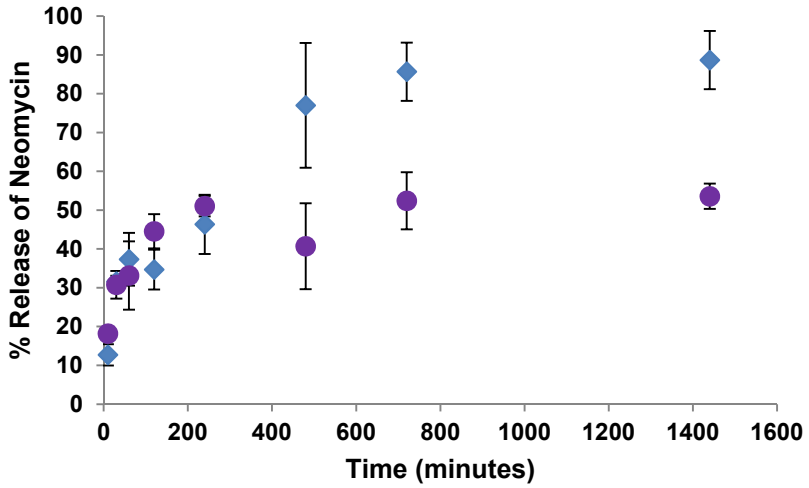

Figure 6.6. Dynamic Release of Neomycin from NAN-NEO and T17CT18C- NAN-NEO Combination Nano-Carrier. Release of neomycin at 22 ± 1°C from (♦) 1:1 NAN-NEO and T17CT18C-NAN-NEO combination conjugated nano-carrier and (●) 1:2 NAN-NEO and T17CT18C-NAN-NEO combination conjugated nano-carrier. N = 3.

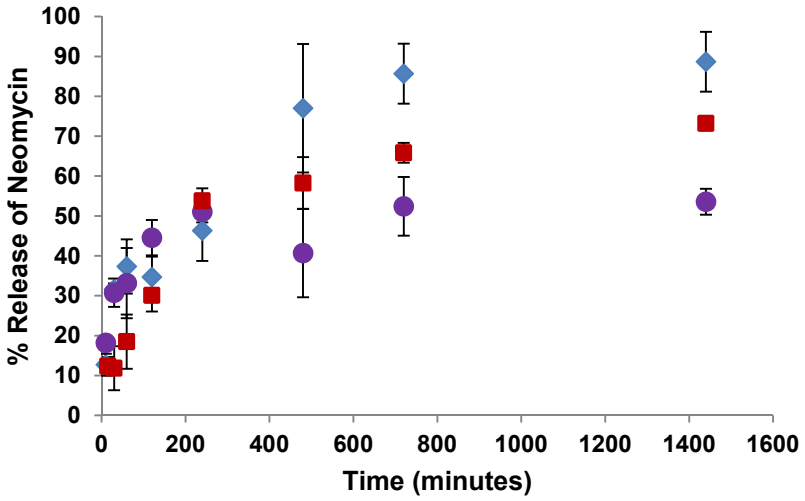

Figure 6.7. Comparison of Dynamic Release of Neomycin from NAN-NEO and T17CT18C- NAN-NEO Combination Nano-Carrier with NAN-NEO Nano-Carrier. Release of neomycin at 22 ± 1°C from (■) NAN-NEO conjugated nano-carrier, (♦) 1:1 NAN-NEO and T17CT18C-NAN-NEO combination conjugated nano-carrier and (●) 1:2 NAN-NEO and T17CT18C-NAN-NEO combination conjugated nano-carrier. N = 3.

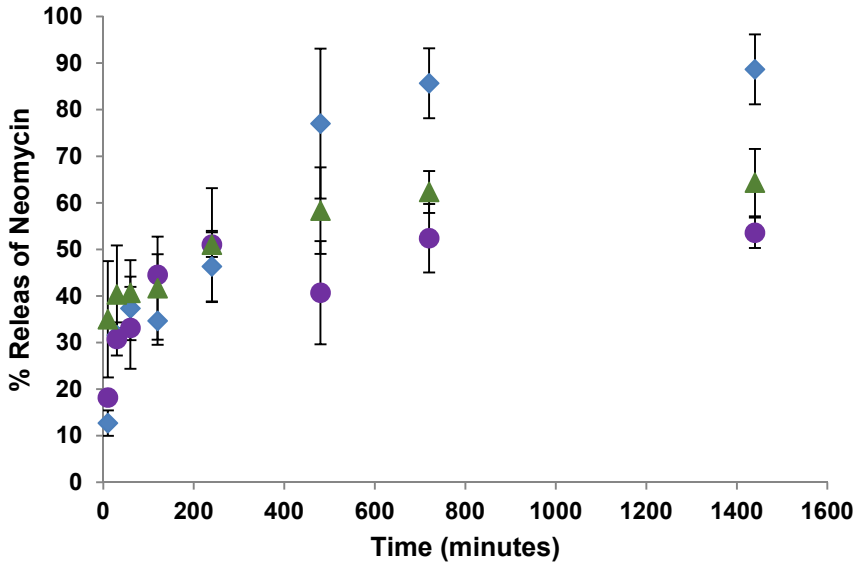

Figure 6.8. Comparison of Dynamic Release of Neomycin from NAN-NEO and T17CT18C- NAN-NEO Combination Nano-Carrier with T17CT18C-NAN-NEO Nano-Carrier. Release of neomycin at 22 ± 1ºC from (▲) T17CT18C-NAN-NEO conjugated nano-carrier, (♦) 1:1 NAN-NEO and T17CT18C-NAN-NEO combination conjugated nano-carrier and (●) 1:2 NAN-NEO and T17CT18C-NAN-NEO combination conjugated nano-carrier. N = 3.

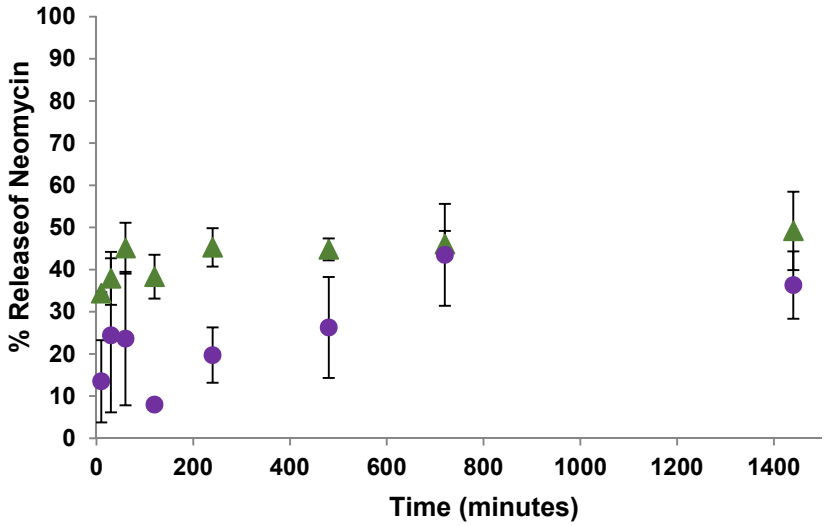

Figure 6.9. Dynamic Release of Neomycin from NAN-NEO and A13G- NAN-NEO Combination Nano-Carrier. Release of neomycin at 22 ± 1°C from (▲)1:1 NAN-NEO and A13G-NAN-NEO combination conjugated nano-carrier and (●) 1:2 NAN-NEO and A13G-NAN-NEO combination conjugated nano-carrier. N = 3.

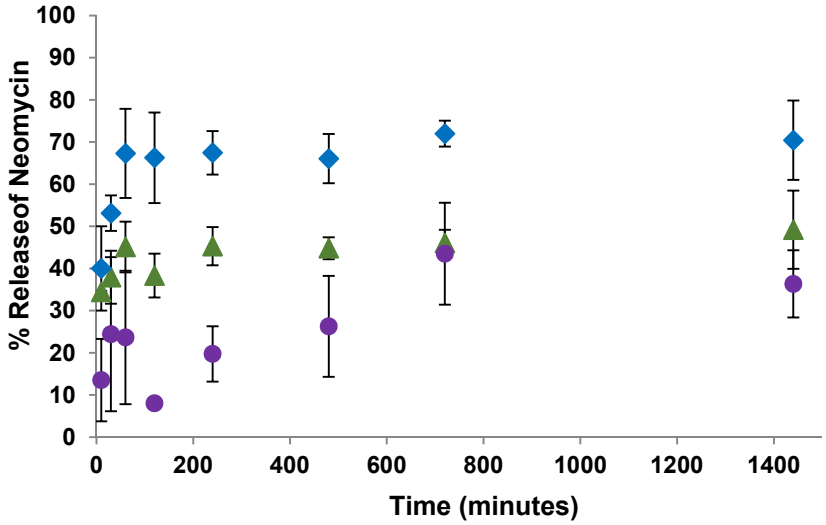

Figure 6.10. Comparison of Dynamic Release of Neomycin from NAN-NEO and A13G- NAN-NEO Combination Nano-Carrier with A13G-NAN-NEO Nano-Carrier. Release of neomycin at 22 ± 1°C from (♦) A13G-NAN-NEO conjugated nano-carrier, (▲)1:1 NAN-NEO and A13G-NAN-NEO combination conjugated nano-carrier and (●) 1:2 NAN-NEO and A13G-NAN-NEO combination conjugated nano-carrier. N = 3.

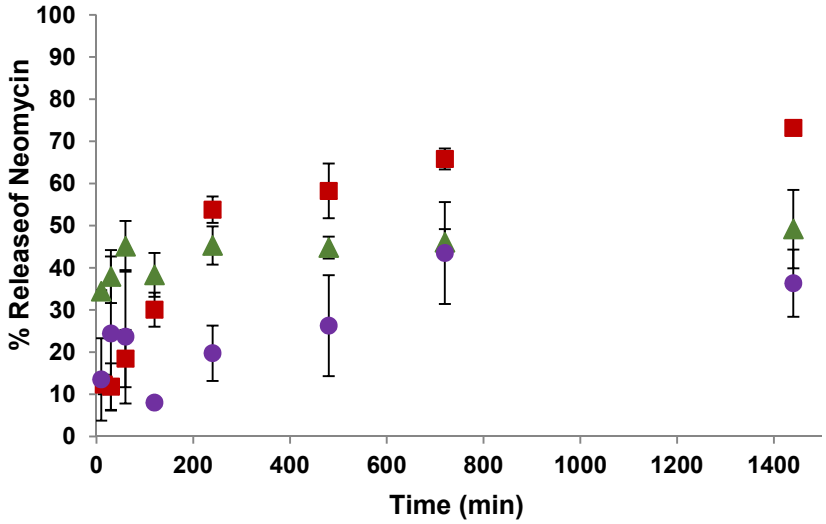

Figure 6.11. Comparison of Dynamic Release of Neomycin from NAN-NEO and A13G- NAN-NEO Combination Nano-Carrier with NAN-NEO Nano-Carrier. Release of neomycin at 22 ± 1ºC from (■) NAN-NEO conjugated nano-carrier, (▲) 1:1 NAN-NEO and A13G-NAN-NEO combination conjugated nano-carrier and (●) 1:2 NAN-NEO and A13G-NAN-NEO combination conjugated nano-carrier. N = 3.

Chapter 7. Non-Toxic Drug Delivery Nano-Carrier for Targeted and Controlled Release of Daunomycin

In this chapter, synthesis, characterization and performance of a novel drug delivery carrier for anticancer drug daunomycin is reported. Daunomycin is a very frequently used and highly toxic anticancer drug that binds to the DNA and inhibits RNA synthesis. Taking advantage of the binding ability of daunomycin to DNA, we developed a high payload nano-carrier capable of targeted and extended release of drug. We hypothesized that covalent incorporation of nucleic acids on gold nanoparticles would produce a novel delivery carrier with very low, if any, toxicity, and capable of targeted delivery of daunomycin. We established the potential of our nano-carrier by recording in vitro continuous release of daunomycin from it for an extended period of time. In the course of testing our carrier in physiological landscape, we demonstrated its performance in delivering daunomycin to MCF7 breast cancer cells.

7.1. Scientific Rationale

Daunomycin is an antitumor antibiotic that belongs to the anthracyclin family. It was obtained from Streptomyces peucetius in 1963[1]. It is constituted of an aglycon chromophore (daunomycinone) linked to an amino sugar (daunosamine)[2] as shown in **Figure 7.1**. It has been used in the clinical practice for over 40 years to treat various kinds

of cancers including breast, bile ducts, endometrial tissue, esophagus and liver, soft tissue sarcoma, lungs, and also acute myeloid leukemia[3].

A number of different mechanisms have been proposed for the cytostatic and cytotoxic effects of daunomycin. Initially, daunomycin was reported to preferentially inhibit RNA synthesis by binding to DNA in the cell[1]. Later, Theologidies *et al*., showed that daunomycin inhibits the synthesis of DNA to a much greater degree than the synthesis of RNA[2]. Over the years various mechanisms of action were suggested to explain the antitumor activity of daunomycin including intercalation into DNA resulting in inhibition of macromolecular bio-synthesis[4-7], free radical formation inducing DNA damage[8-11], DNA alkylation[12-14], DNA crosslinking[15, 16], interference with DNA unwinding[17-19], initiation of DNA damage with the inhibition of topoisomerase II[20-22], and induction of apoptotic cell death[23-25]. It should be noted that all these mechanisms were observed at different drug concentrations and experimental conditions. At a clinically relevant submicromolar drug concentration, interference with DNA unwinding/helicase, and induction of cell differentiation may be the most evident mechanisms. At peak plasma concentration, the primary drug mechanism is likely through interaction with topoisomerase II which triggers growth arrest and/or cell killing through a signaling pathway leading to apoptosis.

During chemotherapy, daunomycin is administered intravenously. This method of drug administration leads to rapid biodistribution and absorption of daunomycin by various organs including heart, lungs, liver, spleen, kidney, and intestine, and induces unwanted toxicity and side effects[26]. Moreover, due to the small size of the drug molecule, a large amount of daunomycin gets excreted first into bile and then gradually into urine[27]. For an

anticancer drug to be effective, it has to reach the tumor overcoming the barriers posed by the body with minimal loss of its volume or activity in the blood. After reaching the tumor, the drug should be able to selectively kill cancer cells without affecting the normal cells. This can be achieved by delivering the drug using a nanoparticle carrier that can circulate for longer time in the blood stream, and target the drug to the cancer cells. Such drug carrier can also reduce the side effects and drug loss.

Nanoparticles are the best choice for formulating such drug carrier as the fate of the injected nanoparticle can be well controlled by adjusting their size and surface properties. The nanoparticle has to be large enough to prevent rapid leakage into blood capillary, and small enough to escape capture by fixed macrophages present in the reticuloendothelial system such as the liver and spleen[28]. The physiological upper limit of pore size in capillary walls is about 15 nm[29], in spleen and liver ranges from 150 to 200 nm[28], and in cancer cell vasculature ranges from 100 to 600 nm[30]. Thus the size of nanoparticles for drug delivery can range from 16 to 100 nm.

Another advantage of nanoparticles is that they can be targeted to cancer cells by two methods: passive targeting and active targeting method. In passive mode, nanoparticles accumulate preferentially at tumor sites by enhanced permeability and retention effect[31, 32]. This phenomenon is caused due to imbalanced angiogenic regulatory factors, such as growth factor and matrix metalloproteinases, in tumor cells producing dilated tumor vasculature with enlarged gap junction between endothelial cells, and the lack of effective lymphatic drainage system in tumors[31-33]. Thus a nanoparticle of size above the pore size of normal vasculature (15 nm) and under the upper limit of the pore size of cancer cell vasculature (100 to 600) can be passively targeted to cancer cells in vivo. In active mode,

the nanoparticles are functionalized with targeting ligands or antibodies that can specifically binds to a receptor over expressed on cancer cells and there by specifically accumulate at tumor site[28].

Here, we report a nano-carrier for anticancer drug daunomycin, synthesized using non-toxic gold nanoparticle and oligonucleotides. This nano-carrier is capable of high drug payload, passive targeting, and controlled release of drug inside the cancer cells for an extended period of time.

7.2. Daunomycin- DNA Interaction

Although many mechanisms of action have been suggested for daunomycin, the inhibition of RNA synthesis by binding to DNA in the cell is believed as the clinically relevant mode of action. Thus, scientist have extensively studied the interaction of daunomycin with various DNA and synthetic oligonucleotides. The characteristics of the drug:DNA complex, and the structural changes in DNA due to the drug interactions have been studied.

7.2.1. Daunomycin Interaction with Double Stranded DNA

Calendi *et al*., suggested that daunomycin binds to DNA through two bonds: one at the chromophore and other at the amino sugar[5]. A year later Kresten *et al*., suggested that the chromophore of daunomycin intercalates between the successive base pairs of DNA[34]. This theory was supported by the X-ray diffraction study of daunomycin:DNA complex by

Pigram *et al*[35]. According to Pigram model, the amino sugar of the daunomycin is accommodated in the large grove of the DNA, and the hydrophobic faces of the base pair and the drug overlap extensively. In such arrangement, the amino group can interact strongly with the second DNA phosphate away from the site of intercalation. The other possible interaction suggested was the hydrogen bond between the first phosphate and the hydroxyl of the daunomycin chromophore[35]. Later, the equilibrium binding studies of daunomycin and dsDNA interactions by Chaires *et al*., demonstrated that the daunomycin binds tightly to dsDNA and shows negative cooperativity. Using neighbor exclusion model, they calculated the association constant to be $7 \times 10^5\ M^{-1}$ and that daunomycin intercalates after every four base pairs in the DNA. The subsequent drug molecules are excluded from binding to nearby sites, either by physical blockage or steric alteration of DNA. Their study also demonstrated that daunomycin has a slight binding preference to G-C base pair over A-T, and the daunomycin binding to DNA is exothermic.

In addition to the equilibrium study, Chaires *et al*., studied the kinetics of the binding reaction to obtain a complete understanding of the daunomycin-DNA interaction. Kinetic studies provided information necessary for the formulation of plausible reaction mechanism. Moreover, the biological and pharmacological activity of the drug may be more readily correlated to kinetics rather than the binding equilibrium of the drug-DNA complex. Chaires *et al*., studies the kinetics of daunomycin-DNA interaction with calf thymus DNA by stopped-flow and temperature-jump relaxation methods[36]. Their data suggested that the three steps of daunomycin binding to DNA corresponds to rapid formation of weak binding of drug to the outsides of DNA, followed by intercalation of drug into the DNA helix, followed by either conformation adjustment of the DNA or

redistribution of the intercalated drug to the preferred site by internal transfer. Two more possible alternative models were developed by them: formation of two different complexes, and formation two interchangeable complexes allowing for the unimolecular interconversion of the two types of complexes such as drug bound to A-T or G-C sites. Another interesting and important observation from this study was that daunomycin was found to have a slow isomerization step along its dissociation path which implies that the drug will be bound to DNA for a longer lifetime relative to other DNA intercalators.

7.2.2. Daunomycin Interaction with Nucleosome

Thought the binding of daunomycin to DNA has been well studied, in the cell it is not the naked DNA that the drug binds to, but rather chromatin, consisting of DNA complexed with histones and other nuclear proteins. To understand how the drug acts in vivo, it is important to know how the presence of these protein affects the binding of daunomycin. To answer this question, Chaires *et al*., studied the binding of daunomycin to calf thymus nucleosome[37]. Their study suggested that daunomycin, because of its special intercalation geometry, strongly prefers binding to free DNA region than bent helices found in nucleosomes and chromatin. Hence, In vivo the drug is focused in the genetically active regions of DNA which has less nucleosome structure. Moreover, they found that the presence of core histidine drastically reduces the affinity of daunomycin to DNA. Hydrodynamic studies showed that daunomycin causes unfolding of nucleosome particles and, at saturation, promotes their aggregation.

7.2.3. DNA Conformation Specificity of Daunomycin-DNA Interaction

Double stranded DNA exists in many possible conformation including A-DNA, B-DNA and Z-DNA. The conformation of DNA depends on the hydration level, nucleotide sequence, presence of metal ion, and modification of the bases. In functional organism, the types of DNA conformation observed are B-DNA and Z-DNA. As all the above mentioned studies of DNA-daunomycin interactions were carried out with B-DNA, to test the structural preference of daunomycin interaction to DNA Chaires *et al*., studied the binding of daunomycin to the Z- DNA. The results revealed that daunomycin preferentially binds to right handed B-form of the DNA and selectively discriminates all the alternate DNA conformations[36, 38, 39] .

7.2.4. Sequence Specificity of Daunomycin-DNA Interaction

For a detailed understanding of the action of the daunomycin it is very important to identify its preferred binding site in the DNA sequences. Many laboratories studied the possible site or sequence specificity of DNA-daunomycin interactions and the data obtained are contradictory. In 1981, Patel *et al*., suggested alternating purine-pyrimidine specificity for daunomycin binding based on the NMR study of daunomycin:poly(dA-dT)-poly(dA-dT) complex. Later, the solution studies utilizing purified, well characterized, and synthetic deoxypolynucleotides by Chaires *et al*., demonstrated that daunomycin preferentially binds to polynucleotides of alternating purine-pyrimidine sequence[40], in accord with the earlier study by Patel. Solution studies on natural DNA showed that G-C

base pair is slightly preferred by daunomycin, and it intercalates preferentially to GC-rich DNA[41]. However, the conclusions regarding the sequence specificity of daunomycin derived from the theoretical calculations contradicted these studies. In 1984, Newlin *et al*., modeled the daunomycin interaction with tetrameric duplex DNA sequences and predicted that the drug prefers adjacent AT base pairs to intercalate[42]. Later, a theoretical computational study by Chen *et al*., using six self-complemetary, double stranded hexanucleotides concluded that triplet sequences serves as specific sites with the optimal site being A-T base pair flanked by the adjacent G-C base pairs such as 5'ACG and 5'TCG[43]. This finding was consistent with the crystal structure of daunomycin-oligonucleotide complex determined by X-ray crystallography where daunomycin was intercalated between G-C base pairs and flanked by an AT base pair at the 5' position[44]. In spite of the availability of the A-T base pair as the potential binding site, binding of daunomycin to the G-C base pair suggests that the G-C pair is the optimal, energetically, and most favorable intercalation site in the crystalline form. Further equilibrium binding and DNase I footprinting study by Chaires *et al*., using natural DNA in solution demonstrated that the optimal daunomycin binding site is a triplet sequence comprised of AT base pairs at the 5' position, flanked by two contiguous GC base pairs. The requirement of the AT base pair at the 5' position was found not to be strict, however, a triplet GC base pair was also demonstrated as acceptable site although possibly forms weaker binding[45]. However, another DNase I footprinting by Skorobogaty *et al*., identified dinucleotide sequence 5'CA as the preferred daunomycin binding site[46, 47], which contradicted the previously suggested triplet binding site theory. This discrepancy in the preferential binding data was justified by another high resolution footprinting study by Chaires. The

data from this study demonstrated that the triplet sequence 5'(A/T)CG, 5'(A/T)GC, and 5'(A/T)CA as the most preferred daunomycin binding sites[48]. This data is in agreement with the previous theoretical calculations by Chen[43], DNases I footprinting by Chaires[45], and also crystallographic study of daunomycin-hexanucleotide complex[49, 50]. The crystallographic structure of daunomycin bound to 5'd(GCTACG)[49] and 5'd(GCATCG)[50] showed that daunomycin intercalates between the CpG with daunosomine moiety extending down the minor groove to physically cover the AT base pair. The drug is stabilized in the complex by both direct hydrogen bonds, and indirect hydrogen bonds stabilized by water molecules with the cytosine of GC base pair at the end of the complex. On reconciling data by Skorobogaty with this DNases footprinting data and considering the molecular basis of daunomycin sequence preference, it was suggested that 5' AT base pair and the central CG base pair are the predominant determinants for preferential binding[48].

7.2.5. Daunomycin Interaction with ssDNA, DNA Triplexes and Tetraplexes

As mentioned earlier, scientist discovered that daunomycin selectively binds to the B-form DNA rather than the alternative forms. However, binding of daunomycin to DNA is not restricted to duplex DNA. Daunomycin was observed to binds to single stranded DNA[51], DNA triplexes[52, 53] and tetraplexes[53]. Daunomycin was found to intercalate to single stranded DNA with self-complementary G-C base pair[51]. Wochner *et al*., isolated an aptamer for daunomycin using SELEX procedure, which was found to bind daunomycin very strongly (K_d = 20 nM)[54]. Daunomycin was also found to intercalate to human

telomeric DNA, telomeric ends of chromosome that consists of tandem repeats of guanine-rich DNA capable of associating either by inter- or intramolecularly to form a variety of four stranded quadruplex structure, and act as the quadruplex stabilizing agent[55, 56]. In spite of their lack of quadruplex selectivity, unlike other quadruplex stabilization ligands, daunomycin was also found to bind to quadruplex DNA in solution[53]. Clark *et al*., reported the first structure of a parallel DNA quadruplex-daunomycin complex[57]. The asymmetric unit contained four parallel d(TGGGGT) strands forming a discrete intermolecular quadruplex together with three daunomycin molecules, three Na^+ cation, and 129 water molecules. The set of three daunomycin was stacked at the 5' end of the quadruplex where they form weak π- π interactions with the guanines in the terminal tetrad. No drug molecule was found to intercalate into the guanine core of the quadruplex[57].

7.3. Materials and Methods

In this section, the materials and methods used for the preparation of the novel drug delivery carrier for daunomycin, and demonstration of extended and controlled in-vitro release of daunomycin from the nano-carrier and inside the MCF7 breast cancer cells are described.

7.3.1. Materials

Gold nanoparticles of 15 nm diameter (AuNPs) were purchased from Ted Pella, Inc (Redding, CA). Modified and unmodified oligonucleotides were synthesized by Operon

Biotechnologies. NAP-5 columns (Sephadex G-25 DNA grade) were purchased from G.E. Healthcare (Piscatiway, NJ). Sterile, 6 well clear multiple well plates and 384 well low flange solid black microplates were obtained from Corning, Inc. (Corning NY). Polyester sealing films were purchased from VWR International (West Chester, PA), and drop dialysis membranes (13 mm, 0.025 μm) were obtained from Millipore (Billerica, MA). Daunomycin hydrochloride was purchased from Sigma-Aldrich (St. Louis, MO). The cell culture media DMEM, Penicillin/Streptomycin, Glutamax, and sodium pyruvate were purchased from GIBCO (Grand Island, NY). 10% fetal bovine serum and non-essential amino acids were purchased from Atlanta Biologicals (Flowery Branch, GA) and Lonza (Basil, Switzerland), respectively. Live/Dead cell viability kit was obtained from Invitrogen (Grand Island, NY). Silver enhancement kit for light and electron microscopy was purchased from Ted Pella, Inc (Redding, CA), XTT cell viability kit was obtained from Biotium (Hayward, CA), Trypsin and EDTA were obtained from Corning cellgro (Manassas, VA). MCF7 human breast adenocarcinoma cells were kindly provided by Dr. Richard Bird, Auburn University College of Veterinary Medicine. Tissue culture treated 96 well plates with lid (BD Falcon ^{TM}) and μ- Slide 96 well plates were purchased from BD Biosciences (San Jose, CA) and Ibidi (Verona, WI), respectively. All other chemicals were molecular biology grade, and unless specified were from Sigma-Aldrich (St. Louis, MO).

7.3.2. Methods. DNA-Daunomycin Titration

A fixed concentration of daunomycin (1.5 μM) in daunomycin binding buffer (DBB; 20 mM Tris-Hcl [pH 7.4], 140 mM NaCl, 5 mM KCl, 1 mM $MgCl_2$, 1 mM $CaCl_2$) was incubated with the increasing molar ratio of DNA (0.1, 0.2, 0.5, 1, 3 and 5 equivalence). The decrease in the fluorescence of daunomycin due to binding was measured using NanoDrop 3300 fluorospectrometer. The binding constant was calculated using Hill plot equation as given below, where Y is the fractional saturation of sites (occupied sites/total sites), [B] is concentration of daunomycin, and n_H is the Hill coefficient.

$$\text{Hills Equation: } \log\left(\frac{Y}{1-Y}\right) = n_H(\log[B]) - \log(K_D)$$

7.3.3. Methods. Assessment of DNA Complex Formation

A reaction mixture containing 1 μL of 1 mM anchor DNA (ANC-oligo), 1 μL of 0.1 mM [5'–^{32}P]-labeled oligo-93, 1 μL of 10X NEBuffer 2 (1X NEBuffer 2: 50 mM NaCl, 10mM Tris-HCl, 10 mM MgCl2, 1mM DTT; pH 7.9), and 5 μL of DI water was incubated at 37^{o}C for 10 minutes. To this mixture, 1 μL of 4 mM dNTPs and 1 μL of Klenow enzyme (5000 units/mL) were added and incubated at 37^{o}C for 45 minutes. Similarly, a control reaction mixture containing 1 μL of 0.1 mM [5'–^{32}P]-labeled oligo-93, 1 μL of 10X NEBuffer 2, and 8 μL of DI water was incubated for 45 minutes at 37^{o}C. Both, the reaction mixture and the control mixture, were subjected to electrophoresis in a 10% non-denaturing gel for 12 hours at 100 volts. Band intensity was quantified using FLA-5100 imager (Fujji).

7.3.4. Methods. Preparation of Daunomycin Nano-carrier

Hybridization reaction mixture (65 μL) containing ANC-oligo (2 nmoles), and oligo-93 (2 nmoles), 0.18 M phosphate buffer solution (PB; pH 7.2) and 0.1 M dithiothreitol (DTT) was incubated at 37ºC for 3 hours. The DNA complexes were then desalted on NAP-5 column and concentrated to ~ 20 μL using a Speed Vac. Then 1 mL of AuNps (15 nm, $1.4x10^{12}$ particles/mL) and 1 μL of 10% SDS solution were added. The mixture was vortexed for 16 hours at room temperature. PB was added until a final concentration of 0.01 M was achieved, and then the DNA/AuNps solution was incubated at room temperature for 2 hours. Aliquots of 10 μL of 5 M NaCl solution were added to the DNA/AuNps solution. The mixture was sonicated for 10 seconds using a sonic dismembrator (Fisher Scientific) and incubated for 20 minutes at room temperature after every addition of 5 M NaCl. This process was repeated to a final concentration of 0.4 M NaCl. The mixture was then vortexed for 24 hours at room temperature. The solution was centrifuged for 30 minutes at 10,000 rpm to remove unbound oligonucleotides. The DNA complexes conjugated AuNps was resuspended in DI water and then vortexed overnight. Later, 40 μL of 17.8 μM daunomycin in DBB was added and continued vortexing overnight. The mixture was centrifuged twice for 20 minutes at 10,000 rpm to remove the unbound daunomycin, and then the daunomycin loaded nano-carrier was resupended in 10 mM PB and 0.2 M NaCl solution (PBS; pH 7).

[5'–^{32}P]-labeled oligonucleotides were prepared according to the protocol developed by Fedor and Uhlenbeck[58]. The amount of radioactivity was quantified by Cerenkov counting using the LKE Wallac scintillation counter. The mean diameter of

oligonucleotides conjugated AuNps was measured using Dynamic Light Scattering (DLS) instrument (PSS-NICOMP).

7.3.5. Methods. Quantitative Analysis of Oligo-93 Binding to AuNps

ANC-oligo: oligo-93 conjugated AuNps were prepared according to the protocol. To avoid labelling of ANC-oligo, the oligo-93 conjugated to AuNps were then labelled at the 5' end with [γ–^{32}P] ATP, according to the protocol developed by Fedor and Uhlenbeck[58],. A 5 µl aliquot of this sample along with 0.5 nmoles of [5'–^{32}P]-labeled oligo-93, and 0.5 nmoles of [5'–^{32}P]-labeled ANC-oligo were subjected to electrophoresis in a 10% denaturing TBE (Tris base, boric acid, EDTA) gel for 1 hour. The gel was then dried and scanned for [5'–^{32}P]-labeled DNA using Fuji FLA-5100 imager.

7.3.6. Methods. In-Vitro Analysis of Dynamic Release of Daunomycin from the Nano-Carrier

A 100 µL aliquot of the daunomycin-loaded nano-carrier suspended in PBS was pipetted on to a drop dialysis membrane floating on 10 mL of PBS in a clear 6 well plate, and placed on a rocker platform at 37^{o}C. To minimize evaporation losses, well plates were covered with adhesive polyester sealing films. The sample was collected from the membrane after 1 hour and corrected for any volume loss due to evaporation. The DNA were removed from AuNps by incubating them in 0.05 M DTT for 16 hours at room temperature, centrifuged for 30 minutes at 13,000 rpm in Eppendorf centrifuge, and then

the supernatant was measured for absorbance of daunomycin at 480 nm. The experiment was repeated for different dialysis times from 1 hour to 6 days.

7.3.7. Methods. Procedure for Cell Culture

MCF7 human breast adenocarcinoma cells were kindly provided by Dr. Richard Bird (Auburn University College of Veterinary Medicine). MCF7 cells were cultured in DMEM supplemented with 10% fetal bovine serum, 1%(v/v) non-essential amino acids, 1%(v/v) Penicillin/Streptomycin, 1% (v/v) Glutamax and 1%(v/v) sodium pyruvate (cell culture media). The cells were maintained in tissue-culture flasks in a humidified atmosphere of 5% CO_2 and at constant temperature of 37°C. Cells cultured in 2D matrix were enzymatically dissociated with 0.25% Trypsin/2.21 mM EDTA; an equal volume of cell culture media was added to neutralize the trypsin. The cell suspension was centrifuged at 200 g for 5 minutes to collect a cell pellet. The supernatant liquid was aspirated and the cell pellet was resuspended homogenously in 1 mL media. A 10 µl aliquot of the cell suspension was added to a hemocytometer and the cell density was counted under the microscope. The desired numbers of cells were seeded in well plates and appropriate volume of media was added for overnight cell adhesion.

7.3.8. Methods. Assessment of Cellular Uptake of Nano-Carrier

MCF7 cells were seeded into µ- Slide 96 well plates at a density of 15,000 cells per well with 150 µL of cell culture media (DMEM supplemented with 10% fetal bovine

serum, 1%(v/v) non-essential amino acids, 1%(v/v) Penicillin/Streptomycin, 1% (v/v) Glutamax and 1%(v/v) sodium pyruvate) and grown to 80% confluence. Then the media was aspirated, and cells were washed twice with PBS. Incubated for 4 hours at 37°C with 100 µL of 50 nM nano-carrier suspended in the cell culture media or 100 µL media. Then the cells were washed thrice with PBS, stained with silver enhancement kit for 3 minutes, and washed three more times with PBS. Stained cells were subjected to bright field imaging using Eclipse Ti inverted microscope (Nikon).

7.3.9. Methods. XTT Cell Viability Assay

MCF7 cells were grown in gelatin coated 96 well plate to 80% confluence at 37°C. Then the cells were washed thrice with PBS and treated with 100 µL of fresh media containing different concentration of daunomycin loaded nano-carrier or free daunomycin, or 50 nM nano-carrier for 4 hours or 12 hours. The cells were washed with PBS and incubated at 37°C for 6 hours. Activated XTT solution of 50 µL was added to the cells with 100 µL of cell culture media after PBS wash, and the assay was performed as per manufacturer recommended protocol. The absorbance signal of the samples were measure using Synergy 2 Multimode Microplate Reader (BioTek) spectrophotometer at a wavelength of 450-500 nm, and the background absorbance was measured between 630-690 nm. The background absorbance was subtracted from the sample absorbance reading to obtain normalized absorbance values.

7.3.10. Methods. Live/Dead Fluorescent Cell Viability Assay

The MCF7 cells were grown in the gelatin coated 96 well plates to 80% confluence and treated with different concentration of daunomycin loaded nano-carrier or free daunomycin for 4 or 12 hours. The cells were then washed with PBS and incubated in fresh media for 6 hours. After washing the cells thrice with PBS, 50 µl of a pre-prepared solution of 0.5 µl/ml of calcein-AM and 2 µl/ml of ethidium homodimer-1 in PBS was added and incubated at room temperature for 30 minutes. The cells were then washed twice with PBS, and imaged using Eclipse Ti inverted microscope (Nikon).

7.4. Results and Discussion

Daunomycin is an anthracycline antibiotic very commonly used to treat various types of cancer. The drug binds to the DNA and inhibits both DNA replication and RNA transcription of cancer cells. Taking advantage of this property of daunomycin, we developed a nano-carrier by functionalizing AuNps with a daunomycin-binding DNA.

Similar to our previously developed nano-carrier for neomycin, we developed a nano-carrier for the anti-cancer drug daunomycin by conjugating DNA aptamer for daunomycin to AuNps via an anchor DNA **(Figure 7.2)**. To construct this nano-carrier, we selected the DNA aptamer identified by Wochner *et al.*, which was found to bind daunomycin with high affinity (K_D = 20 nM)[54]. To the 3'end of the aptamer sequence, we added a short sequence complementary to an anchor DNA (ANC-oligo) (oligo-93; **Figure**

7.2). Therefore, the aptamer can be hybridized to the anchor DNA modified at its 5' end with a thiol group, and then covalentlyattached to AuNps via thiol-gold bond **(Figure 7.2)**.

The physical complex between daunomycin and oligo-93 was studied by monitoring the fluorescent spectrum of free daunomycin (1.5 μM) in daunomycin binding buffer (DBB; 20 mM Tris-Hcl [pH 7.4], 140 mM NaCl, 5 mM KCl, 1 mM $MgCl_2$, 1 mM $CaCl_2$) incubated with the increasing molar ratios of oligo-93 (0.1, 0.2, 0.5, 1, 3 and 5 equivalence). The decrease in the fluorescence of daunomycin due to binding to oligo-93 was measured **(Figure 7.3 A)**. The titration results suggest that each oligo-93 is able to bind three daunomycin molecules. The binding constant (K_D) of 60 nM for daunomycin-oligo-93 complex was calculated using Hills plot. This binding constant for daunomycin-oligo-93 interaction is different than that published by Wochner et al. It should be noted that in our experiment the binding of daunomycin to oligo-93 was analyzed in solution, whereas Wocher investigated the binding of the biotinylated daunomycin to the 5' biotinylated DNA attached to the microtiter plate. These differences in the experimental conditions could account for the observed difference in the binding constants. Further, to verify the sequence specificity of oligo-93 in binding daunomycin, we synthesized a 93mer oligonucleotide with same nucleotides composition as oligo-93, whose sequence was randomized (oligo-93R; **Figure 7.2**), and tested it daunomycin binding properties **(Figure 7.3 B)**. The titration results showed that oligo-93R can bind about 5 daunomycin molecules but with a K_D of 187 nM. This finding suggests that the high affinity of oligo-93 to daunomycin is due to its sequence.

To construct our nano-carrier by conjugating oligo-93 to AuNps via ANC-oligo, we first tested the hybridization of ANC-oligo and oligo-93 by electrophoresis on non-

denaturing gel. The oligo-93: ANC-oligo was unstable when fractionated on this gel. To stabilize the interaction ANC-oligo was used as a primer to synthesize DNA strand complementary to oligo-93 using Klenow enzyme. On the gel, oligo-93 hybridized ANC-oligo with the duplex sequence extended by Klenow enzyme ran higher than the unhybridized oligo-93 **(Figure 7.4A)**. This showed the successful hybridization of oligo-93 to ANC-oligo. As daunomycin intercalates to the double stranded DNA, we testes the binding capacity of the ANC-oligo:oligo-93 DNA complex by titration **(Figure 7.4B)**. The results suggested that ANC-oligo:oligo-93 complex has a binding capacity of 7 daunomycin molecules.

The nano-carrier was prepared by conjugating oligo-93:ANC-oligo complex to AuNps. The change in hydrodynamic size of the AuNps upon the binding of DNA was measured using Dynamic Light Scattering (DLS). The diameter of nanoparticles increased from 16 ± 1 nm (free AuNp) to 41 ± 2 nm (nano-carrier) suggesting the attachment of DNA on AuNps. As the energy gained from the formation of thiol-gold bond favors the attachment of DNA via thiol-gold bond rather than adsorption[59, 60], the increase in the mean diameter of the AuNps suggests the conjugation of oligo-93:ANC-oligo complex to AuNps via thiol-gold bond. The hydrodynamic size of this nano-carrier (41 ± 2 nm) makes it perfect for passive targeting of cancer cells in-vivo. As mentioned in section 7.2, the ideal size of the nano-carrier can range from 15 to 100 nm to avoid rapid renal clearance, escape RES macrophages, and passive targeting to cancer cells via leaky vasculature. Our nano-carrier being 41 ± 2 nm in diameter has a high potential to passively target daunomycin to cancer cells in-vivo and reduce the side of effects of daunomycin, and avoid rapid renal as well as RES clearance.

To double check the attachment of oligo-93 to AuNps, the nano-carrier was incubated with polynucleotide kinase and [γ–^{32}P] ATP. This procedure is expected to label the 5' ends of oligo-93 bound to ANC-oligo derivatized AuNps. Aliquots of ^{32}P-labelled nano-carrier were fractionated by denaturing polyacrylamide electrophoresis. The gel was then scanned using Fuji FLA-5100 imager to obtain the binding profile of oligonucleotide on AuNps **(Figure 7.5)**. The binding profile showed that in addition to oligo-93 (~ 68%) shorter oligonucleotide (~ 32%) were present on AuNps. These shorter oligonucleotides are represents the abortive products of the solid phase synthesis of oligo-93. These shorter fragments of oligo-93 were also found to bind daunomycin but with a weaker affinity (data not shown). Thus in our nano-carrier, AuNps is conjugated to AuNps along with a small percentage of shorter oligonucleotide fragments of oligo-93 **(Figure 7.6)**.

Using [5'–^{32}P]-labeled oligo-93, we measured the number of ANC-oligo:oligo-93 complexes conjugated per AuNps to be 111 ± 8 oligonucleotides. Previously, we found that the maximum number of ANC-oligo that can be attached to a 15 nm AuNp to be 101 ± 8[61]. Thus our measurement of 111 ± 8 oligo-93 conjugated onto AuNp suggests that some oligo-93 might be forming complexes. This possibility was confirmed experimentally by fractionation of oligo-93 on a non-denaturing polyacrylamide gel. The result revealed that about 15% of the oligo-93 forms a high molecular weight complex **(Figure 7.7)**. A small percent of oligo-93 self-complexes conjugated to AuNps explains the high oligonucleotide loading.

After characterizing our nano-carrier, we prepared daunomycin loaded nano-carrier as per protocol and measured the maximum attainable drug payload on the nano-carrier. Analysis of nano-carrier charged with daunomycin revealed a drug payload of 1157 ± 18

daunomycin molecules per AuNp. To our knowledge, this is one of the very high drug payload obtained on a 15 nm AuNps. Some of the previously reported drug loading on AuNps are, ~100 drug molecules per 5 nm AuNps reported by Chen et al[62]., Zubarev et al., loaded 70 molecules of paclitaxel on a 2 nm AuNp[63], Hue et al., succeeded in coupling ~ 201 molecules of paclitaxel on a 15 nm AuNp[64], Nakshini et al., reported a loading of 200 thiol form of disulfide capping with an ability to bind one histamine molecule each on AuNps[65], and recently Kim et al., reported a high loading of 615 ± 34 molecules of daunomycin on a 29.4 ± 7.7 nm AuNp[66]. Taking into account the titration results of ANC-oligo:oligo-93 complex and the oligo-93 loading to AuNps data, we expected a drug loading of 833 daunomycin molecules per AuNp which is lesser than the experimentally observed loading of 1157 ± 18 daunomycin per AuNp . The difference between the expected and observed drug loading might be due to two reasons: (1) the small number of self-complexed oligo-93 conjugated on the AuNps binds more than 7 daunomycin molecules resulting in higher drug loading, (2) the DNA oligonucleotides loaded on the AuNps in the parallel orientation interacts with each other and produce additional binding sites for daunomycin. DNA with repeated G-tetrads can form inter and intramolecular quadruplexes with parallel or antiparallel DNA strands at favorable conditions. Clark *et al*., demonstrated the binding of daunomycin to a parallel G-quadruplex[57]. As the sequence of oligo-93 consists of repeated d(GGGG) there is a possibility of parallel strands of oligo-93 conjugated on AuNps to interact and produce more daunomycin binding sites. The parallel oligo-93 can also interact to form duplexes[67] and triplexes[68, 69] but such interactions of parallel DNA are not well studied yet and thus there is a gap in the scientific knowledge about them.

Further studies of these interactions of the daunomycin binding oligonucleotides on AuNps have to be considered. However, as our study focuses on developing and testing the nano-carrier for extended release of the drug into cancer cells, we extended our work in the direction of studying the release of daunomycin from the developed nano-carrier. The in vitro release study of daunomycin from the nano-carrier was performed on a drop dialysis setup at 37^{o}C. The release data showed that the daunomycin can be released from the nano-carrier in a continuously increasing pattern for an extended period of time **(Figure 7.8)**. The initial release of daunomycin in the first 12 hours corresponds to the weaker daunomycin binding to shorter oligonucleotide and the double stranded region of oligo-93:ANC-oligo hybridization. The slow and continuous release of daunomycin after 12 hours corresponds to the daunomycin bound to oligo-93. About 75% of the bound drug was released from the nano-carrier after 6 days suggesting that the nano-carrier can release the drug for even longer period of time.

We tested the cellular uptake of the nano-carrier by MCF7 breast cancer cells. The cells were incubated with nano-carrier (50 nM) in cell culture medium or the media alone (control) at 37^{o}C for 4 hours, and then washed with PBS to remove the unbound nano-carrier. The nano-carrier inside the cells were visualized by staining the cells with silver enhancement kit for 3 minutes. The silver stained images of MCF7 cells with and without nano-carrier are shown in **Figure 7.9.** Clear black aggregates of silver were seen in the cells incubated with nano-carrier due to silver deposit on AuNps, while no such black spots were observed in the control cells incubated in just the cell culture media. This result indicate that our nano-carrier is well taken up by MCF7 cells.

We next examined the potential of the nano-carrier as daunomycin delivery carrier to cancer cells. As daunomycin is a fluorescent molecule, the presence of daunomcyin inside the cells can be examined using fluorescent imaging. MCF7 cells were treated with various concentrations of daunomycin loaded nano-carriers, and subjected to fluorescent imaging to assess the uptake of nano-carrier and release of daunomycin inside the cell. Strong fluorescence was observed in the cells in each case indicating the presence of free daunomycin in the cytoplasm of the cells. More daunomycin fluorescence was observed in the cells treated with different concentrations of daunomycin loaded nano-carrier than that in the cells treated with same concentration of free daunomycin **(Figure 7.10)**. Which is expected as the nano-carriers are loaded with a large amount of daunomycin.

The ability of daunomycin loaded nano-carrier to kill cancer cells was tested by assessing the cytotoxicity of the daunomycin and daunomycin loaded nano-carrier as a function of concentration using XTT cell viability assay. The cells were either incubated with daunomycin or daunomycin loaded nano-carrier. **Figure 7.11** shows the cell death induced by different concentrations of daunomycin and daunomycin loaded nano-carrier after 4 and 12 hours of incubation. After 4 hours cellular uptake, the cell death induced by different concentrations of daunomycin loaded nano-carrier was always greater than or equal to the cell death induced by the same concentration of daunomycin. A significantly higher cell death was observed with 100 nM of daunomycin loaded nano-carrier than the same concentration of daunomycin. After 12 hours cellular uptake, significantly higher cell death was observed with 50 nM and 100 nM of daunomycin loaded nano-carrier than the same concentration of free daunomycin. Almost 98 % cell death was observed with 100 nM of daunomycin loaded nano-carrier which was ~50% more cell death induced by same

concentration of daunomycin. In addition, to visualize the cell death induced by the free drug and the drug loaded nano-carrier, we performed live-dead cell fluorescent assay. **Figure 7.12** shows the live and dead MCF7 cells after 4 hours cellular uptake of 100 nM of daunomycin loaded nano-carrier and free daunomycin followed by 6 hours of incubation. The live cells produce a green fluorescence while the dead cells do not. This microscopic fluorescent image provides a visual demonstration of differences in cell viability observed with free daunomycin and daunomycin loaded nano-carrier. Our observation strongly suggest that the daunomycin loaded nano-carrier is superior to the free drug alone in inducing apoptosis in cancer cells.

To prove that the cytotoxicity of daunomycin loaded nano-carrier does not involve toxicity induced by AuNps or DNA, we tested the cytotoxicity of the nano-carrier. Although AuNps and DNA were previously found to be non-toxic, we tested the cytotoxicity of the nano-carrier by assessing the cell viability of MCF7 cells treated with the 50 nM nano-carrier for 4 hours **(Figure AI.2)**. Only about 6% cell death was induced by 50 nM nano-carrier in contrast to 49% cell death induced by the same concentration of daunomycin loaded nano-carrier **(Figure 7.13)**. This proves that the high cytotoxicity of the daunomycin loaded nano-carrier is due to the daunomycin released from the carrier.

7.5. Conclusions

We have developed a drug delivery carrier for anti-cancer drug daunomycin by conjugating the DNA capable of binding daunomycin (oligo-93) onto AuNps via an anchor DNA (ANC-oligo). A short sequence complementary to ANC-oligo was added to the 3'

end of oligo-93. The oligo-93 was hybridized to the ANC-oligo with a thiol modification at its 5' end, and then the oligo-93: ANC-oligo complex was covalently attached to AuNps via thiol-gold chemistry. We tested the daunomycin binding capability of oligo-93 by titrating daunomycin with increasing concentration of oligo-93. These experiments demonstrated that oligo-93 can bind 3 molecules of daunomycin per oligonucleotide, and the binding constant (K_D) was calculated to be 60 nM using Hill plot. Titration of daunomycin with oligo-93R, whose sequence was randomized, suggests that daunomycin:oligo-93 interactions are sequence specific.

The hydrodynamic size of oligo-93 conjugate AuNps was measured using DLS. The diameter of AuNps increased from 15 nm to 41 ± 2 nm upon binding of oligo-93. This size of nano-carrier suitable for passive targeting of drug to the cancer cells, in vivo. By targeting the drug we could reduce non-specific absorption and toxicity of the drug. Our studies measured an unexpected complexity in the structure of the nano-carrier. Additional possible interactions between parallel and antiparallel oligo-93 strands seem to contribute to high binding of daunomycin to the nano-carrier. The drug payload on the nano-carrier was found to be very high, 1157 ± 18 daunomycin per AuNp. This is one of the highest drug loading reported on a 15 nm AuNp.

The daunomycin loaded nano-carrier was found to efficiently release the drug in a continuously increasing pattern for an extended time period. The nano-carrier was well uptaken by MCF7 breast cancer cells and was found to be superior to daunomycin in inducing apoptosis of cancer cell. Using 100 nM of daunomycin loaded nano-carrier about 98% cell death was achieved after 12 hours of cellular uptake which is ~ 50% more than cell death induced by 100 nM daunomycin. The cytotoxicity study of the nano-carrier

without the drug showed that nano-carrier has a negligible toxicity and therefore the high toxicity induced by the daunomycin loaded nano-carrier is due to the high loading of daunomycin. Thus, we have developed a non-toxic nano-carrier with high therapeutic payload, capable of extended drug release and proven to be more effective than the daunomycin alone in killing cancer cells.

7.6. REFERENCES

1. Dimarco A, Soldati M, Fioretti A, Dasdia T. Activity of Daunomycin, a New Antitumour Antibiotic, on Normal and Neoplastic Cells Grown In Vitro. Cancer Chemotherapy Reports. Part 1. 1964;38: 39.

2. Theologides A, Yarbro JW, Kennedy BJ. Daunomycin Inhibition of DNA and RNA Synthesis. Cancer. 1968;21: 16-21.

3. Gewirtz D. A Critical Evaluation of The Mechanisms Of Action Proposed for the Antitumor Effects of the Anthracycline Antibiotics Adriamycin and Daunorubicin. Biochemical Pharmacology. 1999;57: 727-741.

4. Di Marco A, Silvestrini R, Di Marco S, Dasdia T. Inhibiting Effect of the New Cytotoxic Antibiotic Daunomycin on Nucleic Acids and Mitotic Activity of Hela Cells. The Journal of Cell Biology. 1965;27: 545-550.

5. Calendi E, Di Marco A, Reggiani M, Scarpinato B, Valentini L. On Physico-Chemical Interactions Between Daunomycin and Nucleic Acids. Biochimica Et Biophysica Acta (BBA). Nucleic Acids and Protein Synthesis. 1965;103: 25-49.

6. Dano K, Frederiksen S, Hellung-Larsen P. Inhibition of DNA and RNA Synthesis by Daunorubicin in Sensitive and Resistant Ehrlich Ascites Tumor Cells in Vitro. Cancer Research. 1972;32: 1307-1314.

7. Tanaka M, Yoshida S. Mechanism of the Inhibition of Calf Thymus DNA Polymerases α and β by Daunomycin and Adriamycin. Journal of Biochemistry. 1980;87: 911-918.

8. William LJ, Sim S-K, Majumdar KC, Chang R-Y. Strand Scission of DNA by Bound Adriamycin and Daunorubicin in the Presence of Reducing Agents. Biochemical and Biophysical Research Communications. 1977;76: 705-710.

9. Bachur NR, Gordan SL, Gee MV. Anthracycline Antibiotic Augmentation of Microsomal Electron Transport and Free Radical Formation. Molecular Pharmacology. 1977;13: 901-910.

10. Muindi JRF, Sinha BK, Gianni L, Myers CE. Hydroxyl Radical Production and DNA Damage Induced by Anthracycline-Iron Complex. FEBS Letters. 1984;172: 226-230.

11. Feinstein E, Canaani E, Weiner LM. Dependence of Nucleic Acid Degradation on In Situ Free-Radical Production by Adriamycin. Biochemistry. 1993;32: 13156-13161.

12. Sinha BK, Chignell CF. Binding Mode of Chemically Activated Semiquinone Free Radicals From Quinone Anticancer Agents to DNA. Chemico-Biological Interactions. 1979;28: 301-308.

13. Wallace KB, Johnson JA. Oxygen-Dependent Effect of Microsomes on the Binding of Doxorubicin to Rat Hepatic Nuclear DNA. Molecular Pharmacology. 1987;31: 307-311.

14. Cullinane C, Phillips DR. Induction of Stable Transcriptional Blockage Sites by Adriamycin: GpC Specificity of Apparent Adriamycin-DNA Adducts and Dependence on Iron(III) Ions. Biochemistry. 1990;29: 5638-5646.

15. Skladanowski A, Konopa J. Interstrand DNA Crosslinking Induced by Anthracyclines in Tumour Cells. Biochemical Pharmacology. 1994;47: 2269-2278.

16. Skladanowski A, Konopa J. Relevance of Interstrand DNA Crosslinking Induced by Anthracyclines for their Biological Activity. Biochemical Pharmacology. 1994;47: 2279-2287.

17. Fornari FA, Randolph JK, Yalowich JC, Ritke MK, Gewirtz DA. Interference by Doxorubicin with DNA Unwinding in MCF-7 Breast Tumor Cells. Molecular Pharmacology. 1994;45: 649-656.

18. Montecucco A, Pedrali-Noy G, Spadari S, Zanolin E, Ciarrocchi G. DNA Unwinding And Inhibition of T4 DNA Ligase by Anthracyclines. Nucleic Acids Research. 1988;16: 3907-3918.

19. Bachur NR, Yu F, Johnson R, Hickey R, Wu Y, Malkas L. Helicase Inhibition by Anthracycline Anticancer Agents. Molecular Pharmacology. 1992;41: 993-998.

20. Tewey KM, Chen GL, Nelson EM, Liu LF. Intercalative Antitumor Drugs Interfere with the Breakage-Reunion Reaction of Mammalian DNA Topoisomerase II. Journal of Biological Chemistry. 1984;259: 9182-9187.

21. Tewey K, Rowe T, Yang L, Halligan B, Liu L. Adriamycin-Induced DNA Damage Mediated by Mammalian DNA Topoisomerase II. Science. 1984;226: 466-468.

22. Capranico G, Riva A, Tinelli S, Dasdia T, Zunino F. Markedly Reduced Levels of Anthracycline-induced DNA Strand Breaks in Resistant P388 Leukemia Cells and Isolated Nuclei. Cancer Research. 1987;47: 3752-3756.

23. Ling Y-H, Priebe W, Perez-Soler R. Apoptosis Induced by Anthracycline Antibiotics in P388 Parent and Multidrug-resistant Cells. Cancer Research. 1993;53: 1845-1852.

24. Skladanowski A, Konopa J. Adriamycin and Daunomycin Induce Programmed Cell Death (Apoptosis) in Tumour Cells. Biochemical Pharmacology. 1993;46: 375-382.

25. Zaleskis G, Berleth E, Verstovsek S, Ehrke MJ, Mihich E. Doxorubicin-Induced DNA Degradation in Murine Thymocytes. Molecular Pharmacology. 1994;46: 901-908.

26. Fujita H. Comparative Studies on the Blood Level, Tissue Distribution, Excretion and Inactivation of Anticancer Drugs. Japanese Journal of Clinical Oncology. 1971;1: 151-162.

27. Yesair DW, Schwartzbach E, Shuck D, Denine EP, Asbell MA. Comparative Pharmacokinetics of Daunomycin and Adriamycin in Several Animal Species. Cancer Research. 1972;32: 1177-1183.

28. Cho K, Wang X, Nie S, Chen Z, Shin DM. Therapeutic Nanoparticles for Drug Delivery in Cancer. Clinical Cancer Research. 2008;14: 1310-1316.

29. Sarin H. Physiologic Upper Limits of Pore Size of Different Blood Capillary Types and Another Perspective on the Dual Pore Theory of Microvascular Permeability. Journal of Angiogenes Research. 2010;2: 10.1186.

30. Yuan F, Dellian M, Fukumura D, et al. Vascular Permeability in a Human Tumor Xenograft: Molecular Size Dependence and Cutoff Size. Cancer Research. 1995;55: 3752-3756.

31. Jain RK. Transport of Molecules, Particles, and Cells in Solid Tumors. Annual Review of Biomedical Engineering. 1999;1: 241-263.

32. Jain RK. Delivery of Molecular Medicine to Solid Tumors: Lessons from in Vivo Imaging of Gene Expression and Function. Journal of Controlled Release. 2001;74: 7-25.

33. Gao X, Cui Y, Levenson RM, Chung LWK, Nie S. In Vivo Cancer Targeting and Imaging with Semiconductor Quantum Dots. Nature Biotechnology. 2004;22: 969-976.

34. Kersten W, Kersten H, Szybalski W, Fiandt M. Physicochemical Properties of Complexes between Deoxyribonucleic Acid and Antibiotics Which Affect Ribonucleic Acid Synthesis (Actinomycin, Daunomycin, Cinerubin, Nogalamycin, Chromomycin, Mithramycin, and Olivomycin)*. Biochemistry. 1966;5: 236-244.

35. Pigram W, Fuller W, Hamilton L. Stereochemistry of Intercalation: Interaction of Daunomycin with DNA. Nature. 1972;235: 17-19.

36. Chaires JB, Dattagupta N, Crothers DM. Kinetics of the Daunomycin-DNA Interaction. Biochemistry. 1985;24: 260-267.

37. Chaires JB, Dattagupta N, Crothers DM. Binding of Daunomycin to Calf Thymus Nucleosomes. Biochemistry. 1983;22: 284-292.

38. Chaires JB. Daunomycin Inhibits the B ← Z Transition in Poly d(G-C). Nucleic Acids Research. 1983;11: 8485-8494.

39. Chaires JB. Allosteric Conversion of Z DNA to an Intercalated Right-Handed Conformation by Daunomycin. Journal of Biological Chemistry. 1986;261: 8899-8907.

40. Chaires JB. Equilibrium Studies on the Interaction of Daunomycin with Deoxypolynucleotides. Biochemistry. 1983;22: 4204-4211.

41. Chaires JB, Dattagupta N, Crothers DM. Studies on Interaction of Anthracycline Antibiotics and Deoxyribonucleic Acid: Equilibrium Binding Studies on The Interaction of Daunomycin with Deoxyribonucleic Acid. Biochemistry. 1982;21: 3933-3940.

42. Newlin DD, Miller KJ, Pilch DF. Interactions of Molecules with Nucleic Acids. VII. Intercalation and T·A Specificity of Daunomycin in DNA. Biopolymers. 1984;23: 139-158.

43. Chen K-X, Gresh N, Pullman B. A Theoretical Investigation on the Sequence Selective Binding of Daunomycin to Double-Stranded Polynucleotides. Journal of Biomolecular Structure and Dynamics. 1985;3: 445-466.

44. Quigley GJ, Wang AH, Ughetto G, van der Marel G, van Boom JH, Rich A. Molecular Structure of an Anticancer Drug-DNA Complex: Daunomycin Plus d(CpGpTpApCpG). Proceedings of the National Academy of Sciences. 1980;77: 7204-7208.

45. Chaires JB, Fox KR, Herrera JE, Britt M, Waring MJ. Site and Sequence Specificity of the Daunomycin-DNA Interaction. Biochemistry. 1987;26: 8227-8236.

46. Skorobogaty A, White RJ, Phillips DR, Reiss JA. The 5′-CA DNA-Sequence Preference of Daunomycin. FEBS Letters. 1988;227: 103-106.

47. Skorobogaty A, White RJ, Phillips DR, Reiss JA. Elucidation of the DNA Sequence Preferences of Daunomycin. Drug Design and Delivery. 1988;3: 125-151.

48. Chaires JB, Herrera JE, Waring MJ. Preferential Binding of Daunomycin to 5'TACG and 5'TAGC Sequences Revealed by Footprinting Titration Experiments. Biochemistry. 1990;29: 6145-6153.

49. Wang AHJ, Ughetto G, Quigley GJ, Rich A. Interactions Between an Anthracycline Antibiotic and DNA: Molecular Structure of Daunomycin Complexed to d(CpGpTpApCpG) at 1.2-.ANG. Resolution. Biochemistry. 1987;26: 1152-1163.

50. Moore MH, Hunter WN, d'Estaintot BL, Kennard O. DNA-Drug Interactions: The Crystal Structure of d(CGATCG) Complexed with Daunomycin. Journal of Molecular Biology. 1989;206: 693-705.

51. Bagalkot V, Farokhzad OC, Langer R, Jon S. An Aptamer–Doxorubicin Physical Conjugate as a Novel Targeted Drug-Delivery Platform. Angewandte Chemie International Edition. 2006;45: 8149-8152.

52. Carbone GM, McGuffie E, Napoli S, et al. DNA Binding And Antigene Activity of a Daunomycin Conjugated Triplex Forming Oligonucleotide Targeting the P2 Promoter of the Human C-Myc Gene. Nucleic Acids Research. 2004;32: 2396-2410.

53. Ren J, Chaires JB. Sequence and Structural Selectivity of Nucleic Acid Binding Ligands. Biochemistry. 1999;38: 16067-16075.

54. Wochner A, Menger M, Orgel D, et al. A DNA Aptamer with High Affinity and Specificity for Therapeutic Anthracyclines. Analytical Biochemistry. 2008;373: 34-42.

55. Elmore LW, Rehder CW, Di X, et al. Adriamycin-induced Senescence in Breast Tumor Cells Involves Functional p53 and Telomere Dysfunction. Journal of Biological Chemistry. 2002;277: 35509-35515.

56. Ogretmen B, Kraveka JM, Schady D, Usta J, Hannun YA, Obeid LM. Molecular Mechanisms of Ceramide-mediated Telomerase Inhibition in the A549 Human Lung Adenocarcinoma Cell Line. Journal of Biological Chemistry. 2001;276: 32506-32514.

57. Clark GR, Pytel PD, Squire CJ, Neidle S. Structure of the First Parallel DNA Quadruplex-Drug Complex. Journal of the American Chemical Society. 2003;125: 4066-4067.

58. Fedor MJ, Uhlenbeck OC. Substrate Sequence Effects on "Hammerhead" RNA Catalytic Efficiency. Proceedings of the National Academy of Sciences. 1990;87: 1668-1672.

59. Steel AB, Levicky RL, Herne TM, Tarlov MJ. Immobilization of Nucleic Acids at Solid Surfaces: Effect of Oligonucleotide Length on Layer Assembly. Biophysical Journal. 2000;79: 975-981.

60. Parak WJ, Pellegrino T, Micheel CM, Gerion D, Williams SC, Alivisatos AP. Conformation of Oligonucleotides Attached to Gold Nanocrystals Probed by Gel Electrophoresis. Nano Letters. 2002;3: 33-36.

61. Sundaram P, Wower J, Byrne ME. A Nanoscale Drug Delivery Carrier Using Nucleic Acid Aptamers for Extended Release of Therapeutic. Nanomedicine: Nanotechnology, Biology and Medicine. 2012;8: 1143-1151.

62. Cheng. Y, Samia. A. C, Meyers. J. D et al., Highly Efficient Drug Delivery with Gold Nanoparticle Vectors for *in Vivo* Photodynamic Therapy of Cancer**,** Journal of. American. Chemical. Society. 2008, 130: 10643–10647.

63. Gibson. J.D, Khanal. B.P, Zubarev. E.R, Paclitaxel-Functionalized Gold Nanoparticles, Journal of. American. Chemical. Society. 2007, 129: 11653–11661.

64. Hwu J.R, Lin Y.S, Josephrajan. T et al., Targeted Paclitaxel by Conjugation to Iron Oxide and Gold Nanoparticles, Journal of. American. Chemical. Society. 2009, 131: 66-68.

65. Nakayama. H, Shimizu. T, Ishida. H et al., Light-Regulated Activation of Cellular Signaling by Gold Nanoparticles That Capture and Release Amines, Journal of. American. Chemical. Society. 2009,131: 3822- 3823.

66. Kim D, Jeong YY, Jon S. A Drug-Loaded Aptamer−Gold Nanoparticle Bioconjugate for Combined CT Imaging and Therapy of Prostate Cancer. ACS Nano. 2010;4: 3689-3696.

67. Rippe. K, Ramsing. N. B, Jovin. T. M, Spectroscopic Properties and Helical Stabilities of 25 nt Parallel Stranded Linear DNA Duplex. Biochemistry. 1989, 28: 9536- 9541.

68. Zhurkin. V. B, Raghunathan. G, Ulyanob. N. B, Camerini. R. D, Jernigan. R. L, A Parallel DNA Triplex as a model for the Intermediate Homologous Recombination. Journal of Molecular Biology. 1994, 239: 181- 200.

69. Asensio. J. L, Lane. A. N, Dhesi. J, Bergqvist. S, Brown. T, The Contribution of Cytosine Protonation to the Stability Parallel DNA Triple Helices. Journel of Molecular Biology. 1998, 275: 811- 822.

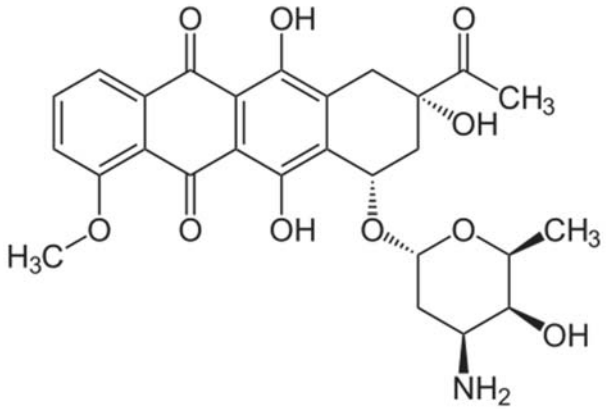

Figure 7.1. Chemical Structure of Daunomycin. Aglycon chromophore (daunomycinone) linked to an amino sugar (daunosamine). **(**Adopted from Wikipedia)

A Oligo-93

5′-GGGAATTCGAGCTCGGTACCATCTGTGTAAGGGGTAAGGGGTGGGGGTGGGTACGTCTA
GCTGCAGGCATGCAAGCTTGG**AATATTGTAAACC**–3′

B Oligo-93R

5′-AGGTGCGTGAGTCGAGGTGATCGTGAGTCGTGAGTGCAGTGACGCGCTGAGTCCGAGTG
AGCGAGTGTGAGTGATGATCC**AATATTGTAAACC**-3′

(Bolded is the extended sequence complementary to ANC-oligo)

C ANC-oligo

5′-(SH) TTTTATGGTTTACAATATT-3′

D

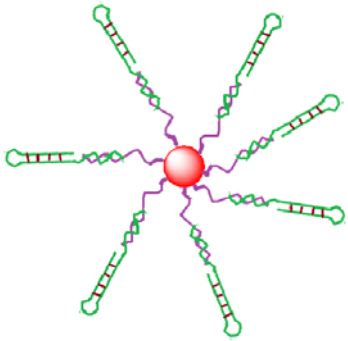

Figure 7.2. Nano-Carrier Construct. Sequence of (A) daunomycin binding DNA, (B) control DNA, (C) anchor DNA, and (D) Representation of daunomycin nano-carrier: anchor DNA(violet) hybridized oligo-93 (Green) conjugated to AuNps.

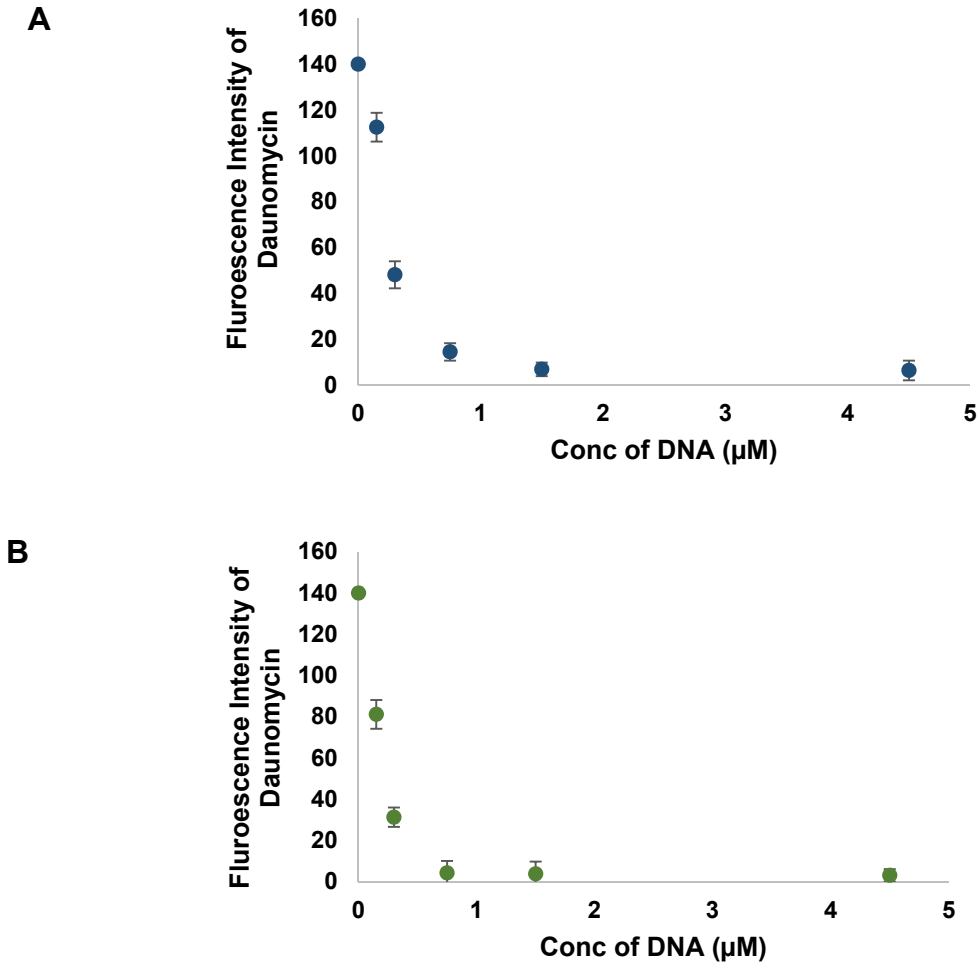

Figure 7.3. Daunomycin – Oligonucleotide Titration. Decrease in the fluorescence intensity of fixed concentration of daunomycin with addition of increasing concentration of (A) oligo-93, (B) oligoR-93. (N=3)

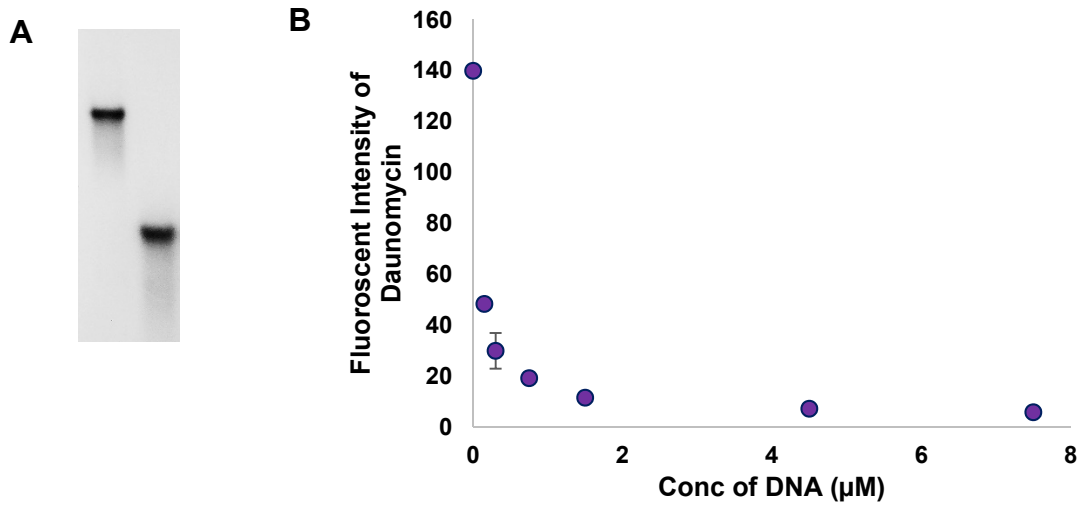

Figure 7.4. Hybridization of oligo-93 to ANC-Oligo. (A) Gel image of a 10% non-denaturing gel with [γ–^{32}P]-labeled oligo-93 on the right, and ANC-oligo hybridized [γ–^{32}P]-labeled oligo-93 with duplex sequence extended using Klenow enzyme on the left. The difference in the position of the bands signifies the duplex formation between oligo-93 and ANC-oligo. (B) Decrease in the fluorescence intensity of fixed concentration of daunomycin with addition of increasing concentration of oligo-93: ANC-oligo complex (N-3).

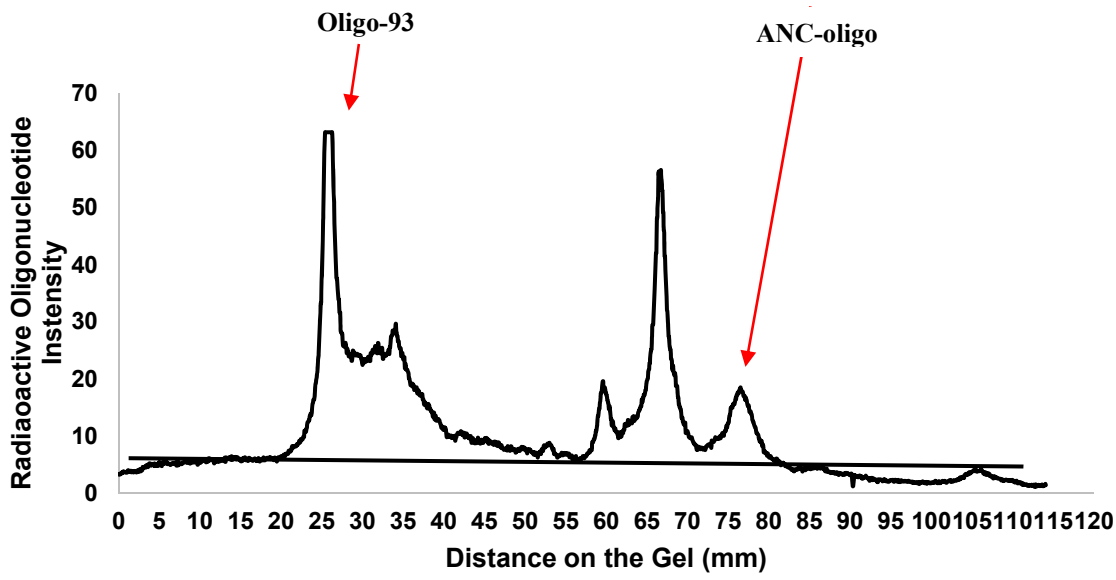

Figure 7.5. Oligo-93 Binding Profile. Along with oligo-93, a small amount of shorter fragments of oligo-93, which are the side products of the solid phase synthesis of oligonucleotides, were conjugated on AuNps.

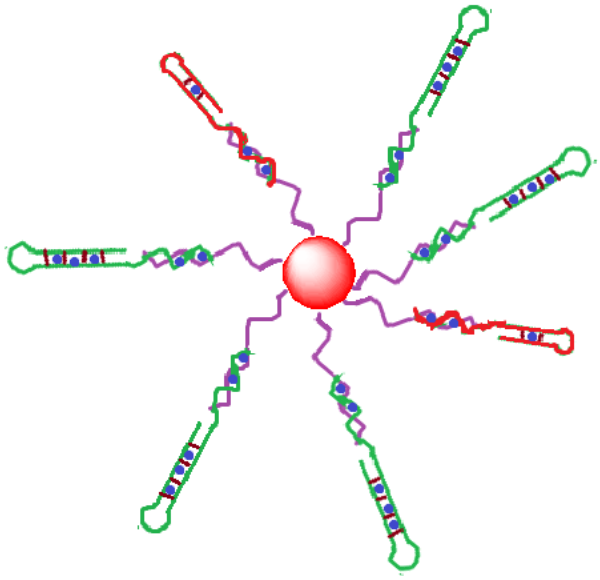

Figure 7.6. Representation of Daunomycin Loaded Nano-Carrier. The green DNA represents oligo-93, the red represents shorter oligonucleotide fragaments of oligo-93, and the blue dots represent daunomycin.

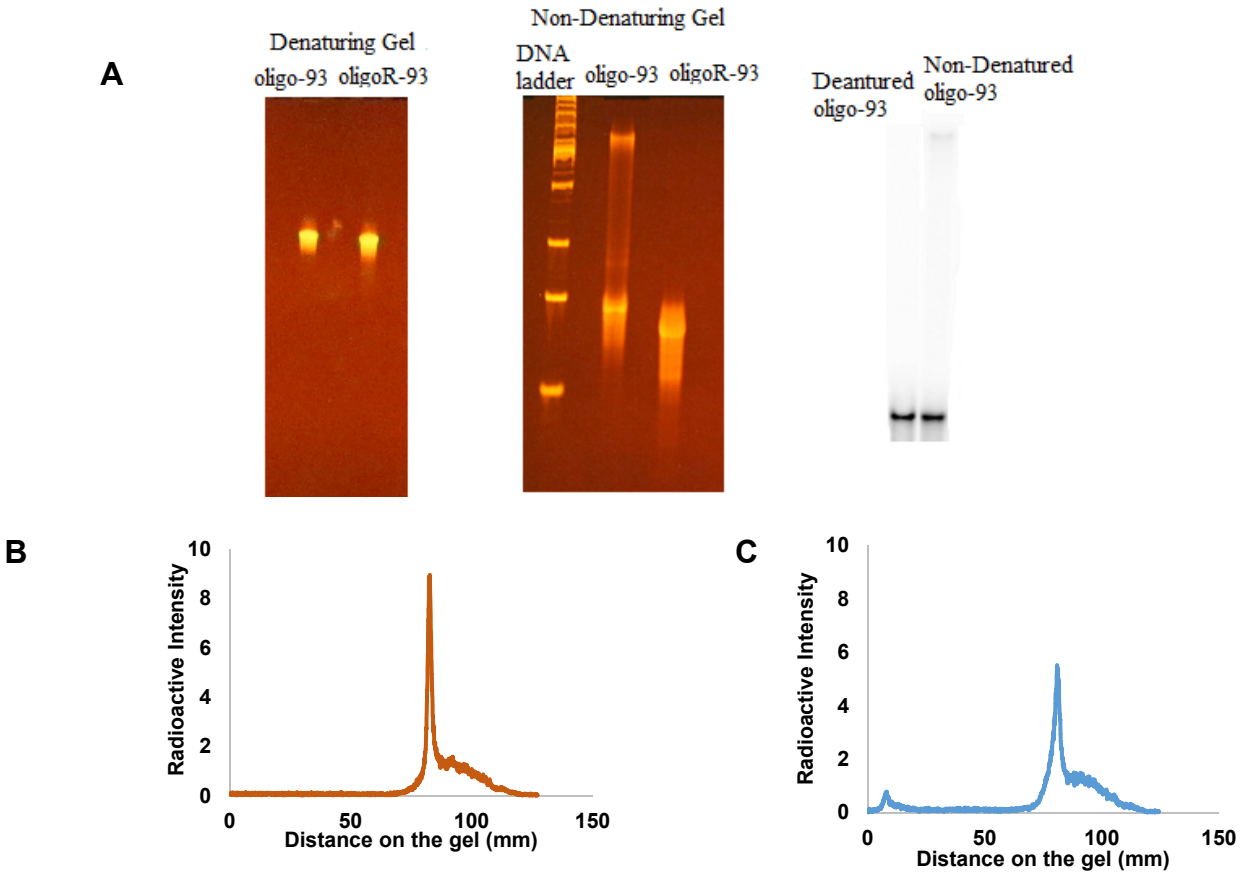

Figure 7.7. Self-Complexes of Oligo-93. (A) Left: gel image of oligo-93 and oligo-93R in a denaturing gel in which the oligonucelotides are in denatured state and so no complexes are present. Middle: gel image of the oligonucleotides in the non-denatured state. It can be observed that oligo-93 forms self-complexes. Right: gel image of denatured and non-denatured [γ–^{32}P]-labeled oligo-93. This gel was scanned using Fuji FLA-5100 imager for radioactive intensity profile. (B) Intensity profile of denatured oligo-93. Single peak was observed corresponding to oligo-93. (C) Intensity profile of non-denatured oligo-93. Two peaks were observed one for oligo-93 and another for oligo-93 complex.

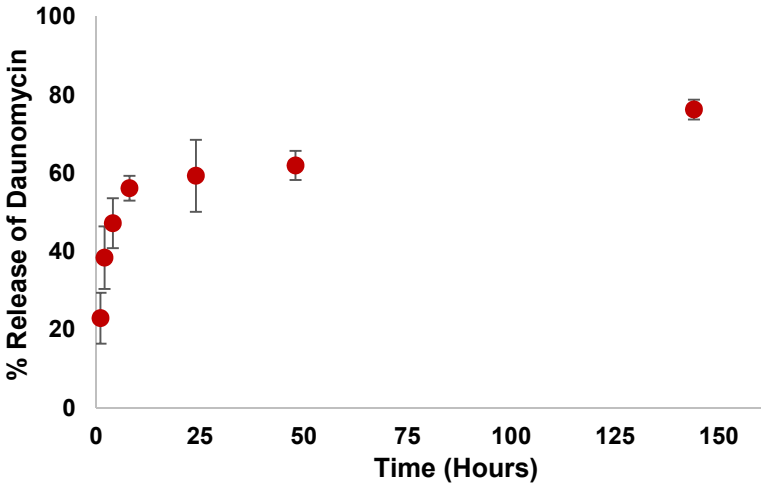

Figure 7.8. In-vitro Release of Daunomycin from the Nano-Carrier. The release of daunomycin from the drug loaded nano-carrier was recorded for 6 day at 37°C. (N=3)

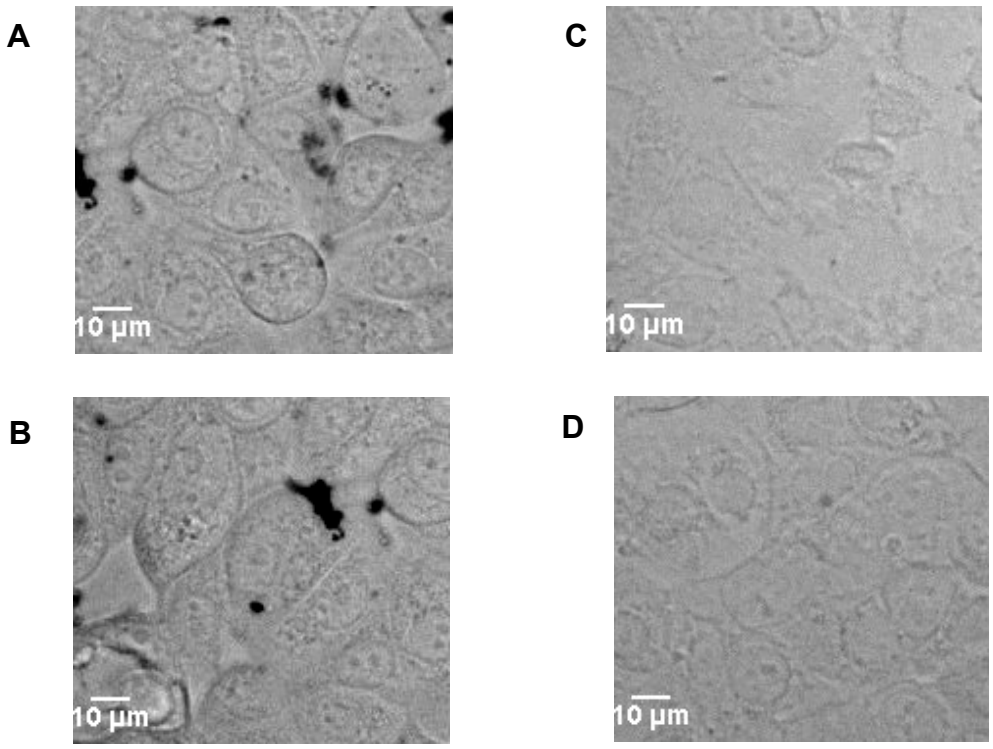

Figure 7.9. Cellular Uptake of Nano-Carrier by MCF7 Breast Cancer Cells. Silver stained MCF7 cells after 4 hours of incubation with (A&B) 50 nM nano-carrier in cell culture media (C&D) plain cell culture media. Dark black spots in A & B correspond to silver deposit on AuNps inside the cell.

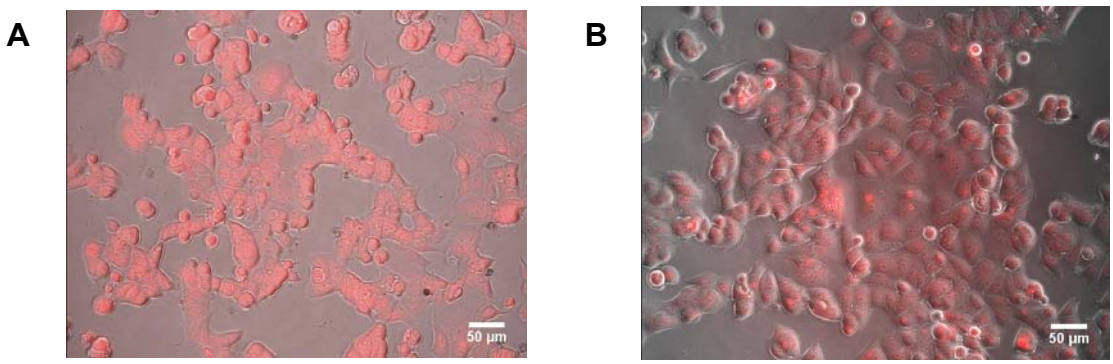

Figure 7.10. Presence of Daunomycin inside MCF7 Cells. The breast cancer cells were incubated with (A) 100 nM nano-carrier (B) 100 nM free daunomycin. The phase contrast and fluorescence infused images of MCF7 cells were obtained using Nikon Eclipse Ti inverted microscope. (Scale bar = 50 µm)

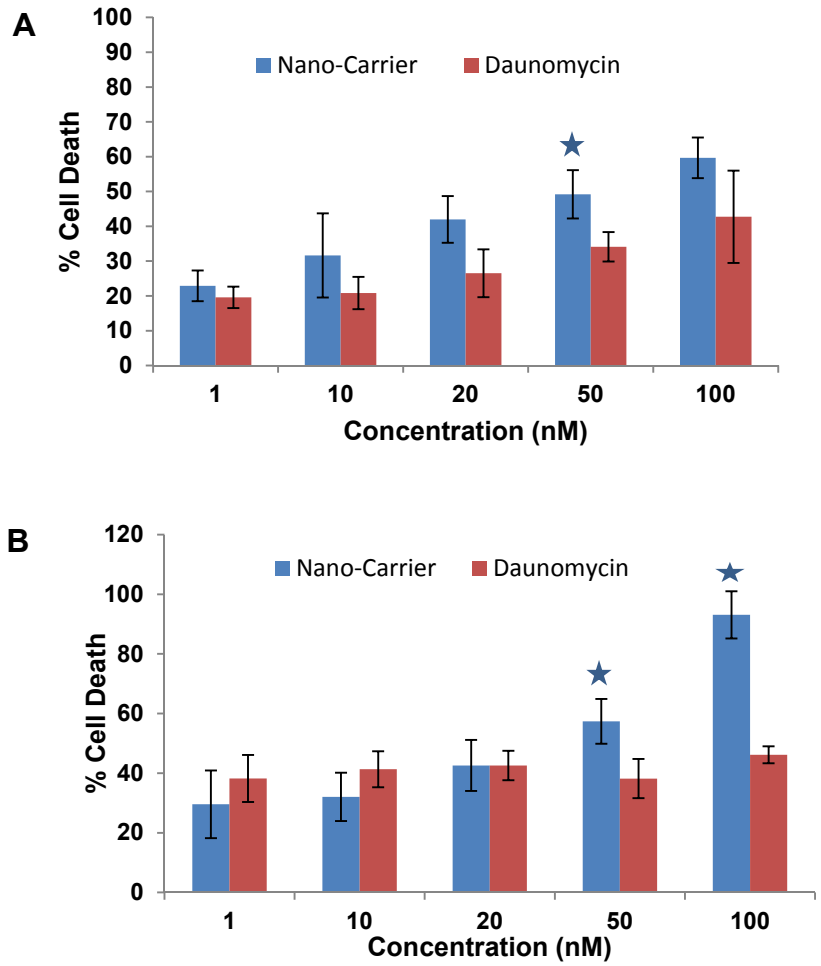

Figure 7.11. In-vitro Cell Viability Measured by XTT Assay. MCF7 cells were incubated with different concentrations of free daunomycin and daunomycin loaded nanao-carrier at 37ºC for (A) 4 hours (B) 12 hours. Cells were then washed and the cell viability was measured after a 6 hours of incubation at 37ºC. (N=3; ★ represents statistically significant difference)

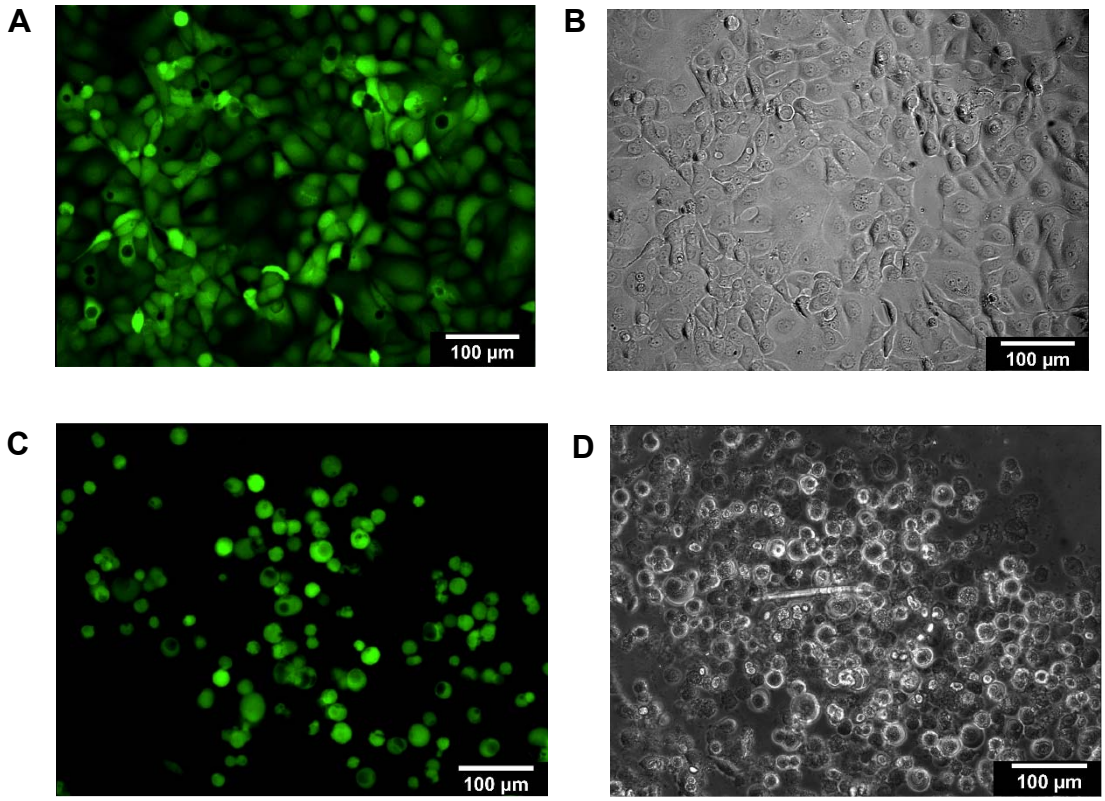

Figure 7.12. In-vitro Live/Dead Fluorescent Cell Viability Assay Images of MCF7 Cells. MCF7 cells were subjected to 4 hours cellular uptake of (A & B) free daunomycin, (C & D) daunomycin loaded nano-carrier, followed by 6 hours incubation and live cell fluorescent assay. (B & D) are the phase contrast images of cells, (A & C) are the green fluorescent images of live cells.

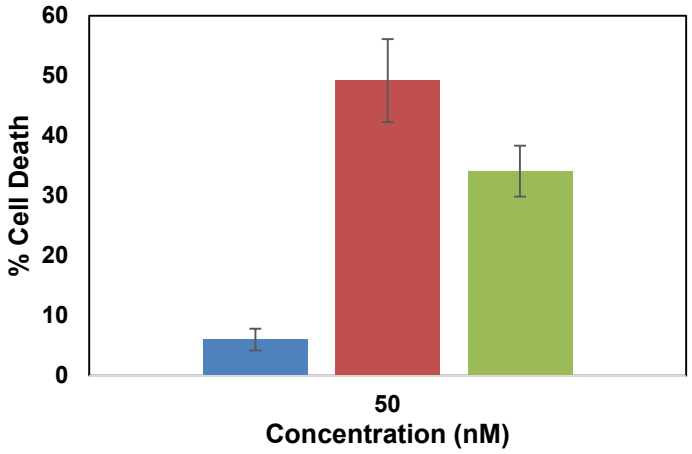

Figure 7.13. Cytotoxicity of Nano-Carrier Compared with Drug Loaded Nano-Carrier. Cell viability of MCF7 cells treated with 50 nM of nano-carrier (blue), daunomycin loaded nano-carrier (red), daunomycin (green). (N = 3)

Chapter 8. Conclusions

Nanotechnology is a rapidly expanding field today and has a great potential in the field of drug delivery. Drug delivery carriers hold tremendous promise in overcoming some of the obstacles imposed by the body to efficiently target drug to affected cells. Biohybrid nanoparticles are prime candidates in creating advanced delivery systems that would profoundly impact the current treatment regimens for various diseases and improve the quality of life of patients. Present research in the field of drug delivery is focused on engineering a non-toxic nano delivery carrier capable of targeted and controlled delivery of drug.

In this work, a novel, biohybrid, nano-delivery carrier for dynamic, targeted and controlled release of drug for an extended period of time was synthesized using gold nanoparticles and DNA. We investigated the factors affecting the loading of DNA on AuNps, and found that DNA loading is a function of salt and DNA concentration. The optimum salt concentration depends on the length and the sequence of the DNA. For loading of single stranded anchor DNA (NAN-ANC) on AuNps the optimum salt concentration was found to be 0.4 M. At optimum salt concentration, DNA loading increased with DNA concentration until 4 μM, at which a maximum loading of 101±8 NAN-ANC per AuNp was observed. For any DNA concentration above 4 μM, the AuNps was observed to aggregate.

The orientation of DNA conjugated to AuNps changed with the number density of DNA. At lower number density, due to the affinity between the nucleotide and gold surface, DNA tended to wrap around the AuNps. While, at higher number density, due to the repulsion forces between the DNA strands, they tended to orient in an erect fashion. The conformation of DNA attached to the AuNps changed from stretched to coiled with an increase in length of the single stranded DNA.

Moreover, for the first time, the binding of neomycin to DNA aptamer with high affinity was demonstrated. This binding could explain some of the side effects of neomycin. Two different strategies for binding the DNA aptamer and neomycin to AuNps were studied, and the best method for maximum loading was identified. A maximum of 22 neomycin molecules were immobilized per AuNp. Taking advantage of the non-covalent complexation between neomycin and aptamer, temperature-triggered release of neomycin from the nano-carrier for an extended period of 24 hours, with no initial burst release, was demonstrated. Also, we obtained an aptamer-drug binding affinity based release of neomycin at a constant temperature for an extended period of 24 hours.

Furthermore, we synthesized a non-toxic nano-carrier for the anticancer drug daunomycin using AuNps and DNA. The hydrodynamic size of the nano-carrier was measured to be 41 ± 2 nm. This size signifies its potential to passively target cancers cells via leaky vasculature, avoid rapid leakage into capillary, and escape macrophages of the reticuloendothelial system. A very high drug loading of 1157 ± 18 daunomycin per 15 nm AuNp was obtained with the daunomycin nano-carrier. The in-vitro dynamic drug release from the nano-carrier at 37^{o}C demonstrated that the drug can be continuously released for an extended period of time. Daunomycin nano-carriers were uptaken well by the MCF7

breast cancer cells, and the drug loaded nano-carrier was found to be superior to daunomycin in causing apoptosis to cancer cells. Moreover, the nano-carrier itself was found to be non-toxic, proving to be better than some of the present drug carriers that have high toxicity and also activate the immune system.

Here, we developed an efficient novel biohybrid delivery carrier for antibiotic drug neomycin and anticancer drug daunomycin using the principles of molecular biology and biochemistry. This nano-carrier is flexible to be easily modified for any drug and is thereby expected to profoundly impact present treatment regimens and revolutionize the field.

Appendix I - Experimental Data

Appendix I consists of data set collected from the experiments which were analyzed for generating results and discussions described in this dissertation.

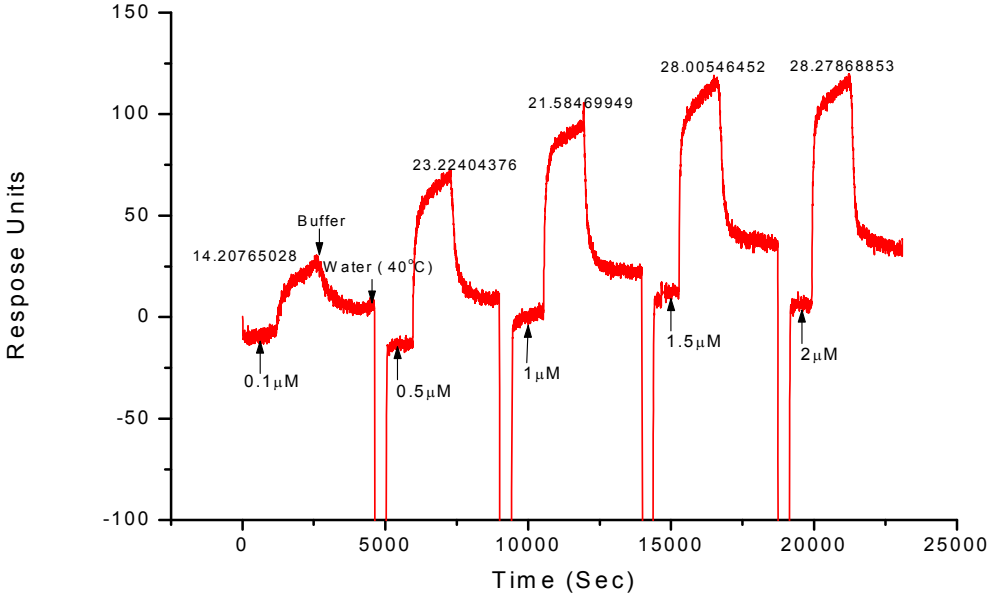

Figure AI.1. Neomycin-DNA Aptamer Binding Analysis on SPR. Increase in the response units with addition of neomycin onto the SPR surface functionalized with DNA aptamer followed by a water wash to remove the bound neomycin, and circulation of neomycin binding buffer to bring back the signal to equilibrium.

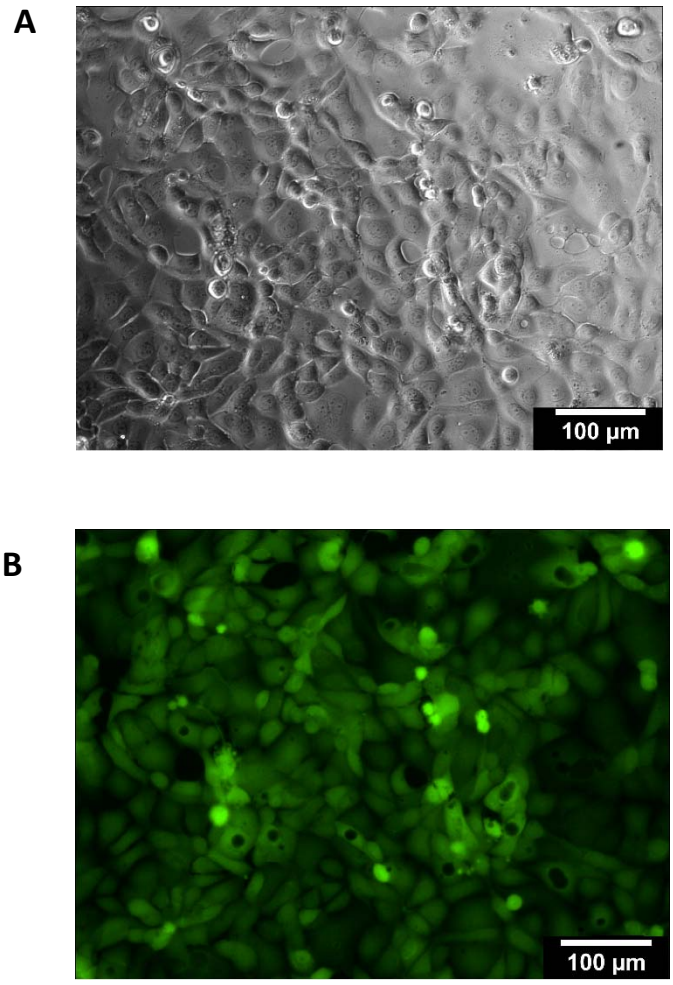

Figure AI.2. Cell Viability Assay with Nano-Carrier. Phase contrast (A) and fluorescent (B) images of MCF7 cells incubated with nano-carrier for 4 hours. All the cells were observed to produce green fluorescence signifying that the cells were alive.

Appendix II – Oligonucleotides Sequences

Anchor DNA	5′-(SH)TTTTATGGTTTACAATATT-3′
Neomycin Aptamer	5′- GGACUGGGCGAGAAGUUUAGUCC -3′
Neomycin DNA Aptamer	5′- GGACTGGGCGAGAAGTTTAGTCC -3′
NAN-NEO	5′- GGACTGGGCGAGAAGTTTAGTCCAATATTGTAAACC -3′
A13G-NAN-NEO	5′- GGACTGGGCGAGGAGTTTAGTCCAATATTGTAAACC -3′
T17C-NAN-NEO	5′- GGACTGGGCGAGGAGTCTAGTCCAATATTGTAAACC -3′
G7C-NAN-NEO	5′- GGACTGCGCGAGAAGTTTAGTCCAATATTGTAAACC -3′
T17CT18C-NAN-NEO	5′- GGACTGGGCGAGGAGTCCAGTCCAATATTGTAAACC -3′
G7TT17A-NAN-NEO	5′- GGACTGTGCGAGAAGTATAGTCCAATATTGTAAACC -3′
NAN-ANC-20mer	5′-(SH)TTTTATGGTTTACAATATTT -3′
NAN-ANC-30mer	5′-(SH)TTTTAT**GGTTTACAATATT** -3′ 3′-**CCAAATGTTATAA**CACACACACAA-5′
NAN-ANC-40mer	5′-(SH)TTTTAT**GGTTTACAATATT** -3′ 3′-**CCAAATGTTATAA**CACACACACACACACACACAA-5′
NAN-ANC-50mer	5-(SH)TTTTAT**GGTTTACAATATT**-3′ 3′-**CCAAATGTTATAA**ACACACACACACACACACACACACACACAA-5′

Table AII.1. Oligonucleotide Sequences used in Neomycin Study

Daunomycin Aptamer I	5′GGGAATTCGAGCTCGGTACCATCTGTGTAAGGGGTAAGGGGTGGGGGT GGGTACGTCTAGCTGCAGGCATGCAAGCTTGG-5′
ANC-oligo	5′-(SH)TTTTATGGTTTACAATATT-3′
Oligo-93	5′-GGGAATTCGAGCTCGGTACCATCTGTGTAAGGGGTAAGGGGTGGGGGT GGGTACGTCTAGCTGCAGGCATGCAAGCTTGGAATATTGTAAACC–3′
Oligo-10	5′- GCAAGCTTGGAATATTGTAAACC – 3
Oligo-20	5′- CTGCAGGCATGCAAGCTTGGAATATTGTAAACC -3′
Oligo-30	5′- GTACGTCTAGCTGCAGGCATGCAAGCTTGGAATATTGTAAACC – 3′
Oligo-40	5′-GTGGGGGTGGGTACGTCTAGCTGCAGGCATGCAAGCTTGGAATAT TGTAAACC – 3′
Oligo-50	5′-GGGGTAAGGGGTGGGGGTGGGTACGTCTAGCTGCAGGCATGCAAGCTTGG AATATTGTAAACC – 3′
Oligo-93R	5′- AGGTGCGTGAGTCGAGGTGATCGTGAGTCGTGAGTGCAGTGACGCGCT GAGTCCGAGTGAGCGAGTGTGAGTGATGATCCAATATTGTAAACC-3′
Oligo-10R	5′- GTGATGATCCAATATTGTAAACC -3′
Oligo-20R	5′- GCGAGTGTGAGTGATGATCCAATATTGTAAACC -3′
Oligo-30R	5′- GTCCGAGTGAGCGAGTGTGAGTGATGATCCAATATTGTAAACC-3′
Oligo-40R	5′- GACGCGCTGAGTCCGAGTGAGCGAGTGTGAGTGATGATCCAATA TTGTAAACC -3′
Oligo-50R	5′-TGAGTGCAGTGACGCGCTGAGTCCGAGTGAGCGAGTGTGAGTGATGATC CAATATTGTAAACC- 3′

Table AII.2. Oligonucleotide Sequences used in Daunomycin Study